SWELLING OF ELASTOMERS IN BIODIESEL AND THE RESULTING MECHANICAL RESPONSE UNDER CYCLIC LOADING

CHAI AI BAO

FACULTY OF ENGINEERING
UNIVERSITY OF MALAYA
KUALA LUMPUR

2013

SWELLING OF ELASTOMERS IN BIODIESEL AND THE RESULTING MECHANICAL RESPONSE UNDER CYCLIC LOADING

CHAI AI BAO

THESIS SUBMITTED IN FULFILMENT
OF THE REQUIREMENTS
FOR THE DEGREE OF DOCTOR OF PHILOSOPHY

FACULTY OF ENGINEERING
UNIVERSITY OF MALAYA
KUALA LUMPUR

2013

UNIVERSITI MALAYA

ORIGINAL LITERARY WORK DECLARATION

Name of Candidate: Chai Ai Bao (I.C./Passport No.:

Registration/Matrix No.: KHA100023

Name of Degree: The Degree of Doctor of Philosophy

Title of Project Paper/Research Report/Dissertation/Thesis ("this Work"): Swelling of elastomers in biodiesel and the resulting mechanical response under cyclic loading

Field of Study: Mechanical Aspect of Polymer

I do solemnly and sincerely declare that:

(1) I am the sole author/writer of this Work;
(2) This work is original;
(3) Any use of any work in which copyright exists was done by way of fair dealing and for permitted purposes and any excerpt or extract from, or reference to or reproduction of any copyright work has been disclosed expressly and sufficiently and the title of the Work and its authorship have been acknowledged in this Work;
(4) I do not have any actual knowledge nor do I ought reasonably to know that the making of this work constitutes an infringement of any copyright work;
(5) I hereby assign all and every rights in the copyright to this Work to the University of Malaya ("UM"), who henceforth shall be owner of the copyright in this Work and that any reproduction or use in any form or by any means whatsoever is prohibited without the written consent of UM having been first had and obtained;
(6) I am fully aware that if in the course of making this Work I have infringed any copyright whether intentionally or otherwise, I may be subject to legal action or any other action as may be determined by UM.

Candidate's Signature Date

Subscribed and solemnly declared before,

Witness's Signature Date

Name:
Designation:

ABSTRACT

The environmental and economic concerns have raised the popularity of biodiesel as the replacement for the conventional fuel. However, the incompatibility of engineering rubber components with biodiesel affects significantly the performance of the components. Majority of the compatibility studies focus on evaluating the degradation of mechanical properties in the rubbers due to contamination of different types of biodiesel. Nevertheless, the resulting mechanical responses of swollen rubbers, in particular under cyclic and fatigue loading conditions, are rarely investigated. In engineering applications where elastomeric components are concurrently subjected to fluctuating mechanical loading and exposure to aggressive liquids such as biodiesel, it is crucial to investigate and to model the mechanical responses of these components for durability analysis.

The first part of this research involves experimental works to investigate the effect of swelling, due to biodiesel diffusion in the elastomers, on the macroscopic mechanical response of elastomers under cyclic compressive loading. First of all, simple immersion tests on stress-free elastomeric specimens were conducted and the resulting mechanical responses were evaluated. The focus of this work is on the effect of swelling on the inelastic responses classically observed in elastomers under cyclic loading conditions, i.e. stress-softening due to Mullins effect, hysteresis and stress relaxation. The results show that inelastic responses decrease significantly when the degree of swelling increases. Secondly, swelling tests on uniaxially-stressed specimens were conducted. For this purpose, an original compression device was developed to investigate the effect of uniaxial mechanical loading on the swelling of rubber in solvent. The apparatus comprises of four stainless steel plates and spacer bars in between which are specifically designed such that compression can be introduced on the rubber specimens while they are simultaneously immersed into biodiesel. Thereby allowing coupled liquid diffusion and large strain to take place. Different pre-compressive strains and biodiesel blends were considered. At the end of each immersion period, the resulting swelling and mechanical responses of rubber specimens under cyclic loading conditions were investigated. Special attention is given to the stress-softening phenomenon.

The second part of this work can be regarded as a first step towards modeling of stress-softening in swollen rubber. For this purpose, the pseudo-elastic model and the two-phase model were considered and extended in order to account for the degree of swelling. Results show that the proposed models were qualitatively in good agreement with experimental observations.

ABSTRAK

Keperhatinan terhadap alam sekitar dan ekonomi telah meningkatkan popularitibiodiesel sebagai pengganti bahan api konvensional. Walau bagaimanapun, ketidakserasian komponen getah kejuruteraan dengan biodiesel telah memberi kesan ketara kepada prestasi komponen. Kebanyakan kajian keserasian menumpu kepada penilaian kemerosotan sifat-sifat mekanikal dalam getah akibat pencemaran daripada pelbagai jenis biodiesel yang berlainan. Sungguh pun demikian, hasil tindak balas mekanikal getah bengkak, terutamanya dalam keadaan pembebanan berulang dan kelesuan, adalah jarang disiasat. Dalam aplikasi kejuruteraan di mana komponen elastomer mengalami bebanan mekanik turun naik dan didedahkan kepada cecair yang agresif seperti biodiesel secara serentak, maka amatlah penting untuk mengkaji dan membina model tindak balas mekanikal komponen ini demi analisis kebolehtahanan.

Dalam bahagian pertama penyelidikan ini melibatkan kerja-kerja eksperimen untuk menyiasat kesan bengkak, disebabkan oleh peresapan biodiesel dalam elastomer, terhadap tindak balas mekanikal makroskopik dalam keadaan bebanan mampatan berulang. Pertama sekali, ujian rendaman yang mudah telah dijalankan pada spesimen elastomer yang bebas dari tegasan dan hasil tindak balas mekanikal yang berkenaan telah dikaji. Tumpuan kerja ini adalah untuk menyiasat kesan bengkak kepada tindak balas mekanikal tidak boleh ubah yang biasa diperhatikan dalam elastomer yang mengalami bebanan berulang, iaitu pelembutan tegasan yang disebabkan oleh kesan Mullins, histerisis dan pengenduran tegasan. Hasil kajian menunjukkan bahawa tindak balas tak kenyal berkurang dengan ketara apabila tahap bengkak meningkat. Kedua, ujian pembengkakan atas spesimen yang mengalami tegasan ekapaksi telah dijalankan. Untuk tujuan ini, alat mampatan yang asal telah dicipta untuk mengkaji kesan bebanan mekanikal kepada kebengkakan getah dalam pelarut. Alat ini terdiri daripada empat plat keluli tahan karat dan bar jarak di antaranya yang direka khusus supaya mampatan boleh dikenakan secara serentak atas spesimen getah semasa spesimen direndam di dalam biodiesel. Justeru membolehkan peresapan cecair dan terikan besar berlaku. Pelbagai terikan pra-mampatan dan campuran biodiesel telah dipertimbangkan. Pada akhir setiap tempoh rendaman, hasil dari ujian bengkak dan hasil tindak balas mekanikal spesimen getah bengkak dalam keadaan bebanan berulang telah dikaji. Perhatian khusus diberikan kepada fenomena pelembutan tegasan.

Bahagian kedua kerja ini boleh dianggap sebagai langkah pertama ke arah membina model pelembutan tegasan dalam getah bengkak. Bagi tujuan ini, model pseudo-elastik dan model dua-fasa telah dipertimbangkan dan diperluaskan dengan mengambil kira tahap kebengkakan. Hasil kerja menunjukkan bahawa model yang dicadangkan adalah mempunyai persetujuan yang baik secara kualitatif dengan pemerhatian eksperimen.

ACKNOWLEDGEMENTS

Foremost I wish to express my sincere appreciation to my supervisors, Dr. Andri Andriyana and Dr. Mohd. Rafie Johan for their consistent guidance, teaching and supervision during the process of working this research. Their advice and comments have helped me significantly in moving forward and completing this thesis report on time. I could not have imagined having a better supervisor and mentor during my PhD study.

I would also thank Prof. Erwan Verron from Ecole Centrale de Nantes (ECN), France for offering me an internship opportunity to work in his research group in Nantes, France. The exchange program has enlighten me and allowed me to work on a diverse exciting project. To my friends in ECN, you have made my stay in France a memorable one!

Besides, I would like to thank my friends in Department of Mechanical Engineering, University of Malaya (UM). I thank them for their continuous support and assistance provided whenever I needed a helping hand. A special thank to Ch'ng Shiau Ying, I treasure the time we spent in the laboratory and endless chat over writing academic journals, and all the fun and joy you brought to me!

Last but not the least, my deepest gratitude goes to my beloved parents, Chai Soong Choon and Chin Nyet Lan and my siblings, Chai Ginn Bao, Chai Ten Poh and Chai Sim Por for their endless love and encouragement. I will not be who I am today without their encouragement. Not to forget the endless support and understanding from my husband, Ong Cheat Wai and my little prince Ong Jun Hean. To those who indirectly contributed in this research, your kindness are highly appreciated. Thank you very much.

TABLE OF CONTENTS

LIST OF FIGURES

LIST OF TABLES

LIST OF SYMBOLS AND ACRONYMS

A	Helmholtz free energy.
A_κ	Thermodynamic force associated with the damage variable κ.
A_v	Avogadro number.
C_0	Dry state (unswollen-unstrained configuration).
C_o	Dry shear modulus.
C_s	Swollen state (swollen-unstrained configuration).
C_t	Swollen state (swollen-strained configuration).
E_s	Supplied energy during uploading.
G	Moduli in the unswollen state.
G'	Moduli in the swollen state.
H	Heat content.
H_5	Amount of hysteresis.
J_s	Degree of swelling.
J_s^e	Equilibrium degree of swelling.
M_w	Molecular weight of the solvent.
N	Number of chain per unit volume (degree of cross linking).
S	Entropy.
T	Temperature.
T_g	glass transition temperature.
U	Internal energy.
V	Volume.
V_0	Volume at dry state (unswollen-unstrained configuration).
V_s	Volume at swollen state (swollen-unstrained configuration).
W	Strain energy function/ elastic potential.
W_m	Strain energy per unit of volume in C_s associated with mechanical loading.
W_s	Strain energy per unit of volume in C_0 associated with isotropic swelling.
X	Strain amplification factor.
ΔG_1	*Gibbs free energy of dilution*.
ΔH_1	Heat of dilution.
ΔS	The entropy of deformation (defined per unit volume of the swollen rubber).
$\Delta S'$	Entropy of deformation of the swollen network (defined per unit volume of the original unswollen rubber).
ΔS_1	Entropy of dilution.
ΔS_o	Change of entropy associated with the initial isotropic swelling.
$\Delta S'_o$	Total entropy change passing from the *unstrained unswollen* state to the *strained swollen* state.
Λ_e	Deformation ratio relative to the length of the freely swollen undeformed gel.
Ω	Region.
χ	Flory-Huggins interaction parameter.
δQ	Heat absorbed by the system.
δW	Work done by the external forces.

$\dot{W}$	Rate change of strain energy.
ε	Strain.
$\hat{\mathbf{P}}$	1st Piola-Kirchhoff stress tensor relative to C_s (engineering stress with respect to swollen-unstrained configuration).
κ	Scalar internal variable.
λ	Stretch ratio.
$\mathscr{D}$	Internal dissipation per unit of volume in C_0.
μ	Shear modulus.
ν	Volume of the solvent molecules.
ϕ	Volume fraction of deswollen gels.
ϕ_e	Volume fraction of the polymer in the freely swollen gel.
ρ	Density in the unswollen state.
$\sqrt{N}$	Locking stretch of a molecule chain.
dA	change of Helmholtz free energy.
dS	Entropy change.
dU	Change in internal energy.
$\mathbf{F}_{\mathrm{m}}$	Mechanical part of the total deformation gradient.
$\mathbf{F}_{\mathrm{s}}$	Swelling part of the total deformation gradient.
$\mathbf{I}$	Identity tensor.
$\mathbf{P}$	1st Piola-Kirchhoff stress tensor relative to C_0 (engineering stress with respect to unswollen-unstrained configuration).
σ	Cauchy stress tensor.
υ_2	Volume fraction of rubber in the mixture of rubber and liquid.
υ_f	Volume fraction of hard phase.
υ_s	Effective volume fraction of the soft phase.
$\upsilon_{so,d}$	Initial soft phase fraction of the dry rubber.
$\upsilon_{so,m}$	Maximum initial soft phase fraction of the swollen rubber.
$\upsilon_{so,s}$	Initial soft phase fraction of the dry rubber.
υ_{ss}	Saturation value of υ_s.
$\mathbf{B}$	Left Cauchy-Green strain tensor.
$\mathbf{F}$	Deformation gradient tensor.
$\mathbf{X}$	Material point.
$\mathbf{x}$	Spatial point.
c_o	Concentration.
d	Damage function.
k	Boltzmann constant.
p	Pressure.
q	Lagrange multiplier.
AFM	Atomic Force Microscopies.
B0	diesel.
B100	biodiesel.
BR	Butadiene Rubber.
CCl_4	Carbon Tetrachloride.
CDM	Continuum Damage Mechanics.
CI	compression ignition.
CR	Polychloroprene Rubber.
EPDM	Ethylene Propylene Diene Monomer.
FAME	fatty acid methyl esters.
FKM	Fluorocarbon rubbers.

FTIR	Fourier Transform Infrared.
GCMS	Gas Chromatography Mass Spectroscopy.
HDPE	High Density Polyethylene.
HNBR	Hydrogenated Nitrile Butadiene Rubber.
KOH	potassium hydroxide.
NaOH	sodium hydroxide.
NBR	Nitrile Butadiene Rubber.
NMR	Nuclear Magnetic Resonance.
NR	Natural Rubber.
phr	per hundred rubber (parts).
PTFE	Polytetrafluroethylene.
PVC	Polyvinyl Chloride.
SBR	Styrene Butadiene Rubber.
SEM	Scanning Electron Microscope.
SR	Silicone Rubber.

CHAPTER 1

INTRODUCTION

1.1 Research background

Petroleum-based fuel is depleted significantly due to its limited reserve and increasing energy demand from various industries. The use of this type of fuel contributes significantly to the greenhouse effect resulting to environmental degradation and climate change. Thus, the energy insecurity and environmental awareness have motivated the world to develop biofuel as partial substitution of petroleum fuels (Jayed et al., 2011). The biofuel which is derived from renewable resources such as animal fat or vegetable oils (palm, rapeseed, sunflower, soya bean, coconut, etc.) are claimed to provide better energy efficiency and cleaner environment (Jayed et al., 2009, 2011). The potential wide use of palm biodiesel is highly beneficial for Malaysia and Indonesia who are currently the world largest and second largest palm oil producers. To this end, the governments have decided to utilize the palm biodiesel as energy source for industrial and transportation (Jayed et al., 2011).

However, the introduction of biofuel is placing additional demands on the material compatibility in the diesel engine system in long term operation. Indeed, in the case of rubber materials, changes in fuel composition often create many problems in rubber seals, pipes, gaskets and o-rings. The compatibility studies of several types of elastomers in diesel and palm biodiesel have been conducted (Trakarnpruk & Porntangjitlikit, 2008; Haseeb et al., 2010, 2011). In these works, only physical degradations related to the swelling, hardness and tensile strength of materials were studied. Moreover, there are collections of experimental studies on mechanical responses of polymeric gels in solvents (Sasaki, 2004; Hirotsu, 2004; Valentín et al., 2010). Nevertheless, it is to note that the works focusing on the effect of palm biodiesel diffusion on the macroscopic mechanical responses of the rubber components, in particular under cyclic and fatigue loading conditions, are less common (Chai et al., 2011).

In many engineering application, exposure of the rubber components to aggressive

liquids, such as organic solvent and oil, may lead to degradation of rubber. A major form of degradation in rubber exposed to liquid is swelling which can be described in terms of mass or volume change (Haseeb et al., 2010; Trakarnpruk & Porntangjitlikit, 2008). During the swelling process, liquids penetrate the polymer network and occupy positions among the polymer molecules. Consequently, the swelling of materials occurs when the macromolecules are forced apart. Furthermore, the mechanical stiffness decreases since the increase in chain separation will result in the reduction of secondary bonding (Callister, 2007). In addition to exposure to potentially hostile environments, a large majority of rubber components are simultaneously subjected to fluctuating multiaxial mechanical loading in service conditions. These two main forms of degradation: swelling due to diffusion of liquid into elastomer and fatigue due to long term cyclic loading need to be studied and understood for durability analysis of these components.

However, in the majority of studies involving fatigue of rubber, only the fatigue behavior in ambient (non-aggressive) environment is investigated. See for example the review of Mars and Fatemi (2002) and the work of Verron and Andriyana (2008); Le Cam et al. (2008); Andriyana et al. (2010); Brieu et al. (2010); Le Cam and Toussaint (2010); Le Cam et al. (2013) among others. Considerably fewer studies which explicitly deal with the fatigue failure analysis of rubber in aggressive environments are available (Zuyev et al., 1964; Magryta et al., 2006; Hanley, 2008; Abu-Abdeen, 2010). A number of static immersion tests investigating the diffusion of liquid in rubber have been extensively studied (see Treloar (1975) and references therein). However, investigations on more complex problems involving the swelling of polymer network in the presence of stresses (strains), in particular multiaxial stress state, are less common. The earliest work dealing with the problem dates back to the work of Flory and Rehner (1943a). Since this pioneering work, more recent accounts on coupling diffusion-deformation can be found in the literature (Soares, 2009; Hong et al., 2008; Baek & Srinivasa, 2004; Nah et al., 2010). It can be noted that these studies deal with the interaction between diffusion of liquid and large deformation without explicitly relating them to cyclic and fatigue response of rubber.

Under cyclic loading condition, it is well-known that dry rubber exhibits strong inelastic responses such as hysteresis and stress-softening. The hysteresis is characterized by different uploading and unloading paths and it can be related to either viscoelasticity

(Bergström & Boyce, 1998), viscoplasticity (Lion, 1996, 1997) or strain-induced crystallization (Trabelsi et al., 2003). The stress-softening corresponds to the significant decrease in stress between two successive cycles, in particular between the first and second uploading responses. This phenomenon was first observed by Bouasse and Carrière (1903) and intensively studied by Mullins (1948). It is often referred to as the Mullins effect. While the Mullins effect is well-known in both filled and unfilled crystallizing dry rubbers (Diani et al., 2009), it is recently demonstrated that the Mullins effect is also observed in swollen rubbers (Chai, Andriyana, et al., 2013; Andriyana et al., 2012). As reviewed by Diani et al. (2009), there are many efforts in proposing different theories to explain the stress-softening phenomenon in dry rubber. In spite of these efforts, there is no unanimous agreement on a microscopic explanation for the stress-softening up to this date (Diani et al., 2009; Marckmann et al., 2002). In contrast to dry rubbers, only few studies dealing with the observation of Mullins effect in swollen rubbers and gels are available (Webber et al., 2007; Lin et al., 2010; Andriyana et al., 2012; Chai, Andriyana, et al., 2013). Moreover, corresponding constitutive models are not available in the literature.

This research work can be regarded as a first step toward an integrated durability analysis of industrial rubber components exposed to aggressive environments, e.g. oil environment in biofuel systems, during their service. More precisely, the effect of swelling on the macroscopic mechanical response of elastomers under cyclic loading conditions is investigated. For this purpose, swelling tests on stress-free specimens and uniaxially-stressed specimens are conducted. An original compression device is developed to investigate the effect of static mechanical loading on the swelling of rubber and the effect of swelling on the mechanical response under cyclic loading. Furthermore, a simple phenomenological model is proposed to capture the Mullins effect observed in swollen rubbers under cyclic loading conditions. Other inelastic responses such as hysteresis and permanent set are not considered. The pseudo-elastic model of Ogden and Roxburgh (1999) and the two phases model of Mullins and Tobin (1957) and Qi and Boyce (2004) for Mullins effect are modified and extended in order to account for the degree of swelling. The dependence of Mullins effect on swelling is probed through a set of mechanical testing on swollen rubbers having different degrees of swelling. Two types of filled rubber

are considered: NBR and CR.

1.2 Objectives

The objectives of this research are summarized below:

1. To investigate the swelling of elastomers in solvent.
2. To investigate the effect of the presence of static mechanical loading on the swelling of elastomers.
3. To investigate the effect of swelling on the mechanical response of elastomers under cyclic loading condition.
4. To develop a continuum mechanical model for the Mullins effect in swollen elastomers.

1.3 Dissertation organization

This thesis is organized as follows. Chapter 1 provides an overview on the background, objectives and scope of the work. Chapter 2 provides a relevant literature review corresponding to the work. The reviews start from general reviews on elastomers and then focuses on the mechanical response of the elastomers under monotonic loading and cyclic loading. Subsequently the swelling of elastomers is reviewed. We also include the review on biodiesel and its effect on elastomers. Chapter 3 describes the research methodology. Experimental work including materials, specimen geometry, development of a specially-designed compression device and the types of test conducted in this study are detailed. The swelling of NBR and CR in diesel and biodiesel in the absence and in the presence of static uniaxial stress are investigated. Both dry and swollen specimens are subsequently subjected to cyclic compressive test to probe the mechanical response. In the modeling work, pseudo-elastic model and two-phase model are extended to model the Mullins effect observed in swollen elastomers. Chapter 4 presents the experimental results and discussion of the data obtained. The modeling results are compared with the experimental results in Chapter 5. Lastly, Chapter 6 summarizes the current research works and suggests directions for future research.

1.4 Scope of the works

This thesis focuses on the swelling behaviours and mechanical responses of two commercial elastomers: NBR and CR. The swelling behaviours of these elastomers are evaluated by immersing the initially dry elastomers in two different fluids: diesel (B0), biodiesel (B100) and different blends of these fuels (B25, B75). Two types of immersion are conducted: immersion test on stress-free specimens and on uniaxially-stressed specimens to study the effect of static mechanical loading on the swelling behaviour. The mechanical responses such as stress-softening due to the Mullins effect, hysteresis and stress relaxation are evaluated for both dry and swollen elastomers through two different mechanical tests: uniaxial cyclic compression test and multi-relaxation compression test. Special attention is given to the Mullins effect in swollen rubber. The experimental data is analysed and simulated using the extended pseudo-elastic model and the extended two-phase model.

CHAPTER 2

LITERATURE REVIEW

This chapter aims at providing some basic information for the entire thesis developed in the following chapters. The subjects discussed in the subsequent sections are:

1. General characteristics of elastomers.
2. A review on mechanical responses of dry elastomers with emphasis on the stress-softening under cyclic loading condition.
3. The swelling of elastomers.
4. A general review of biodiesel including the effect of it on different elastomers.

2.1 Generalities on elastomers

Elastomer is derived from the term "elastic polymer" and is commonly known as "rubber". Through polymerization, the monomer molecules can be arranged in an amorphous (rubbery), glassy or crystalline phase. For elastomers, they are typically categorized as amorphous (single-phase) polymers with random-coiled molecular arrangement. They exist above their T_g with T_g far below room temperature ($-71°$C for unvulcanized rubber and few degree higher for vulcanized rubber (Treloar, 1975)). As shown in Figure 2.1, an amorphous elastomer has a pronounced rubbery plateau above T_g which enables it to have considerable segmental motion. Therefore, elastomers are unique in being soft, exhibit high elasticity and the long chain polymer network is able to return to original configuration after the applied stress is removed. In addition, the polymer network chains which are connected with covalent cross-linkages allow the network to swell in a suitable solvent without being dissolved. In the following, the structures of the elastomer are discussed and different types of common industrial rubber materials are introduced.

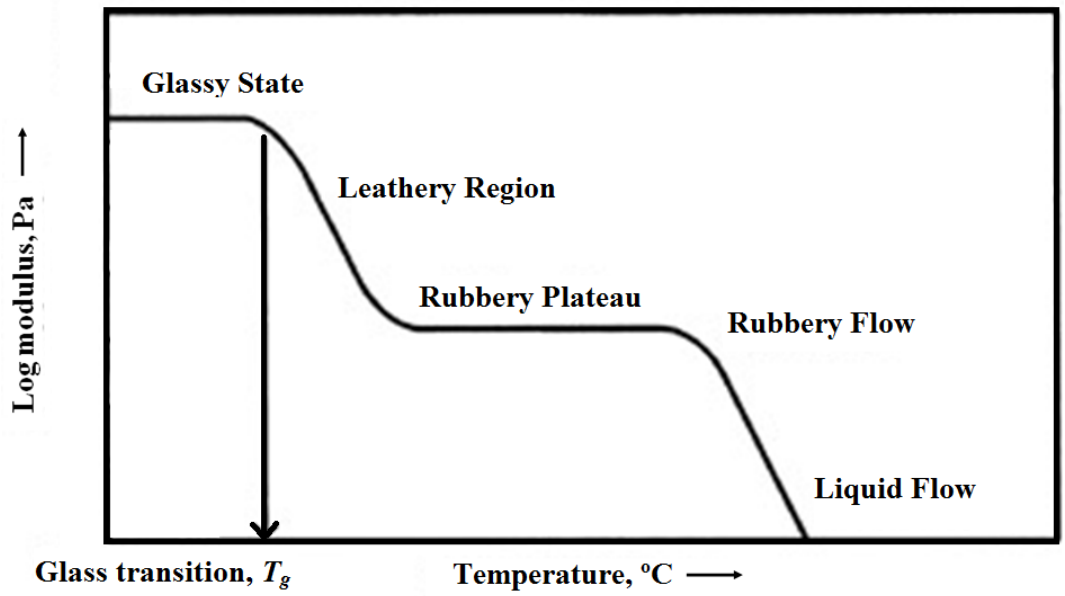

Figure 2.1: The modulus of elasticity versus temperature plot of an elastomer has a pronounced rubbery region (Shackelford, 2000).

2.1.1 Structures of elastomer

The polymer network is formed by linking the polymer chain through physical or chemical linkage. Physical linking is obtained through chains absorption onto the surface of filler, formation of small crystallites, coalescence of ionic groups or glassy sequences in block copolymers. In addition, long chain polymer networks tend to entangle with each other forming temporary physical crosslinks as shown in Figure 2.2. The existence of natural entanglement will increase the number of the effective crosslinks resulting to higher elastic modulus. However, this linkage is temporary and can easily be broke down by the presence of solvent or by increase of temperature. On the other hand, chemical cross-links are obtainable through co-polymerization or cross-linking method of sulphur cures, peroxide cures, and high-energy irradiations. The effect of swelling on the rubber properties will be discussed in the subsequent section in detail.

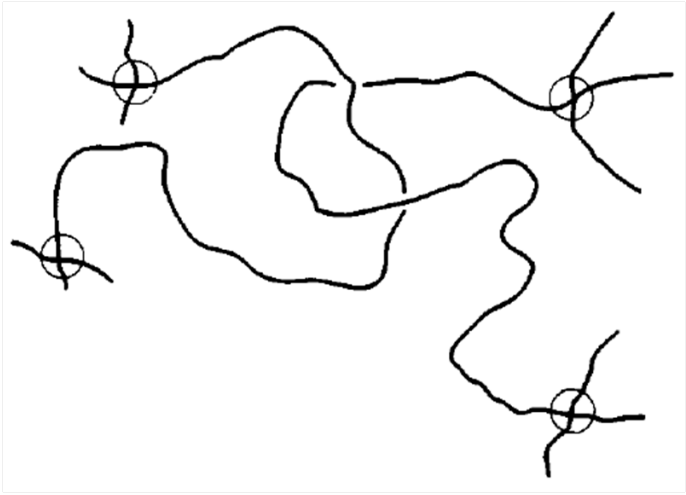

Figure 2.2: Sketch of a molecular entanglement (Gent, 1992).

Vulcanization Vulcanization is a chemical process to produce cross-linking in the rubber network as shown in Figure 2.3. Cross-linking generally restricts swelling in the polymer network (George et al., 1999). A crosslink may be a group of sulphur atoms in a short chain, a single sulphur atom, a carbon to carbon bond, a polyvalent organic radical, an ionic cluster, or a polyvalent metal ion. During vulcanization, the rubber mixed with vulcanizing agent, commonly sulphur or peroxide, is heated for the cross-linkage to take place in a mold under a certain molding pressure. Vulcanization is necessary to produce a cured rubber for industrial usage. It increases the retractile force in the rubber and reduces the amount of permanent deformation remaining after removal of the deforming force during the molding process (Mark et al., 2005).

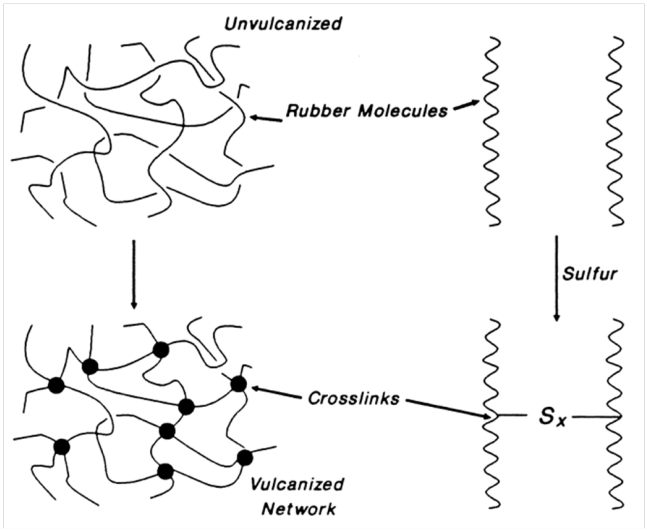

Figure 2.3: Network formation (Mark et al., 2005).

Reinforcement Reinforcement in the rubber refers to mixing the rubber compound with particulate fillers, especially carbon black. This simple action enhances the mechanical properties of crosslinked rubber systems. The addition of reinforcing fillers increases stiffness, modulus and deformation at break of the rubber materials as shown in Figure 2.4. The reinforcement in the rubber system also has the ability to alter the sorption and permeability of penetrants through it (Ramesan, 2005).

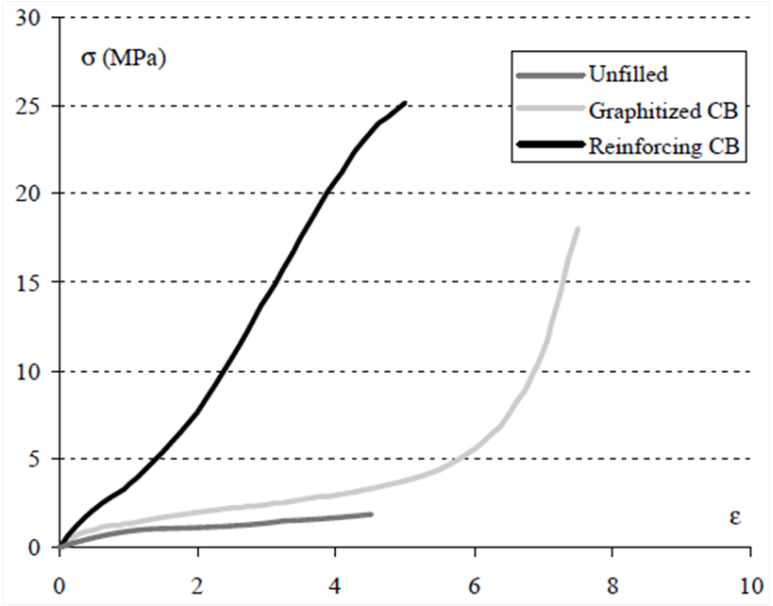

Figure 2.4: Stress-strain curve of unfilled, graphitized, and reinforcing carbon black samples (Mark et al., 2005).

2.1.2 Industrial rubber materials

Natural Rubber (NR) Natural Rubber (NR) is obtained from the latex of the *Hevea brasiliensis* tree. From this latex, the solid rubber is obtained by drying off the water or by adding appropriate preservatives (e.g. ammonia, formaldehde, sodium sulfide). Chemically, NR is a polymer of isoprene called *cis*-1,4-polyisoprene as shown in Figure 2.5. NR crystallizes when it is strained, which imparts outstanding green strength and tack, and gives NR high resistance to crack growth at severe deformation. Therefore, NR is an excellent choice for making tires because of its low hysteretic properties, high tensile strength, and good abrasion resistance.

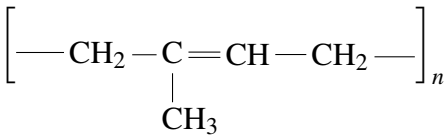

Figure 2.5: Molecular structure of NR.

Styrene Butadiene Rubber (SBR) Styrene Butadiene Rubber (SBR) is the most widely used synthetic general-purpose rubber. It is a copolymer of butadiene and contains about 23% styrene, with a T_g of approximately -55°C. Figure 2.6 shows the structural formula of SBR. SBR is synthesized via free-radical polymerization as an emulsion in water with a fatty acid or a rosin acid, or anionically in solution with butyl lithium. It is extensively used for tire treads because it offers wet skid and traction properties while retaining good abrasion resistance. However, they absorb organic solvents such as gasoline and oil and swell.

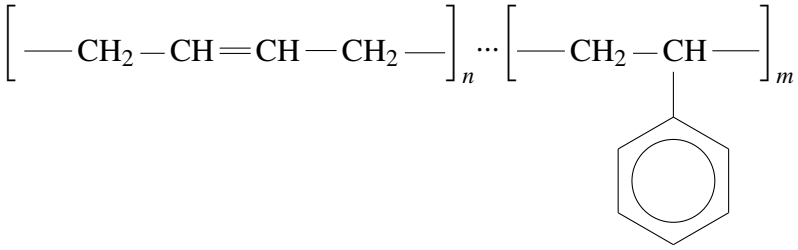

Figure 2.6: Molecular structure of SBR.

Nitrile Butadiene Rubber (NBR) Nitrile Butadiene Rubber (NBR) is an emulsion copolymer of acrylonitrile and butadiene with an acrylonitrile content varying from 18% to 50% (Gent, 1992). Figure 2.7 shows the structural formula of NBR. The polarity in NBR is introduced by copolymerization with the polar monomer, acrylonitrile, which provides excellent chemical, fuel and oil resistance. The higher the acrylonitrile content, the higher the T_g is. This reduces the resilience, swelling and gas permeability in NBR and thus improves the heat resistance and strength of NBR. NBR are more costly than ordinary rubbers. Therefore, usage of NBR is limited to special applications such as in oil rich environments as hydraulic hose and automotive engine components where oil resistance is essential.

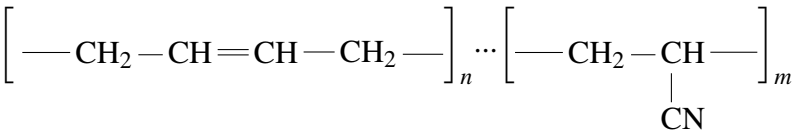

Figure 2.7: Molecular structure of NBR.

Polychloroprene Rubber (CR) Polychloroprene Rubber (CR) is produced from either acetylene or butadiene. Acetylene is reacted to form vinyl acetylene, which is then chlorinated to form chloroprene. Subsequently, this can be polymerized to polychloroprene. Polychloroprene contains approximately 85% trans-,10% cis-,and 5% vinyl-chloroprene. Polychloroprene tends to crystallize because of the C-Cl dipoles which enhance interchain interaction (Gent, 1992). Figure 2.8 shows the structural formulae of CR. In terms of performance, polychloroprene is inferior to NBR for oil resistance but it is still significantly better than NR, SBR, or Butadiene Rubber (BR). Like NBR it is also used extensively as oil seals, gaskets, hose linings, and automotive engine transmission belts where resistance to oil absorption is important.

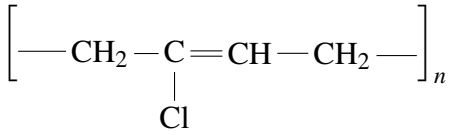

Figure 2.8: Molecular structure of CR.

Fluorocarbon rubbers (FKM) Fluorocarbon rubbers (FKM) are made in emulsion and are among the most inert and expensive elastomers. A typical one is made by copolymerizing the fluorinated analogs of ethylene and propylene. This rubber has a density of 1.85g/cm^3 and has a service temperature exceeding 250°C. It contains high fluorine content of up to 70% which makes it less affected by immersion in acids, bases, or aromatic solvents; but it is attacked by ketones and acetates. It is generally used in applications requiring excellent thermal stability and outstanding sealing capability such as o-rings, seals, and gaskets in aircraft application.

2.2 Mechanical response of elastomers

In this subsection, the general mechanical responses of dry elastomer under static and cyclic loading are discussed. The emphasis is laid on the discussion of Mullins effect

classically observed in elastomer.

2.2.1 Mechanical response under monotonic loading

2.2.1 (a) Non linear elasticity at large strain (hyperelasticity)

Hyperelasticity is a theoretical concept used to describe the characteristics of rubber-like materials which exhibit large deformation even at comparative low stress (Gent, 1992). Under static loading, the stress-strain curve for elastic deformation of a rubber component is shown in Figure 2.9. We observe here that the stress response is highly non-linear (i.e. Hooke's law does not apply), hence there is no constant value of the elastic modulus except in the region of small strains. The elastic modulus of elastomer (given by the slope of the curve) varies with increasing extension. For low strains (λ = 1.0 - 1.5), the elastic modulus is low because the forces needed to overcome secondary bonding and to uncoil the molecules is small. However, at high strains (λ > 3.5), the elastic modulus increases rapidly as a larger force is needed to stretch the primary covalent bonds along the molecular backbone.

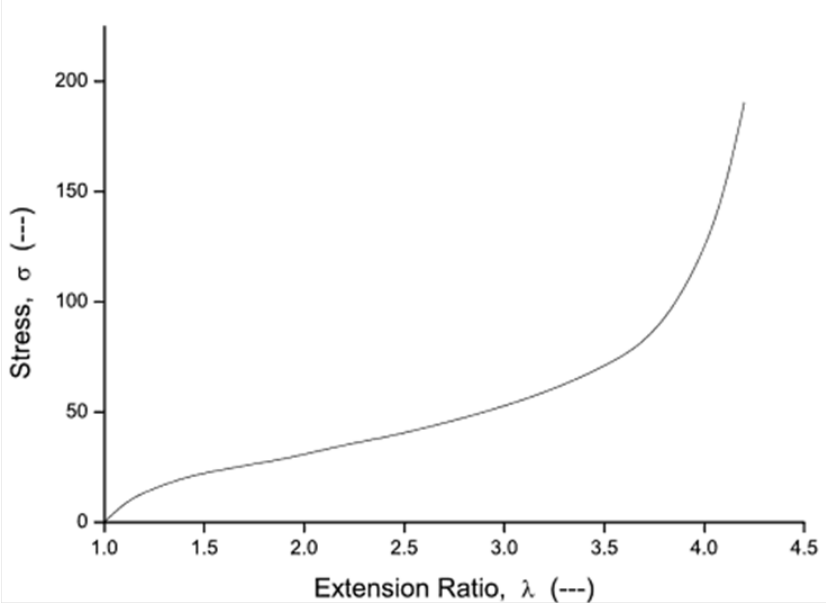

Figure 2.9: Extension of elastomer tensile specimen (Bauman, 2008).

Meyer and Ferri (1935) associated the changes in the conformations of a system of long-chain molecules in passing from the unstrained to the strained state with changes in the configurational entropy of the system where the internal energy remains unchanged. It is shown that the stretching force, for a given state of strain, should be proportional to

the absolute temperature, provided that the extension was sufficiently large (see Figure 2.10). Examining this observation with thermodynamic equation:

$$f = \left(\frac{\partial U}{\partial l}\right)_T - T\left(\frac{\partial S}{\partial l}\right)_T . \tag{2.1}$$

where U is the internal energy, T is the temperature and S is the entropy, it appears that elasticity of elastomer is essentially entropic in nature.

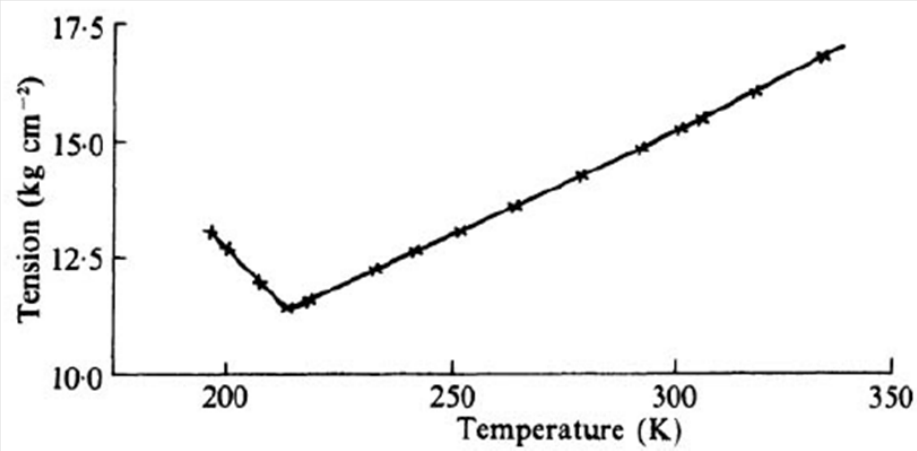

Figure 2.10: Extension of elastomer tensile specimen (Meyer & Ferri, 1935).

2.2.1 (b) Hyperelastic model

The hyperelasticity of different rubber materials can be described using different strain energy functions and the majority of these models are incorporated into commercial FEM software packages. Much work is done to improving the mathematical model with the following considerations (Mars, 2001):

(a) The model should be able to describe the stress responses to various strain loadings (uniaxial or biaxial tension/ compression and simple or pure shear) and not be limited to a single loading condition.

(b) It should involve minimal experimental work to determine the material parameters.

(c) It can be explained physically.

Most of the hyperelastic models have been reviewed. See for the reviews of Treloar (1975); Laraba-Abbes et al. (2003); Marckmann and Verron (2006). Laraba-Abbes et al. (2003) classified the hyperelastic models generally into two categories:

1. The molecular approach (Gaussian or non-Gaussian network theory) which is based on statistical thermodynamics considerations.

2. The phenomenological approach: purely continuum approach without directly considering the microstructure and molecular nature of the material.

Molecular approach (Gaussian network theory) The Gaussian network theory is based on the concept of a vulcanized rubber being an assembly of long-chain molecules which are connected with each other at a relatively small number of points to form an irregular three-dimensional network. The sequence of statistical treatment of the network is listed below:

1. Calculate the entropy of the whole assembly of chains as a function of the macroscopic state of strain in the sample.

2. Derive the free energy or work of deformation.

3. Derive the associated stresses from the work of deformation corresponding to a given state of strain.

From the first law of thermodynamics, the change in internal energy dU is given by:

$$\mathrm{d}U = \delta Q + \delta W. \tag{2.2}$$

where δQ is the heat absorbed by the system and δW is the work done by the external forces. In a *reversible* process, the second law defines the entropy change dS by the relation:

$$T\,\mathrm{d}S = \delta Q. \tag{2.3}$$

Therefore, for a reversible process, Equation (2.2) becomes

$$\mathrm{d}U = T\,\mathrm{d}S + \delta W. \tag{2.4}$$

The Helmholtz free energy A, which is the basic to derive the strain energy function, is defined by the relation:

$$A = U - TS. \tag{2.5}$$

For a change of the Helmholtz free energy dA taking place at constant temperature, the following expression is obtained:

$$\mathrm{d}A = \mathrm{d}U - T\mathrm{d}S. \tag{2.6}$$

Inserting Equation (2.4) into Equation (2.6), we have:

$$\mathrm{d}A = \delta W \text{ (constant temperature)}. \tag{2.7}$$

which implies that in a reversible isothermal process the change in Helmboltz free energy is equal to the work done by the applied forces on the system.

Next, consider a unit strained cube which has three equal edge lengths λ_1, λ_2 and λ_3. For an isochoric deformation, it can be shown that the change in entropy ΔS for the Gaussian network is given by:

$$\Delta S = -\frac{1}{2}Nk(\lambda_1^2 + \lambda_2^2 + \lambda_3^2 - 3). \tag{2.8}$$

where N is the number of chains per unit volume (degree of cross linking) while k is the Boltzmann constant. Taking the basic principles of the kinetic theory and assuming that there is no change of internal energy during deformation, from Equation (2.6) and (2.7):

$$W = -T\mathrm{d}S. \tag{2.9}$$

Therefore, Equation (2.8) becomes:

$$W = \frac{1}{2}G(\lambda_1^2 + \lambda_2^2 + \lambda_3^2 - 3). \tag{2.10}$$

where

$$G = NkT. \tag{2.11}$$

Molecular approach (Non-Gaussian network theory) Under relatively large strains, the chain response deviates from the Gaussian theory. Therefore, the non-Gaussian network theory which takes into account the finite extensibility of the chain should be considered. The simplest model of the non-Gaussian network theory is the three-chain model. This model is based on the assumption that the network of Gaussian chains can be replaced by three independent sets of chains parallel to the axes of a rectangular coordinate system. The four-chain model first developed by Flory and Rehner (1943b) based on the Gaussian theory is later modified by Treloar (1975) in the non-Gaussian theory. The model considers an elementary "cell" of the network consisting of four chains radiating outwards from a common junction point. Following these pioneers, Arruda and Boyce (1993) proposed a similar chain model but with a distribution of eight chains corresponding to the vertices of a cube inscribed in the unit sphere, namely the eight-chain model. This model presents better agreement with experimental data for uniaxial and equibiaxial extensions.

Phenomenological approach The stress-strain behavior of elastomer is often modeled using a pure mathematical approach which is also known as "phenomenological" approach. The strain energy function or elastic potential W, which corresponds to the change in the Helmholtz free energy of the material upon deformation, is used to derive the constitutive equations of elastomeric materials.

A dry elastomer is considered as a continuous body. The natural (undeformed and unstressed) configuration occupies the region Ω and contains a material point $\mathbf{X}$ with Cartesian coordinates X_j (j = 1,2,3). After deformation, the deformed body occupies the region Ω_d, and the point $\mathbf{X}$ is transformed to the spatial position $\mathbf{x}$ with coordinates x_i (i = 1,2,3). The deformation gradient tensor, $\mathbf{F}$ is given by:

$$\mathbf{F} = \mathrm{Grad}\,\mathbf{x} = \frac{\partial \mathbf{x}}{\partial \mathbf{X}}. \tag{2.12}$$

The left Cauchy-Green strain tensor is then simply given by $\mathbf{B} = \mathbf{F}\mathbf{F}^T$. The response of hyperelastic materials is characterized by the existence of a strain energy function W

which depends on **F**:

$$W = W(\mathbf{F}). \tag{2.13}$$

Considering the objectivity principle and isotropy, the form of W for incompressible elastomers can be expressed as a function of the two invariants of **B**, i.e.:

$$W = W(I_1, I_2). \tag{2.14}$$

where:

$$I_1 = \mathrm{tr}\,\mathbf{B} \qquad I_2 = \frac{1}{2}\left(I_1^2 - \mathrm{tr}\,\mathbf{B}^2\right). \tag{2.15}$$

Considering the second law of thermodynamics, it can be shown that the Cauchy stress tensor σ is given by (Holzapfel, 2000):

$$\sigma = q\mathbf{I} + 2\left[\frac{\partial W(I_1, I_2)}{\partial I_1} + I_1\frac{\partial W(I_1, I_2)}{\partial I_2}\right]\mathbf{B} - 2\frac{\partial W(I_1, I_2)}{\partial I_2}\mathbf{B}^2 \tag{2.16}$$

where q is an arbitrary scalar (Lagrange multiplier) due to the incompressibility assumption. It can be determined from the equilibrium equations and appropriate boundary conditions. As indicated in Equation (2.16), the stress response can be entirely determined once the form of strain energy denstiy W is specified. Table 2.1 summarizes some strain energy density functions for hyperelastic models (Mars, 2001).

2.2.2 Mechanical response under cyclic loading

When a dry rubber is subjected to cyclic loading, it exhibits strong inelastic responses such as hysteresis, stress relaxation, Mullins effect and permanent set as shown in Figure 2.11. This figure presents the stress-strain responses of a 50 phr carbon-black filled SBR subjected to a simple uniaxial tension and to a cyclic uniaxial tension with increasing maximum stretch every 5 cycles. In the following, the mechanical responses of hysteresis, stress relaxation, Mullins effect and permanent set are briefly discussed.

Table 2.1: Strain energy density functions for hyperelasticity (Mars, 2001).

Constitutive Model Name	Strain Energy Density Function
Linear Elastic	$W = G(\frac{v}{1-2v}(\varepsilon_1+\varepsilon_2+\varepsilon_3{}^2)+\varepsilon_1^2+\varepsilon_2^2+\varepsilon_3^2)$
Neo-Hookean	$W = \frac{G}{2}(I_1-3)$
Mooney-Rivlin	$W = C_{10}(I_1-3)+C_{01}(I_2-3)$
Generalized Polynomial	$W = \sum_{i=1}^{N}\sum_{j=1}^{N} C_{ij}(I_1-3)^i(I_2-3)^j$
Ogden	$W = \sum_{n=1}^{N}\frac{\mu_n}{\alpha_n}(\lambda_1^{\alpha_n}+\lambda_2^{\alpha_n}+\lambda_3^{\alpha_n}-3)$
Gent	$W = -\frac{G}{2}\lambda_m ln(1-\frac{I_1-3}{\lambda_m})$
Arruda-Boyce	$W = G(\frac{\frac{1}{2}(I_1-3)+\frac{1}{20\lambda_m^2}(I_1^2-9)+\frac{11}{1050\lambda_m^4}(I_1^3-27)}{+\frac{19}{7000\lambda_m^6}(I_1^4-81)+\frac{519}{673750\lambda_m^8}(I_1^5-243)+\cdots})$
Yeoh	$W = C_{10}(I_1-3)+C_{20}(I_1-3)^2+C_{30}(I_1-3)^3$
Note:	$I_1 = \lambda_1^2+\lambda_2^2+\lambda_3^2$, $I_2 = \lambda_1^{-2}+\lambda_2^{-2}+\lambda_3^{-2}$
	$I_3 = 1 = \lambda_1^2\lambda_2^2\lambda_3^2$ (Incompressibility constraint)

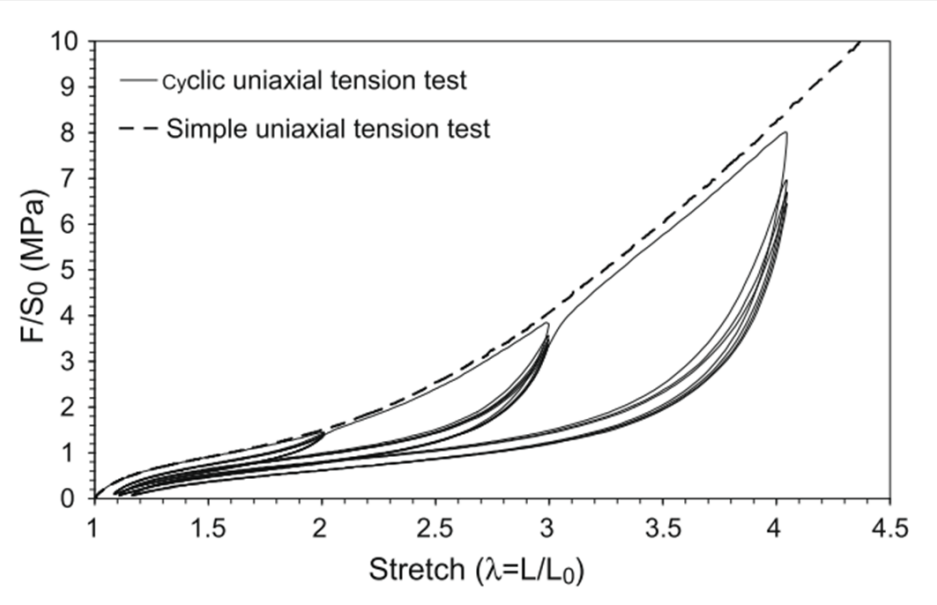

Figure 2.11: Stress-strain responses of a 50 phr carbon-black filled SBR subjected to a simple uniaxial tension and to a cyclic uniaxial tension with increasing maximum stretch every 5 cycles (Diani et al., 2009).

2.2.2 (a) Hysteresis

In Figure 2.12, the unloading curve is well below the uploading curve producing difference in stress, $\Delta\sigma$ which is called hysteresis. The hysteresis is defined as the amount

of energy dissipated during cyclic deformation and characterized by different uploading and unloading path. It can be related to either viscoelasticity (Bergström & Boyce, 1998), viscoplasticity (Lion, 1996, 1997) or strain-induced crystallization (Trabelsi et al., 2003) depending on the material. Hysteresis loss increases with an increase in strain rate, filler loading, resin loading (at high rates), crosslink density, and strain level but decreases with an increase in temperature, particle diameter of filler, and resin loading at high testing temperature (Kar & Bhowmick, 1997).

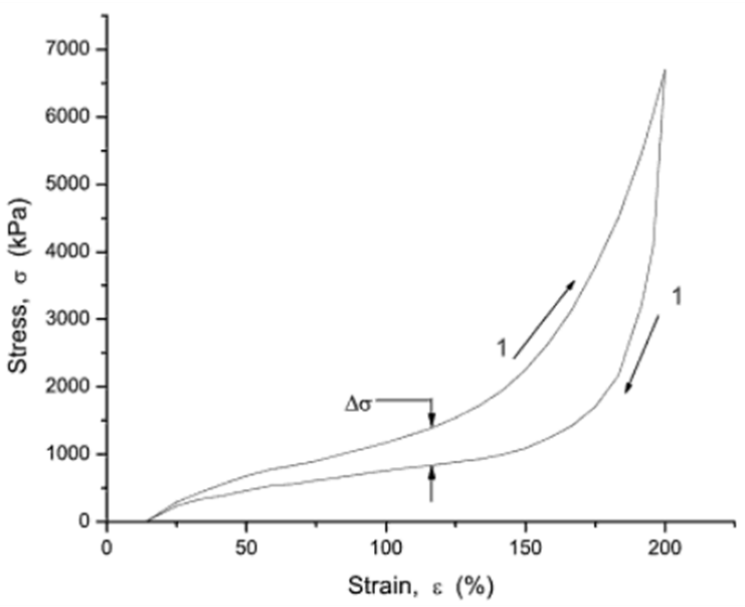

Figure 2.12: Extension and retraction of tensile specimen exhibiting hysteresis (Bauman, 2008).

2.2.2 (b) Viscoelasticity

Viscoelastic behavior is a time-dependent mechanical response and is usually characterized by creep, stress-relaxation, or dynamic mechanical measurements (Gent, 1992). Since our study focuses only on stress-relaxation, a detailed review is discussed next.

Stress Relaxation The ability of rubber to retain its elastic behavior after prolonged compressive stress makes it a favorite material for sealing applications. However, the decrease of stress due to viscoelastic behavior in rubber during compression under constant deformation may reduce the performance of the sealing components after use for a long period of time (Mostafa et al., 2009). Stress relaxation processes can be categorized into: a) Physical relaxation where the stress initially decreases rapidly and slows down with

time. It is caused by the reorientations of molecular network under constant strain when secondary bond between chains, fillers and chain and fillers break apart after disengagement and rearrangement of polymer chain. This internal arrangement of polymer network contributes to the decrease of stress under constant deformation with time. b) Chemical relaxation which is more prominent in a thin sheet of rubber exposed to chemical and is associated to scission of chemical bonds in the polymer chains or in the cross-linking system (Gent, 1992).

2.2.2 (c) Stress-softening (Mullins Effect)

The Mullins effect is the most noticeable effect happening in cyclic deformation. In Figure 2.13, three cyclic loadings with increasing strain are shown.

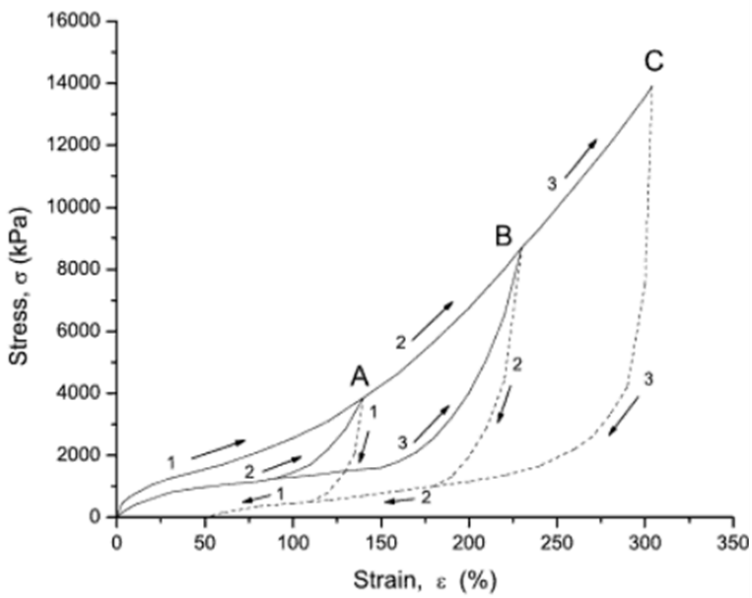

Figure 2.13: Mullins effect (Bauman, 2008).

Stress-softening is refers to the decrease of stress level in both the uploading and the unloading during the first couple of loading cycles. This phenomenon, first observed by Bouasse and Carrière (1903) then intensively studied by Mullins (1948), is often referred to as the Mullins effect. While the Mullins effect is well-known in both filled and unfilled crystallizing dry rubber (Mullins, 1948; Harwood et al., 1966b, 1966a), we have recently observed the Mullins effect in swollen rubber (Andriyana et al., 2012).

2.2.2 (d) Permanent set

When a carbon black filled rubber is loaded to a specific extension and unloaded, it does not return to its original stress-free configuration but exhibit residual strain or permanent set as shown in Figure 2.14. Permanent set occurs during unloading when the old unbroken chain segments try to bring the deformed block back to the original shape, but are resisted by the new bonds formed by the ruptured chain segments. It increases with the time in the deformed state and depends on the amount of carbon black in the rubber and on the maximum elongation of the rubber specimen prior to unloading (Dorfmann & Ogden, 2004). However, permanent set can be recovered when the recovery time is sufficient.

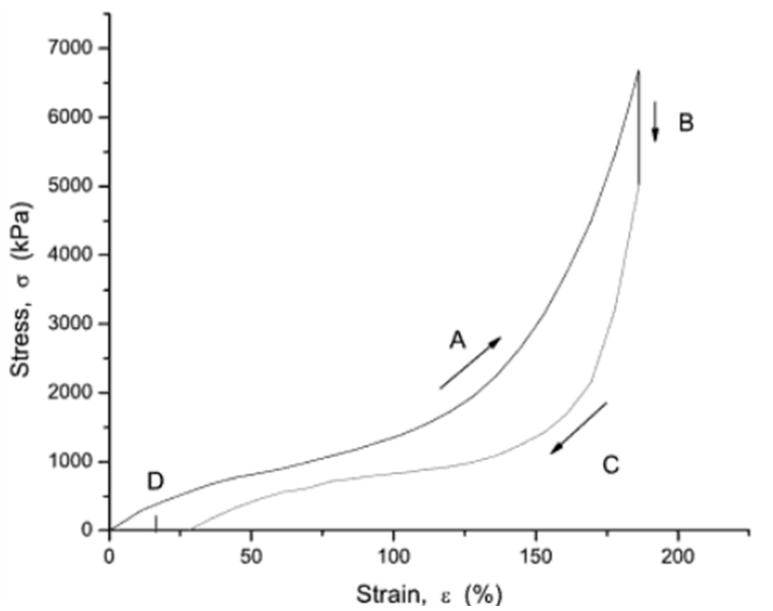

Figure 2.14: Permanent set (Bauman, 2008).

2.2.3 Review on the stress-softening in dry rubber

2.2.3 (a) Experimental observations

Diani et al. (2009) reviewed the Mullins effect and concluded several observations from the materials exhibiting softening effect as listed below:

- Most of the softening, which is characterized by a lower resulting stress for the same applied strain, appears after the first load.
- After a few cycles (values up to 10 are reported in the literature depending on the

material nature), the material responses coincide during the following cycles, aside from a fatigue effect.

- The softening appears for stretches lower or equal to the maximum stretch ever applied.
- When the extension exceeds the maximum extension previously applied, the material stress-strain response returns to the same path as the monotonous uniaxial tension test stress-strain response after a transition, which increases with the amount of strain.
- The softening increases progressively with the increasing maximum stretch.

Filler loading was found to contribute to the stress-softening phenomenon in several rubber compounds. However, it was also revealed that stress-softening is observed in unfilled rubber when it is stretched to a stress level similar to the filled rubber (Harwood et al., 1966b). These unfilled rubbers need to initially contain crystalites like thermoplastic rubbers or crystallize during the deformation process, such as NBR (Kakavas, 1996). Although we generally said stress softening occurred in both filled and unfilled rubber, no stress-softening is observed yet a unfilled non-crystallizing one. It is well documented by Mullins and Tobin (1957) that non-crystallizing pure gum breaks before any stress softening is exhibited. Among various observations, we noted here that stress softening can be recovered by heating or swelling as demonstrated by Harwood and Payne (1966) and Amin and Lion (2010).

2.2.3 (b) Modeling

As reviewed by Diani et al. (2009), there are many efforts in proposing different theories to explain the stress-softening phenomenon in dry rubber. Nevertheless, there is no unanimous microscopic explanation for the stress-softening exists up to this date (Diani et al., 2009; Marckmann et al., 2002). The first attempt to describe the Mullins effect is through a phenomenological approach. It was proposed by Mullins and Tobin (1957) that rubber initially contains both hard and soft phases. During deformation process, the hard phase transforms into the soft one. Their theory was successfully adopted in a number of works (Qi & Boyce, 2004; Beatty & Krishnaswamy, 2000; Huntley et al.,

1997, 1996; Wineman & Huntley, 1994). Simo (1987) adopted the concept of Continuum Damage Mechanics (CDM). The Mullins effect was considered as a damage phenomenon and was described by a scalar damage parameter. Thus, the material response is characterized by multiplying the classical hyperelastic strain energy with a reducing parameter representing damage level. Different forms of damage parameter were proposed in the literature (Chagnon et al., 2004; Ogden & Roxburgh, 1999; Miehe, 1995). In contrast to Chagnon et al. (2004) and Miehe (1995) who assumed that damage evolves when the applied level of deformation is undergone by the material for the first time, Ogden and Roxburgh (1999) proposed that damage stays zero when the material is subjected to a level of deformation never applied, and evolves in the range of submaximal deformation. The latter is known as the pseudo-elastic model.

The second approach is through physical interpretation (Marckmann et al., 2002; Klüppel & Schramm, 2000; Killian et al., 1994; Govindjee & Simo, 1991). Marckmann et al. (2002) reported the development of a new network alteration theory to describe the Mullins effect where they considered the Mullins effect as consequence of breakage of links inside the material, involving both filler-matrix and chain interaction links. This new alteration theory is implemented by modifying the eight-chains constitutive equation of Arruda and Boyce (1993). The accuracy of the resulting constitutive equation is demonstrated on cyclic uniaxial experiments for both natural rubbers and synthetic elastomers. Chagnon et al. (2006) later modified this network alteration theory to include the dangling chains effect in the network and proposed that the number of monomers involved in the elastic response of the material is a decreasing function of the maximum deformation.

2.3 Swelling of elastomers in solvent

The swelling phenomenon of rubber often refers to its solubility in organic media, e.g. hydrocarbon solvents (Treloar, 1975). Whenever rubbers are exposed to liquids, one main form of degradation experienced by the materials is swelling which can be described in terms of mass or volume change (Flory, 1953; Treloar, 1975). During the swelling, liquids penetrate the polymer network and occupy positions among the polymer molecules. Consequently, the macromolecules are forced apart resulting in swelling of material and in a decrease in its strength since the increase in chain separation leads

to the reduction of secondary bonding (Callister, 2007). This section discusses physical description of swelling, thermodynamics of swelling, elastic properties of swollen rubber, effect of deformation on swelling of the polymers and the coupled theory of the diffusion and large deformation in polymers.

2.3.1 Physical description

Diffusion of liquid into polymer network involves two physical processes:

1. The liquid molecules first occupy the polymer surface until reaching a concentration c_o through adsorption.

2. The liquid penetrates further into the depth of the polymer network until reaching equilibrium swelling by absorption.

Since the rate of swelling is diffusion-controlled, increasing the square of the elastomeric components thickness and the viscosity of the liquid will increase the resistance to swelling of an elastomeric component (Gent, 1992).

2.3.2 Thermodynamics of swelling

Equilibrium swelling in polymer is achieved when the change in free energy resulting from the transfer of a small quantity of liquid from the pure liquid phase to the mixed phase (polymer + liquid) is zero. Treloar (1975) introduced the *Gibbs free energy of dilution* ΔG_1 to define the change in the Gibbs free energy of the system due to the transfer of 1 mol of liquid from the liquid phase to a very large quantity of the mixed phase, given by:

$$\Delta G_1 = \Delta H_1 - T\Delta S_1. \tag{2.17}$$

where ΔH_1 is the heat of dilution which corresponds to the changes in the heat content H and ΔS_1 is the entropy of dilution corresponding to the changes in the entropy S of the system per mole of liquid transferred from the liquid phase to the mixed phase. The heat content H is defined by the relation:

$$H = U + pV. \tag{2.18}$$

where U is the internal energy and V is the volume. When p is the atmospheric pressure, the second term pV becomes negligible and the H is practically equivalent to U.

At constant pressure, the condition for equilibrium to be achieved with respect to the transfer of liquid is given by:

$$\Delta G_1 = 0. \tag{2.19}$$

To treat swelling problem statistically, it is essential to determine the increase of mixing entropy of polymer and liquid molecules. The entropy in the mixed state increases from greater probability compared with the unmixed state, and may be calculated based on the number of configurations available to the system at any given composition. Flory (1942) and Huggins (1942) proposed comparatively simple methods for the calculation of the configurational entropy of mixing. Flory (1942) assumed that the liquid and polymer molecules are arranged on a three-dimensional lattice of sites such that each site may be occupied either by a liquid molecule or by a single segment of a polymer chain. Using this consideration, the entropy of dilution ΔS_1 with respect to the liquid component is:

$$\Delta S_1 = -R\ln(1-\upsilon_2) + (1-1/x)\upsilon_2. \tag{2.20}$$

where the volume fraction of the fluid in the mixture υ_1 is written as $1-\upsilon_2$ and x is the segment of the polymer molecules.

For the free energy of dilution ΔG_1, Flory introduced the expression for the heat of dilution ΔH_1 on a semi-empirical basis using this formula:

$$\Delta H_1 = \alpha\upsilon_2^2. \tag{2.21}$$

and the Gibbs free energy of dilution ΔG_1:

$$\Delta G_1 = RT\left(\ln(1-\upsilon_2) + (1-1/x)\upsilon_2 + (\alpha/RT)\upsilon_2^2\right). \tag{2.22}$$

The alternative solution proposed by Huggins (1942) is similar to the one proposed by Flory, but includes a more precise analysis of the number of sites available to sub-

sequent polymer molecule segments after the third segment. His free energy of dilution contains an additional term in υ_2^2 but including the same form of heat of dilution as shown in Equation (2.21), and is expressed as:

$$\Delta G_1 = RT\ \left(\ln(1-\upsilon_2)+(1-1/x)\upsilon_2+\chi\upsilon_2^2\right). \tag{2.23}$$

where χ is a parameter which includes a component χ_o due to additional entropy from the purely energetic contribution ΔH_1, i.e.

$$\chi = \chi_o + \alpha/RT. \tag{2.24}$$

where χ_o and α are constants. Note here Equation (2.22) and (2.23) are identical at any given temperature. In the case where the number of segments in the polymer chain is sufficiently large, $1/x$ becomes very small thus these equations reduce to the form

$$\Delta G_1 = RT\left(\ln(1-v_2)+v_2+\chi v_2^2\right). \tag{2.25}$$

where χ is regarded as a constant. This form of equation is often referred to as the Flory-Huggins equation.

2.3.3 Elastic properties of swollen rubber

Treloar (1975) studied the effect of swelling on the mechanical properties of a cross-linked rubber by assuming that the unswollen sample is a unit cube which contains N chains per unit volume. The degree of swelling is defined in terms of the volume fraction υ_2 of the rubber in the mixture of rubber and liquid. Using this definition, and assuming swelling occurs isotropically, the corresponding linear stretch of the swollen sample is $\lambda_o = \upsilon_2^{-1/3}$

The parameter υ_2 is introduced to measure the state of swelling of the network, whether it is in equilibrium or not with respect to the absorption of liquid. The nature of the swelling agent, or if equilibrium swelling is achieved or not is not considered in the development of this theory.

Swelling corresponds to isotropic expansion of a network and thus will be accompa-

nied by a reduction in the entropy of a network which can be seen from Equation (2.8). Applying stress on the swollen network will further reduce the entropy due to the deformation of the already swollen network. Therefore the total reduction of entropy involved during the transformation of the initial *unswollen unstrained* state to the final *strained swollen* can be described by two separate terms. One due to the swelling and one due to the mechanical loading.

The entropy of deformation $\Delta S'$ of the swollen network (defined per unit volume of the original unswollen rubber) is given by:

$$\Delta S' = \Delta S'_o - \Delta S_o. \tag{2.26}$$

where $\Delta S'_o$ is the total entropy change passing from the *unstrained unswollen* state to the *strained swollen* state. For a Gaussian network (Treloar, 1975), it is given by:

$$\Delta S'_o = -\frac{1}{2}Nk(l_1^2 + l_2^2 + l_3^2 - 3). \tag{2.27}$$

where l_1, l_2, and l_3 are the lengths of the edges of the original unit cube, i.e. the principal extension ratios referred to the unswollen state. The change of entropy associated with the initial isotropic swelling ΔS_o is given by:

$$\Delta S_o = -\frac{1}{2}Nk(3\lambda_o^2 - 3) = -\frac{1}{2}Nk(3\upsilon_2^{-\frac{2}{3}} - 3). \tag{2.28}$$

Inserting Equations (2.27) and (2.28) into Equation (2.26), we obtain the difference between these two quantities:

$$\Delta S' = -\frac{1}{2}Nk(l_1^2 + l_2^2 + l_3^2 - 3\upsilon_2^{-\frac{2}{3}}). \tag{2.29}$$

The extension ratios of λ_1, λ_2, and λ_3 can be defined with reference to the *unstrained swollen* state such that $l_1 = \lambda_1\lambda_0 = \lambda_1\upsilon_2^{-\frac{2}{3}}$, etc. Thus Equation (2.29) becomes:

$$\Delta S' = -\frac{1}{2}Nk\upsilon_2^{-\frac{2}{3}}(\lambda_1^2 + \lambda_2^2 + \lambda_3^2 - 3). \tag{2.30}$$

The entropy of deformation ΔS (defined per unit volume of the swollen rubber) is given by:

$$\Delta S = \upsilon_2 \Delta S' = -\frac{1}{2} N k \upsilon_2^{\frac{1}{3}} (\lambda_1^2 + \lambda_2^2 + \lambda_3^2 - 3). \tag{2.31}$$

The corresponding strain energy function for the swollen rubber thus becomes:

$$W = -T\Delta S = \frac{1}{2} N k T \upsilon_2^{\frac{1}{3}} (\lambda_1^2 + \lambda_2^2 + \lambda_3^2 - 3). \tag{2.32}$$

Equation (2.32) describes the properties of the swollen rubber in terms of the extension ratios measured in the swollen state and the volume fraction of rubber υ_2. Noted here N is the number of chains per unit volume of the unswollen rubber. Comparing the results of swollen rubber expressed in Equation (2.32) with the corresponding expression of the unswollen rubber in Equation (2.10), it is seen that the dependence of the stored energy on strain are the same in both cases, except the value of the shear modulus. Thus, we can write:

$$G' = G\upsilon_2^{\frac{1}{3}} = \rho RT / M_c \upsilon_2^{\frac{1}{3}}. \tag{2.33}$$

where G is the modulus in the unswollen state while G' is the modulus in the swollen state and ρ is the density in the unswollen state. This result implies that the only effect of swelling is to reduce the modulus in inverse proportion to the cube root of the swelling ratio, without changing the form of the stress-strain relations. Moreover, as stated by Treloar (1975) that from a physical standpoint, swelling is a purely physical mixing or interdiffusion process in which there is no chemical attraction between the rubber and liquid molecules.

2.3.4 Effect of deformation on swelling

The effect of deformation in terms of applied strain or stress on the swelling of a polymer network has long been recognized and discussed by Flory and Rehner (1943a). The theory was further developed by Treloar (1975, 1950) and he discussed it for general types of homogeneous strain. Equations for uniaxial extension, bi-axial extension and uniaxial compression strains were developed. He concluded from the experimental data obtained from vulcanized natural rubber specimens swollen in benzene and heptane that

the effect of strain on the equilibrium swelling is satisfactorily predicted for the statistical theory under the three entirely different types of strains. Although swelling under unidirectional compression is the least accurate due to the measuring process that required drying and weighing and lengthy immersion duration, however it is observed that swelling is increasing under tensile strain and decreasing with compressive strain.

Horkay and Zrinyi (1988) compared the effect of deformation and diluent activity on the equilibrium concentration of poly(vinyl acetate) networks swollen with toluene. The swollen gels were deswollen by two methods: gels were subjected to uniaxial compression at fixed activity of the diluent and the activity of the diluent around the free swollen gel specimens was lowered by dissolving a polymer in the surrounding media. They compared the experimental volume fraction data obtained from uniaxial deformed gels equilibrium swollen in pure diluent with calculated values using Equation (2.34).

$$\phi = \phi_e \Lambda_e^{-4/9} \tag{2.34}$$

where ϕ is the volume fraction of deswollen gels, ϕ_e is the volume fraction of the polymer in the freely swollen gel and Λ_e is the deformation ratio relative to the length of the freely swollen undeformed gel. It is found that there is a good agreement between measured and calculated volume fraction data in the cases of natural rubber samples swollen by benzene and heptane conducted by Treloar (1950) and poly(vinyl acetate) networks swollen by toluene in their study. They evaluated the relationships between the swelling pressure, elastic modulus, deformation ratio and polymer concentration and validated this relationship with experimental results.

Fukumori et al. (1990) utilized real time pulse Nuclear Magnetic Resonance (NMR) to evaluate the initial swelling rate of the filled and unfilled NBR under tensile deformation swollen in non polar solvent, e.g. Carbon Tetrachloride (CCl_4) as shown in Figure 2.15. The specimen studied is a ring specimen with outside diameter = 22mm and inner diameter=19mm. The rubber contents filler concentration of 0, 20, 40 and 60 phr. The swelling ratio of the rubber matrix at equilibrium is evaluated with volume swelling measurements. They found that the initial swelling rate and the swelling ratio of the rubber matrix at equilibrium increased with the increase of the stretch ratio. The molecular

mobility of the swollen rubber is also enhanced with the increase of the tensile strain. It was found that the presence of reinforcing filler in NBR reduced the initial swelling rate because of transient spatial effect caused by some oriented structures induced by tensile deformation. However, the presence of reinforcing fillers in the swollen rubbers under tensile strain has a strain amplification effect proportionally to the filler concentration, which resulted in an increase of the average local strain in the rubber matrix and enhanced the swelling ratio relative to the unfilled system.

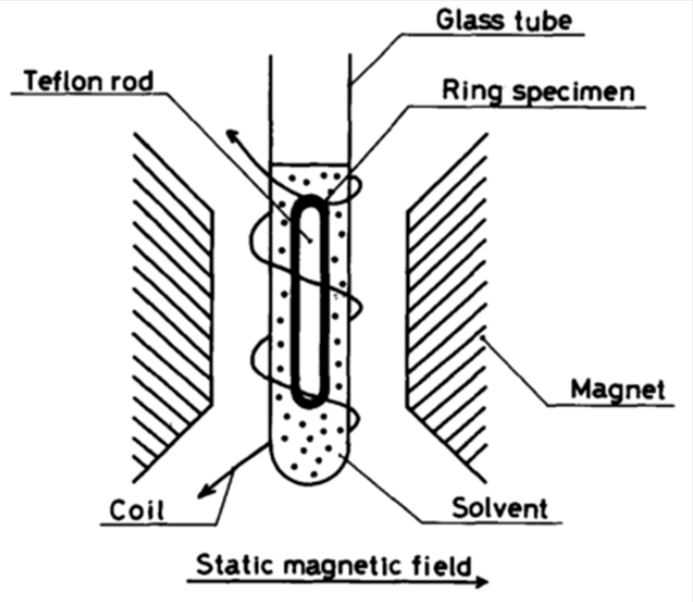

Figure 2.15: Schematic illustration of the real-time NMR, measurement of a stretched rubber specimen immersed in a solvent (Fukumori et al., 1990).

A free oscillation technique has been adopted to study the effect of swelling on the dynamic storage and loss moduli of carbon black filled and unfilled natural rubber materials on a range of tensile pre-strains (Busfield et al., 2000). It is observed that the dynamic storage and loss moduli are independent of the pre-strain at small pre-strains. Both the storage and the loss moduli increase with pre-strains. Swelling the materials in liquids with a wide range of viscosity produces a relatively large decreases in both the storage and the loss moduli. The authors attributed the dynamic behaviour of the swollen filled rubbers to the combined effects of a reduction in the modulus of the rubber matrix (caused by the swelling action) and a reduction in the effective volume fraction of the filler. However, the effect of the viscosity of the swelling liquid on these dynamic

behaviours are insignificant. They concluded that the swelling liquids might be affecting the filler-filler or the filler-rubber interaction.

Botros and Sayed (2001) investigated the effect of compressive strain on the swelling behavior of different blend compositions of NR/Ethylene Propylene Diene Monomer (EPDM) swollen in motor oil. The compression recovery of all blend ratios investigated had positive values at low applied compression strain (3%). However, at high compressive strain (18% and 35%), the compression recovery had negative values. The lowest weight uptake of motor oil was shown by the EPDM vulcanizate, whereas the 25/75 NR/EPDM blend showed the highest compression recovery.

Most recently, Nah et al. (2011) investigated the swelling of bent natural rubber sheet in dodecane. Following Treloar's theory, they proposed that when rubber sheets are bent, they are expected to swell more on the tension side and less on the compression side. Moreover, when the bending constraint is removed, recovery toward the initial flat state is expected to be only partial at first and then followed by a slow further recovery. They found that the measured "set" following release from bending is agreed with simple swelling theory. The time dependence of later recovery is shown to be in agreement with the rate of diffusion of the swelling liquid. It is concluded that internal migration of compatible liquids will cause temporary delays in deformation kinetics and make a significant contribution to energy losses. Also, the bending experiment itself appears to provide a simple and generally applicable method for determining the internal diffusion coefficients of absorbed liquids.

2.3.5 Modeling of coupling between deformation and swelling

Several theories have been developed to account for the coupled diffusion and large deformation in polymers (Gandhi, 1989; Inci et al., 2001; Baek & Srinivasa, 2004; Ramtani, 2006; Hong et al., 2008; Deng & Pence, 2009; Soares, 2009; Hong et al., 2009; Deng & Pence, 2010; Joshi & Muliana, 2010; Cai et al., 2010; Nah et al., 2011; Johlitz & Lion, 2012). Gandhi (1989) considered the problem of a cylindrical specimen of a nonlinearly elastic solid and an ideal fluid medium subjected to combined finite axial extension and torsion. He discussed the general problem for the finite deformation of the swollen cylinder in the context of Mixture Theory and presented the computational results

for the variation of the radial and tangential stretch ratios and the distribution of the fluid in the swollen deformed state. He found that the swollen volume of a cylinder reduces with twisting when the axial extension ratio is held constant. Simulation agreed well with experimental results.

Baek and Srinivasa (2004) modeled slow diffusion of a fluid into a swelling solid undergoing large deformation and predicted the stress in the solid as well as the diffusion rates. The approach is based on the balance laws of a single continuum with mass diffusion, and overcame the difficulties inherent in the theory of mixtures in specifying boundary conditions. The authors derived a "natural" boundary condition based on the continuity of the chemical potential by the use of a variational approach, based on maximizing the rate of dissipation. They found that the differential equations resulting from the use of mixture theory can be recast into a form that is identical to the equations obtained in the absence of the initial effect and they successfully solved the boundary value problem of the steady flow of a solvent through a gum rubber membrane.

Hong et al. (2008) formulated a theory of the coupled mass transport and large deformation. The free energy of the gel results from two molecular processes: stretching the network and mixing the network with the small molecules. They assumed that both the small molecules and the long polymers are incompressible, a constraint enforced by using a Lagrange multiplier, which coincides with the osmosis pressure or the swelling stress. The gel can undergo large deformation of two modes. The first mode results from the fast process of local rearrangement of molecules, allowing the gel to change shape but not volume. The second mode results from the slow process of long-range migration of the small molecules, allowing the gel to change both shape and volume. They also assumed that the local rearrangement is instantaneous, and model the long-range migration by assuming that the small molecules diffuse inside the gel. The theory is illustrated with a layer of a gel constrained in its plane and subject to a weight in the normal direction.

Soares (2009) described a single-constituent constitutive model for diffusion of fluids in nonlinear elastic solids, originally presented by Baek and Srinivasa (2004) and based on a variational method and on the assumption of continuity of chemical potential across the solid-fluid interface. The balance laws for a single continuum with mass diffusion are cast in spherical coordinates, and suitable boundary conditions are posed to

describe the radial diffusion of fluid through an elastic spherical shell with finite thickness. They modeled its inner surface adjacent to a rigid wall, either impermeable or permeable, while the outside surface is in contact with the fluid that swells the solid, diffuses through it, and exerts a hydrostatic pressure on its surface.

Hong et al. (2009) investigated the effect of mechanical load and geometric constraint on the inhomogeneous swelling of a polymeric gel. When the network, solvent, and mechanical load equilibrate, inside the gel the chemical potential of the solvent is homogeneous, but the concentration of the solvent and the deformation of the network can be inhomogeneous. They used the chemical potential of the solvent and the deformation gradient of the network as the independent variables of the free-energy function, and concluded that the boundary value problem of the swollen gel is equivalent to that of a hyperelastic solid. They implemented the approach in a finite-element package, ABAQUS, and analyzed examples of swelling-induced deformation, contact, and bifurcation.

Deng and Pence (2009) considered the connection between diffusion and large deformation in polymer and the broader hyperelastic theory that treats the effect of mechanical loading in deforming the swollen polymer network. They pointed out that fluid loss (swelling reduction) or fluid gain (swelling increase) occurred when there is a change in mechanical loading. In such cases the gel reestablishes equilibrium only when the relative motion of the liquid through the polymer has ceased and processes have come to rest. Such processes are inherently dissipative. Their study focused on reestablished equilibria depending on mechanical load. They considered that the amount of available fluid is limited for quasi-static loadings that give fluid gain. It is predicted that maximum fluid gain in the gel system will be reached by increasing the quasi-static loading. The gel system transitions from a saturated state to an unsaturated state. This quasi-static transition is considered in the context of homogeneous deformation where an appropriate hyperelastic analysis shows that the equilibrium mechanical response is inherently stiffer after loss of saturation. They concluded from the study of inhomogeneous deformation of an everted tube subject to an axial load and found that loss of saturation leads to an inherently stiffer quasi-static response.

In addition, Deng and Pence (2010) discussed a continuum model for the absorption and redistribution of fluid in swollen elastomers due to mechanical loading for both

saturated and unsaturated systems. They considered the effect of various boundary displacement and traction in the problem of radial displacement combined with azimuthal shear for an annular cylinder consisting of a fluid infused hyperelastic medium. The fluid distribution is monitored through a numerical model. It is found that certain boundary tractions generate overall volume increase after free swelling and the overall mechanical response after loss of saturation is stiffer than the saturated system.

Cai et al. (2010) suggested that when an elastomer imbibes a solvent and swells, a force is generated if the elastomer is constrained by a hard material. The magnitude of the force depends on the geometry of the constraint, as well as on the chemistry of the elastomer and solvent. They modeled an elastomer crosslinked on the exterior surface of a metallic tubing. The elastomer then imbibes a solvent and swells. After the swollen elastomer touches the wall of the borehole, a significant amount of time is needed for the solvent in the elastomer to redistribute, building up the sealing pressure to the state of equilibrium. They calculated the sealing pressure and the sealing time from the geometric parameters (i.e., the thickness of the elastomer and the radii of the tubing and borehole), the number of monomers along each polymer chain of the elastomer, and the affinity between the elastomer and the solvent.

2.4 Biodiesel

2.4.1 What is biodiesel?

Biodiesel fuels are methyl ester based oxygenates derived from a wide range of renewable natural sources such as animal fats (beef tallow), vegetable oils (soybean oil, cottonseed oil, canola oil), and recycled cooking grease or oils (e.g., yellow grease) (Trakarnpruk & Porntangjitlikit, 2008). It is a diesel replacement fuel in a compression ignition (CI) engine.

The biodiesel is manufactured through transesterification which can be illustrated in Figure 2.16. The transesterification process converts oils and fats into chemicals called long-chain mono alkyl esters, or biodiesel. These chemicals are better known as fatty acid methyl esters (FAME) (Laboratory, 2009). From the schematic diagram, it is easy to explain that the oil/fat are reacted with a short-chain alcohol (i.e. methanol) with the aid of a catalyst (i.e. sodium hydroxide (NaOH) or potassium hydroxide (KOH)) to produce

biodiesel and glycerin. Glycerin is a sugar alcohol that is formed as by-product in the manufacturing process of biodiesel.

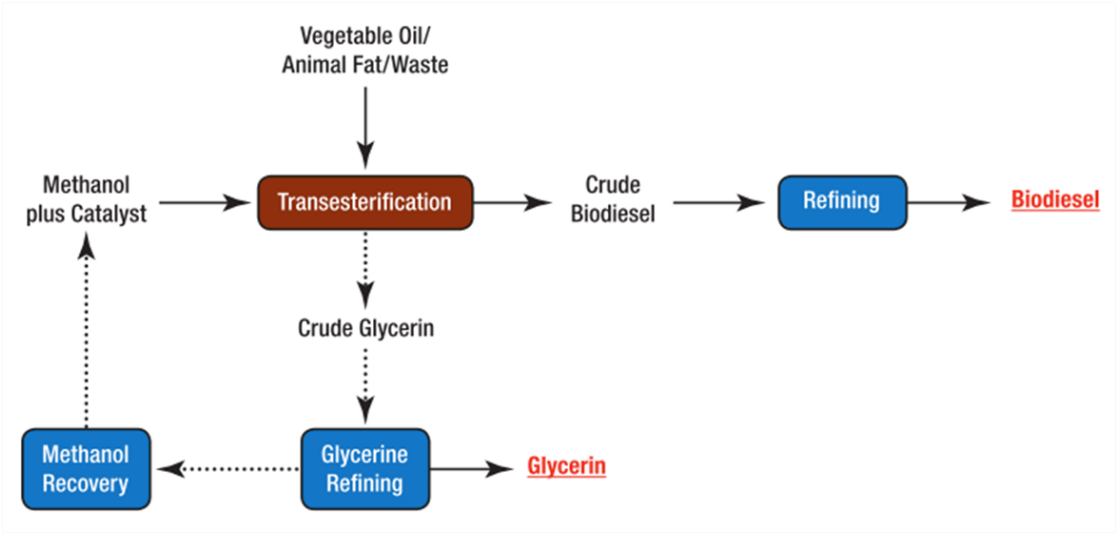

Figure 2.16: Basic transesterification process (Laboratory, 2009).

Biodiesel has been proven to be environmentally friendly and to provide properties similar to that of conventional fuel. However, the biodiesel has a different composition than conventional diesel. Indeed, while biodiesel consists of a mixture of fatty acid ester, conventional fuel consists of a mixture of hydrocarbon (Haseeb et al., 2010). This change of composition leads to difficulties in terms of material compatibility especially in industrial applications involving elastomeric materials.

2.4.2 Effect of biodiesel on elastomers

Compatibility studies of several types of elastomers in diesel and palm biodiesel have been conducted (Trakarnpruk & Porntangjitlikit, 2008; Haseeb et al., 2010, 2011). However in these works, only physical degradation related to the swelling, hardness and tensile strength of materials was studied.

The material compatibility has been studied by Trakarnpruk and Porntangjitlikit (2008) who evaluated six types of elastomer (NBR, Hydrogenated Nitrile Butadiene Rubber (HNBR), NBR/ Polyvinyl Chloride (PVC), acrylic rubber, co-polymer Fluorocarbon rubbers (FKM), and terpolymer FKM) in B10 (10% palm biodiesel in diesel) after immersion of 22, 670, and 1008 h at 100°C. They found that NBR, NBR/PVC and acrylic rubber were affected more than other elastomers due to the absorption and dissolving of

biodiesel by rubber in these samples and concluded that Co-polymer FKM and terpolymer FKM are more resistant in B10 biodiesel environment.

Haseeb et al. (2010) evaluated the degradation behaviour of NBR, CR, and fluoro-viton A in B0 (diesel), B10, B100 (palm biodiesel) after 500 h immersion at (25 °C) room temperature and 50 °C. The mass and volume change, hardness, tensile strength and elongation were investigated. The exposed elastomer surface was studied by Scanning Electron Microscope (SEM). Fourier Transform Infrared (FTIR) spectroscopy was conducted to identify the chemical and structural changes. It is found that the physical degradation was higher for both CR and NBR while fluoro-viton has good resistance in biodiesel.

In addition, Haseeb et al. (2011) investigated the physical property degradation of EPDM, Silicone Rubber (SR), Polytetrafluroethylene (PTFE) CR, and NBR upon exposure to diesel and palm biodiesel. Static immersion tests in B0 (diesel), B10 (10% biodiesel in diesel), B20, B50 and B100 (biodiesel) were carried out at (25 °C) room temperature for 1000 h. They measured changes in weight and volume, hardness and tensile strength at every 250 h of immersion time. Compositional changes in biodiesel due to exposure of different elastomers were investigated by Gas Chromatography Mass Spectroscopy (GCMS). They concluded that the overall sequence of compatible elastomers in palm biodiesel is found to be PTFE > SR > NBR > EPDM > CR.

Other than palm biodiesel, compatibility studies of rubber components in other types of biodiesel are investigated (Maru et al., 2009; Berlanga-Labari et al., 2011). Maru et al. (2009) analyzed the interaction between three fuels (petroleum diesel and two types of biofuel: soybean and sunflower) and High Density Polyethylene (HDPE) after static immersion of 75 and 125 days under constant temperature of 60 °C. A wide range of characterization methods were used to evaluate the changes in both rubber materials and the fuels: including weight change measurement, optical, scanning electron and Atomic Force Microscopies (AFM), Raman and FTIR and differential scanning calorimetry. They detected the maximum weight gain by fluid absorption in the polyethylene immersed in petroleum diesel by the spectroscopic techniques. However, no significant differences in the HDPE surface morphology after immersion in these fuel medias. They concluded that ageing took place only in biodiesels, but this phenomenon did not cause degradation or

corrosion of HDPE, since petroleum diesel did not age but exerted the most significant material degradation.

On the other hand, Berlanga-Labari et al. (2011) also evaluated the compatibility of the same material (HDPE) but in E5 (5% v/v bioethanol, 95% v/v gasoline) and E10 (10% v/v bioethanol, 90% v/v gasoline) after static immersion of 2000 h at 45 °C. Different mechanical and physical-chemical properties of HDPE have been assessed before and after the execution of these tests. Additional information about biofuels-HDPE interaction has been obtained by infrared spectroscopy and solubility tests. Although they observed a slight variation of mechanical properties in HDPE, both studies concluded that no defects on the chemical structure and physical properties of this polymer have been detected.

Moreover, there are collections of experimental studies on mechanical responses of polymeric gels in solvents (Sasaki, 2004; Hirotsu, 2004; Valentín et al., 2010). Nevertheless, it is to note that the works focusing on the effect of palm biodiesel diffusion on the macroscopic mechanical responses of the rubber components, in particular under cyclic and fatigue loading conditions, are less common.

CHAPTER 3

RESEARCH METHODOLOGY

The literature review has shown that very limited work has been done on studying the mechanical responses, i.e. hysteresis, stress-softening, etc. of swollen rubber under cyclic loading conditions. The present research is therefore carried out to establish a database of swollen rubbers, namely NBR and CR using mechanical tests. The mechanical tests involved are compressive cyclic test and compressive multiple relaxation test.

Experimental procedures to prepare swollen rubbers, including the design of the uniaxial compression test specimen, the development of an original compression device and details of the immersion test are described in this chapter. The swelling behaviours for both stress-free and uniaxially-stressed rubber specimens are investigated. Subsequently, the following mechanical responses are investigated: stress-softening and hysteresis from compressive cyclic test and viscoelasticity from compressive multiple relaxation test.

Next, the stress-softening in swollen rubbers is modeled using an extended pseudo-elastic model and an extended two-phase model. These are conducted as a first attempt towards understanding and modeling of the stress-softening phenomenon in swollen rubbers.

The overall research work is described using flow chart in Figure 3.1.

Remark 1 *It is to note that large parts of the content in this chapter and the following chapters have been published (Chai et al., 2011; Andriyana et al., 2012; Chai, Andriyana, et al., 2013; Chai, Verron, et al., 2013). The rest of the thesis is written based on the inspiration from these papers, aiming at producing a well-organized and easy to understand research output.*

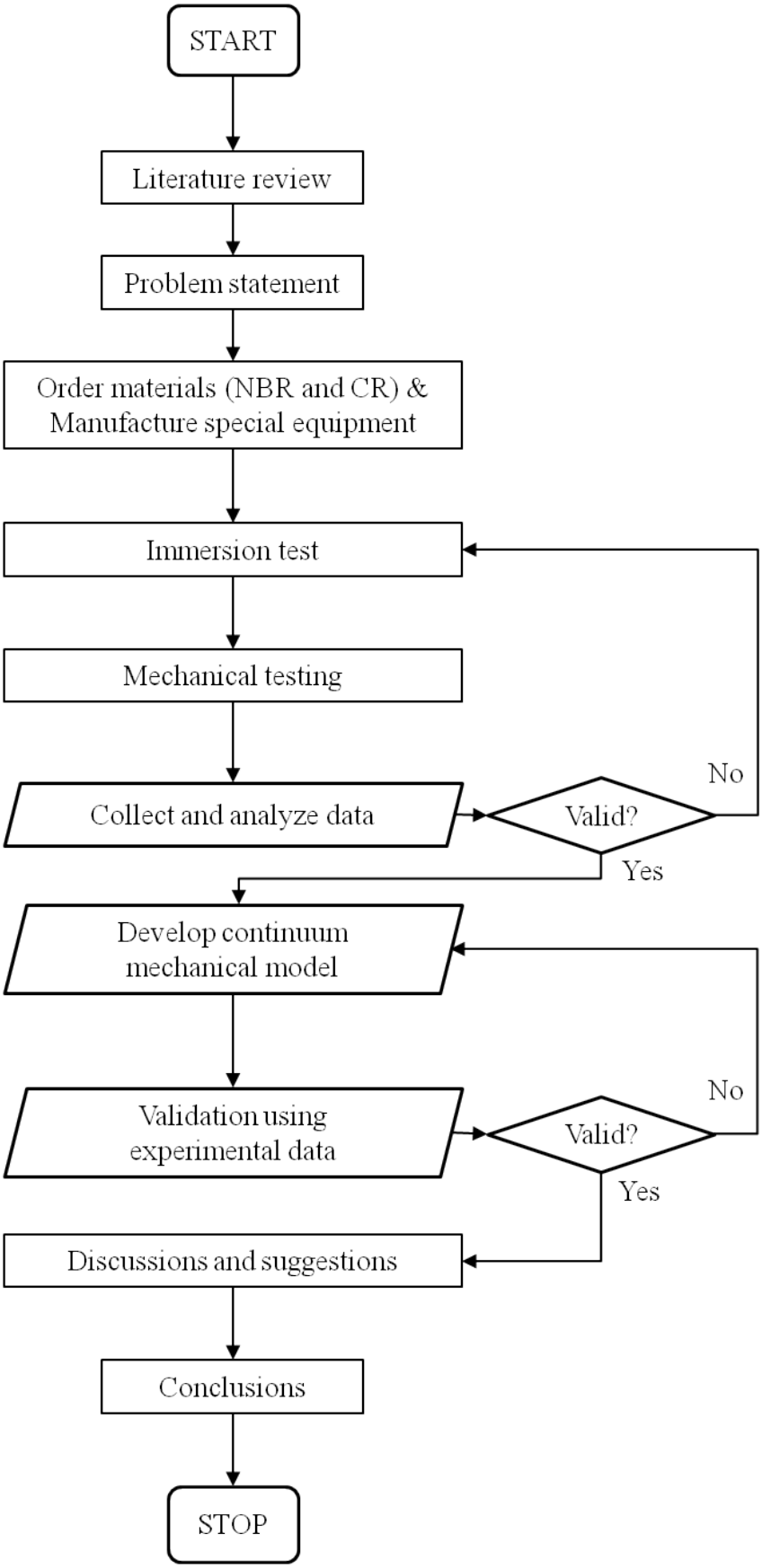

Figure 3.1: General research methodology.

3.1 Experimental program

3.1.1 Materials and specimen geometry

Commercial grade NBR and CR with 60 shore hardness are purchased from MAKA Engineering Sdn. Bhd., Malaysia. The NBR and CR have a specific gravity of 1.4 ± 0.1 and 25 wt.% of carbon black. Due to confidentiality constraints, the detailed compound ingredients are not provided here. For each type of rubber compound, the vulcanization process is performed by compression molding process at 165 °C for 5 min under a pressure of approximately 6.89 MPa from an electrical resistance heating press. The rubber specimens for swelling and mechanical tests are annular cylindrical blocks. Note that no standard is followed in the determination of specimen geometry. The wall thickness of the specimen is optimized with the help of finite element simulation software to ensure that equilibrium diffusion (swelling) in the rubber can be achieved within a reasonable period of time and the wall thickness is able to sustain the compression load to prevent buckling. It is found that the optimum height, outer diameter and wall thickness of the specimen are respectively 10 mm, 50 mm and 6 mm.

Different biodiesel blends are prepared by blending palm biodiesel (provided by Am Biofuels Sdn. Bhd., Malaysia) with diesel. Table 3.1 shows the analysis report of the investigated palm biodiesel. The palm biodiesel blends prepared are B0 (100% diesel), B25 (blend of 25% of biodiesel and 75% of diesel), B75 (blend of 75% of biodiesel and 25% of diesel) and B100 (100% biodiesel).

3.1.2 Experimental setup

3.1.2 (a) Swelling tests on stress-free specimens (free swelling)

The tests are conducted in diesel (B0) and biodiesel (B100) respectively at room temperature for various immersion durations: 2, 5, 10, 20 and 30 days. Figure 3.2 shows the simple immersion test where the specimens are hung and immersed in a stainless steel container containing biodiesel. Each specimen is completely immersed in the tested fuel. Thereby allowing stress-free swelling to occur in the rubber specimens.

Table 3.1: Properties of B100 palm biodiesel.

Test	Unit	Methods	Results
Ester content	% (m/m)	EN 14103	96.9
Density at 15 °C	kg/m^3	EN ISO 12185	875.9
Viscosity at 40 °C	mm^2/s	EN ISO 3104	4.667
Flash point	°C	EN ISO 3679	168
Cetane number	-	EN ISO 5165	69.7
Water content	mg/kg	EN ISO 12937	155
Acid value	mgKOH/g	EN ISO 3679	0.38
Methanol content	% (m/m)	EN 14110	<0.01
Monoglyceride content	% (m/m)	EN 14105	0.67
Diglyceride content	% (m/m)	EN 14105	0.2
Triglyceride content	% (m/m)	EN 14105	0.2
Total glycerine	% (m/m)	EN 14105	0.25

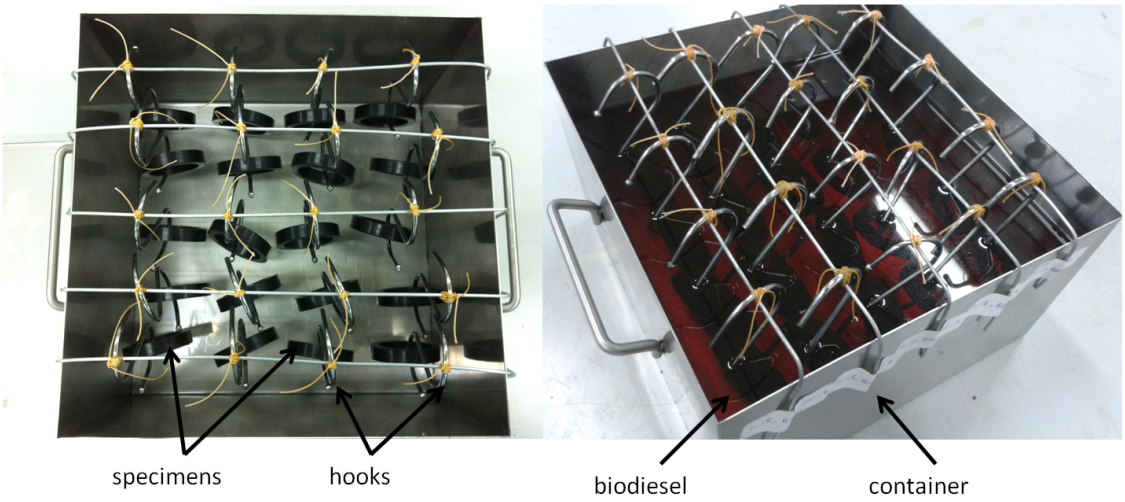

Figure 3.2: Swelling test on stress-free specimens. Before (left) and after (right) immersion in tested fuel (B100).

3.1.2 (b) Swelling tests on uniaxially-stressed specimens (constrained swelling)

The specially made rubber specimens are compressed to different degrees of compressive strain by attaching them to a custom-made compression device prior to immersion as shown in Figure 3.3. The compression device has special features as described below:

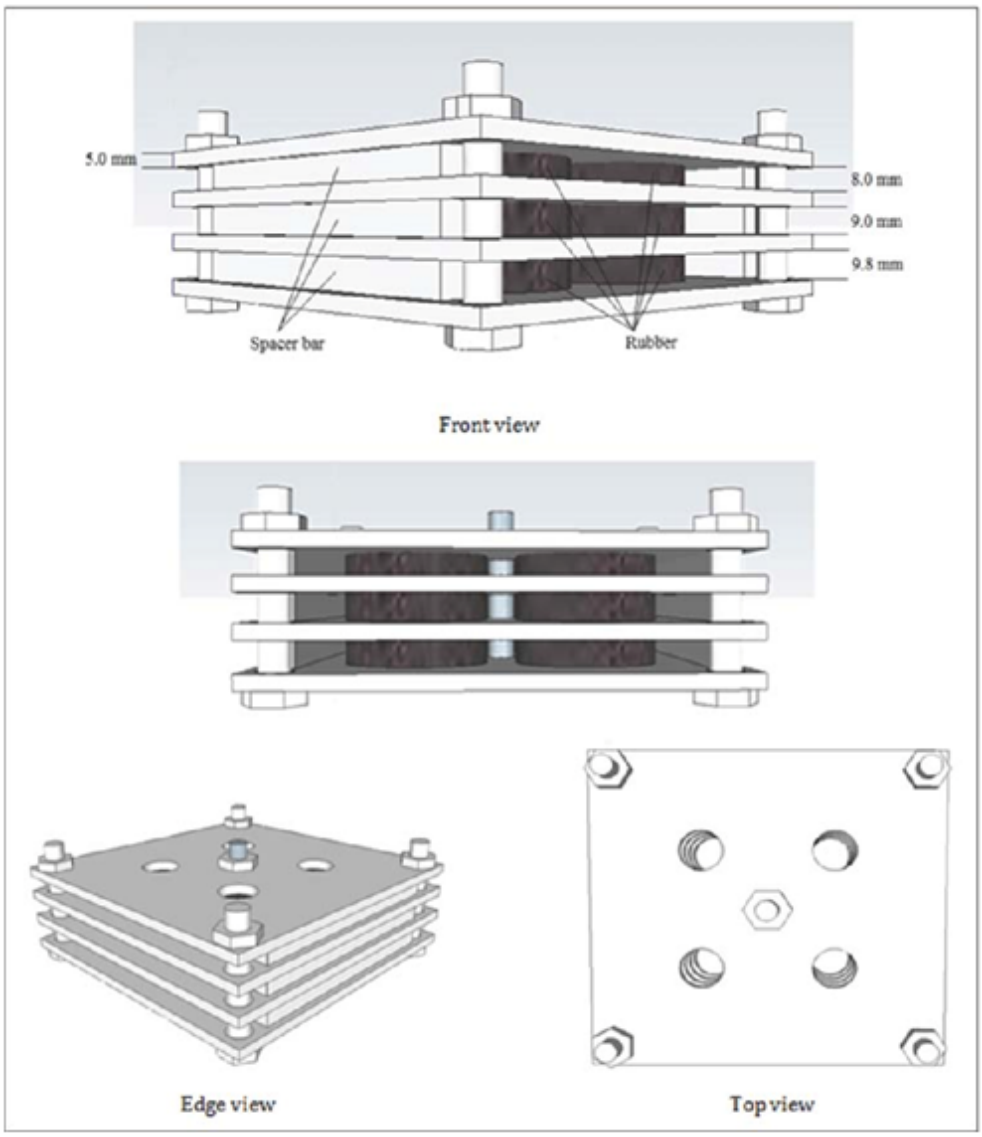

Figure 3.3: Compression device.

1. It consists of four rectangular stainless steel plates. Stainless steel plates are used for corrosion resistance because the device is needed to be immersed into diesel and biodiesel which are deemed to be corrosive.

2. The device is able to accommodate a total of 12 specimens arranged in 3 different levels between two successive plates.

3. Each plate has 4 main holes to allow the liquid to flow and diffuse into the inner surface of the rubber specimens. In this way, each rubber specimen is subjected to diffusion of liquid from both inner and outer wall surfaces, i.e. diffusion along radial direction only as illustrated in Figure 3.4.

4. For each level between two successive plates, a compressive strain is applied to the specimens located at the corresponding level: 20% for the level 1, 10% for the level 2 and 2% for the level 3. Different height of spacers are used at each level to limit the degree of compressive strains. Bolts and nuts located at each corner of the plates are tightened until the compression plates are uniformly in contact with the spacers. Additional ring spacers are placed around the bolt in the middle of the plates to prevent bending of the plates.

5. In practice, the 2% strain is so small that its effect on the macroscopic mechanical response is negligible. Nevertheless, this level of strain is retained to represent initially stress-free condition while ensuring that the diffusion occurs only along radial direction.

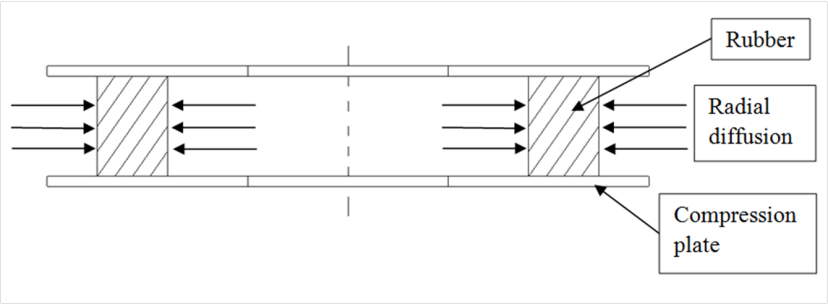

Figure 3.4: Diagram of radial diffusion for swelling under compressive strain.

3.1.2 (c) Swelling measurement

Free swelling When the stress-free samples reached the desired immersion duration, they are removed from the container and dipped quickly into acetone to remove the oil excess. The samples are then blotted dry with filter paper and the weight of stress-free swollen rubber specimens in the air and in the distilled water are measured immediately.

The percentages of mass change and volume change are calculated using the following relations (ASTM, 1957):

$$\% \text{ Mass Change} = \frac{M_2 - M_1}{M_1} \times 100 \tag{3.1}$$

$$\% \text{ Volume Change} = \frac{(M_2 - M_4) - (M_1 - M_3)}{(M_1 - M_3)} \times 100 \tag{3.2}$$

where M_1 and M_2 are the mass in air (gram) before and after immersion while M_3 and M_4 are mass in water (gram) before and after immersion. For each test, at least four specimens are used to measure volume and mass changes.

Constrained swelling The test procedure for swelling measurement of uniaxially-stress free swollen specimens is summarized as followed:

1. Before the immersion, the weight of the rubber specimen is measured in air and in distilled water. The specimen is then quickly dipped into alcohol and blotted dry with filter paper.

2. After weight measurement, the rubber specimens are placed in sequence on the compression plates. Grease is applied on the surface of the specimens that are in contact with the compression plate to avoid bulging and hence ensuring that the specimens are in a simple uniaxial compressive stress state.

3. Bolts and nuts are used to tighten the compression device until the compression plates are uniformly in contact with the spacers. The device containing rubber specimens is subsequently immersed into different palm biodiesel blends for different durations. The detail of the immersion tests is given in Table 3.2. All the tests are conducted at room temperature.

4. At the end of each immersion period, the specimens are removed from the compression device and quickly dipped into acetone; they are then cleaned with filter paper to remove the excess oil. Specimens are left for 30 minutes to allow for recovery before any measurement is made after immersion.

5. Step 1 is repeated to measure the weight of rubber specimen after immersion.

The percentages of mass change and volume change are calculated following Equations (3.1) and (3.2)

Table 3.2: Immersion tests.

Biodiesel Blend	Level of Compressive Strain (%)	Immersion Duration (days)
B0	2/10/20	30/90
B25	2/10/20	30/90
B75	2/10/20	30/90
B100	2/10/20	30/90

3.1.2 (d) Mechanical tests

To gain insight in the effect of swelling due to solvent diffusion, on the mechanical response of swollen rubber, mechanical tests on dry and swollen samples are carried out using an Instron 5500 uniaxial test machine equipped with a 10 kN load cell at room temperature. Circular compression plates are attached to the machine to ensure uniform displacement control on the specimens. The experimental setup is connected to a computer to record the experimental data. The tests are conducted at a constant displacement rate of 0.1 mm/s to avoid excessive increase in the temperature of the specimens, i.e. temperature effects are not considered in the present study. Figure 3.5 shows the experimental setup of the compression test.

Figure 3.5: Experimental setup of the compression test.

Two types of mechanical tests are conducted:

1. Cyclic compression test: This is conducted to observe the stress-softening and hysteresis behaviors of the rubber. The test is conducted at 0.01 s^{-1} strain rate using displacement-controlled mode with two different maximum compressive strains, 30% and 40%, of 6 cycles each.

2. Multi-relaxation test: This test is conducted to observe the viscoelasticity of the rubber. The test is conducted at 0.01 s^{-1} strain rate using displacement-controlled mode initially with 6 cycles of maximum compressive strain of 40% to remove the stress-softening effect. It is then followed by compressing the specimen to strain levels of 10%, 20% and 30% and hold it for 30 minutes as illustrated in Figure 3.6. The stress during the holding time is recorded for both loading and unloading of the strain levels.

In order to ensure repeatability of the results, at least three specimens are used in each test.

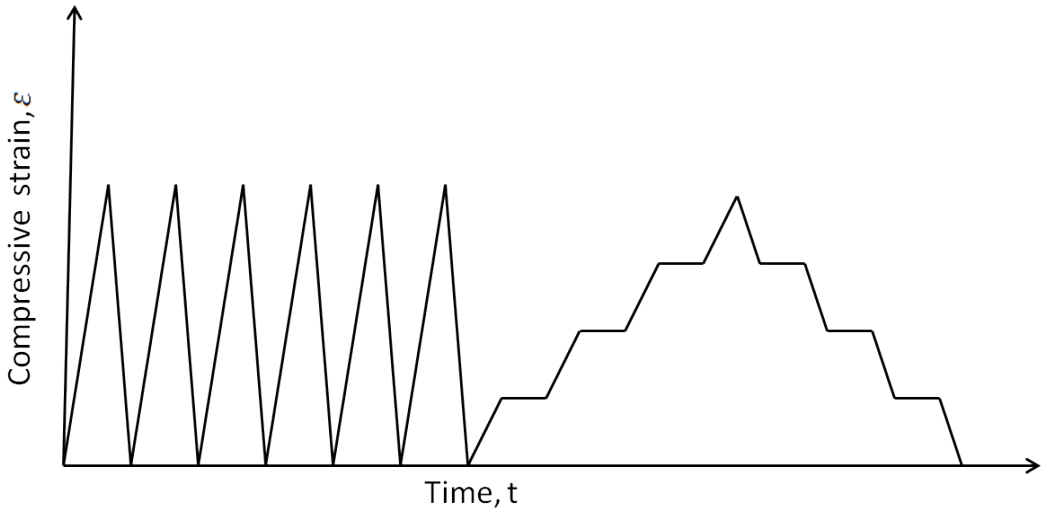

Figure 3.6: Multi-relaxation test.

3.1.2 (e) Microstructure observations

The dry and swollen specimens were cut with a sharp blade and the cross sectional surface was observed with a low vacuum and low pressure scanning electron microscope (FE1 Quanta FEG 250). The aim is to obtain information regarding microstructural change due to oil penetration.

3.2 Continuum mechanical modeling

As a first step to modeling the mechanical response of swollen rubber under cyclic loading, only the Mullins effect is considered. Other inelastic phenomena such as permanent set, hysteresis, etc. will not be considered. For this purpose, data treatment is required and will be discussed in Section 5.1 in Chapter 5.

The constitutive equations of swollen rubber experiencing irreversible softening (damage) due to cyclic mechanical loading is addressed. For this purpose, we first layout the chemical potential equation to obtain the Flory-Huggins interaction parameter for different rubber-fuel combinations. These parameters are needed for continuum mechanical modeling of the Mullins effect in swollen rubber. Next, the discussion is confined to the hyperelasticity of swollen rubber with and without internal damage. The classical multiplicative decomposition of the deformation gradient tensor into swelling and mechanical parts is adopted to replicate the experimental procedure whereby the rubber is first subjected to isotropic swelling before undergoing mechanical loading. The stress response is then derived by considering the second law of thermodynamics.

In order to capture the Mullins effect in swollen rubber, two models available in the literature are considered: the pseudo-elastic model of Ogden and Roxburgh (1999) and the two-phase model of Mullins and Tobin (1957) and Qi and Boyce (2004). These two models are extended to account for the effect of swelling.

3.2.1 Determination of the Flory-Huggins interaction parameter, χ

The Flory-Huggins Interaction parameter χ, is the dimensionless interaction parameter describing the interaction between rubber and solvent, i.e. palm biodiesel and diesel. Following the Flory-Huggins equation from Equation (2.25), these parameters can be calculated at equilibrium swelling using the following chemical potential equation:

$$\frac{kT}{\nu C_0}\left[ln\left(1-\frac{1}{J_s^e}\right)+\frac{1}{J_s^e}+\chi\frac{1}{(J_s^e)^2}\right]+(J_s^e)^{-1/3}-(J_s^e)^{-1}=0 \tag{3.3}$$

where k is Boltzmann constant, T is temperature during swelling, ν is the molar volume of the solvent molecules, C_o is the dry shear modulus and J_s^e is equilibrium degree of swelling.

3.2.2 Hyperelasticity of swollen rubber

3.2.2 (a) Description of the deformation

In the experimental procedure, stress-free dry rubber specimens are immersed in a solvent to allow isotropic swelling to occur in the material. After a desired degree of swelling is achieved, the resulting swollen specimens are subjected to various mechanical loadings. The corresponding procedure is illustrated in Figure 3.7.

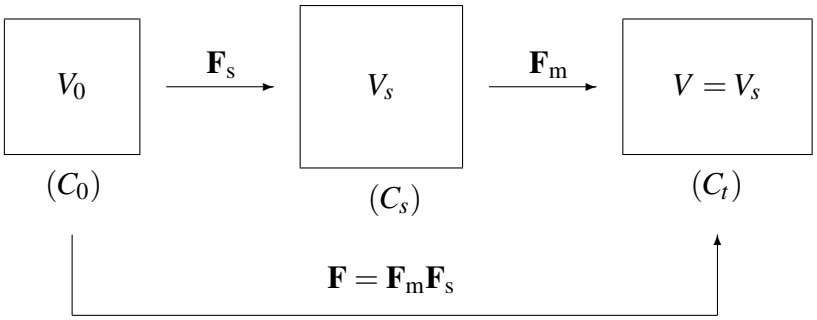

Figure 3.7: Illustration of experimental procedure.

Initially, the rubber specimen is in a dry state at C_0 (unswollen-unstrained configuration) having a volume of V_0. It undergoes isotropic swelling characterized by the swelling part of the total deformation gradient $\mathbf{F}$, denoted $\mathbf{F}_\mathrm{s}$. Due to swelling, the specimen volume changes to V_s at C_s (swollen-unstrained configuration). The degree of swelling, J_s, is simply defined by the ratio between the volume of swollen specimen V_s and the volume of dry specimen V_0, i.e.

$$J_s = \frac{V_s}{V_0}. \tag{3.4}$$

Consequently, $\mathbf{F}_\mathrm{s}$ can be written as a function of J_s as follow:

$$\mathbf{F}_\mathrm{s} = J_s^{1/3}\mathbf{I} \tag{3.5}$$

where $\mathbf{I}$ is the identity tensor.

The next stage of deformation consists of imposing a mechanical loading on the swollen specimen. The corresponding deformation is characterized by the mechanical part of the deformation gradient tensor, denoted $\mathbf{F}_\mathrm{m}$. Here, it is assumed that the swollen

rubber undergoes deformation at constant volume, i.e. swollen rubber is assumed to be incompressible. Thus, the kinematic constraint to respect during this stage of deformation is det $\mathbf{F}_{\mathrm{m}}$=1. In summary, the transformation of material from C_0 to C_t (swollen-strained configuration) can be described by:

$$\mathbf{F} = \mathbf{F}_{\mathrm{m}}\mathbf{F}_{\mathrm{s}} = J_s^{1/3}\mathbf{F}_{\mathrm{m}}. \tag{3.6}$$

Noted that the above decomposition is originally proposed by Flory (1961). Thermal expansion effects can be taking into accouny in a similar way.

3.2.2 (b) Constitutive equations

General stress response In order to describe the stress response, we postulate the existence of a strain energy function W, defined per unit of volume in C_0, which depends on the degree of swelling J_s and on the mechanical part of deformation gradient tensor $\mathbf{F}_{\mathrm{m}}$ as follows:

$$W = \tilde{W}(\mathbf{F}) = \hat{W}(J_s, \mathbf{F}_{\mathrm{m}}) = W_{\mathrm{s}}(J_s) + J_s W_{\mathrm{m}}(J_s, \mathbf{F}_{\mathrm{m}}). \tag{3.7}$$

In this expression, W_{s} is the strain energy per unit of volume in C_0 associated with isotropic swelling while W_{m} is the strain energy associated with mechanical loading. It is to note that W_{m} is defined per unit of volume in C_s. Moreover, the dependence of W_{m} on J_s is through material parameters which *explicitly* depend on the degree of swelling.

For a purely mechanical process, the second law of thermodynamics reduces to:

$$\mathscr{D} = \mathbf{P} : \dot{\mathbf{F}} - \dot{W} \geq 0 \tag{3.8}$$

where $\mathscr{D}$ is the internal dissipation per unit of volume in C_0, $\mathbf{P}$ is the 1st Piola-Kirchhoff stress tensor relative to C_0 (engineering stress with respect to unswollen-unstrained configuration). For swollen rubber of a given degree of swelling (constant degree of swelling), the rate of change of the strain energy $\dot{W}$ is given by:

$$\begin{aligned} \dot{W} &= \frac{\partial \hat{W}}{\partial J_s}\Big|_{\mathbf{F}_{\mathrm{m}}} \dot{J}_s + \frac{\partial \hat{W}}{\partial \mathbf{F}_m}\Big|_{J_s} : \dot{\mathbf{F}}_{\mathrm{m}} \\ &= \frac{\partial \hat{W}}{\partial \mathbf{F}_m}\Big|_{J_s} : \dot{\mathbf{F}}_{\mathrm{m}} \end{aligned} \tag{3.9}$$

since $\dot{J}_s = 0$.

In view of Equation (3.6), $\dot{\mathbf{F}}_{\mathrm{m}}$ can be related to $\dot{\mathbf{F}}$ through:

$$\dot{\mathbf{F}} = \overline{\dot{J_s^{1/3}}\mathbf{F}_{\mathrm{m}}} = \frac{1}{3}J_s^{-2/3}\dot{J}_s\mathbf{F}_{\mathrm{m}} + J_s^{1/3}\dot{\mathbf{F}}_{\mathrm{m}}. \tag{3.10}$$

Thus, the internal dissipation becomes:

$$\mathscr{D} = \left(J_s^{1/3}\mathbf{P} - \frac{\partial \hat{W}}{\partial \mathbf{F}_m}\Big|_{J_s}\right) : \dot{\mathbf{F}}_{\mathrm{m}} = 0. \tag{3.11}$$

which must be satisfied for all possible values of $\dot{\mathbf{F}}_{\mathrm{m}}$ respecting the incompressible constraint, i.e. (Holzapfel, 2000):

$$\det\mathbf{F}_{\mathrm{m}} = 1 \quad \Leftrightarrow \quad \overline{\det\dot{\mathbf{F}}_{\mathrm{m}}} = 0 \quad \Leftrightarrow \quad \mathbf{F}_{\mathrm{m}}^{-\mathrm{T}} : \dot{\mathbf{F}}_{\mathrm{m}} = 0. \tag{3.12}$$

Considering Equation (3.11) and the right term of Equation (3.12), we deduce:

$$\left(J_s^{1/3}\mathbf{P} - \frac{\partial \hat{W}}{\partial \mathbf{F}_m}\Big|_{J_s}\right) = q\mathbf{F}_{\mathrm{m}}^{-\mathrm{T}}. \tag{3.13}$$

where q is an arbitrary scalar (Lagrange multiplier) due to incompressibility assumption which can be determined from the equilibrium equations and appropriate boundary conditions. Hence, we obtain the stress response as follow:

$$\mathbf{P} = qJ_s^{-1/3}\mathbf{F}_{\mathrm{m}}^{-\mathrm{T}} + J_s^{-1/3}\frac{\partial \hat{W}}{\partial \mathbf{F}_{\mathrm{m}}}\Big|_{J_s}. \tag{3.14}$$

Recalling Equation (3.7), the above equation can be recast to:

$$\mathbf{P} = qJ_s^{-1/3}\mathbf{F}_{\mathrm{m}}^{-\mathrm{T}} + J_s^{2/3}\frac{\partial W_{\mathrm{m}}}{\partial \mathbf{F}_{\mathrm{m}}}. \tag{3.15}$$

The Cauchy stress tensor σ (defined in C_t) is simply given by:

$$\begin{aligned}\sigma = (\det\mathbf{F})^{-1}\mathbf{P}\mathbf{F}^{\mathrm{T}} &= J_s^{-1}\left(qJ_s^{-1/3}\mathbf{F}_{\mathrm{m}}^{-\mathrm{T}} + J_s^{2/3}\frac{\partial W_{\mathrm{m}}}{\partial \mathbf{F}_{\mathrm{m}}}\right)\mathbf{F}^{\mathrm{T}} \\ &= qJ_s^{-1}\mathbf{I} + \frac{\partial W_{\mathrm{m}}}{\partial \mathbf{F}_{\mathrm{m}}}\mathbf{F}_{\mathrm{m}}^{\mathrm{T}}.\end{aligned}$$

Noting that (Holzapfel, 2000):

$$\frac{\partial W_{\mathrm{m}}}{\partial \mathbf{F}_{\mathrm{m}}}\mathbf{F}_{\mathrm{m}}^{\mathrm{T}} = \mathbf{F}_{\mathrm{m}}\left(\frac{\partial W_{\mathrm{m}}}{\partial \mathbf{F}_{\mathrm{m}}}\right)^{\mathrm{T}} = 2\mathbf{F}_{\mathrm{m}}\frac{\partial W_{\mathrm{m}}}{\partial \mathbf{C}_{\mathrm{m}}}\mathbf{F}_{\mathrm{m}}^{\mathrm{T}}. \tag{3.16}$$

where $\mathbf{C}_{\mathrm{m}} = \mathbf{F}_{\mathrm{m}}^{\mathrm{T}}\mathbf{F}_{\mathrm{m}}$, the Cauchy stress tensor becomes:

$$\boldsymbol{\sigma} = qJ_s^{-1}\mathbf{I} + 2\mathbf{F}_{\mathrm{m}}\frac{\partial W_{\mathrm{m}}}{\partial \mathbf{C}_{\mathrm{m}}}\mathbf{F}_{\mathrm{m}}^{\mathrm{T}}. \tag{3.17}$$

Assuming that swollen rubber is isotropic, we may express $W_{\mathrm{m}}(J_s, \mathbf{C}_{\mathrm{m}}) = \hat{W}_{\mathrm{m}}(J_s, I_{1\mathrm{m}}, I_{2\mathrm{m}})$, where:

$$I_{1\mathrm{m}} = \mathrm{tr}\,\mathbf{C}_{\mathrm{m}} \qquad I_{2\mathrm{m}} = \frac{1}{2}(I_{1\mathrm{m}} - \mathrm{tr}\,\mathbf{C}_{\mathrm{m}}^2). \tag{3.18}$$

Using chain rules, the above expression can be recast to:

$$\boldsymbol{\sigma} = qJ_s^{-1}\mathbf{I} + 2\left[\left(\frac{\partial \hat{W}_{\mathrm{m}}}{\partial I_{1\mathrm{m}}} + I_{1\mathrm{m}}\frac{\partial \hat{W}_{\mathrm{m}}}{\partial I_{2\mathrm{m}}}\right)\mathbf{B}_{\mathrm{m}} - \frac{\partial \hat{W}_{\mathrm{m}}}{\partial I_{2\mathrm{m}}}\mathbf{B}_{\mathrm{m}}^2\right]. \tag{3.19}$$

where $\mathbf{B}_{\mathrm{m}} = \mathbf{F}_{\mathrm{m}}\mathbf{F}_{\mathrm{m}}^{\mathrm{T}}$. The 1st Piola-Kirchhoff stress tensor relative to C_s (engineering stress with respect to swollen-unstrained configuration), $\hat{\mathbf{P}}$, can be obtained from $\hat{\mathbf{P}} = (\det\mathbf{F}_{\mathrm{m}})\boldsymbol{\sigma}\mathbf{F}_{\mathrm{m}}^{-\mathrm{T}}$, which yields:

$$\hat{\mathbf{P}} = qJ_s^{-1}\mathbf{F}_{\mathrm{m}}^{-\mathrm{T}} + 2\left[\left(\frac{\partial \hat{W}_{\mathrm{m}}}{\partial I_{1\mathrm{m}}} + I_{1\mathrm{m}}\frac{\partial \hat{W}_{\mathrm{m}}}{\partial I_{2\mathrm{m}}}\right)\mathbf{F}_{\mathrm{m}} - \frac{\partial \hat{W}_{\mathrm{m}}}{\partial I_{2\mathrm{m}}}\mathbf{F}_{\mathrm{m}}\mathbf{C}_{\mathrm{m}}\right]. \tag{3.20}$$

Finally, recalling that $\boldsymbol{\sigma} = (\det\mathbf{F})^{-1}\mathbf{P}\mathbf{F}^{\mathrm{T}}$, the tensors $\hat{\mathbf{P}}$ and $\mathbf{P}$ are simply related through:

$$\mathbf{P} = J_s^{2/3}\hat{\mathbf{P}}. \tag{3.21}$$

Special case of uniaxial extension Without loss of generality, we focus on the special case when the swollen rubber is subjected to uniaxial extension along the $\mathbf{e}_1$ direction. In this case, the tensors $\mathbf{F}_{\mathrm{m}}$ and $\mathbf{B}_{\mathrm{m}}$ are simply given by:

$$\mathbf{F}_{\mathrm{m}} = \lambda_{\mathrm{m}}\,\mathbf{e}_1\otimes\mathbf{e}_1 + \lambda_{\mathrm{m}}^{-1/2}\,(\mathbf{e}_2\otimes\mathbf{e}_2 + \mathbf{e}_3\otimes\mathbf{e}_3) \qquad \mathbf{B}_{\mathrm{m}} = \lambda_{\mathrm{m}}^{2}\,\mathbf{e}_1\otimes\mathbf{e}_1 + \lambda_{\mathrm{m}}^{-1}\,(\mathbf{e}_2\otimes\mathbf{e}_2 + \mathbf{e}_3\otimes\mathbf{e}_3) \tag{3.22}$$

where λ_{m} is the mechanical extension ratio defined by the ratio between the length of *swollen-strained* rubber with the one of *swollen-unstrained* rubber. Using boundary condition $\sigma_{22} = \sigma_{33} = 0$ to determine q, it can be shown that the non-zero Cauchy stress σ_{11} reduces to:

$$\sigma_{11} = 2\left(\frac{\partial \hat{W}_{\mathrm{m}}}{\partial I_{1\mathrm{m}}} + \frac{1}{\lambda_{\mathrm{m}}}\frac{\partial \hat{W}_{\mathrm{m}}}{\partial I_{2\mathrm{m}}}\right)\left(\lambda_{\mathrm{m}}^2 - \frac{1}{\lambda_{\mathrm{m}}}\right). \tag{3.23}$$

Assuming that the swollen rubber obeys the neo-Hookean model, we have:

$$\hat{W}_{\mathrm{m}}(J_s, I_{1\mathrm{m}}) = \frac{\mu(J_s)}{2}(I_{1\mathrm{m}} - 3). \tag{3.24}$$

where $\mu = \mu(J_s)$ is the shear modulus of swollen rubber. Note that its value explicitly depends on the degree of swelling J_s. In this case, the Cauchy stress becomes:

$$\sigma_{11} = \mu(J_s)\left(\lambda_{\mathrm{m}}^2 - \frac{1}{\lambda_{\mathrm{m}}}\right). \tag{3.25}$$

and the two engineering stresses are:

$$P_{11} = \mu(J_s)\left(\lambda_{\mathrm{m}} - \frac{1}{\lambda_{\mathrm{m}}^2}\right) \qquad \hat{P}_{11} = J_s^{-2/3}\mu(J_s)\left(\lambda_{\mathrm{m}} - \frac{1}{\lambda_{\mathrm{m}}^2}\right). \tag{3.26}$$

Remark 2 *The dependence of shear modulus on the swelling can be described with a power-law as follows:*

$$\mu(J_s) = \mu_0 J_s^{-n}. \tag{3.27}$$

where μ_0 is the shear modulus of dry rubber and $n > 0$ is a material parameter. In the case where n=1/3, we recover the classical swelling model of Treloar (1975) in Equation (2.33). For elastomers swollen by palm biodiesel and conventional diesel fuel, n=2.5, is experimentally obtained (Chai, Verron, et al., 2013).

Remark 3 *For the non-Gaussian network model, Boyce and Arruda (2001) showed that swelling affects both the shear modulus and the stretch of network chain.*

3.2.3 Hyperelasticity of swollen rubber with damage

3.2.3 (a) Description of the deformation

In this section, we consider the softening phenomenon (Mullins effect) observed in swollen rubber under cyclic mechanical loading (Chai, Andriyana, et al., 2013). Here, the softening is considered as irreversible isotropic damage which can be represented by a scalar internal variable κ. In this case, the general multiplicative decomposition of the deformation gradient tensor illustrated in Figure 3.7 remains applicable. Nevertheless, the following points are worth noting:

1. During the transformation from C_0 to C_t, rubber undergoes softening of two kinds:

   (a) Softening due to isotropic expansion (swelling) of the polymeric network, i.e. transition from C_0 to C_t. This network expansion increases the chain separation resulting in a reduction of the secondary intermolecular bonding forces. As a consequence, the material becomes softer.

   (b) Softening associated with the Mullins effect under cyclic mechanical loading. This softening, which occurs during the transition from C_s to C_t, is often regarded as essentially being caused by the fillers in rubber matrix (Holzapfel, 2000).

2. Experiments showed that increasing the degree of swelling (i.e. increasing softening due to swelling) reduces the Mullins softening (Andriyana et al., 2012). While the precise link between the above two kinds of softening remains unclear, it appears that swelling softening affects the material capacity to accommodate further softening under mechanical loading.

3.2.3 (b) Constitutive equations

General stress response To describe the Mullins softening, the expression of strain energy in Equation (3.7) is extended below:

$$W = \tilde{W}(\mathbf{F}) = \hat{W}(J_s, \kappa, \mathbf{F}_{\mathrm{m}}) = W_{\mathrm{s}}(J_s) + J_s W_{\mathrm{m}}(J_s, \kappa, \mathbf{F}_{\mathrm{m}}). \tag{3.28}$$

Consequently, the internal dissipation in Equation (3.11) becomes:

$$\mathscr{D} = \left(J_s^{1/3}\mathbf{P} - \frac{\partial \hat{W}}{\partial \mathbf{F}_m}\Big|_{J_s,\kappa} \right) : \dot{\mathbf{F}}_{\mathrm{m}} - \frac{\partial \hat{W}}{\partial \kappa}\Big|_{J_s,\mathbf{F}_{\mathrm{m}}} \dot{\kappa} \geq 0. \tag{3.29}$$

for a given (constant) degree of swelling. The above inequality must be respected for all values of $\dot{\mathbf{F}}_{\mathrm{m}}$ and $\dot{\kappa}$ with a kinematic constraint of $\det \mathbf{F}_{\mathrm{m}} = 1$, i.e. incompressibility of swollen rubber. Following the arguments of (Coleman & Gurtin, 1967), we deduce the following constitutive relation:

$$\mathbf{P} = qJ_s^{-1/3}\mathbf{F}_{\mathrm{m}}^{-\mathrm{T}} + J_s^{-1/3}\frac{\partial \hat{W}}{\partial \mathbf{F}_{\mathrm{m}}}\Big|_{J_s,\kappa}. \tag{3.30}$$

which has a similar form as Equation (3.14). Hence, the tensors σ, $\hat{\mathbf{P}}$, $\mathbf{P}$ are respectively:

$$\sigma = qJ_s^{-1}\mathbf{I} + 2\left[\left(\frac{\partial \hat{W}_{\mathrm{m}}}{\partial I_{1\mathrm{m}}} + I_{1\mathrm{m}}\frac{\partial \hat{W}_{\mathrm{m}}}{\partial I_{2\mathrm{m}}} \right)\mathbf{B}_{\mathrm{m}} - \frac{\partial \hat{W}_{\mathrm{m}}}{\partial I_{2\mathrm{m}}}\mathbf{B}_{\mathrm{m}}^2 \right]. \tag{3.31}$$

$$\hat{\mathbf{P}} = qJ_s^{-1}\mathbf{F}_{\mathrm{m}}^{-\mathrm{T}} + 2\left[\left(\frac{\partial \hat{W}_{\mathrm{m}}}{\partial I_{1\mathrm{m}}} + I_{1\mathrm{m}}\frac{\partial \hat{W}_{\mathrm{m}}}{\partial I_{2\mathrm{m}}} \right)\mathbf{F}_{\mathrm{m}} - \frac{\partial \hat{W}_{\mathrm{m}}}{\partial I_{2\mathrm{m}}}\mathbf{F}_{\mathrm{m}}\mathbf{C}_{\mathrm{m}} \right]. \tag{3.32}$$

$$\mathbf{P} = J_s^{2/3}\hat{\mathbf{P}}. \tag{3.33}$$

Remark 4 *While Equations (3.31), (3.32) and (3.33) appear to be similar to their counterparts in Equations (3.19), (3.20) and (3.21), it is to note that their final expressions are actually different since $\hat{W}_m$ in Equations (3.31), (3.32) and (3.33) depends additionally on the damage variable κ.*

Evolution equation The constitutive relation in Equation (3.31) or (3.32) must be complemented by a kinetic relation which describes the evolution of the involved internal variable κ. The corresponding evolution equation has to be consistent with the non-negativity of the internal dissipation. To this end, we consider now the remaining term in inequality

(3.29) as follow:

$$\mathscr{D} = A_\kappa \dot{\kappa} \geq 0 \qquad \text{where} \qquad A_\kappa = -\frac{\partial \hat{W}}{\partial \kappa}\Big|_{J_s,\mathbf{F}_\mathrm{m}} = -J_s \frac{\partial \hat{W}_\mathrm{m}}{\partial \kappa}\Big|_{J_s,\mathbf{F}_\mathrm{m}}. \tag{3.34}$$

In the above expression, A_κ is the thermodynamic force associated with the damage variable κ. Depending on the nature of the variable κ, different evolutions of $\dot{\kappa}$ can be adopted provided that they respect inequality (3.34). For instance, the simplest sufficient condition to fulfil the above inequality is:

$$\dot{\kappa} = \frac{1}{\tau(J_s)} A_\kappa \tag{3.35}$$

where $\tau = \tau(J_s) > 0$ is a material parameter.

To propose any form of constitutive model for Mullins effect in swollen rubber, the above inequality must be respected during deformation. Next, the form of strain energy function $\hat{W}_\mathrm{m}$ and how the evolution rule $\dot{\kappa}$ describing the Mullins effect evolves in swollen rubber are specified for the pseudo-elastic and two-phase models in Section 3.2.4 and 3.2.5 respectively.

3.2.4 Pseudo-elastic model for the Mullins effect

3.2.4 (a) Brief recall on the pseudo-elastic model for the Mullins effect in dry elastomers

The basic assumption used in the pseudo-elastic model is the description of the materials response by the introduction of an additional continuous scalar parameter κ_{pe} into the classical hyperelastic strain energy function of a dry incompressible materials as follows (Ogden & Roxburgh, 1999):

$$\hat{W} = \hat{W}\left(I_1, I_2, \kappa_{pe}\right). \tag{3.36}$$

Due to the nature of κ_{pe}, the authors regarded $\hat{W}$ as the pseudo-energy function and the ensuing constitutive theory as pseudo-elasticity.

In the context of rubber where the Mullins effect is considered as a damage phenomenon, the parameter κ_{pe} can be related to the damage in the materials. The authors assumed that during loading to a new maximum deformation state, the damage stays zero.

In this case, $\kappa_{pe} = 1$ and the material response follows the classical undamaged (virgin) hyperelastic response. During unloading and subsequent reloading to submaximal deformation, κ_{pe} evolves and its value depends on the current deformation state. In this case, the material response is described by another energy function as follows:

$$\hat{W} = \hat{W}\left(I_1, I_2, \kappa_{pe}\left(I_1, I_2\right)\right) = \kappa_{pe}\left(I_1, I_2\right) \cdot W\left(I_1, I_2\right). \tag{3.37}$$

Using W as a measure of deformation state, the authors showed that the parameter κ_{pe} is given by:

$$\kappa_{pe} = 1 - d \qquad \text{where} \qquad d = \frac{1}{r}\text{erf}\left[\frac{1}{m}\left(W_{\max} - W\left(I_1, I_2\right)\right)\right]. \tag{3.38}$$

In the above expression, d is the damage function. r and m are material parameters. r corresponds to a measure of the extent of the damage relative to the virgin state while m controls the dependence of the damage on the extent of deformation. $W_{\max}$ is the value of W at the maximum deformation state ever experienced during the loading history. For our purpose, which is detailed in Section 5.3.1 in Chapter 5, the role of parameters r and m is investigated by plotting d for various values of r and m as depicted in Figures 3.8 and 3.9.

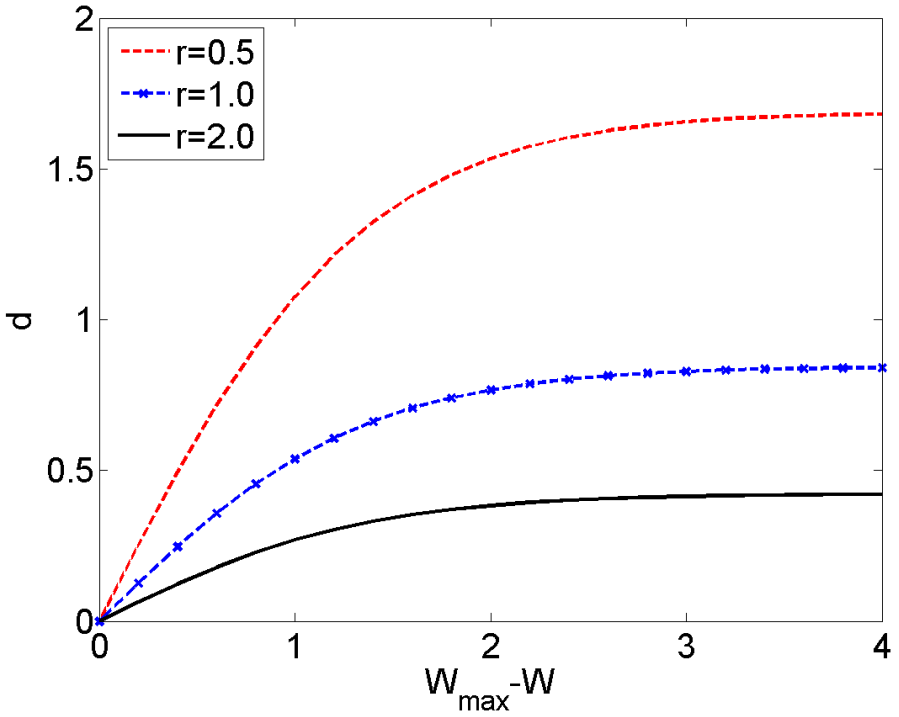

Figure 3.8: Evolution of d as a function of $W_{\max} - W$ for $m = 1$ and different values of r.

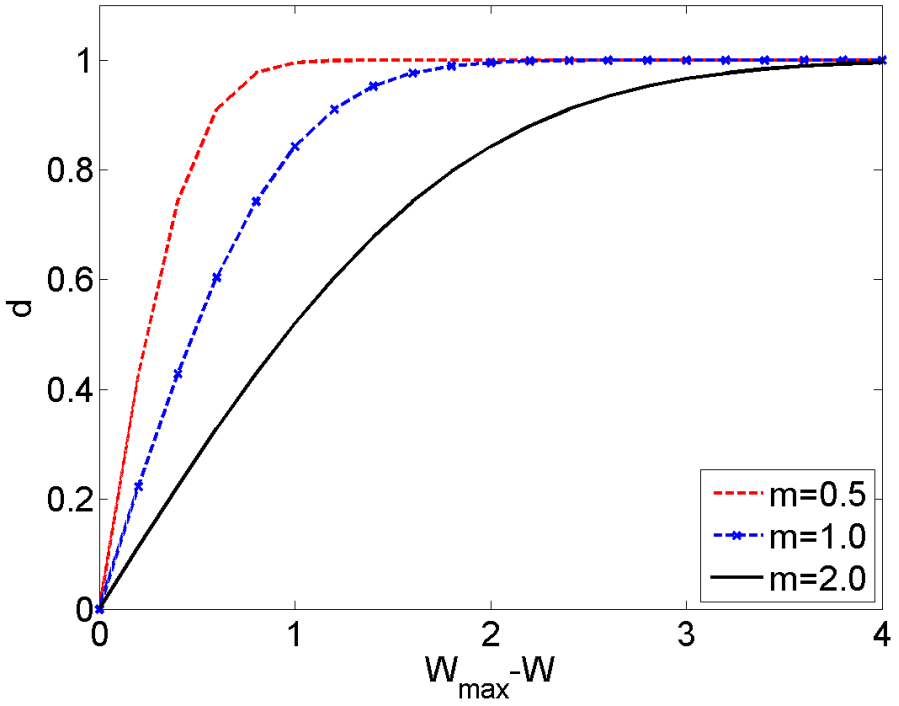

Figure 3.9: Evolution of d as a function of $W_{\max} - W$ for $r = 1$ and different values of m.

It is observed that m dictates the initial slope of d while r simply scales the curve vertically to higher or lower value. More precisely, the initial slope of d is an increasing

function of $\frac{1}{m}$ (decreasing function of m) and the maximum value of d is an increasing function of $\frac{1}{r}$ (decreasing function of r).

3.2.4 (b) Extension of the pseudo-elastic model to Mullins effect in swollen elastomers

In the case of swollen rubbers, the parameters r and m depend on the degree of swelling J_s and the nature of interaction between rubber and solvent χ. In order to investigate the dependence of r and m on the swelling using experimental data, the damage function d in Equation (3.38) is phenomenologically modified and extended as follow:

$$d = d\left(J_s, \chi, I_{1\mathrm{m,\,max}} - I_{1\mathrm{m}}\right) = \frac{1}{r\left(J_s, \chi\right)} \operatorname{erf}\left[\frac{1}{m\left(J_s, \chi\right)}\left(I_{1\mathrm{m,\,max}} - I_{1\mathrm{m}}\right)\right]. \tag{3.39}$$

In this expression, χ is the dimensionless interaction parameter describing the interaction between rubber and solvents, i.e. palm biodiesel and diesel. Note that W has been replaced by $I_{1\mathrm{m}} = \mathrm{tr}\mathbf{B}_{\mathrm{m}}$ as the measure of deformation state where $\mathrm{tr}\mathbf{B}_{\mathrm{m}} = \mathbf{F}_{\mathrm{m}}\mathbf{F}_{\mathrm{m}}^{\mathrm{T}}$. $I_{1\mathrm{m,\,max}}$ is the value of $I_{1\mathrm{m}}$ at the maximum deformation state ever experienced during the loading history. In this framework, during unloading and subsequent reloading to submaximal deformation, the Cauchy stress tensor in Equation (3.31) becomes:

$$\boldsymbol{\sigma} = qJ_s^{-1}\mathbf{I} + 2(1-d)\left[\left(\frac{\partial \hat{W}_{\mathrm{m}}}{\partial I_{1\mathrm{m}}} + I_{1\mathrm{m}}\frac{\partial \hat{W}_{\mathrm{m}}}{\partial I_{2\mathrm{m}}}\right)\mathbf{B}_{\mathrm{m}} - \frac{\partial \hat{W}_{\mathrm{m}}}{\partial I_{2\mathrm{m}}}\mathbf{B}_{\mathrm{m}}^2\right]. \tag{3.40}$$

where

$$\hat{W}_{\mathrm{m}} \equiv \hat{W}_{\text{m-pe}}(J_s, \kappa_{pe}, I_{1\mathrm{m}}, I_{2\mathrm{m}}). \tag{3.41}$$

The choice of $\hat{W}_{\mathrm{m}}$ and the proposed explicit forms of $r\left(J_s, \chi\right)$ and $m\left(J_s, \chi\right)$ are discussed in Section 5.3.1 in Chapter 5.

3.2.4 (c) Special case of uniaxial compression

For our purpose, we focus attention on the case of swollen elastomers under uniaxial compression. In this case, the deformation gradient tensor reduces to:

$$\mathbf{F}_{\mathrm{m}} = \lambda_{\mathrm{m}}\,\mathbf{e}_1 \otimes \mathbf{e}_1 + \frac{1}{\sqrt{\lambda_{\mathrm{m}}}}\left(\mathbf{e}_2 \otimes \mathbf{e}_2 + \mathbf{e}_3 \otimes \mathbf{e}_3\right) \tag{3.42}$$

where λ_{m} is the stretch relative to the swollen-unstrained state of elastomeric specimens. Applying boundary conditions $\sigma_{22} = \sigma_{33} = 0$ to determine q, the Cauchy stress along direction of compression is given by:

$$\sigma_{11} = 2(1-d)\left(\frac{\partial \hat{W}_{\mathrm{m}_{pe}}}{\partial I_{1\mathrm{m}}} + \frac{1}{\lambda_{\mathrm{m}}}\frac{\partial \hat{W}_{\mathrm{m}_{pe}}}{\partial I_{2\mathrm{m}}}\right)\left(\lambda_{\mathrm{m}}^2 - \frac{1}{\lambda_{\mathrm{m}}}\right). \tag{3.43}$$

and the corresponding first Piola-Kirchhoff (engineering) stress relative to the *swollen-unstrained* area is

$$\hat{P}_{11} = 2(1-d)\left(\frac{\partial \hat{W}_{\mathrm{m}_{pe}}}{\partial I_{1\mathrm{m}}} + \frac{1}{\lambda_{\mathrm{m}}}\frac{\partial \hat{W}_{\mathrm{m}_{pe}}}{\partial I_{2\mathrm{m}}}\right)\left(\lambda_{\mathrm{m}} - \frac{1}{\lambda_{\mathrm{m}}^2}\right). \tag{3.44}$$

3.2.5 Two-phase model for the Mullins effect

3.2.5 (a) Brief recall on the two-phase model for Mullins effect in dry elastomers

The two-phase model for Mullins effect in dry elastomer developed by Qi and Boyce (2004) is based on the model using a strain amplification factor X proposed by Mullins and Tobin (1957) for the uniaxial stress-strain response of elastomers to capture the effects of rigid filler particles. Mullins and Tobin (1957) described filled-rubber as a two-phase system containing a hard and a soft phase. The strain is sustained only by the soft phase of which the percentage increases with the maximum stretch applied to the material. The authors suggested that the irreversible conversion from hard phase to soft phase is the origin of the softening observed in rubber under cyclic loading. Since the strain is sustained by the soft phase, the local strain in the soft phase is amplified with the strain amplification factor X, given as:

$$X = \frac{\hat{\lambda} - 1}{\varepsilon}. \tag{3.45}$$

where $\hat{\lambda}$ is the amplified extension ratio of the rubber matrix while ε is the macroscopic (average) strain. It is clearly shown in Equation (3.45) that in the Mullins-Tobin model, the strain amplification factor amplifies the uniaxial stretch. This concept has been extended by Bergström and Boyce (1999) to amplify the first invariant of the stretch:

$$X = \frac{\hat{I}_1 - 3}{I_1 - 3}. \tag{3.46}$$

where $\hat{I}_1$ is the amplified I_1 in the rubber matrix, and I_1 is the overall macroscopic I_1 of the material.

For incompressible isotropic dry rubber undergoing stress-softening due to the Mullins effect, the strain energy function corresponding to the soft phase has the form:

$$W \equiv \tilde{W}\left(\bar{I}_1, \bar{I}_2, X\left(\upsilon_s\right), \upsilon_s\right) = W\left(I_1, I_2, \upsilon_s\right). \tag{3.47}$$

where υ_s is the effective volume fraction of the soft phase, $\bar{I}_1$ and $\bar{I}_2$ are the amplified first and second invariants in the soft phase respectively. They are related to the macroscopic (average) invariants I_1 and I_2 as follows (Bergström & Boyce, 1999):

$$\bar{I}_1 = X\left(I_1 - 3\right) + 3 \qquad\qquad \bar{I}_2 = X\left(I_2 - 3\right) + 3 \tag{3.48}$$

where X is the amplification factor which depends on υ_s. Here, it is to note that the amplification factor of I_2 is assumed to be the same as that of I_1.

Following Qi and Boyce (2004), the amplification factor, X is given in a general polynomial form of:

$$X = 1 + 3.5\upsilon_f + 18\upsilon_f^2. \tag{3.49}$$

where υ_f is the volume fraction of hard phase in the two-phase model. Since $\upsilon_f = 1 - \upsilon_s$, we have $X = 1 + 3.5(1 - \upsilon_s) + 18(1 - \upsilon_s)^2$.

The Cauchy stress tensor in Equation (2.16) is now modified for the two-phase model for Mullins effect in dry rubber as:

$$\sigma = -p\mathbf{I} + 2\left[\frac{\partial W\left(I_1, I_2, \upsilon_s\right)}{\partial I_1} + I_1 \frac{\partial W\left(I_1, I_2, \upsilon_s\right)}{\partial I_2}\right]\mathbf{B} - 2\frac{\partial W\left(I_1, I_2, \upsilon_s\right)}{\partial I_2}\mathbf{B}^2. \tag{3.50}$$

and the dissipation due to irreversible conversion of hard phase to soft phase is:

$$-\frac{\partial W}{\partial \upsilon_s}\dot{\upsilon}_s \geq 0. \tag{3.51}$$

Qi and Boyce (2004) assume that the rate change of the soft phase follow a modified saturation law as follows:

$$\dot{\upsilon}_s = A(\upsilon_{ss} - \upsilon_s)\dot{\lambda}_{\text{chain}}^{\max}. \tag{3.52}$$

where A is a parameter that characterizes the evolution in υ_s with increasing $\dot{\lambda}_{chain}^{max}$, the maximum amplified local chain stretch in the deformation history and υ_{ss} is the saturation value of υ_s. To capture the observed dependence of softening rate on stretch, Equation (3.52) is then modified:

$$\dot{\upsilon}_s = A(\upsilon_{ss} - \upsilon_s)\frac{\sqrt{N}-1}{\left(\sqrt{N}-\lambda_{\text{chain}}^{\max}\right)^2}\dot{\lambda}_{\text{chain}}^{\max} \tag{3.53a}$$

$$\dot{\lambda}_{\text{chain}}^{\max} = \begin{cases} 0 & \text{if} \quad \lambda_{\text{ch,sp}} < \lambda_{\text{chain}}^{\max} \\ \dot{\lambda}_{\text{chain}}^{\max} & \text{if} \quad \lambda_{\text{chain}} = \lambda_{\text{chain}}^{\max}. \end{cases} \tag{3.53b}$$

where $\sqrt{N}$ is the locking stretch of a molecule chain.

3.2.5 (b) Extension of the two-phase model to Mullins effect in swollen elastomers

In the case of swollen rubbers, in addition to the dependence on the effective volume fraction of soft phase υ_s, the strain energy density $\hat{W}_m$ also depends on the degree of swelling J_s. In this framework, during loading and unloading, the Cauchy stress tensor in Equation (3.31) becomes:

$$\boldsymbol{\sigma} = qJ_s^{-1}\mathbf{I} + 2\left[\left(\frac{\partial \hat{W}_{\text{m}}}{\partial I_{1\text{m}}} + I_{1\text{m}}\frac{\partial \hat{W}_{\text{m}}}{\partial I_{2\text{m}}}\right)\mathbf{B}_{\text{m}} - \frac{\partial \hat{W}_{\text{m}}}{\partial I_{2\text{m}}}\mathbf{B}_{\text{m}}^2\right]. \tag{3.54}$$

where

$$\hat{W}_{\text{m}} \equiv W_{\text{m-2p}}(J_s, \upsilon_s, I_{1\text{m}}, I_{2\text{m}}). \tag{3.55}$$

and the remaining dissipation reduces to:

$$-\frac{\partial \hat{W}_{\text{m-2p}}}{\partial \upsilon_s}\bigg|_{J_s, I_{1\text{m}}, I_{2\text{m}}} \dot{\upsilon}_s \geq 0. \tag{3.56}$$

The choice of $\hat{W}_{\text{m}}$ and the evolution rule $\dot{\upsilon}_s$ describing the increase of soft phase with deformation are specified in the Section 5.4.1.

3.2.5 (c) Special case of uniaxial compression

For our purpose, we focus attention on the case of swollen elastomers under uniaxial compression. In this case, the deformation gradient tensor reduces to:

$$\mathbf{F}_{\mathrm{m}} = \lambda_{\mathrm{m}}\,\mathbf{e}_1 \otimes \mathbf{e}_1 + \frac{1}{\sqrt{\lambda_{\mathrm{m}}}}\left(\mathbf{e}_2 \otimes \mathbf{e}_2 + \mathbf{e}_3 \otimes \mathbf{e}_3\right) \tag{3.57}$$

where λ is the stretch relative to the swollen-unstrained state of elastomeric specimens. Applying boundary conditions $\sigma_{22} = \sigma_{33} = 0$ to determine p, the Cauchy stress along direction of compression is given by:

$$\sigma_{11} = 2\left(\frac{\partial \hat{W}_{\mathrm{m}_{2p}}}{\partial I_{1\mathrm{m}}} + \frac{1}{\lambda_{\mathrm{m}}}\frac{\partial \hat{W}_{\mathrm{m}_{2p}}}{\partial I_{2\mathrm{m}}}\right)\left(\lambda_{\mathrm{m}}^2 - \frac{1}{\lambda_{\mathrm{m}}}\right). \tag{3.58}$$

and the corresponding first Piola-Kirchhoff (engineering) stress relative to the swollen-unstrained area is

$$\hat{P}_{11} = 2\left(\frac{\partial \hat{W}_{\mathrm{m}_{2p}}}{\partial I_{1\mathrm{m}}} + \frac{1}{\lambda_{\mathrm{m}}}\frac{\partial \hat{W}_{\mathrm{m}_{2p}}}{\partial I_{2\mathrm{m}}}\right)\left(\lambda_{\mathrm{m}} - \frac{1}{\lambda_{\mathrm{m}}^2}\right). \tag{3.59}$$

CHAPTER 4

EXPERIMENTAL RESULTS AND DISCUSSION

This chapter presents the experimental results obtained from the experimental works discussed in the previous chapter. Discussions are drawn from the results obtained from both the swelling test and mechanical test for the stress-free and uniaxially-stressed swollen rubbers.

4.1 Results of swelling tests on stress-free specimens

4.1.1 Mass and volume changes

The variation of mass change and volume change of dry and swollen NBR and CR as a function of immersion duration are shown in Figures 4.1 and 4.2.

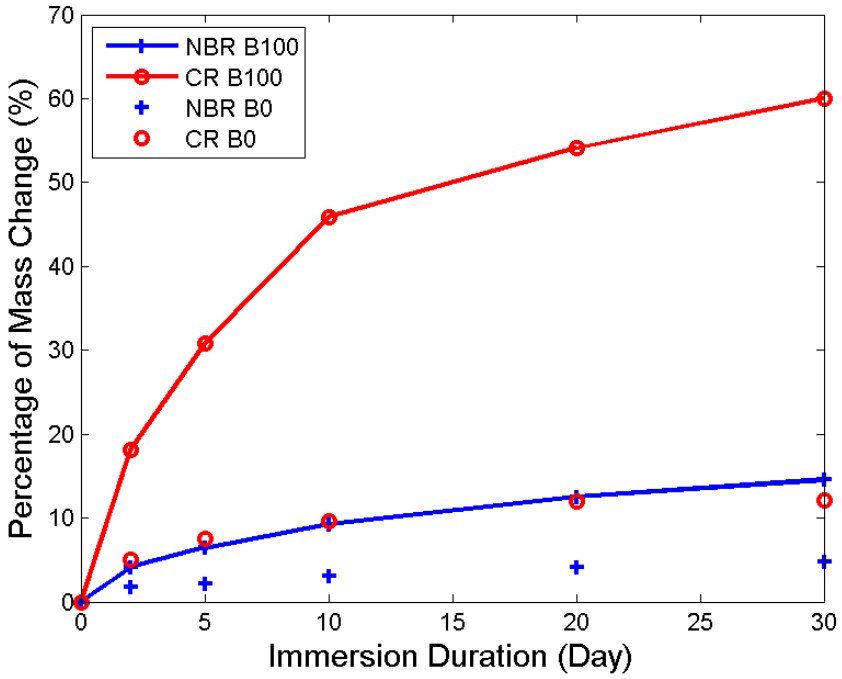

Figure 4.1: Mass change exhibited by NBR and CR after stress-free immersion in diesel and palm biodiesel at different immersion durations.

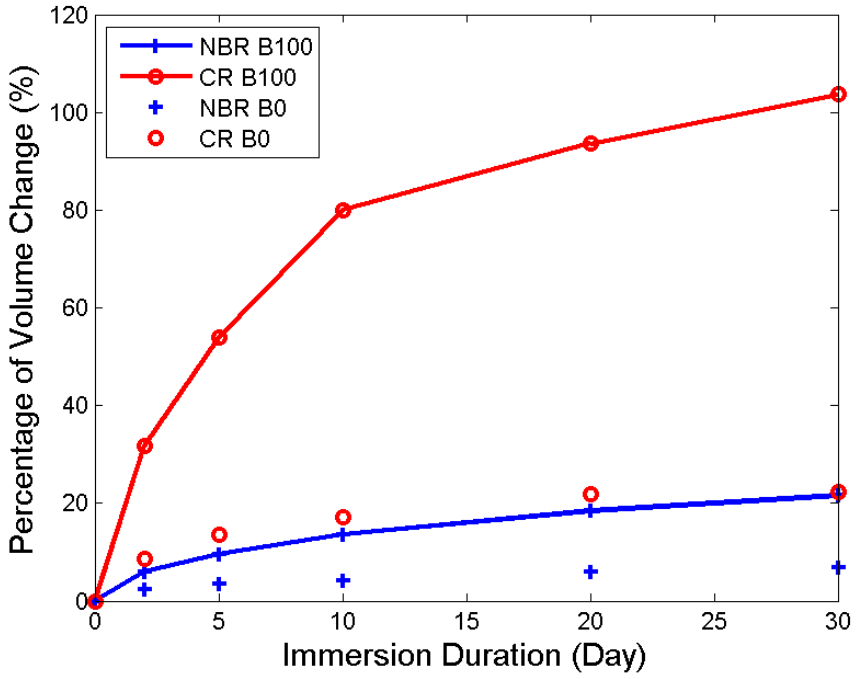

Figure 4.2: Volume change exhibited by NBR and CR after stress-free immersion in diesel and palm biodiesel at different immersion durations.

It can be seen that both graphs show similar trends. The swelling of NBR and CR increases when the exposure time (immersion duration) is increased from 2 to 30 days. For rubbers immersed in B0, it appears that equilibrium swelling has been achieved after 30 days of immersion. This is shown by relatively small increase in the mass and volume change between 20 and 30 days of immersion. In general, the fuel uptake is relatively fast at the initial stage, especially for rubber immersed in biodiesel due to great affinity in rubber for oil uptake (Mostafa et al., 2009). The rate of swelling, either expressed in terms of mass change or volume change, appears to be high at short exposure time before decreasing at longer exposure time. Accelerated swelling is initiated with absorption of liquids when the liquids dissolve on the surface layer of the rubber (adsorption) up to a certain concentration. Subsequently, the liquids penetrate slowly into the rubber by diffusion until the rubber specimen achieves equilibrium swelling (Gent, 1992).

From Figures 4.1 and 4.2, it is obvious that the swelling of CR is higher than NBR. This is because CR is made from emulsion polymerization of 2-chloro-1, 3-butadiene and NBR is emulsion copolymer of acrylonitrile and butadiene (Dick, 2001). The bulky substituent in NBR increases the rigidity of the polymer backbone and decreases the

free volume available for biodiesel diffusion (George & Thomas, 2001). In addition, the swelling of rubber is by the principle of "like dissolve like" - polar solvent are more likely to dissolve polar substances and non-polar substances are more likely to dissolve in non-polar solvent (Zhang & Cloud, 2007). The high polarity of ester in palm biodiesel favors the forming of polymer-solvent interaction in CR resulting in the increase of swelling in CR (Pekcan & Uğur, 2002). Similar results were found by Haseeb et al. (2011).

4.1.2 Mechanical response

The stress-strain response of dry and swollen rubbers (after immersion in B0 and B100 for the maximum immersion duration (30 days)) under cyclic compressive loading is presented in Figures 4.3 and 4.4. Generally, it is observed that the nature of stress-strain curves is preserved. However, for a given strain, lower stresses are recorded for swollen rubbers. CR and NBR swollen by B100 show lower stress levels than the rubbers swollen by B0. The significant decrease of stress in CR after immersion in B100 can be related to the high swelling level due to the strong interaction of rubber-solvent matrix system (George et al., 1999). Both dry and swollen rubbers exhibit inelastic responses such as stress-softening and hysteresis. The stress-softening disappears after around five loading cycles while the hysteresis stabilizes after five loading cycles. Moreover, it is to be noted that for both NBR and CR, the inelastic responses appear to be significantly smaller in the case of swollen rubbers.

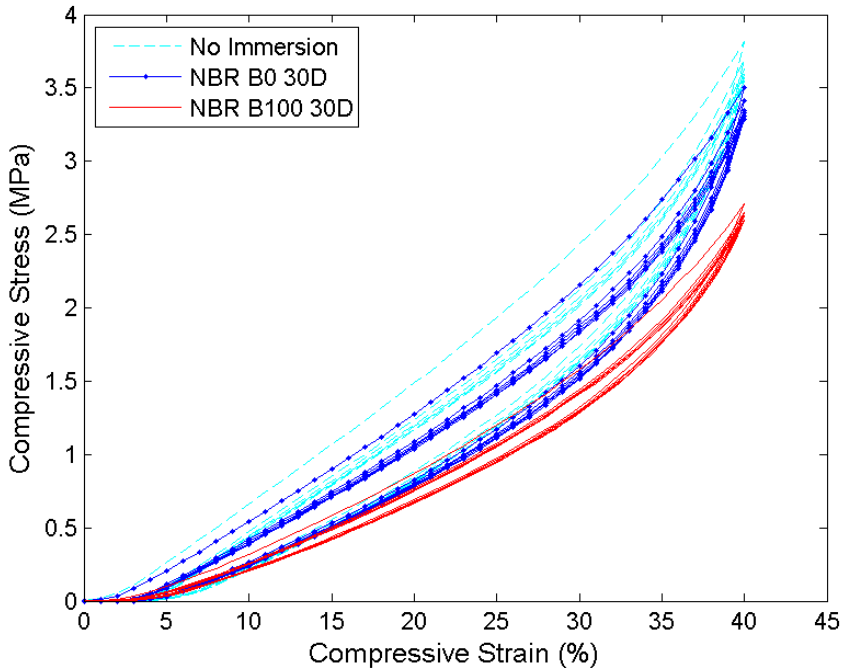

Figure 4.3: Stress-strain curves of NBR at dry (without immersion) and swollen states (after 30 days immersion in B0 and B100). For immersed rubbers, the stress is expressed with respect to the *swollen-unstrained* configuration (initial swollen cross section).

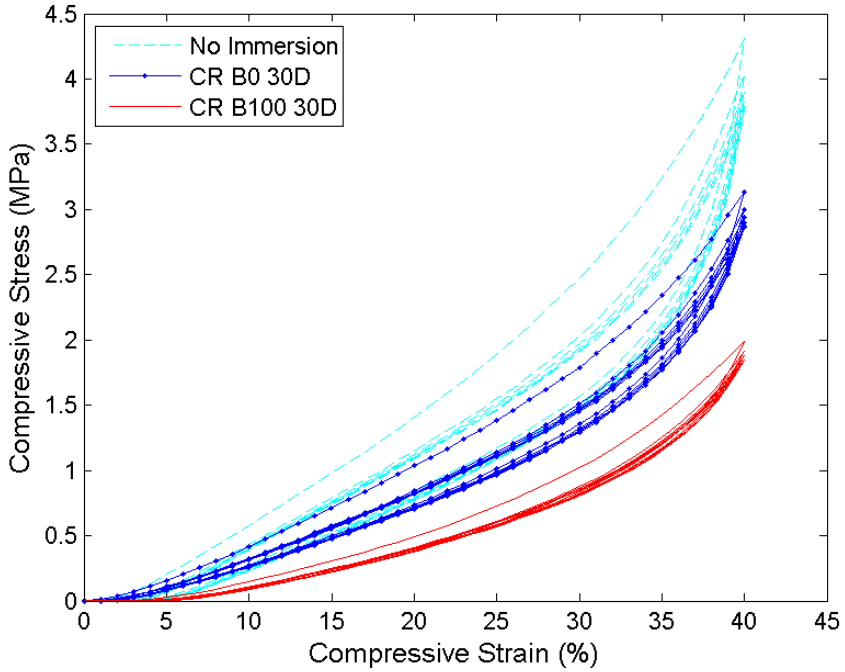

Figure 4.4: Stress-strain curves of CR at dry (without immersion) and swollen states (after 30 days immersion in B0 and B100). For immersed rubbers, the stress is expressed with respect to the *swollen-unstrained* configuration (initial swollen cross section).

To highlight the effect of degree of swelling resulting from different immersion durations and different fuel, the mechanical response of NBR and CR specimens during the first cyclic loading are depicted in Figures 4.5 to 4.8. In these figures, the stress is defined with respect to the *swollen-unstrained* configuration (initial swollen cross section). For each material and each tested fuel, stress-strain curves of dry rubber and swollen rubbers (corresponding to 5, 10, 20 and 30 days immersion durations) are presented. The figure suggests that generally, the inelastic responses in both NBR and CR, i.e. hysteresis, appears to be smaller when the degree of swelling is higher. In the next subsections, further discussions on the nature of swelling and the inelastic responses such as stress-softening, hysteresis and stress relaxation are presented.

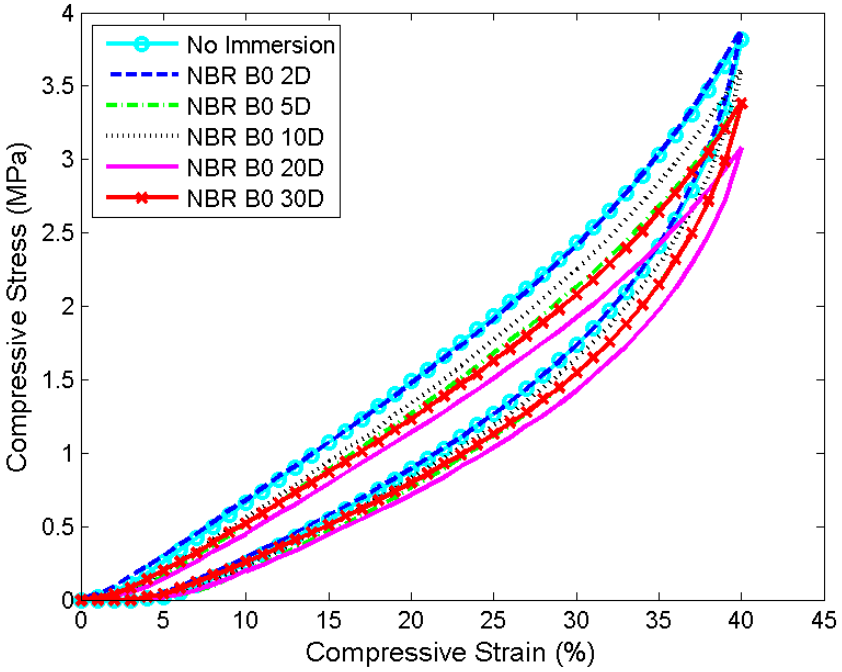

Figure 4.5: Stress-strain curves of NBR at dry states (without immersion) and after 2, 5, 10, 20 and 30 days immersion in B0. For immersed rubbers, the stress is expressed with respect to the *swollen-unstrained* configuration (initial swollen cross section).

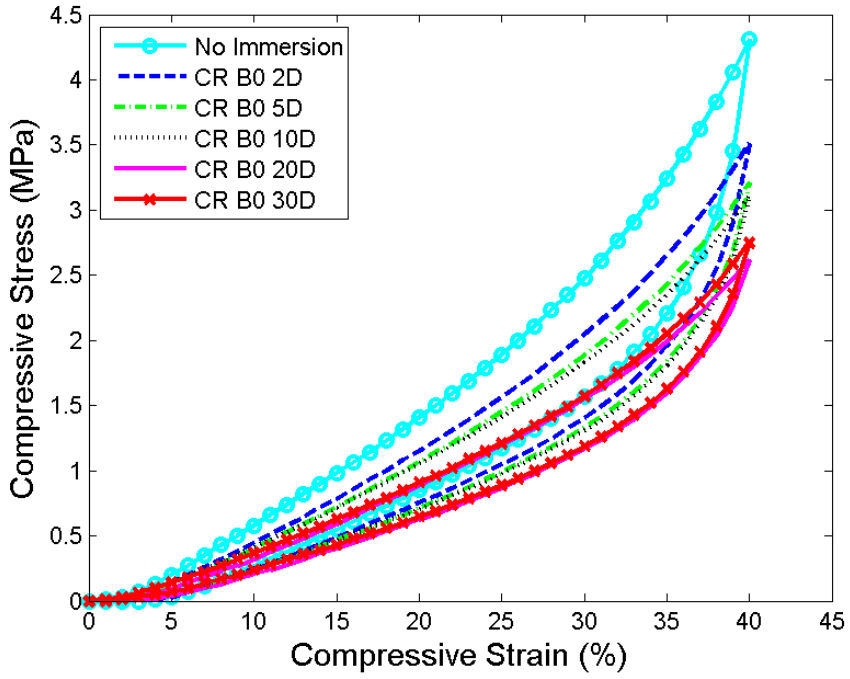

Figure 4.6: Stress-strain curves of CR at dry states (without immersion) and after 2, 5, 10, 20 and 30 days immersion in B0. For immersed rubbers, the stress is expressed with respect to the *swollen-unstrained* configuration (initial swollen cross section).

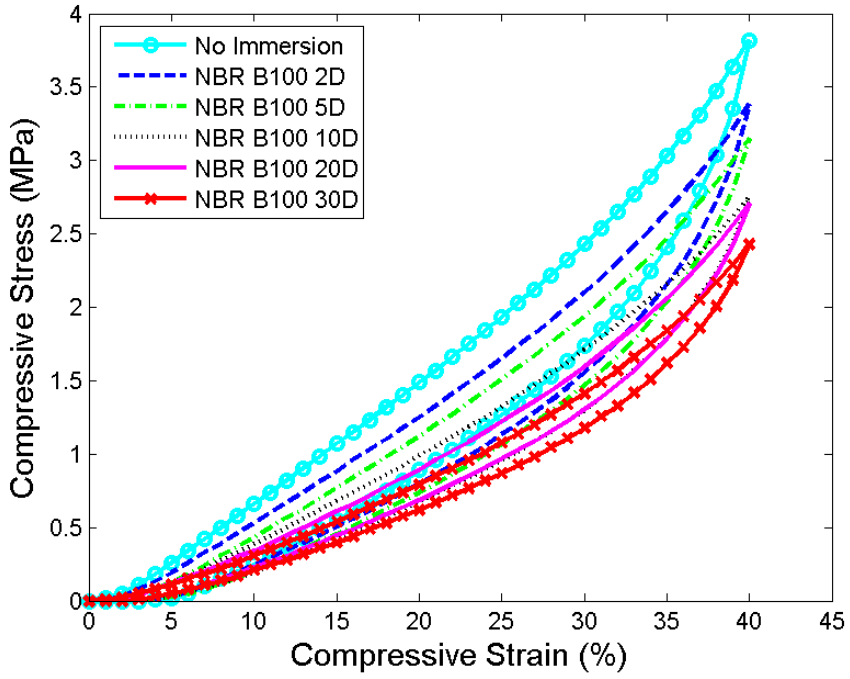

Figure 4.7: Stress-strain curves of NBR at dry states (without immersion) and after 2, 5, 10, 20 and 30 days immersion in B100. For immersed rubbers, the stress is expressed with respect to the *swollen-unstrained* configuration (initial swollen cross section).

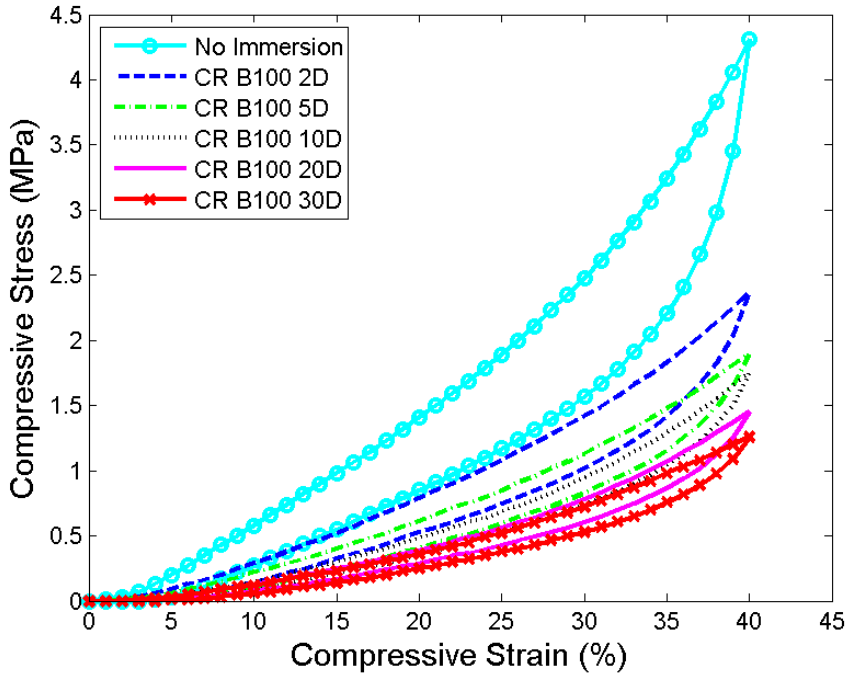

Figure 4.8: Stress-strain curves of CR at dry states (without immersion) and after 2, 5, 10, 20 and 30 days immersion in B100. For immersed rubbers, the stress is expressed with respect to the *swollen-unstrained* configuration (initial swollen cross section).

4.1.2 (a) Nature of swelling

According to Treloar's theory (Treloar, 1975), swelling in rubber is purely a mixing or diffusion process with no chemical attraction between rubber and liquid molecules. Furthermore, the only effect of swelling is to reduce the modulus in inverse proportion to the cube root of the swelling ratio without changing the form of the stress-strain curves, i.e.,

$$\frac{G}{G_o} = \upsilon_2{}^{1/3} \tag{4.1}$$

where G and G_o are the shear modulus in swollen and dry state respectively, and υ_2 is the volume fraction of rubber in the mixture of rubber and liquid. It is related to the change of volume in rubber, ΔV due to the presence of liquids via the following equation:

$$\upsilon_2 = \frac{1}{1+\Delta V} \tag{4.2}$$

Next, the nature of swelling experienced by NBR and CR due to the presence of biodiesel is investigated, i.e. we examine whether it follows swelling in the sense of Treloar (1975)

mentioned previously. For this purpose, the values of G and G_o are required. Unlike rubber materials considered in Treloar (1975) which follow the neo-Hookean hyperelastic response, our materials exhibit strong inelastic responses as clearly depicted in Figures 4.3 and 4.4. For this reason, the following methods are used for the determination of the shear modulus ratio:

1. Method 1 (M-1): The shear modulus ratio is calculated via cube root of the swelling ratio as predicted by Treloar (Eq. (4.1)).

2. Method 2 (M-2): G and G_o are identified by fitting the first uploading stress response of swollen and dry rubbers respectively. In both rubbers, the first uploading stress response is assumed to follow a simple neo-Hookean hyperelastic model.

3. Method 3 (M-3): The shear modulus ratio is calculated by dividing the first uploading stress response of swollen rubber with the one that corresponds to dry rubber. Thereby allowing the observation of possible strain-dependent shear modulus ratio.

4. Method 4 (M-4): G and G_o are identified by fitting the estimated equilibrium stress response of swollen and dry rubbers respectively. Following Bergström and Boyce (1998), the equilibrium stress response is given by the imaginary curve lines between the uploading and unloading of the sixth cycle, i.e. after the stress-softening effect is removed. Here, the equilibrium response is also assumed to follow a simple neo-Hookean hyperelastic model.

5. Method 5 (M-5): The shear modulus ratio is calculated by dividing the estimated equilibrium stress response of swollen rubber with the one that corresponds to dry rubber. Similarly to M-3, this method also allows the observation of possible strain-dependent shear modulus ratio.

The five methods above are compared. In Figures 4.9 to 4.12, shear modulus ratio obtained using M-1, M-2 and M-3 methods are plotted as a function of applied compressive strain for NBR and CR immersed in B0 and B100 respectively. In each graph, results that correspond to 2, 10 and 30 days of stress-free immersion are presented. Similarly, in Figures 4.13 to 4.16, shear modulus ratios are plotted, but this time using M-1, M-4 and M-5 methods.

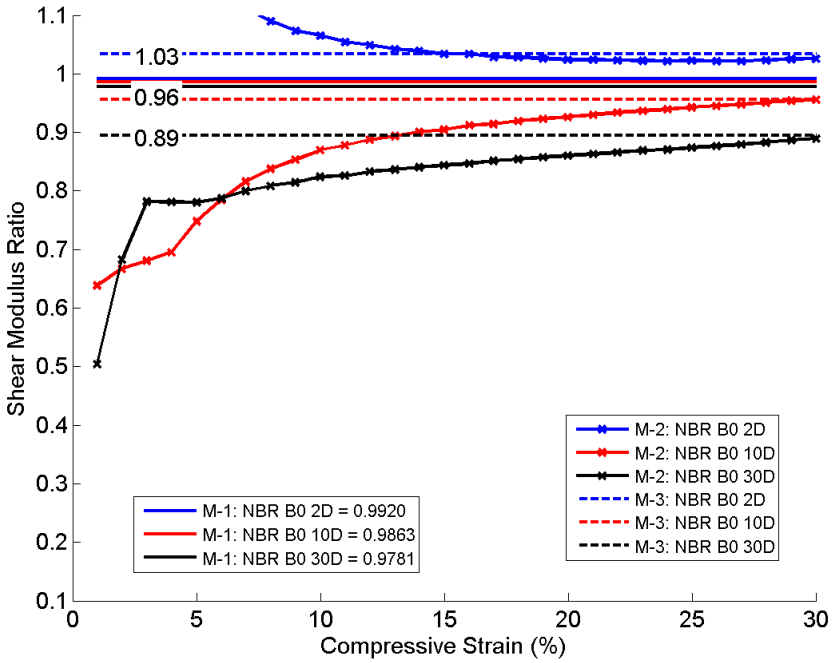

Figure 4.9: Shear modulus ratio obtained using M-1, M-2 and M-3 methods as a function of applied compressive strain for NBR after immersion in B0. Results correspond to 2, 10 and 30 days of stress-free immersion.

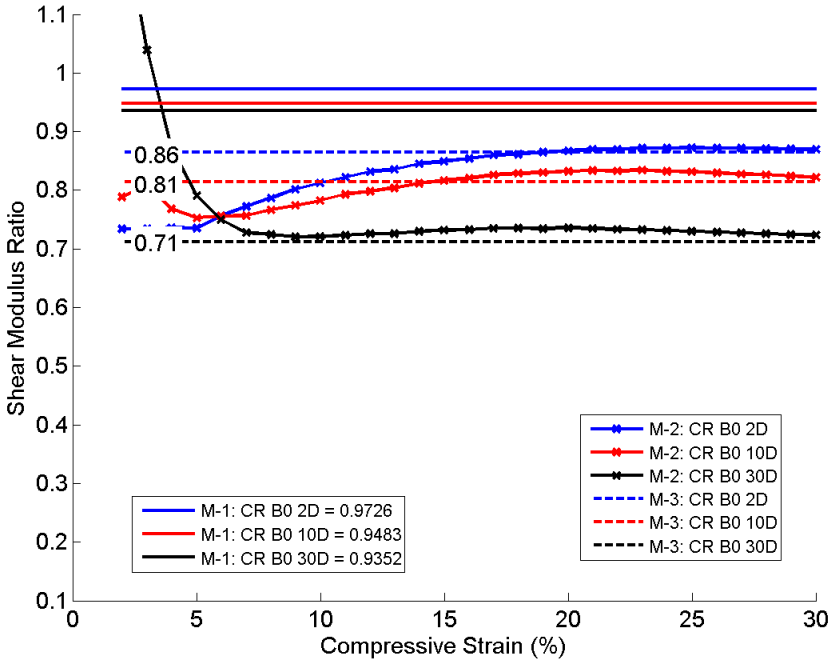

Figure 4.10: Shear modulus ratio obtained using M-1, M-2 and M-3 methods as a function of applied compressive strain for CR after immersion in B0. Results correspond to 2, 10 and 30 days of stress-free immersion.

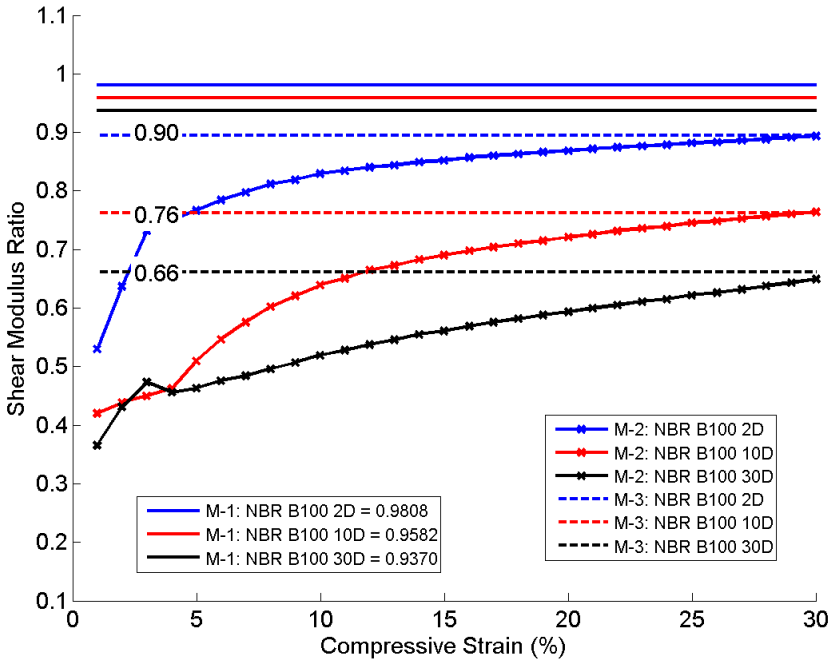

Figure 4.11: Shear modulus ratio obtained using M-1, M-2 and M-3 methods as a function of applied compressive strain for NBR after immersion in B100. Results correspond to 2, 10 and 30 days of stress-free immersion.

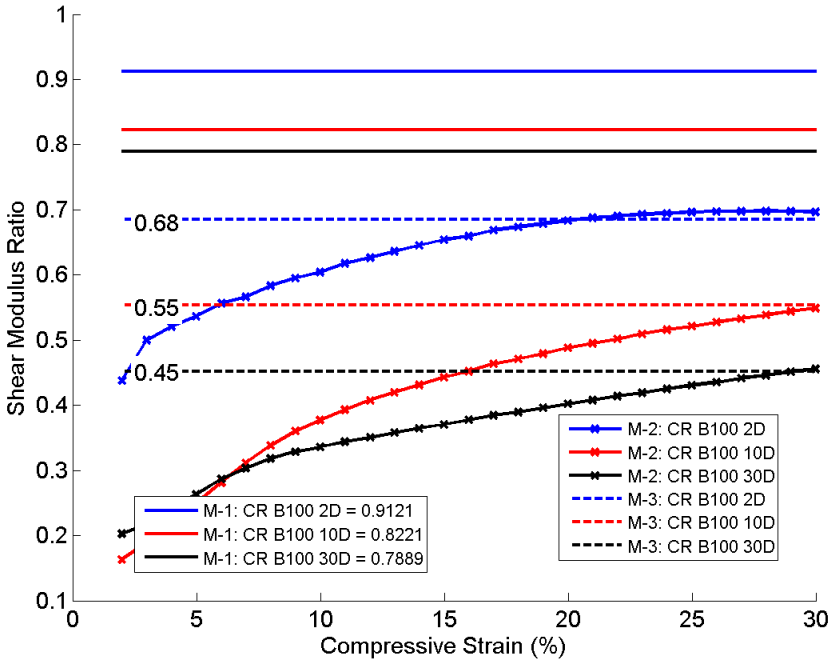

Figure 4.12: Shear modulus ratio obtained using M-1, M-2 and M-3 methods as a function of applied compressive strain for CR after immersion in B100. Results correspond to 2, 10 and 30 days of stress-free immersion.

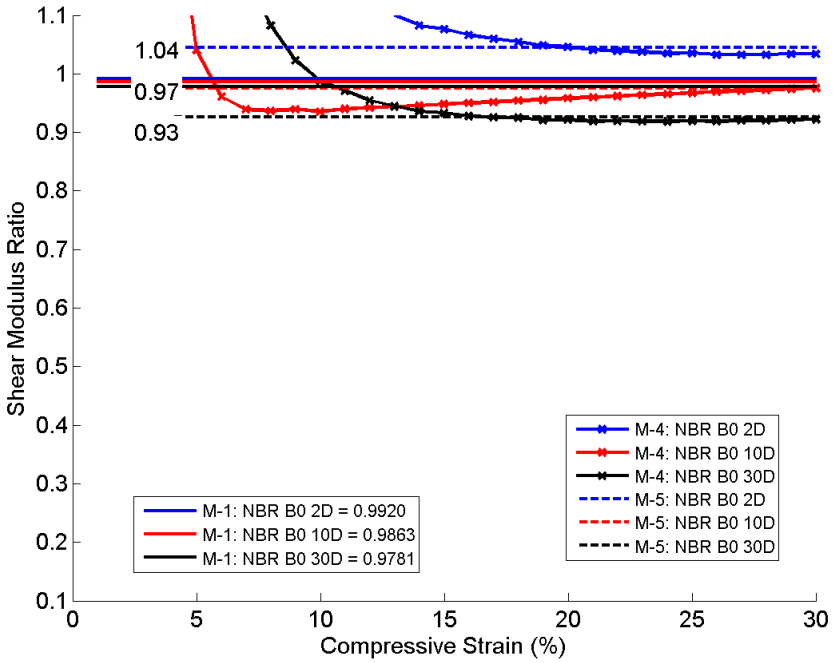

Figure 4.13: Shear modulus ratio obtained using M-1, M-4 and M-5 methods as a function of applied compressive strain for NBR after immersion in B0. Results correspond to 2, 10 and 30 days of stress-free immersion.

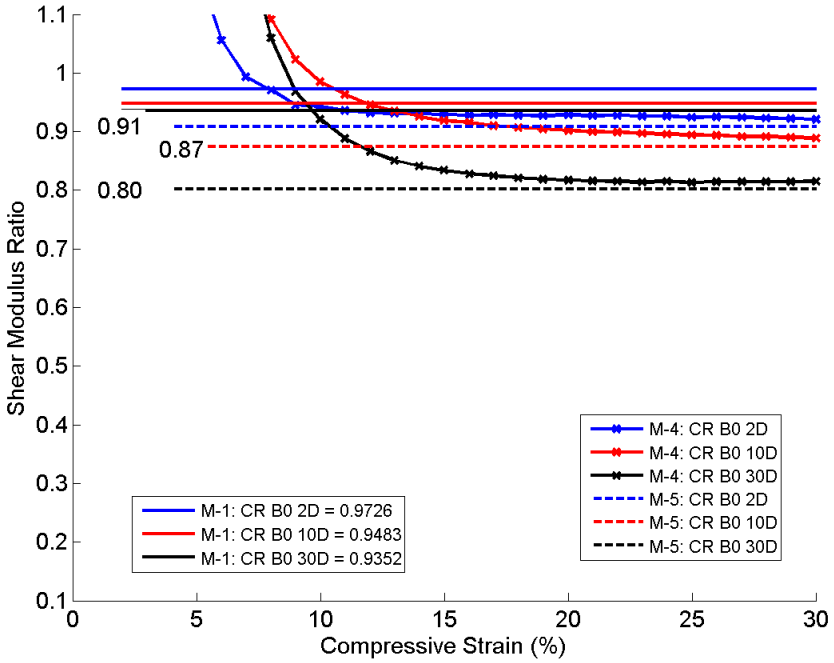

Figure 4.14: Shear modulus ratio obtained using M-1, M-4 and M-5 methods as a function of applied compressive strain for CR after immersion in B0. Results correspond to 2, 10 and 30 days of stress-free immersion.

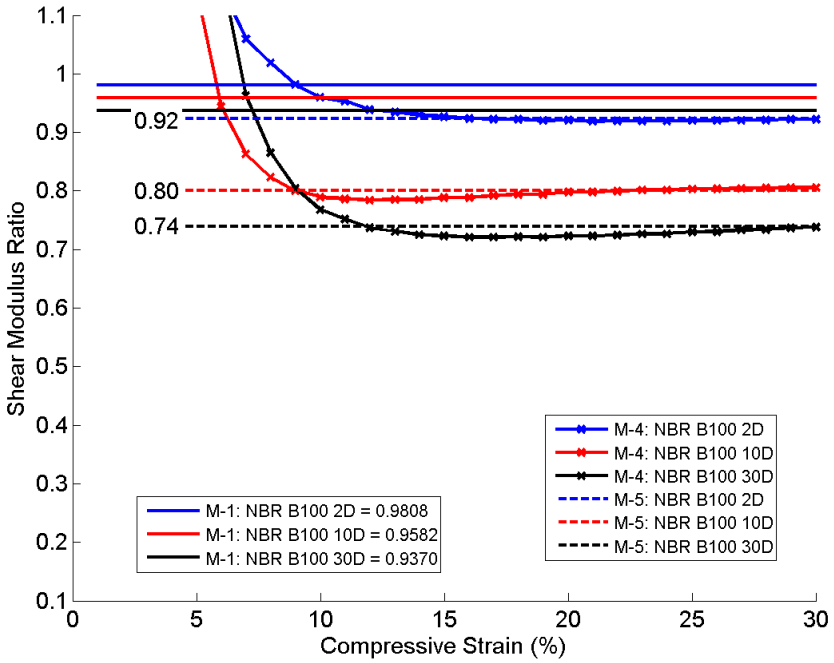

Figure 4.15: Shear modulus ratio obtained using M-1, M-4 and M-5 methods as a function of applied compressive strain for NBR after immersion in B100. Results correspond to 2, 10 and 30 days of stress-free immersion.

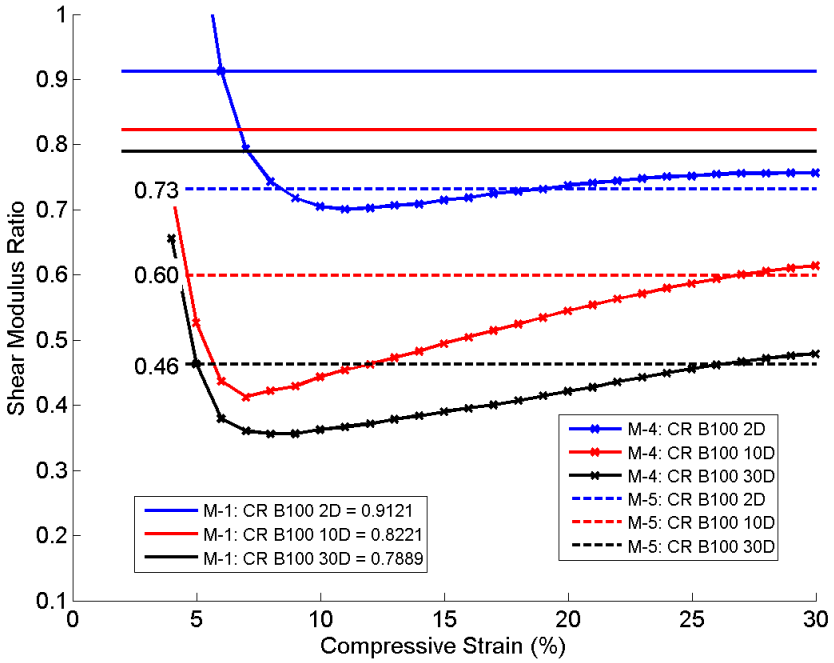

Figure 4.16: Shear modulus ratio obtained using M-1, M-4 and M-5 methods as a function of applied compressive strain for CR after immersion in B100. Results correspond to 2, 10 and 30 days of stress-free immersion.

In general, as depicted in Figures 4.9 to 4.16, it is found that the shear modulus ratio deviates from the cube root of the swelling ratio as predicted by Treloar, i.e. results obtained using M-2, M-3, M-4 and M-5 methods are different from those issued from M-1. Regardless of the type of rubber and the method considered, the deviation from Treloar theory in the shear modulus ratio resulting from immersion in B100 is systematically larger than the one resulting from immersion in B0. This observation suggests that a stronger interaction occurs between rubbers and B100 than between rubbers and B0. Increasing the duration of immersion from 2 to 30 days also increases the corresponding deviation. Finally, it is found that the shear modulus ratios calculated using the estimated equilibrium stress response, i.e. M-4 and M-5, appear to give closer values to the one predicted by Treloar than using the first uploading stress response, i.e. M-2 and M-3.

The deviation from Treloar theory can be attributed to the fact that Treloar assumes rubber networks to follow a hyperelastic Gaussian statistical model. In our case, as clearly shown in Figures 4.3 and 4.4, our materials exhibit a strong inelastic response. Hence, the use of the hyperelastic assumption becomes questionable. Furthermore, unlike the Treloar theory, the swelling phenomenon in NBR and CR due to the presence of biodiesel might also involve a strong chemical interaction between rubbers and biodiesel (Haseeb et al., 2011). However, this statement cannot be fully verified in the present study.

4.1.2 (b) Stress drop and stress-softening

It is observed that swollen elastomers exhibit stress-softening which disappears after around five cycles of loading (see Figures 4.3 and 4.4). In the following, only stress-softening occurring between the first uploading and second uploading is considered.

Before proceeding further with the evolution of stress-softening in swollen rubbers under cyclic loading, it is important to recall the difference between the stress decrease associated with the decrease in strength of rubber with that associated with the stress-softening. In the former, the idea is to compare the stress level during the first uploading between dry rubber and swollen rubber while the latter compares the stress level during the first uploading and the second uploading in one rubber (either dry or swollen). To characterize the former and the latter, we use the terms stress drop and stress-softening respectively defined by (see Figure 4.17):

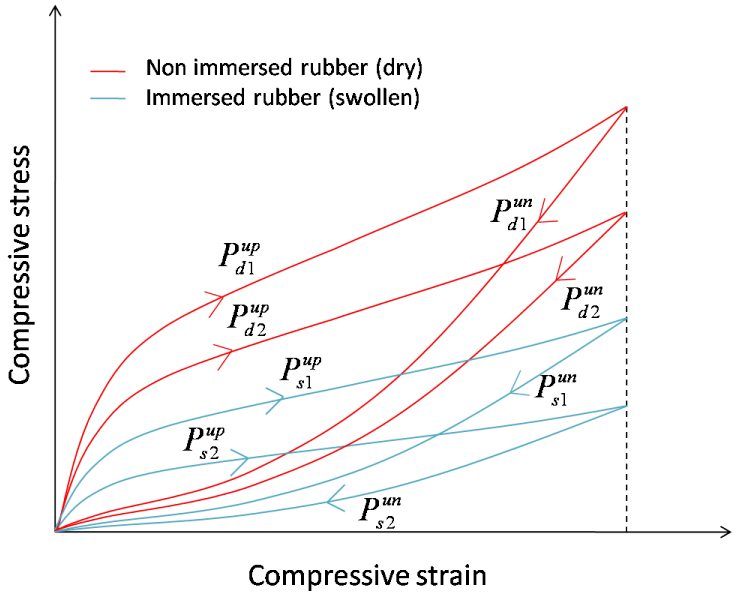

Figure 4.17: Illustration of two first cycles stress-strain curve of previously non immersed (dry) and immersed (swollen) rubbers under cyclic loading.

$$\text{Stress drop} = \frac{P_{d1}^{up} - P_{s1}^{up}}{P_{d1}^{up}} \tag{4.3}$$

$$\text{Stress softening (dry)} = \frac{P_{d1}^{up} - P_{d2}^{up}}{P_{d1}^{up}}; \qquad \text{Stress softening (swollen)} = \frac{P_{s1}^{up} - P_{s2}^{up}}{P_{s1}^{up}} \tag{4.4}$$

where P_{d1}^{up} is the stress in dry rubber during uploading of the first cycle, P_{d2}^{up} is the stress in dry rubber during uploading of the second cycle, P_{s1}^{up} is the stress in swollen rubber during uploading of the first cycle and P_{s2}^{up} is the stress in swollen rubber during uploading of the second cycle. In the next paragraph, the effect of swelling on the evolution of stress drop and stress-softening is discussed.

Remark 5 *It is important to remember that for the calculation of "stress drop", the stresses P_{d1}^{up} and P_{s1}^{up} have to be defined in the same configuration, e.g. unswollen-unstrained configuration.*

The stress drops exhibited by NBR and CR after immersion in B0 and B100, respectively, for 2, 5, 10, 20 and 30 days are shown in Figures 4.18 - 4.21. Note that, the stress drop in dry (non-immersed) rubbers is zero by definition.

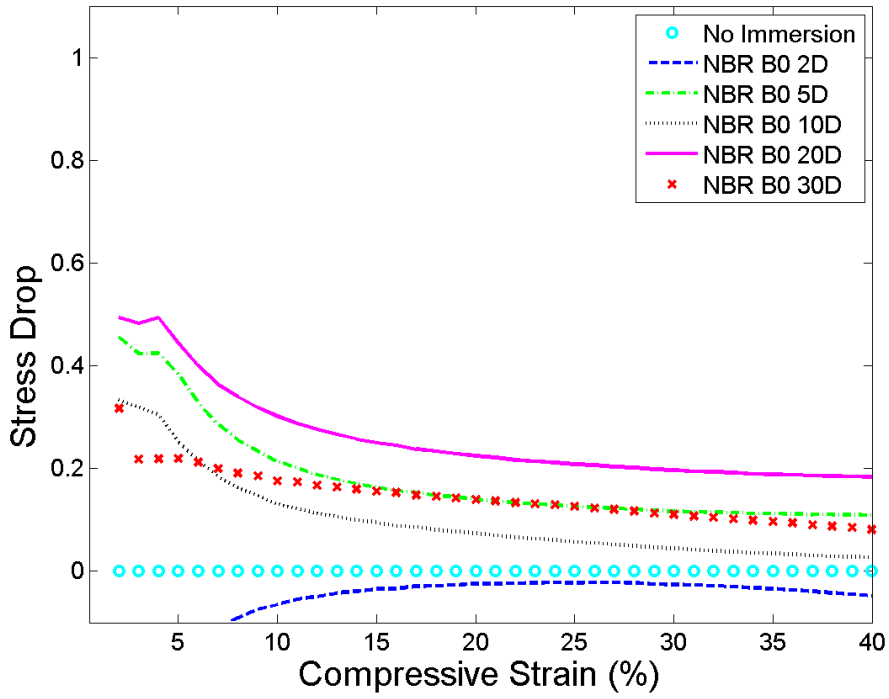

Figure 4.18: Stress drop in NBR previously immersed in B0. Results correspond to 2, 5, 10, 20 and 30 days of immersion duration.

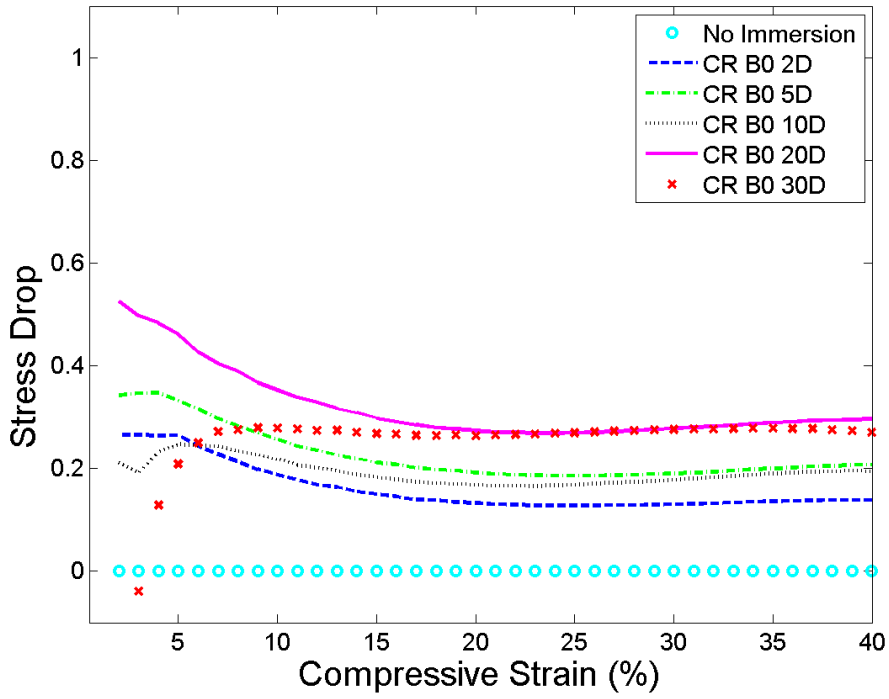

Figure 4.19: Stress drop in CR previously immersed in B0. Results correspond to 2, 5, 10, 20 and 30 days of immersion duration.

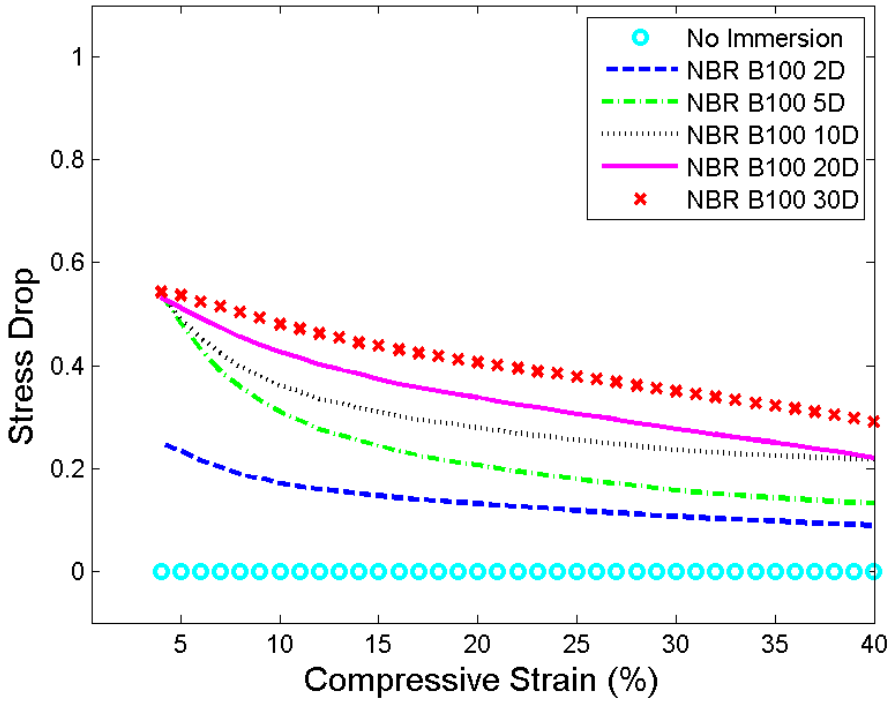

Figure 4.20: Stress drop in NBR previously immersed in B100. Results correspond to 2, 5, 10, 20 and 30 days of immersion duration.

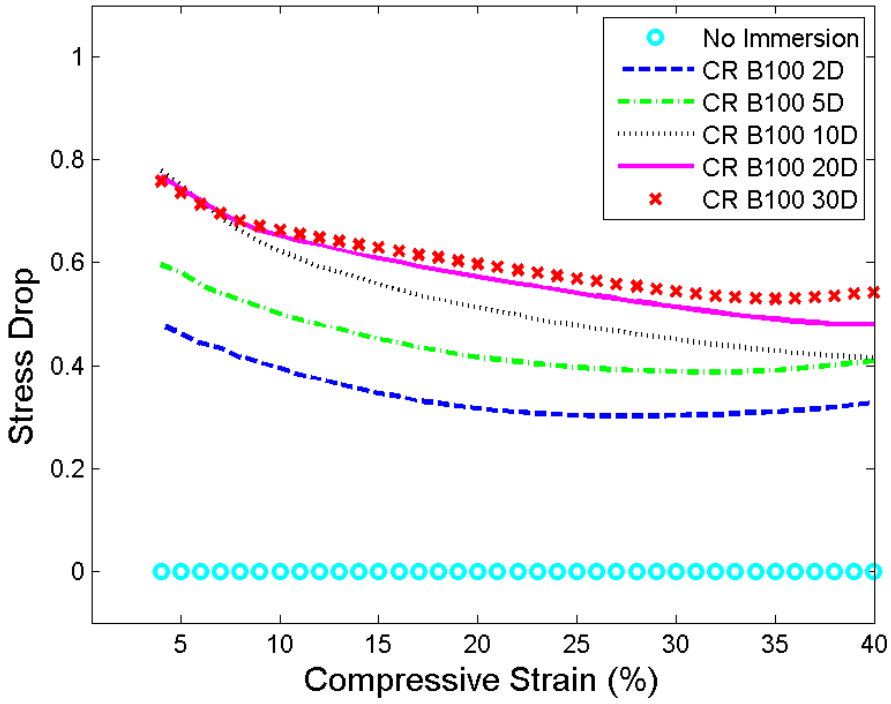

Figure 4.21: Stress drop in CR previously immersed in B100. Results correspond to 2, 5, 10, 20 and 30 days of immersion duration.

As depicted in these figures, both NBR and CR experience stress drop in the presence of liquid, either in diesel (B0) or biodiesel (B100). The stress drop appears to decrease linearly with the applied compressive strain in the range of 10% - 40% for NBR and CR immersed in B0 and 5% - 40% for NBR and CR immersed in B100 respectively. For given immersion duration, stress drop in CR after immersion (either in B0 or B100) is higher than that in NBR. As underlined by George et al. (1999), the high degree of swelling experienced by CR as shown in Figures 4.1 and 4.2 appears to contribute significantly to the decrease of its strength.

Concerning the stress-softening, it is observed that the stress-softening decreases as the strain level approaches the maximum strain previously endured by the material as classically observed in rubber under cyclic loading conditions (Diani et al., 2009). Unlike the stress drop, an opposite trend is found in stress-softening, i.e. the presence of liquids (swelling) decreases the stress-softening as can be seen in Figures 4.22 - 4.25. While in the case of NBR after immersion in B0 and B100, this trend is easily observed, in the case of CR it is less noticeable. Indeed, for relatively low compressive strains, discrepancies are found in CR previously immersed in B100 during 5, 10 and 20 days. While the exact reason of these discrepancies is not known, it could be attributed to the fact that at low compressive strain, the stress P_{s1}^{up} is so small that the corresponding level of stress-softening cannot be correctly described by Equation $(4.4)_2$.

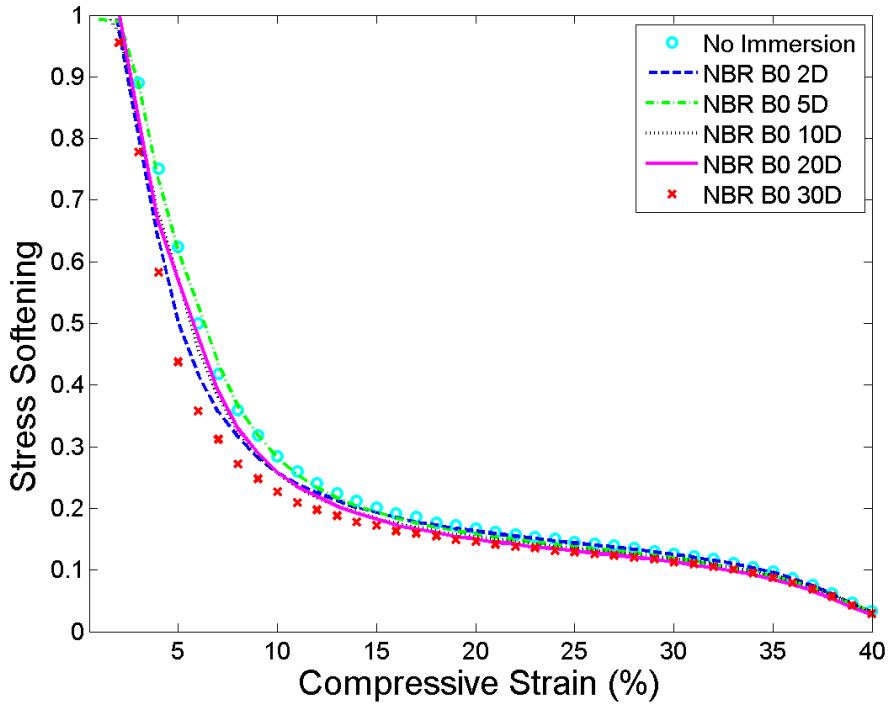

Figure 4.22: Stress-softening in NBR previously immersed in B0. Results correspond to 2, 5, 10, 20 and 30 days of immersion duration.

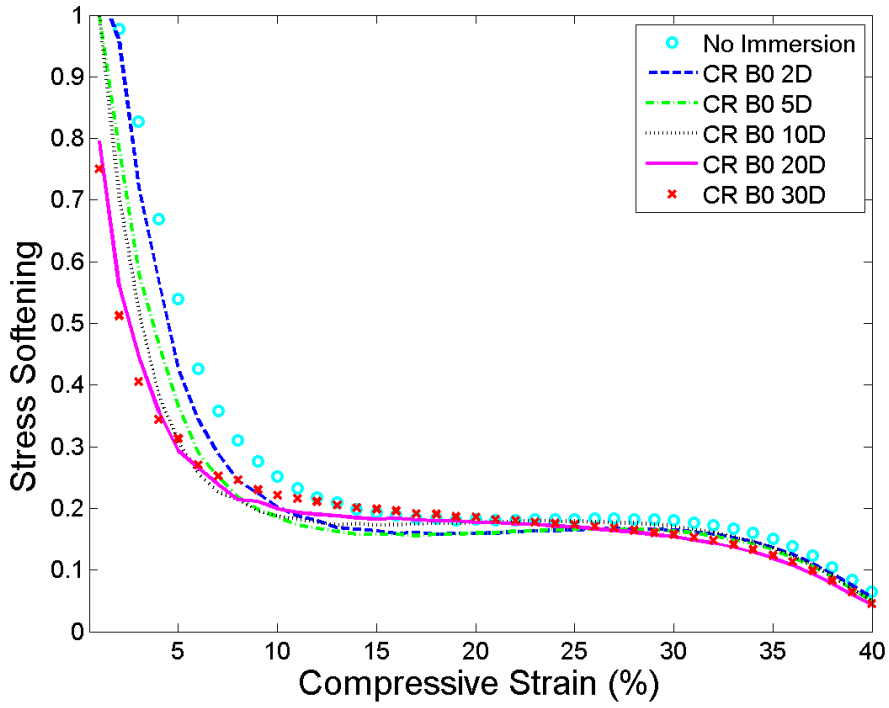

Figure 4.23: Stress-softening in CR previously immersed in B0. Results correspond to 2, 5, 10, 20 and 30 days of immersion duration.

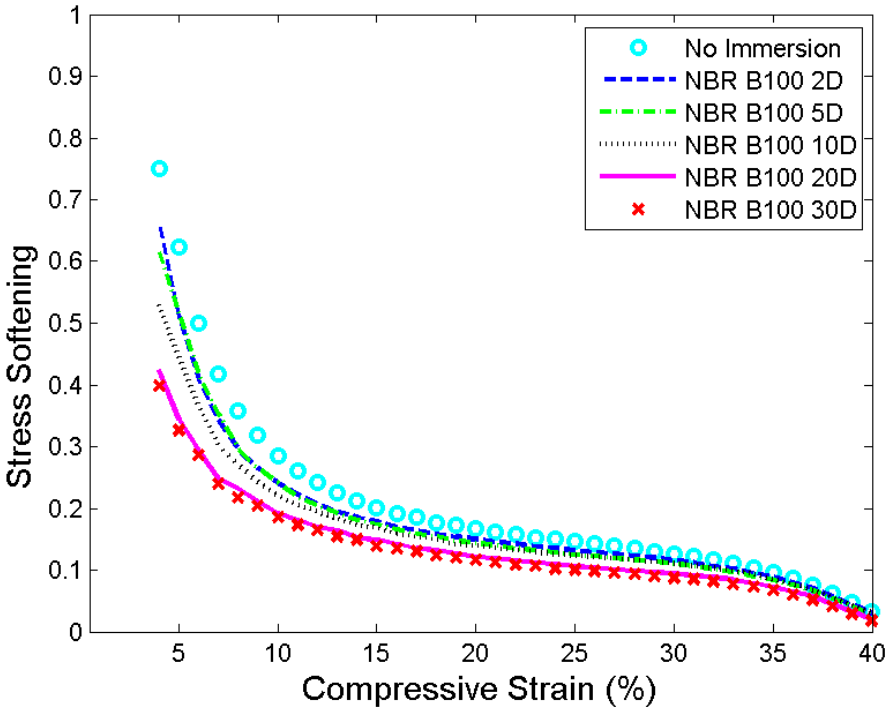

Figure 4.24: Stress-softening in NBR previously immersed in B100. Results correspond to 2, 5, 10, 20 and 30 days of immersion duration.

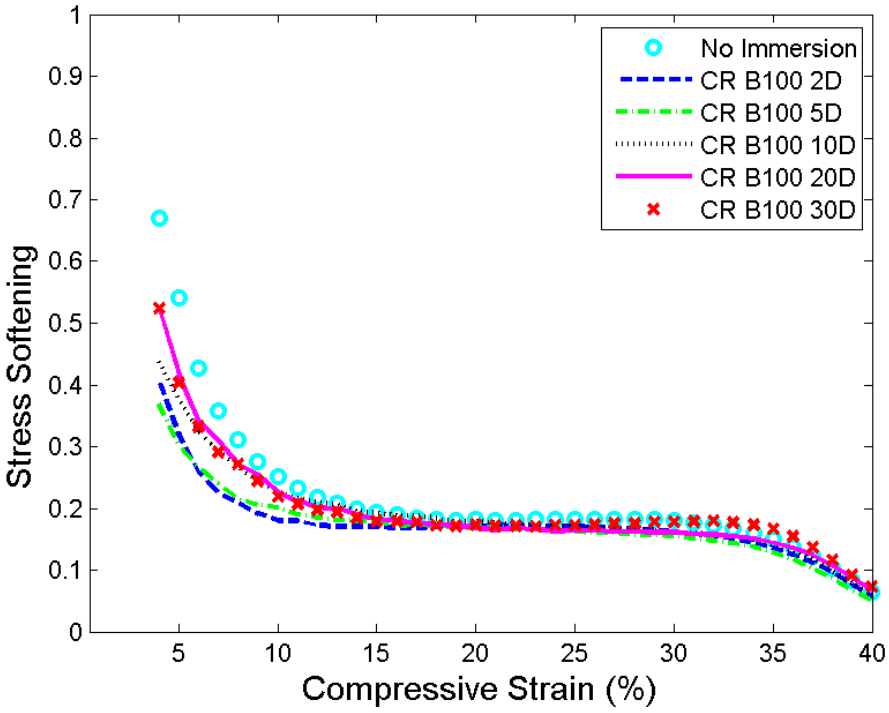

Figure 4.25: Stress-softening in CR previously immersed in B100. Results correspond to 2, 5, 10, 20 and 30 days of immersion duration.

4.1.2 (c) Hysteresis

The hysteresis in our materials is found to stabilize after five cycles of loading (see Figures 4.3 and 4.4). In order to investigate the effect of swelling on hysteresis of elastomers, the amount of hysteresis loss ratio at different immersion durations and different tested fuel is investigated.

Following Bergström and Boyce (1998), the hysteresis loss ratio is calculated from the stabilized hysteresis (after the fifth cycle). In the following, the hysteresis loss ratio is defined by:

$$\text{Hysteresis loss ratio} = \frac{H_5}{E_s} \tag{4.5}$$

where H_5 is the amount of hysteresis (dissipated energy, given by the difference of the area under the uploading and the unloading path of stress-strain curve) and E_s is the supplied energy during uploading (given by the area under the uploading path of the stress-strain curve) as depicted in Figure 4.26.

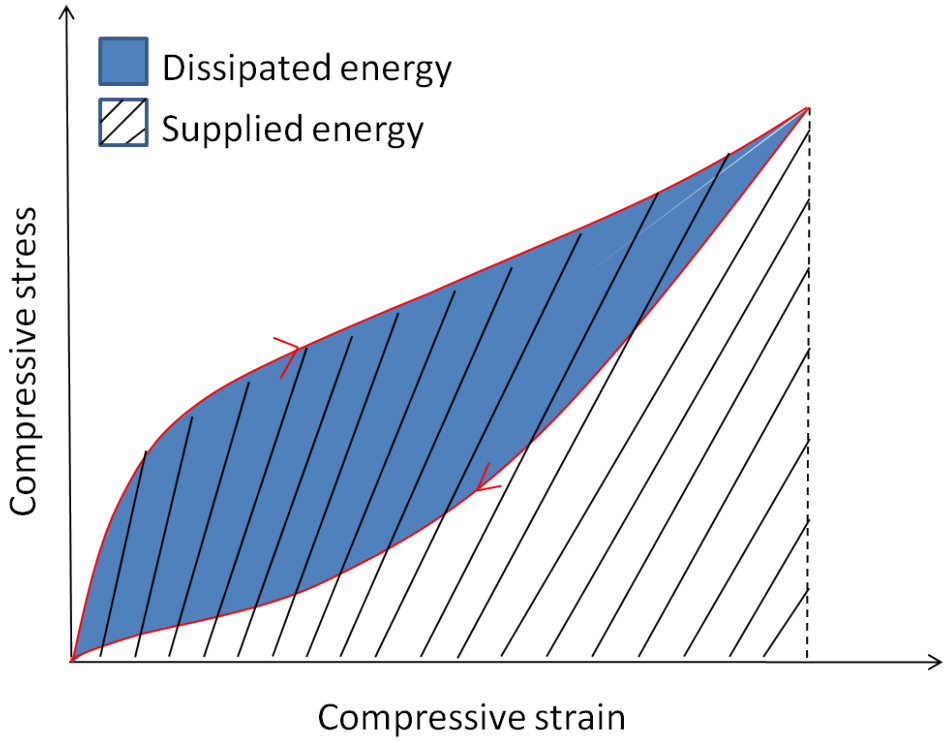

Figure 4.26: Definition of hysteresis loss ratio.

Figure 4.27 depicts the hysteresis loss ratio in NBR and CR after immersion in B0 and B100 for different immersion durations. The plot clearly indicates that for both NBR

and CR the hysteresis loss ratio decreases when the immersion duration increases, i.e. when swelling increases. The change in hysteresis loss ratio is the least in NBR swollen by B0, only decreased by 16% after 30 days immersion. Initially at dry state, CR has higher hysteresis loss ratio. As swelling occurs, the hysteresis loss ratio in CR decreases significantly and becomes consistently lower than that of NBR. Indeed, when the immersion duration is increased to 30 days, the hysteresis loss ratio in CR swollen by B100 decreases by 84% from 0.278 (dry state) to as low as to 0.045 (swollen state). In the case of NBR in B100, the hysteresis loss ratio decreases by 66% from 0.236 (dry state) to 0.081 (swollen state). These results highlight the decrease of viscous effect in elastomers as degree of swelling increases. Note that in the context of fatigue, Cho et al. (2000) attributes the increase of fatigue crack growth in swollen rubbers (decrease in fatigue life) to the decrease of hysteresis.

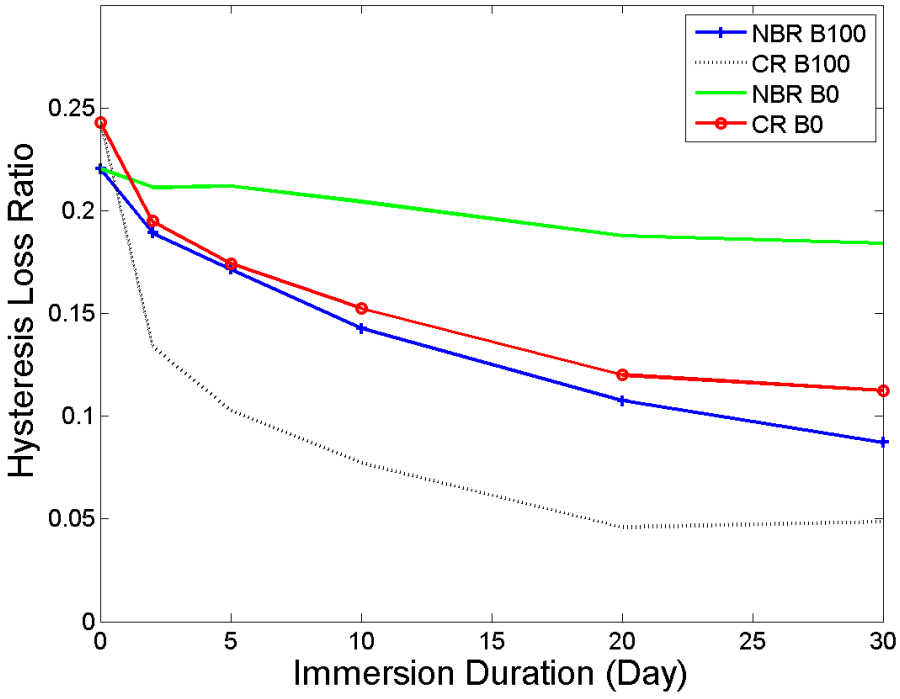

Figure 4.27: Hysteresis loss ratio in NBR and CR under cyclic compressive loading at 40% maximum strain. Results correspond to 2, 5, 10, 20 and 30 days of immersion duration in B0 and B100 respectively.

4.1.2 (d) Stress-relaxation

The effect of the biodiesel diffusion on the time-dependent behavior of the elastomeric materials can be probed with experiments illustrated in the inset of Figure 4.28.

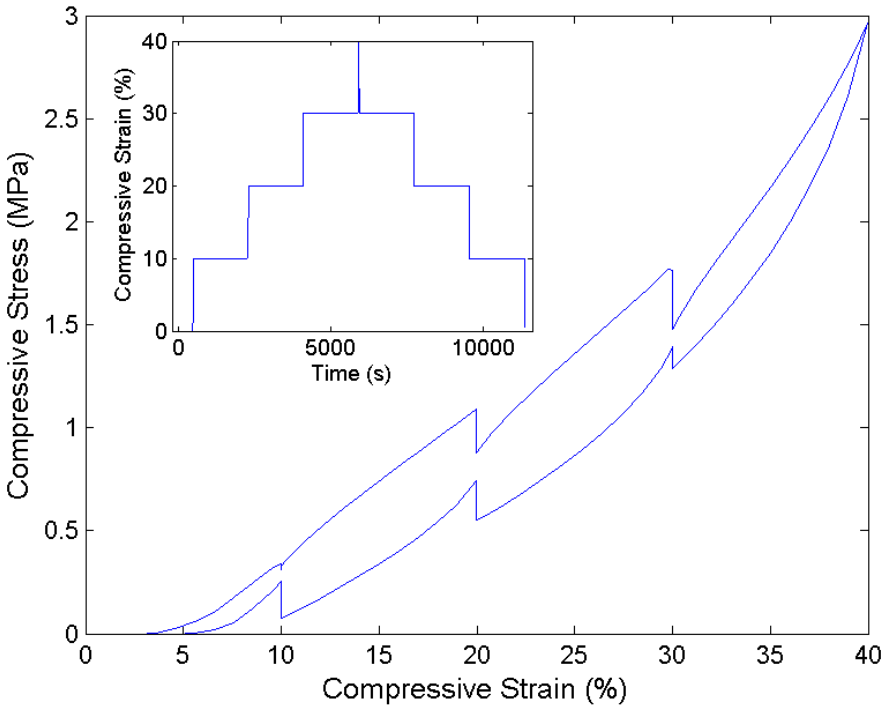

Figure 4.28: Engineering stress-strain response of dry NBR under multi step relaxation test at 0.1 mms^{-1} displacement rate.

In this experiment, after the specimen was pre-conditioned with six cycles of compressive loading to a maximum compressive strain level of 40%, the multi-relaxation tests at strain levels of 10, 20 and 30% were conducted during the uploading and unloading. Similar tests were conducted for dry elastomers by Lion (1997) and Bergström and Boyce (1998) among others. It is observed that the compressive stress decreases during the relaxations in the uploading and increases during the relaxations in the unloading approaching what appears to be an equilibrium state (Bergström & Boyce, 1998) as depicted in Figure 4.28.

Further investigation of the stress relaxation is presented in Figures 4.29 to 4.32 where the normalized stress is plotted as a function of relaxation duration for different immersion durations.

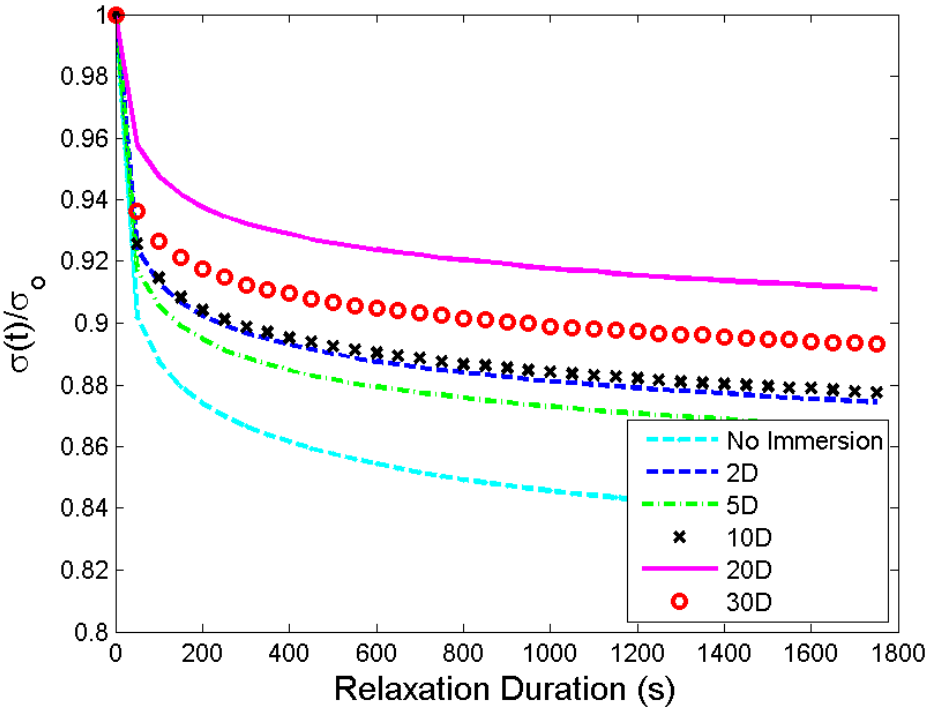

Figure 4.29: Stress relaxation of NBR under compressive strain levels of 30% during 1800 s. Results correspond to 2, 5, 10, 20 and 30 days of immersion in B0.

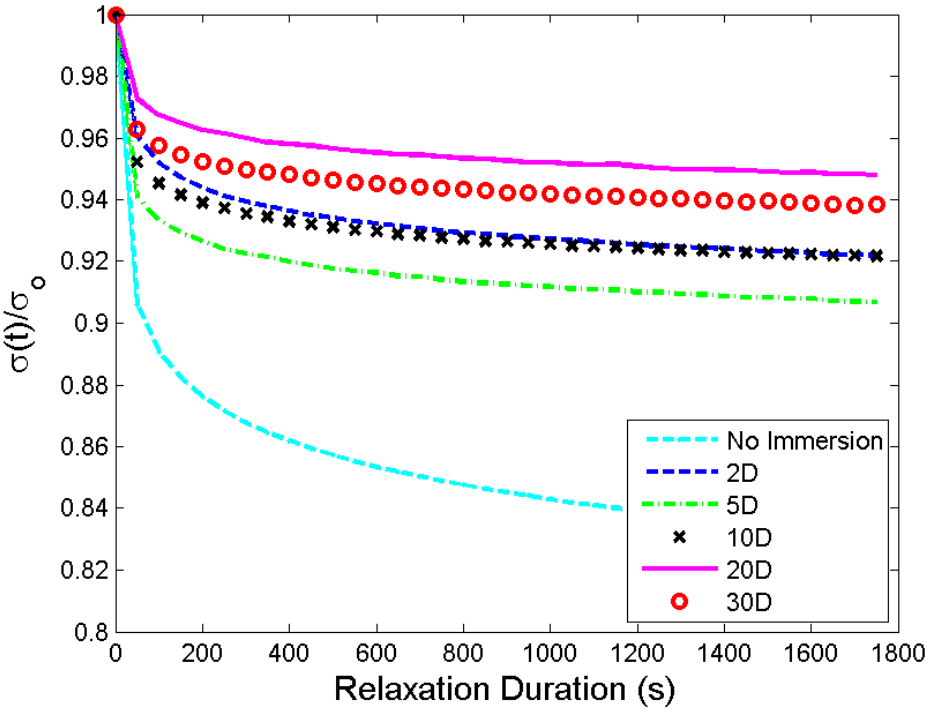

Figure 4.30: Stress relaxation CR under compressive strain levels of 30% during 1800 s. Results correspond to 2, 5, 10, 20 and 30 days of immersion in B0.

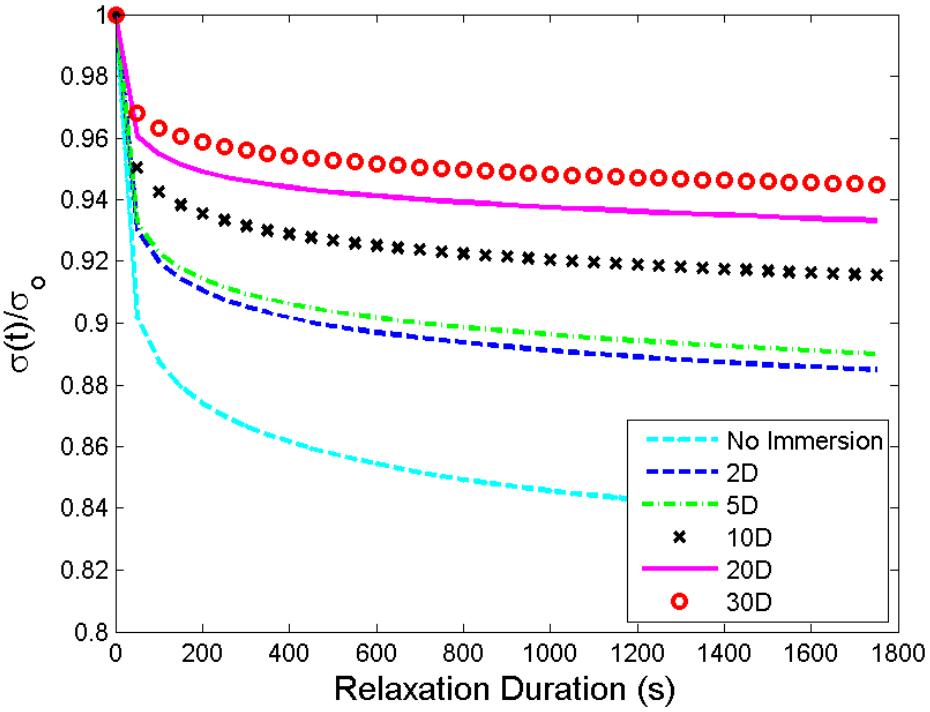

Figure 4.31: Stress relaxation of NBR under compressive strain levels of 30% during 1800 s. Results correspond to 2, 5, 10, 20 and 30 days of immersion in B100.

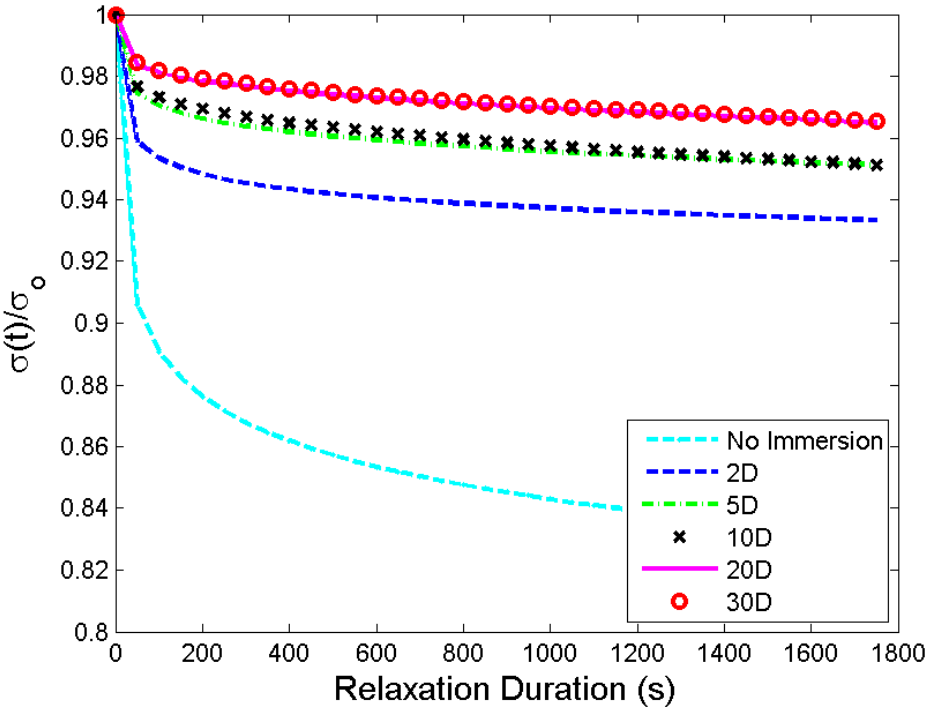

Figure 4.32: Stress relaxation of CR under compressive strain levels of 30% during 1800 s. Results correspond to 2, 5, 10, 20 and 30 days of immersion in B100.

In these figures, the normalized stress is defined by the ratio between the value of stress during relaxation at specific time, $\sigma(t)$ and the maximum stress achieved at the beginning of the corresponding relaxation, σ_o. Only stress relaxation at strain level of 30% during uploading is presented, since the stress relaxation at other strain levels give qualitatively similar results. As clearly shown, the graphs in Figures 4.29 to 4.32 show similar trends. The presence of liquids (swelling) appears to render the material under loading to become closer to the equilibrium state, i.e. the viscous (time-dependent) contribution to the macroscopic mechanical response of material becomes smaller which is consistent with the results of the hysteresis discussed in the previous subsection. Indeed, after 1800 s of relaxation, the stress decreases by the amount of 16% for dry NBR and by 6% when the specimen is immersed in B100 for 30 days. While for CR, the stress only decreases by 3% after immersion for 30 days whereas the stress in dry CR decreased by 17% after 1800 s of relaxation. In the case of NBR after 30 days of immersion in B0, the stress decays the most, to 11% showing that the viscous effect in the rubber is still preserved. As emphasized by Radhakrishnan Nair (1997); Wypych (2004), the palm biodiesel appears to act as lubricant facilitating movement of the polymer chain segments. The distances between the molecules become lesser (physical bonds become weaker).

4.1.3 SEM results

Figure 4.33 shows the micrographs of the cross sectional surface of the dry and swollen elastomers after immersion in B0 and B100 for 5 days and 30 days, respectively. The cross sectional surface of swollen CR shows larger voids than swollen NBR and dry CR and NBR.

NBR in diesel shows an insignificant effect compared to those in B100. Larger voids were found in NBR and CR after swollen in biodiesel. As pointed out by Ismail, Nordin, and Noor (2002), weak filler-matrix interaction is indicated by the presence of many holes or loose fillers on the cross-sectional surface as shown by swollen CR in B100. On the other hand, the void formation could be the result of the introduction of polar oxygen groups into elastomers or cross-linking or macromolecule chain scission (Haseeb et al., 2010). The microstructural changes can be attributed to the increasing surface energy, subsequently leading to localized decreases or increases in density, which will

cause the creation of voids, cracks or pits. In addition, freezing a large amount of stress energy in the polymer can cause crack formation in the rubber (Miller-Chou & Koenig, 2003). According to Ueberreiter (1968), elastomer can be dissolved in solvent either by exhibiting a thick swollen layer or by undergoing extensive cracking, depending on the osmotic pressure stress release rate that builds up in the polymer matrix. In other words, elastomers that exhibit more swelling or cracking tend to dissolve during immersion. Therefore, nitrile rubber and polychloroprene show more cracks and voids in B100 than in B0 due to higher solubility in palm biodiesel.

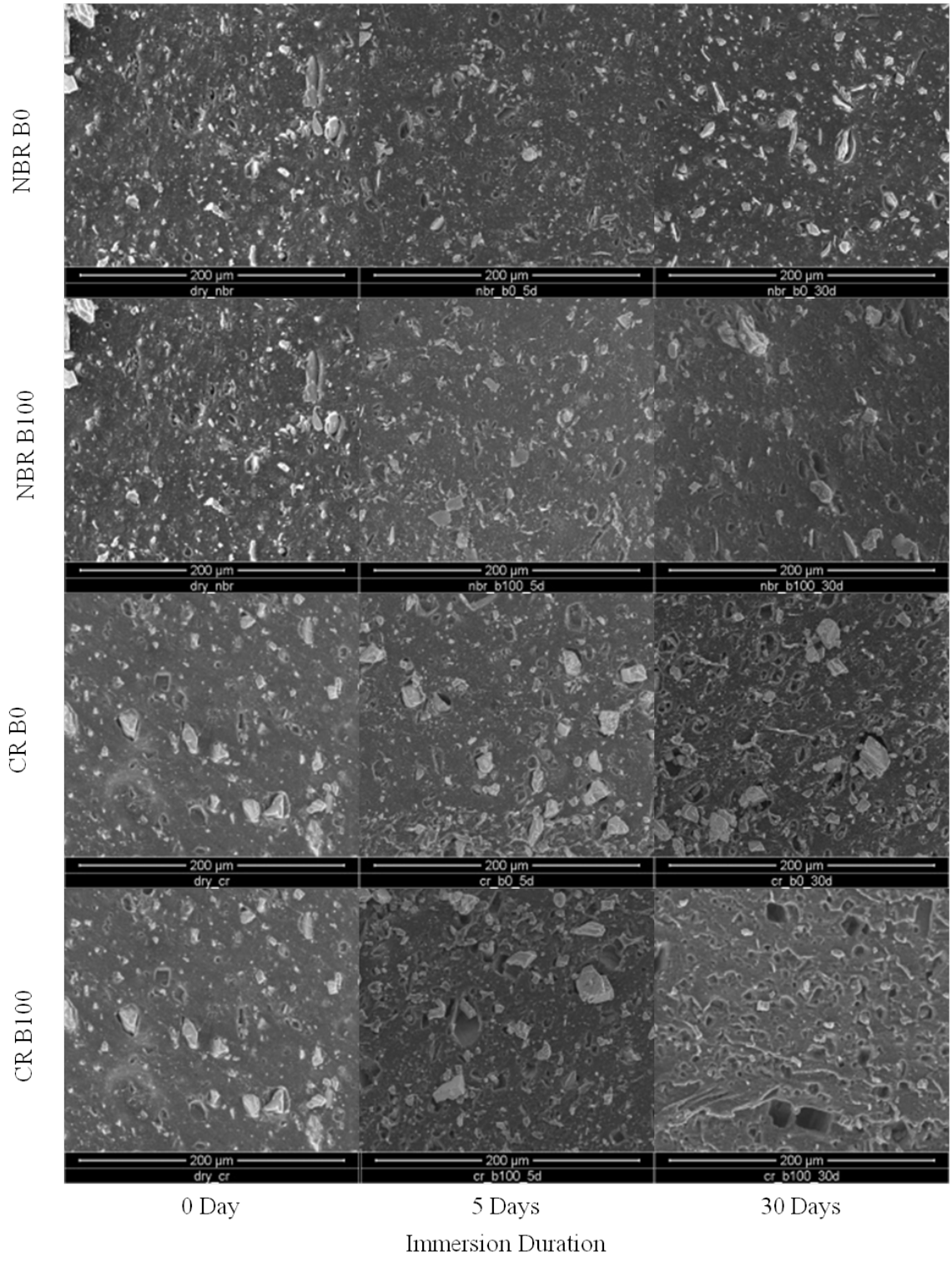

Figure 4.33: SEM images of the cross sectional surface of the dry and swollen elastomers after immersed in B0 and B100 for 5 and 30 days respectively, X500.

4.2 Results of swelling tests on uniaxially-stressed specimens

4.2.1 Mass and volume changes

To determine the effect of static mechanical loading on swelling behavior of NBR and CR specimens, the swelling test is conducted by initially constrained the specimens at different compressive strains using a compression device and subsequently immersing into different biodiesel blends for 30 and 90 days. Figures 4.34 to 4.41 show the percentage of mass change and volume change of NBR and CR with different compressive strains (2%, 10% and 20%) after immersion in different biodiesel blends (B0, B25, B75 and B100) for 30 and 90 days respectively.

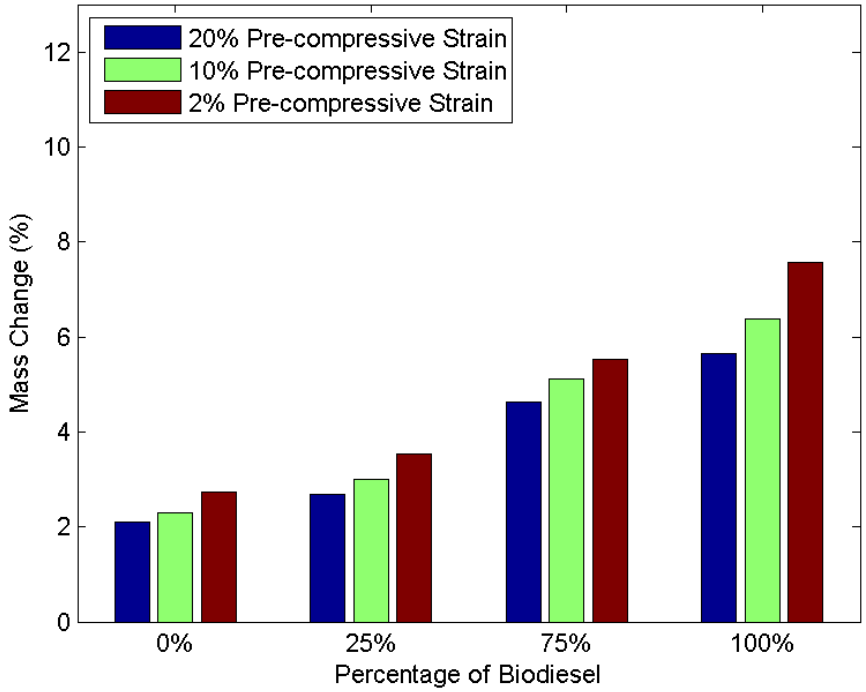

Figure 4.34: Mass change of NBR at different compressive strains after 30 days immersion in different percentage of biodiesel blends.

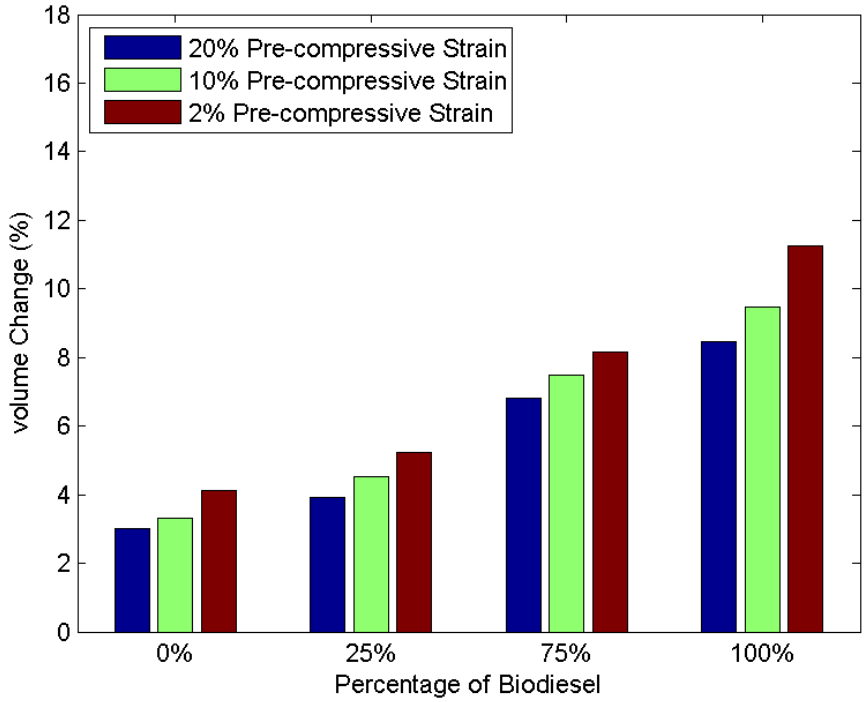

Figure 4.35: Volume change of NBR at different compressive strains after 30 days immersion in different percentage of biodiesel blends.

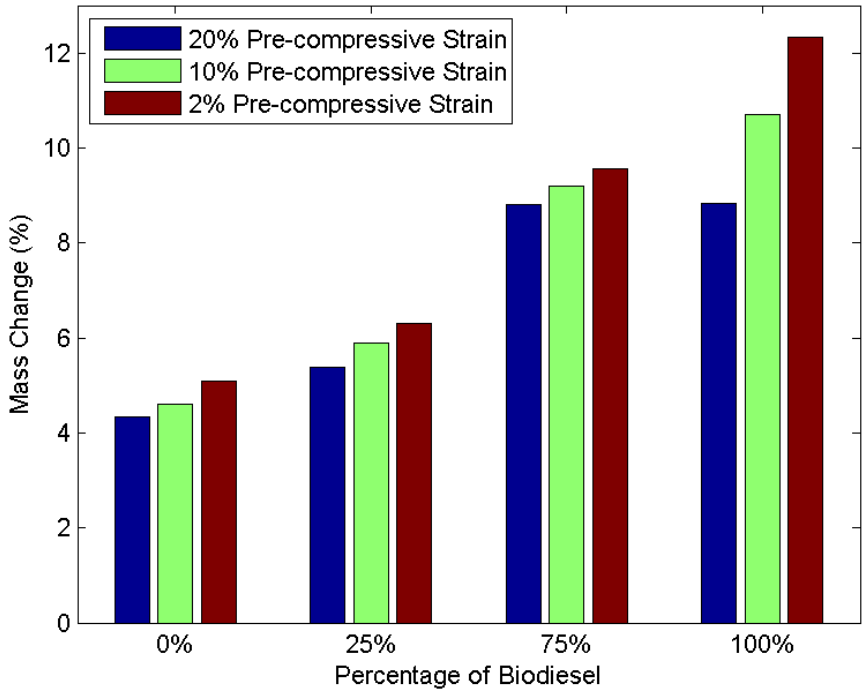

Figure 4.36: Mass change of NBR at different compressive strains after 90 days immersion in different percentage of biodiesel blends.

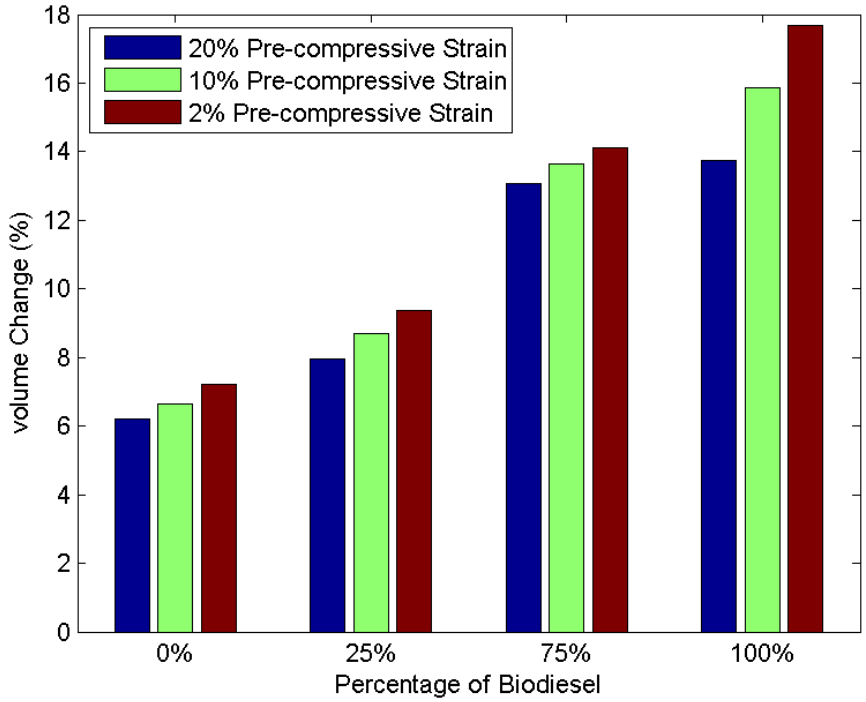

Figure 4.37: Volume change of NBR at different compressive strains after 90 days immersion in different percentage of biodiesel blends.

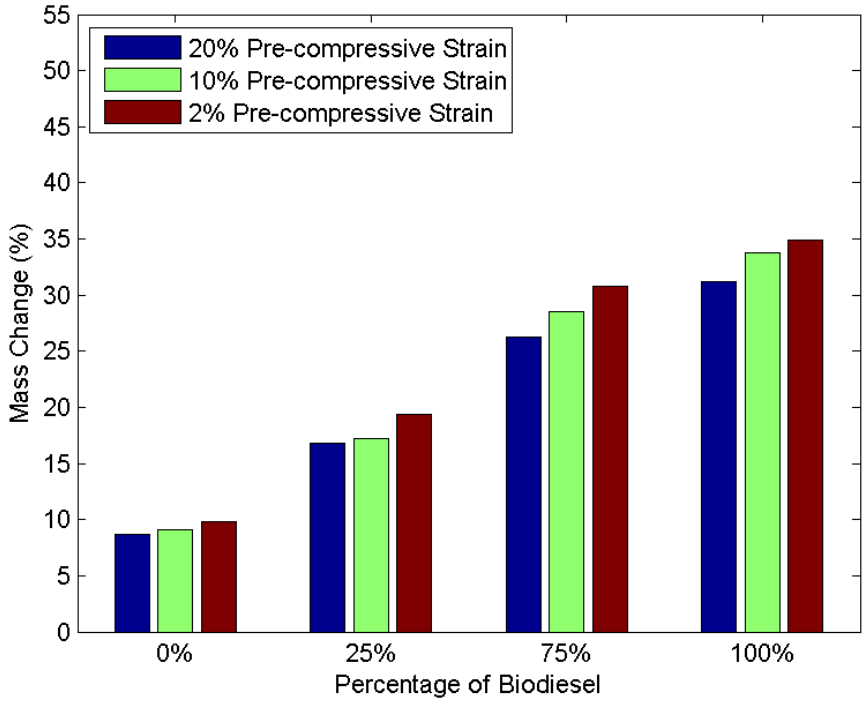

Figure 4.38: Mass change of CR at different compressive strains after 30 days immersion in different percentage of biodiesel blends.

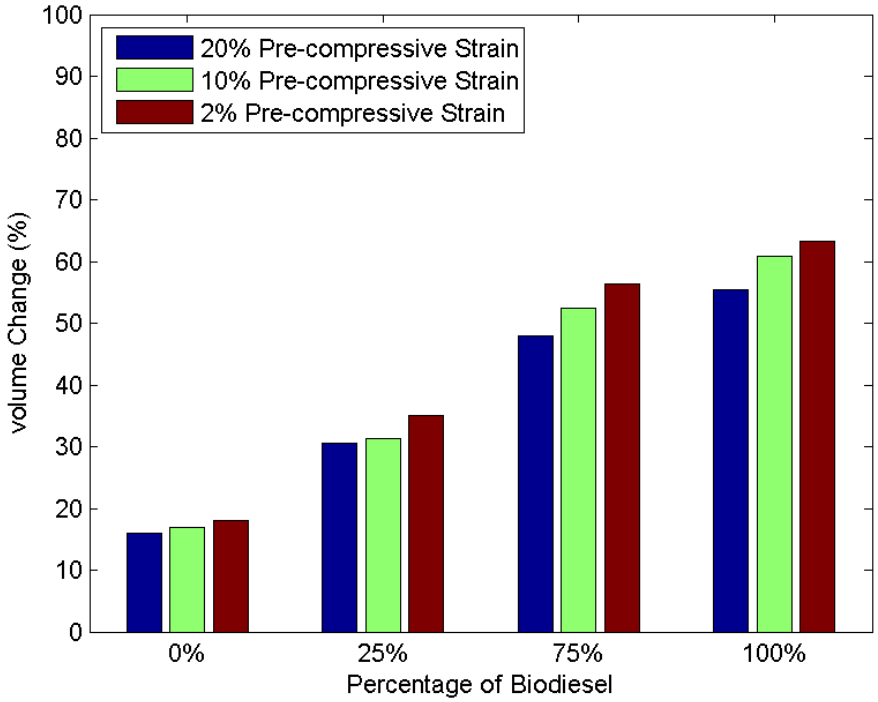

Figure 4.39: Volume change of CR at different compressive strains after 30 days immersion in different percentage of biodiesel blends.

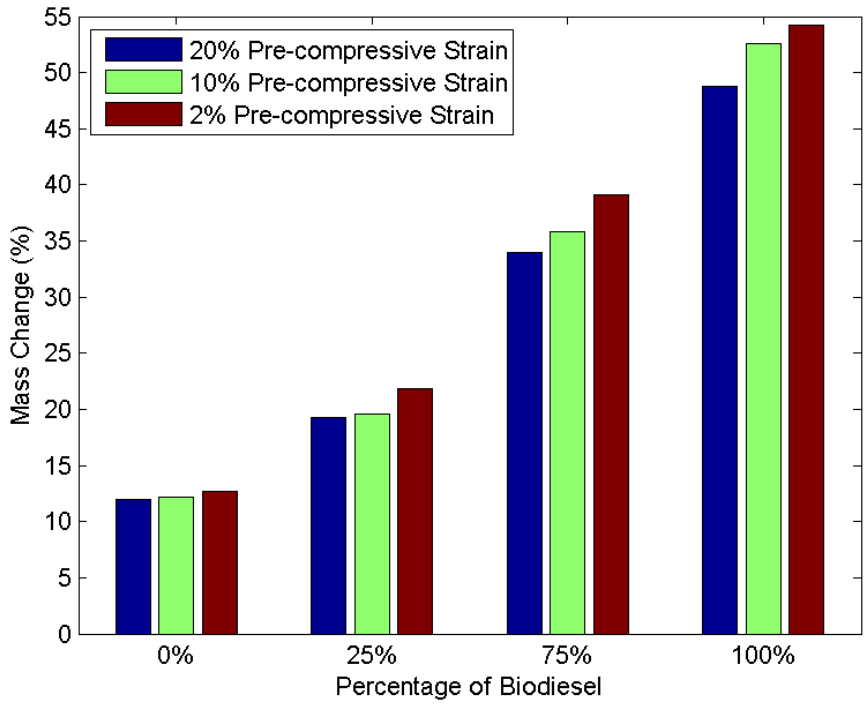

Figure 4.40: Mass change of CR at different compressive strains after 90 days immersion in different percentage of biodiesel blends.

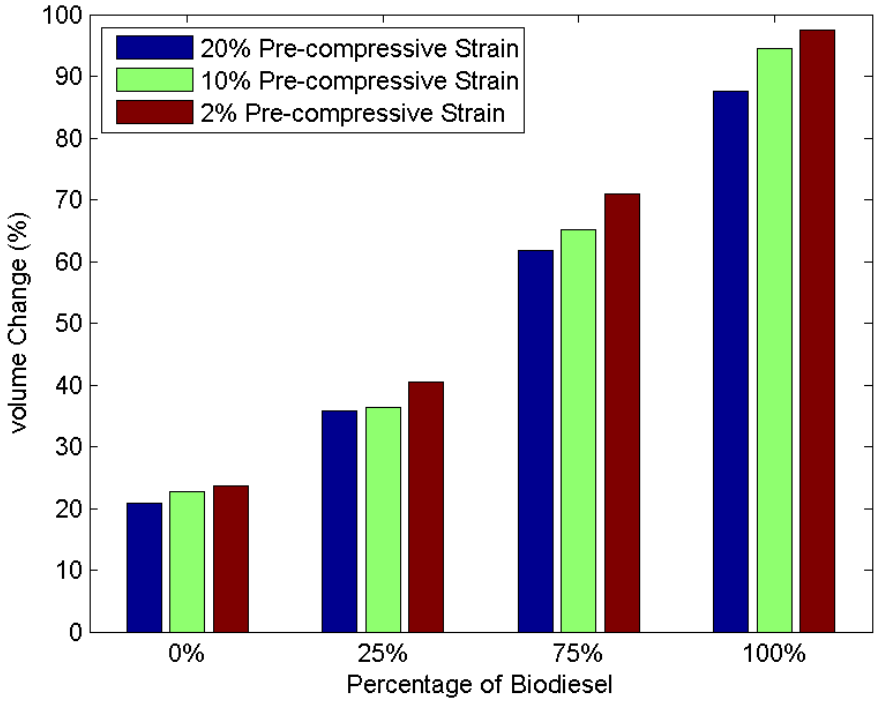

Figure 4.41: Volume change of CR at different compressive strains after 90 days immersion in different percentage of biodiesel blends.

All the plots show similar patterns. Both NBR and CR show increases in mass and volume change when the exposure time is increased from 30 to 90 days. The percentage of fuel uptake is increasing with the increase of palm biodiesel content. It is clear that for low biodiesel content (B0 and B25) no significant fuel uptake (less than 10% mass and volume change) is recorded for NBR. At higher percentage of biodiesel content (B100), both NBR and CR show significant mass and volume change. The corresponding trend can be attributed to the segmental mobility of the polymer and free volume of the polymer (George & Thomas, 2001).

Generally, it is also observed that the fuel uptake is affected by the level of pre-compression. The increase of pre-compressive strain has restricted the fuel uptake into the elastomeric material, i.e. the compressive stress appears to reduce the amount of swelling compared to that for stress-free rubber. As the compressive strain increases, the effective area for diffusion to occur along the radial direction in hollow cylindrical rubber specimens becomes smaller. Hence, the resulting swelling is lower. Furthermore, the reduction in swelling of rubber is affected by the hydrostatic component of the applied

stress (Treloar, 1975; Fukumori et al., 1990). According to the authors, a compressive stress, for which the hydrostatic components is positive, leads to a decrease in the swelling of rubber. In the next subsection, only results that correspond to 2% pre-compressive strain are presented since the pre-compressive strain of 2% yields the highest degree of swelling.

4.2.2 Mechanical response

The stress-strain curves of dry and swollen NBR and CR under cyclic compressive loading at two different maximum compressive strains are illustrated in Figures 4.42 and 4.43. For each maximum compressive strain, the specimen experiences six cycles of loading. It is shown that there is not much difference in the nature of stress-strain behavior after immersion. However, lower stress is recorded for CR after 90 days immersion given the same pre-compressive strain. The corresponding behavior can be related to the swelling in the CR which decreases its strength due to strong interaction of rubber-solvent matrix system (George et al., 1999).

Under cyclic loading conditions, both dry NBR and CR exhibit significant inelastic responses, i.e. mechanical hysteresis and stress-softening. Though a number of works are devoted to the understanding of this stress-softening, no general agreement has been reached either on the physical source or on the mechanical modeling of this softening at the microscopic or meso-scopic scales (Diani et al., 2009). Similar to the observation from stress-free swollen specimens, when uniaxially-stressed NBR and CR are in swollen state, the above inelastic responses decrease significantly, i.e. smaller hysteresis and stress-softening are observed. The following paragraphs focus only on stress responses that correspond to maximum cyclic compressive strain of 30% since the data at larger strain shows similar trend.

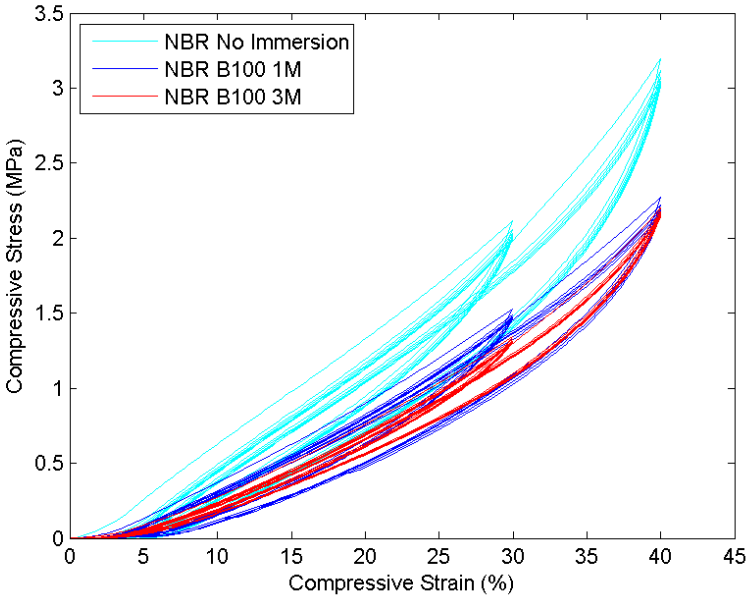

Figure 4.42: Stress-strain curves of NBR at dry states (without immersion) and after 30 days (1M) and 90 days (3M) immersion in B100. Results correspond to pre-compressive strain of 2%. For immersed rubbers, the stress is expressed with respect to the *swollen-unstrained* configuration (initial swollen cross section).

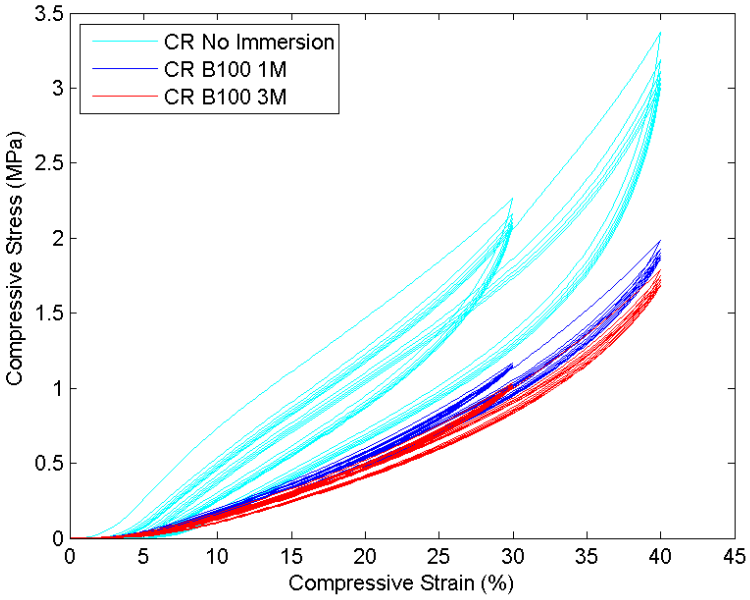

Figure 4.43: Stress-strain curves of CR at dry states (without immersion) and after 30 days (1M) and 90 days (3M) immersion in B100. Results correspond to pre-compressive strain of 2%. For immersed rubbers, the stress is expressed with respect to the *swollen-unstrained* configuration (initial swollen cross section).

4.2.2 (a) Nature of swelling

Following the methods used to evaluate the nature of swelling of stress-free specimens proposed in Section 4.1.2 (a), the five methods are compared using stress-strain data obtained from uniaxially-stressed swollen rubbers. In Figures 4.44 to 4.47, the shear modulus ratios obtained using M-1, M-2 and M-3 methods are plotted as a function of applied compressive strain for NBR and CR immersed in B0 and B100 respectively. In each graph, results that correspond to 30 days (1M) and 90 days (3M) immersion are presented. Similarly, in Figures 4.48 to 4.51, shear modulus ratios are plotted, but this time using M-1, M-4 and M-5 methods.

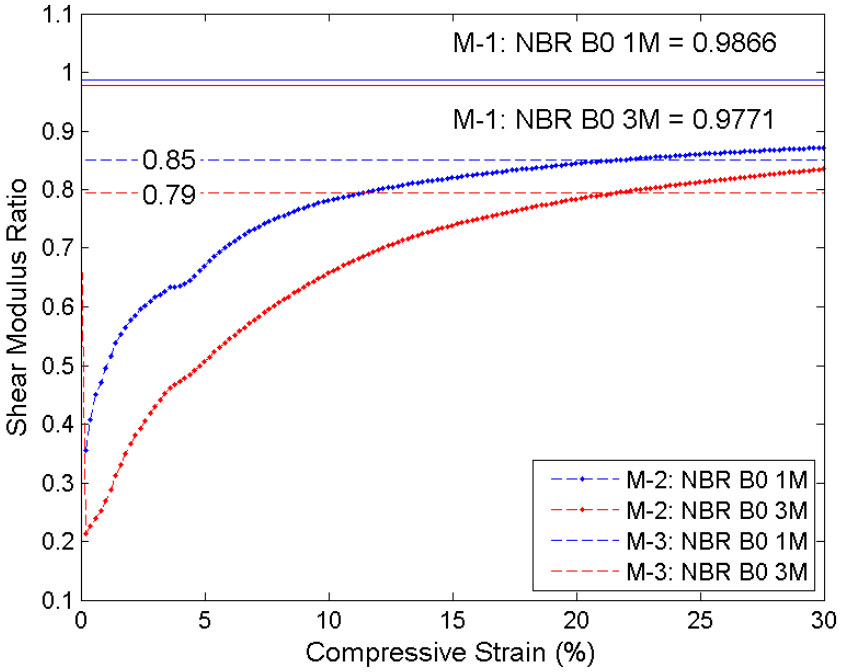

Figure 4.44: Shear modulus ratio obtained using M-1, M-2 and M-3 methods as a function of applied compressive strain for NBR after immersion in B0. Results correspond to 2% pre-compressive strain.

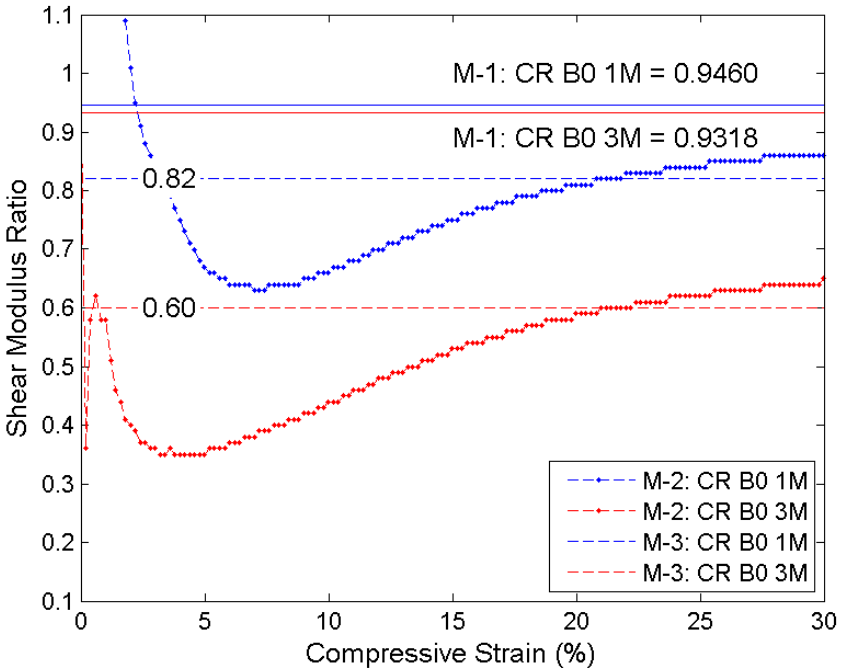

Figure 4.45: Shear modulus ratio obtained using M-1, M-2 and M-3 methods as a function of applied compressive strain for CR after immersion in B0. Results correspond to 2% pre-compressive strain.

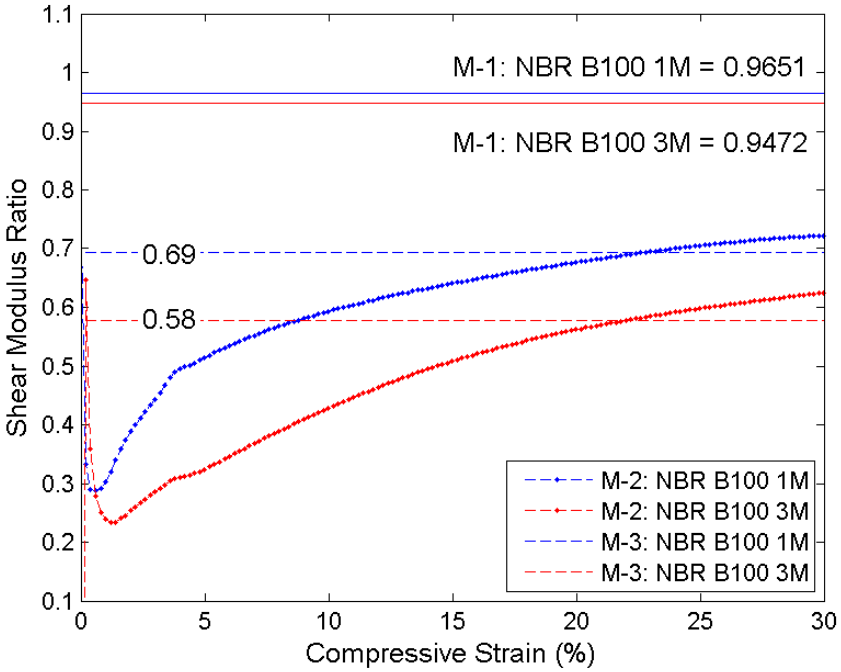

Figure 4.46: Shear modulus ratio obtained using M-1, M-2 and M-3 methods as a function of applied compressive strain for NBR after immersion in B100. Results correspond to 2% pre-compressive strain.

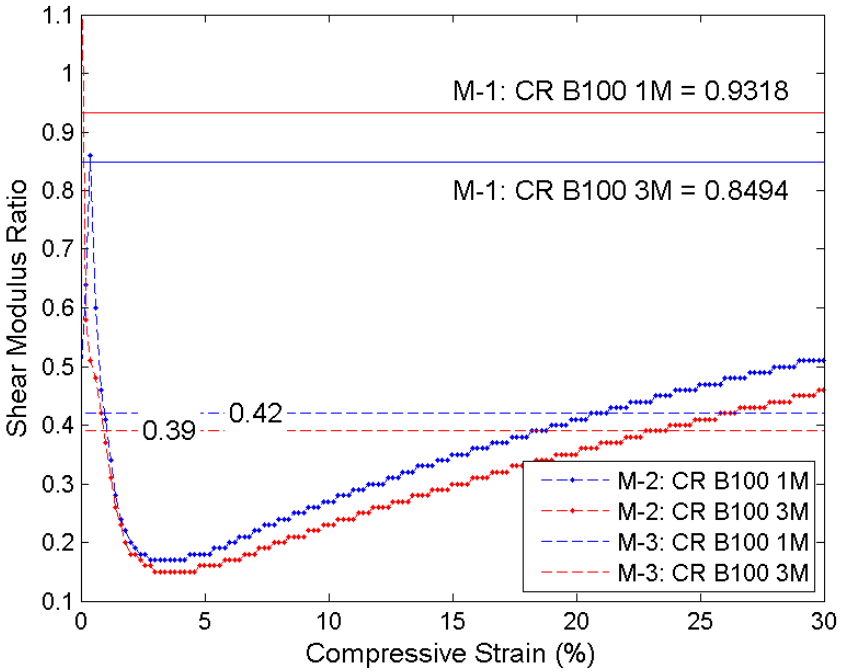

Figure 4.47: Shear modulus ratio obtained using M-1, M-2 and M-3 methods as a function of applied compressive strain for CR after immersion in B100. Results correspond to 2% pre-compressive strain.

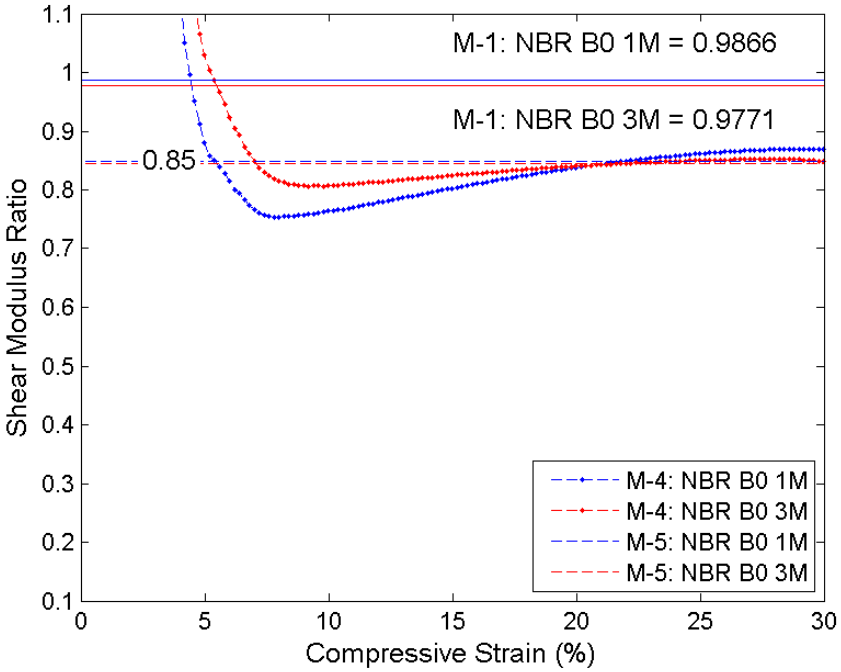

Figure 4.48: Shear modulus ratio obtained using M-1, M-4 and M-5 methods as a function of applied compressive strain for NBR after immersion in B0. Results correspond to 2% pre-compressive strain.

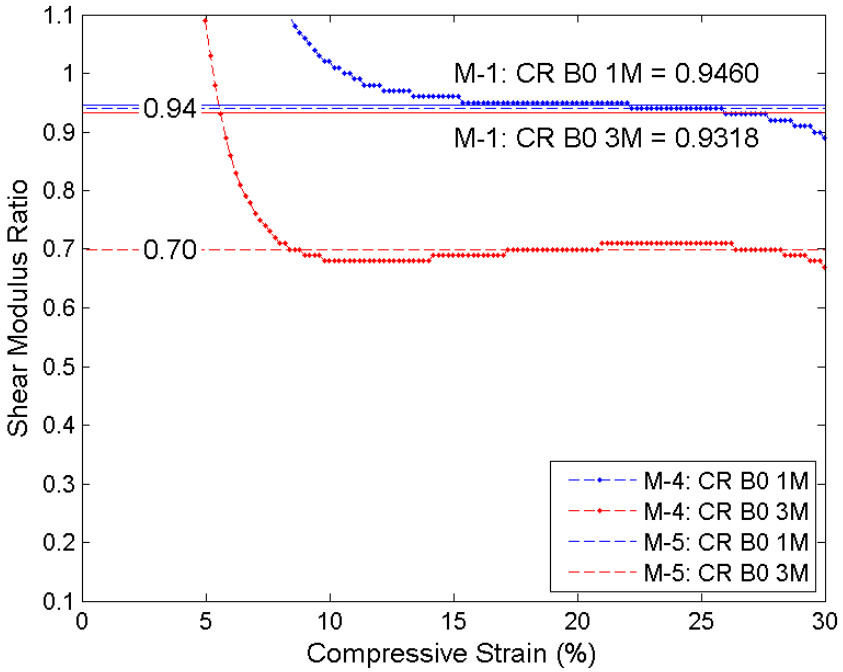

Figure 4.49: Shear modulus ratio obtained using M-1, M-4 and M-5 methods as a function of applied compressive strain for CR after immersion in B0. Results correspond to 2% pre-compressive strain.

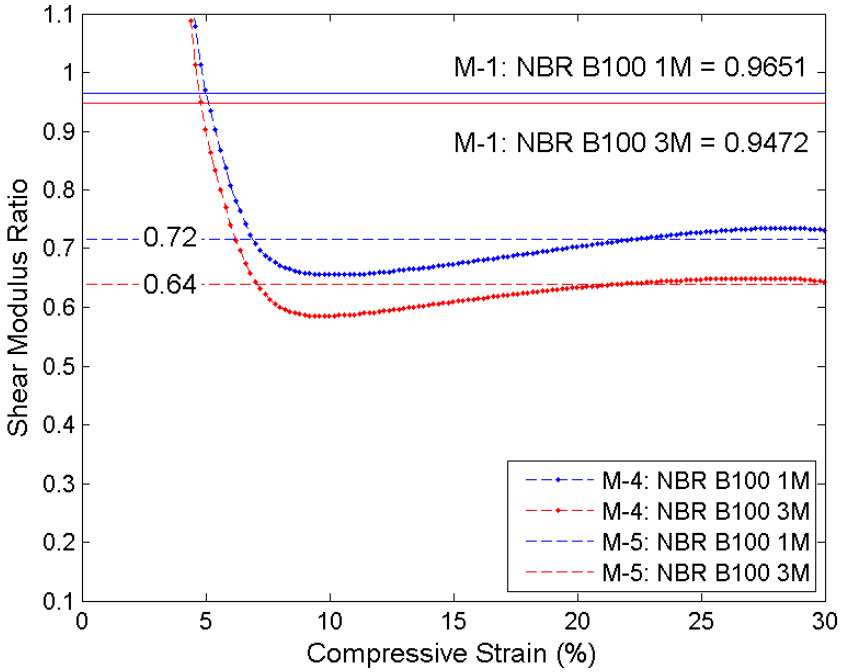

Figure 4.50: Shear modulus ratio obtained using M-1, M-4 and M-5 methods as a function of applied compressive strain for NBR after immersion in B100. Results correspond to 2% pre-compressive strain.

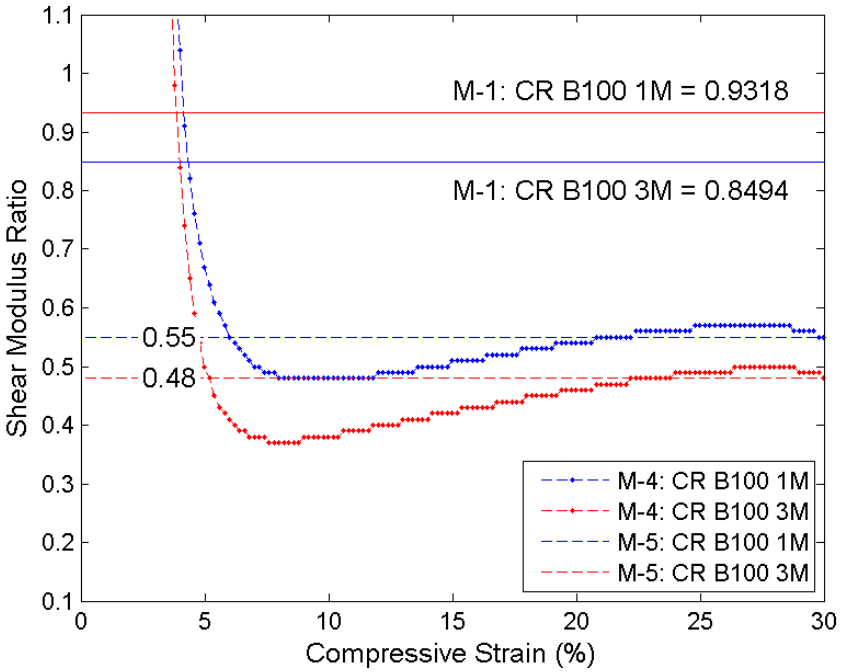

Figure 4.51: Shear modulus ratio obtained using M-1, M-4 and M-5 methods as a function of applied compressive strain for CR after immersion in B100. Results correspond to 2% pre-compressive strain.

Similar to the results obtained from the stress-free swollen rubbers, as depicted in Figures 4.44 to 4.51, it is found that the shear modulus ratio deviates from the cube root of the swelling ratio as predicted by Treloar, i.e. results obtained using M-2, M-3, M-4 and M-5 methods are different from those obtained from M-1. Regardless of the type of rubber and the method considered, qualitatively similar results are obtained from the uniaxially-stressed swollen rubbers:

1. The deviation from Treloar theory in the shear modulus ratio resulting from immersion in B100 is systematically larger than the one resulting from immersion in B0.

2. Increasing the duration of immersion from 1 month to 3 months increases the corresponding deviation.

3. The shear modulus ratios calculated using the estimated equilibrium stress response, i.e. M-4 and M-5, appear to give closer values to the one predicted by Treloar than using the first uploading stress response, i.e. M-2 and M-3.

4.2.2 (b) Stress drop

Using Equation 4.3, the stress drops for the uniaxially-stressed specimens is calculated. Figures 4.52 to 4.55 show the stress drop exhibited by NBR and CR after immersion in various biodiesel blends for 1 month (1M) and 3 months (3M).

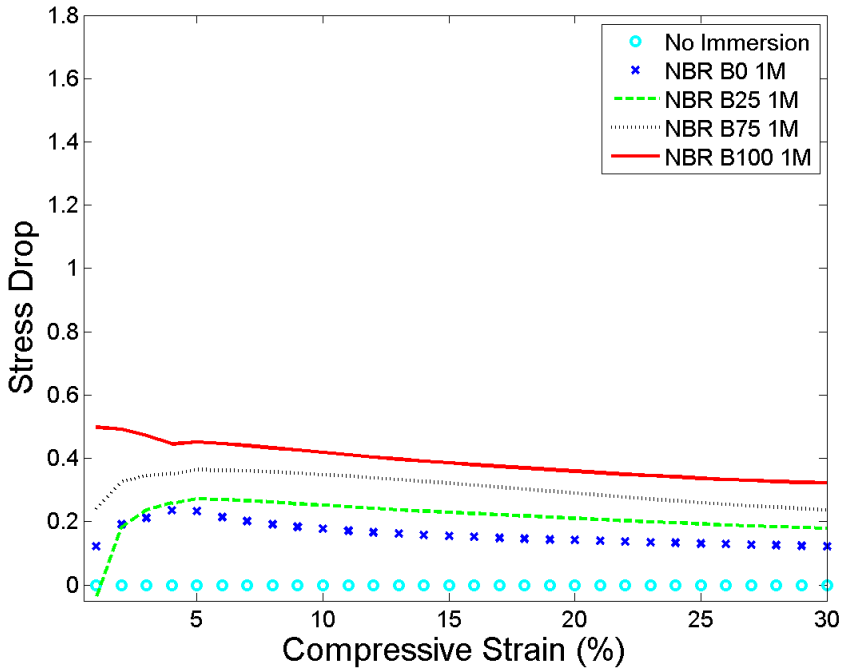

Figure 4.52: Stress drop in NBR previously immersed in various biodiesels for 1 month (1M). Results correspond to pre-compressive strain of 2%.

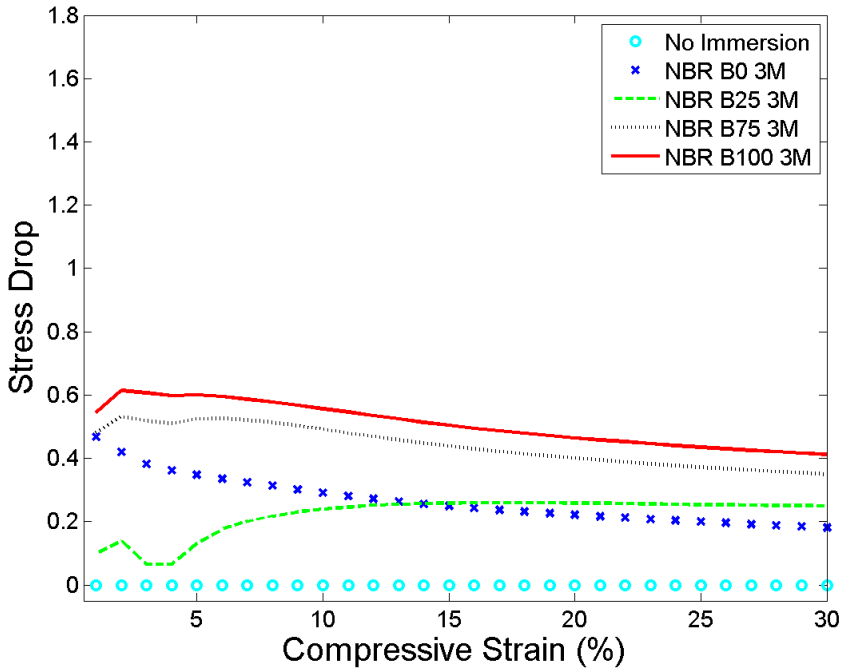

Figure 4.53: Stress drop in NBR previously immersed in various biodiesels for 3 months (3M). Results correspond to pre-compressive strain of 2%.

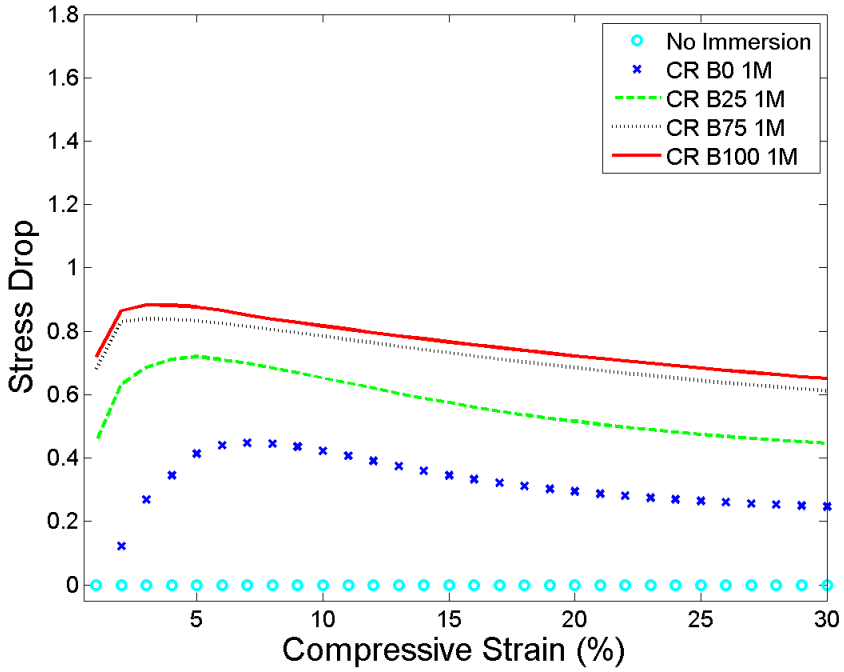

Figure 4.54: Stress drop in CR previously immersed in various biodiesels for 1 month (1M). Results correspond to pre-compressive strain of 2%.

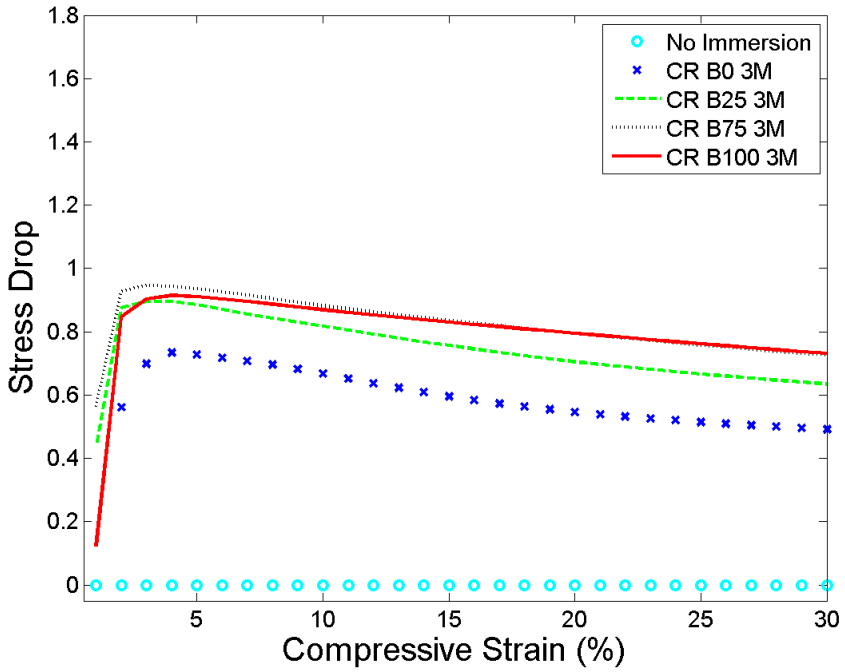

Figure 4.55: Stress drop in CR previously immersed in various biodiesels for 3 months (3M). Results correspond to pre-compressive strain of 2%.

As depicted in these figures, both NBR and CR experience a stress drop in the presence of biodiesels. Moreover, in the range of 5 - 30% strain, the stress drop appears to be decreasing slightly with the applied strain. However, the corresponding drop increases with the biodiesel content and duration of immersion, i.e. the strength of rubber decreases further with the increase of biodiesel content and duration of immersion. For a given biodiesel content and duration of immersion, CR exhibits a larger stress drop than NBR. The high degree of swelling experienced by CR as shown in Figures 4.38 to 4.41 contributes significantly to the decrease of its strength.

4.2.2 (c) Stress-softening

Using Equation 4.4, the stress-softenings for the uniaxially-stressed specimens is calculated. Figures 4.56 to 4.65 show the stress-softening in NBR and CR previously immersed in various biodiesel blends for two different immersion durations: 1 month (1M) and 3 months (3M). Initially, at dry state, CR exhibits slightly more stress-softening than NBR as depicted in Figures 4.56 and 4.57.

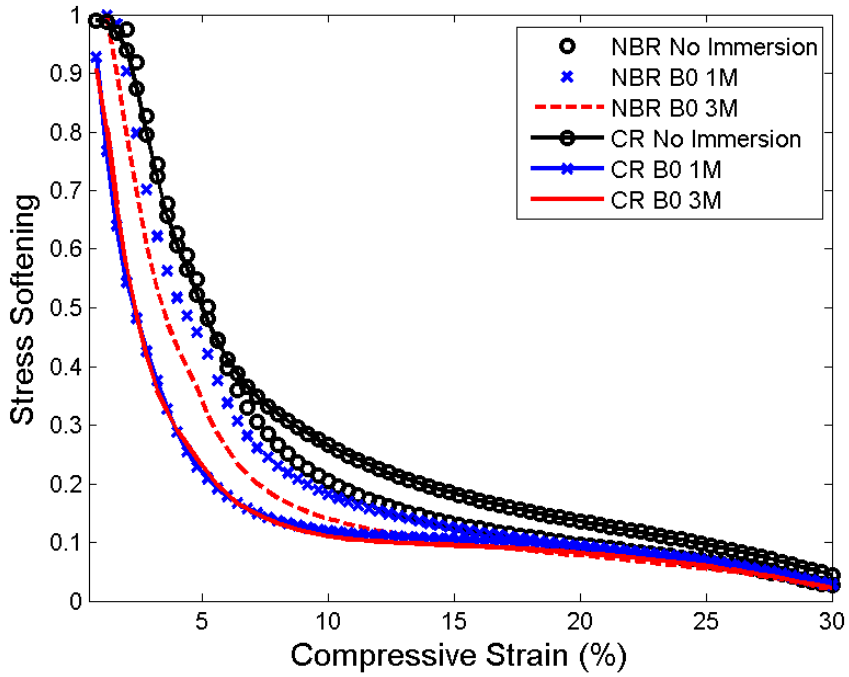

Figure 4.56: Stress-softening in NBR and CR previously immersed in B0 for two different durations of immersion: 1 month (1M) and 3 months (3M). Results correspond to pre-compressive strain of 2%.

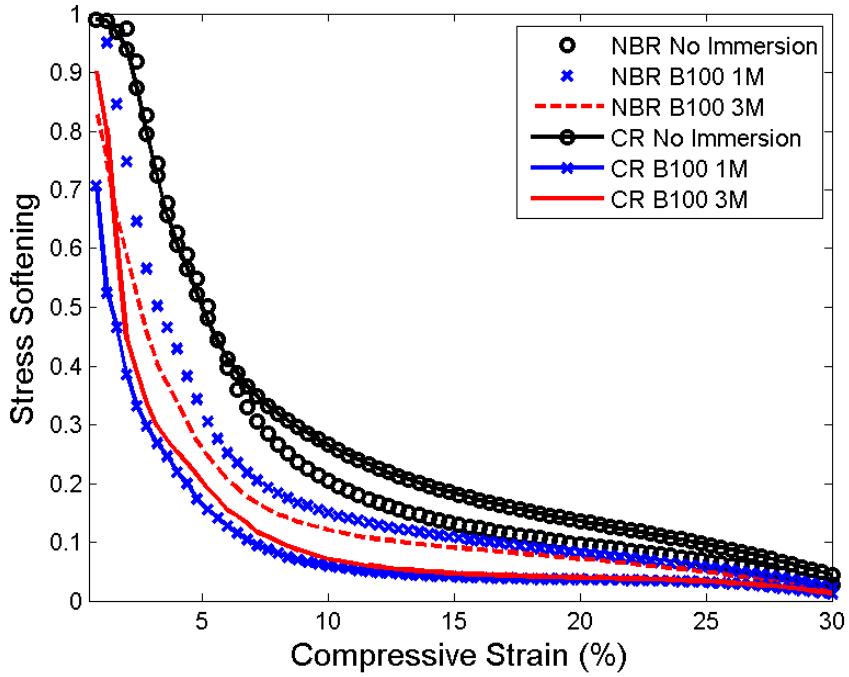

Figure 4.57: Stress-softening in NBR and CR previously immersed in B100 for two different durations of immersion: 1 month (1M) and 3 months (3M). Results correspond to pre-compressive strain of 2%.

Nevertheless, as the material is immersed for 1 month in either B0 or B100, the stress-softening decreases significantly in CR and becomes lower than that of NBR. In NBR, for a compressive strain of 10%, the amount of stress-softening drops from 20% at dry state to 18% and 15% at swollen state (immersed in B0 and B100 respectively for 1 month) as presented in Figures 4.58 and 4.59.

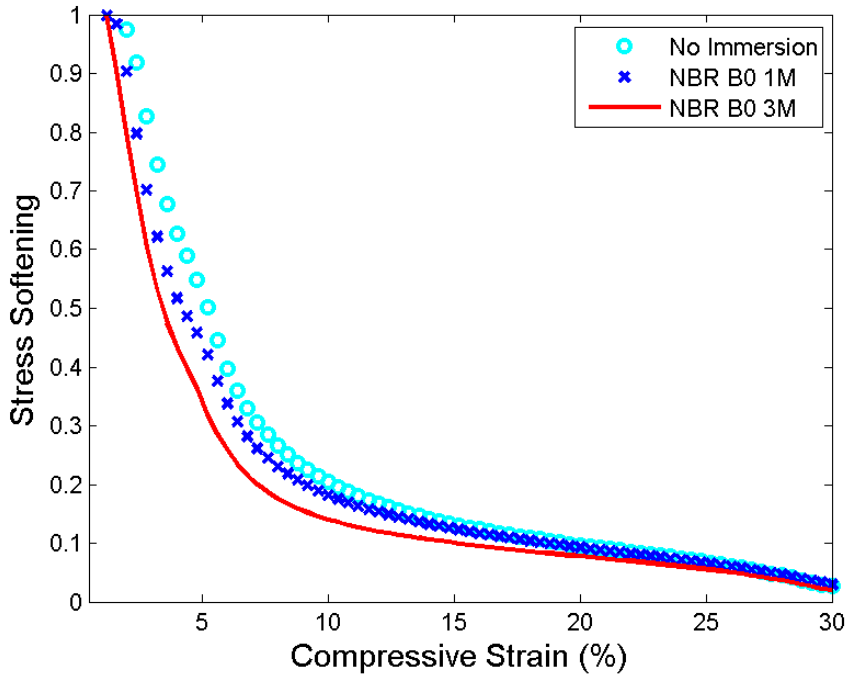

Figure 4.58: Stress-softening in NBR previously immersed in B0 for two different durations of immersion: 1 month (1M) and 3 months (3M). Results correspond to pre-compressive strain of 2%.

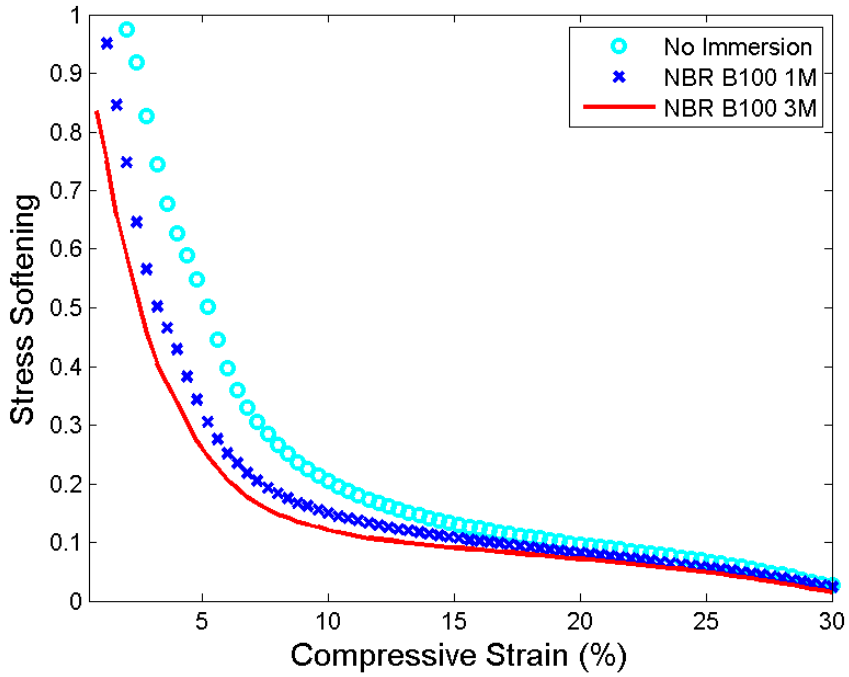

Figure 4.59: Stress-softening in NBR previously immersed in B100 for two different durations of immersion: 1 month (1M) and 3 months (3M). Results correspond to pre-compressive strain of 2%.

Increasing the duration of immersion from 1 to 3 months yields a further decrease of stress-softening to around 15% and 12% in B0 and B100 respectively. Referring to Figures 4.35 and 4.37, this corresponds to the volume change of 11% and 18% respectively.

In the case of CR, at an applied compressive strain of 10%, the amount of stress-softening changes from 28% for dry state to only 12% and 8% when it is immersed respectively in B0 and B100 for 1 month as shown in Figures 4.60 and 4.61. Note that in the latter condition, the volume change exhibited by the material is around 18% and 64% respectively (see Figures 4.39 and 4.41).

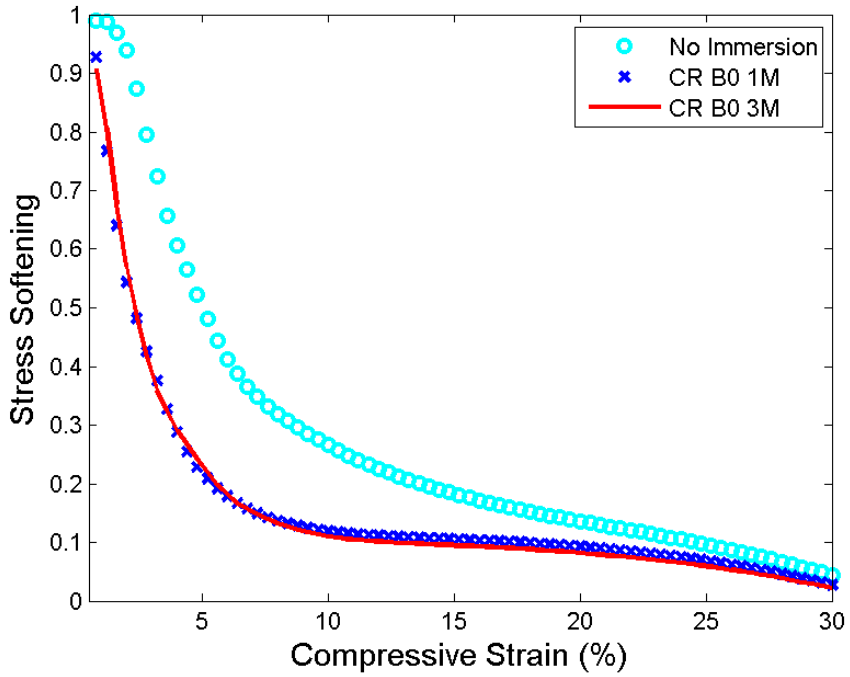

Figure 4.60: Stress-softening in CR previously immersed in B0 for two different durations of immersion: 1 month (1M) and 3 months (3M). Results correspond to pre-compressive strain of 2%.

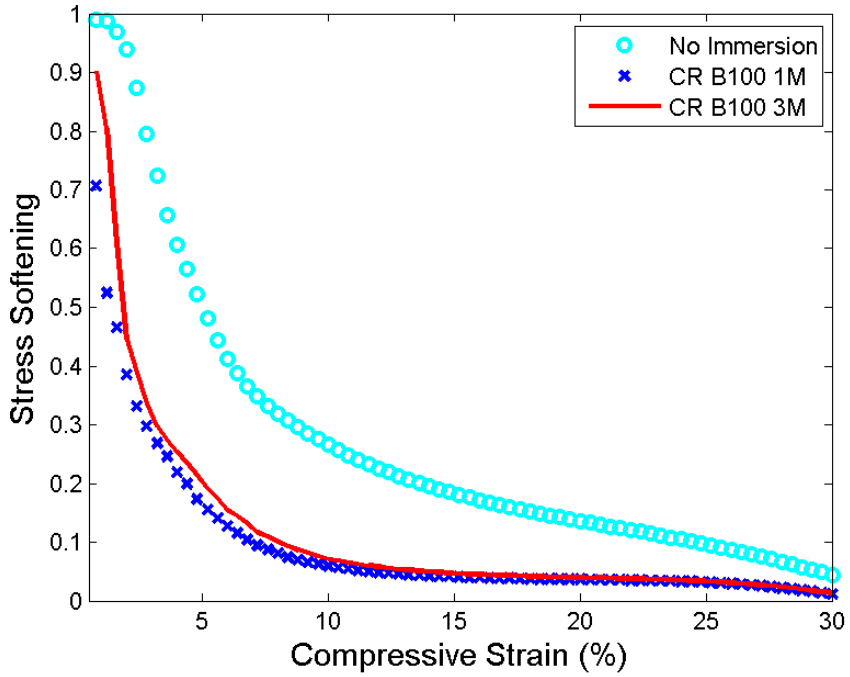

Figure 4.61: Stress-softening in CR previously immersed in B100 (right) for two different durations of immersion: 1 month (1M) and 3 months (3M). Results correspond to pre-compressive strain of 2%.

Increasing the duration of immersion from 1 to 3 months yields a significant increase in the volume change to around 24% and 90% in B0 and B100 respectively. However, the level of stress-softening appears to be unaffected by the corresponding further increase in swelling. Finally, the effect of biodiesel content on stress-softening in NBR and CR is presented in Figures 4.62 to 4.65. In these figures, it is found that for both materials, the increase in the content of biodiesel decreases the level of stress-softening.

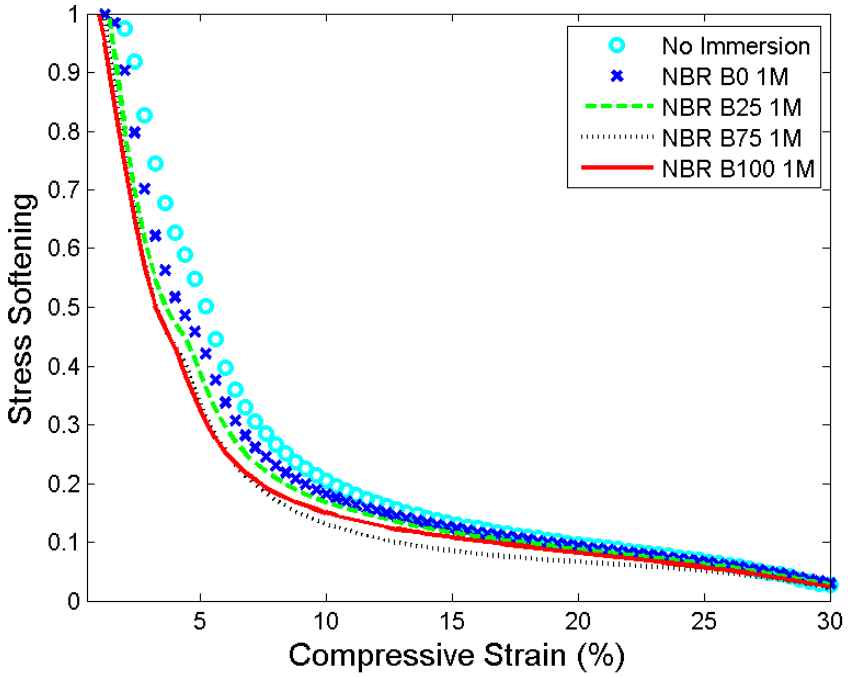

Figure 4.62: Stress-softening in NBR previously immersed in various biodiesels for 1 month (1M). Results correspond to pre-compressive strain of 2%.

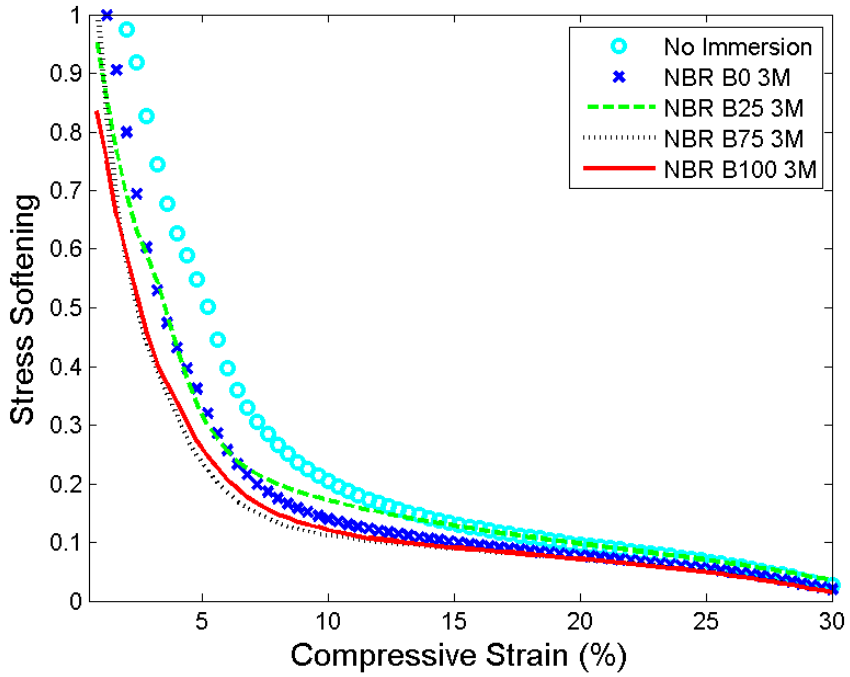

Figure 4.63: Stress-softening in NBR previously immersed in various biodiesels for 3 months (3M). Results correspond to pre-compressive strain of 2%.

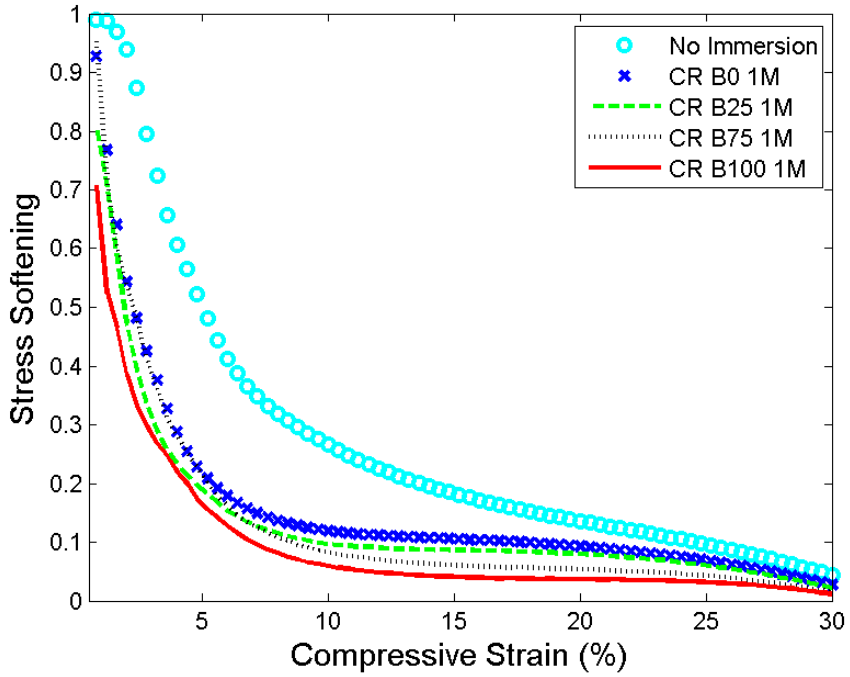

Figure 4.64: Stress-softening in CR previously immersed in various biodiesels for 1 month. Results correspond to pre-compressive strain of 2%.

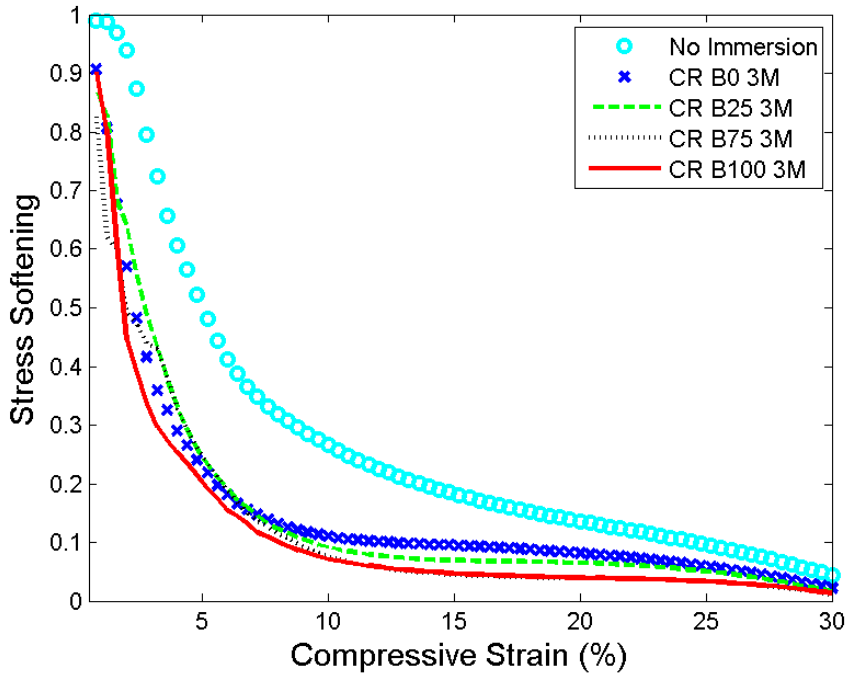

Figure 4.65: Stress-softening in CR previously immersed in various biodiesels for 3 months (3M). Results correspond to pre-compressive strain of 2%.

4.2.2 (d) Hysteresis

Following Equation (4.5), the hysteresis behavior after stabilization for the uniaxially-stressed swollen rubbers is characterized. Figures 4.66 to 4.69 show the hysteresis loss ratio of different elastomers (NBR and CR) under various initial compressive strains (2%, 10% and 30%) after immersion of 30 days in various biodiesel blends. It is shown that for low degree of swelling as exhibited by NBR after 30 days of immersion in different biodiesel blends (see Figure 4.66), the hysteresis loss ratio does not evolve significantly which suggested that the viscoelastic characteristic of the material remains essentially unchanged. However, the hysteresis loss ratio for higher degree of swelling (see Figures 4.67 to 4.69) decrease significantly. In this case, the high degrees of swelling are obtained either by long duration of immersion (90 days) or by increasing biodiesel content. Furthermore, it is to noted that the pre-compressive strains appeared to restrict the decrease of hysteresis loss ratio in the highly swollen rubbers, e.g. CR after immersion in B75 and B100.

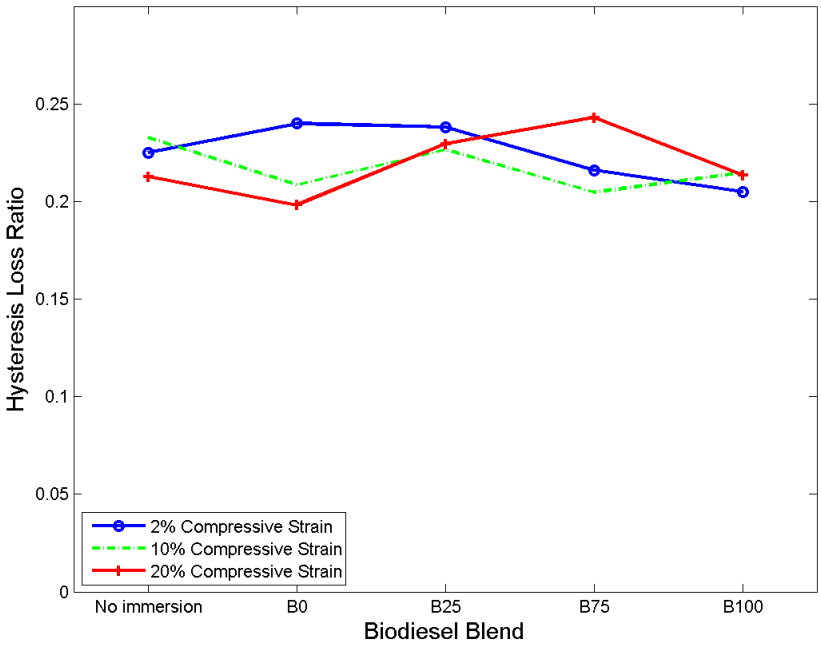

Figure 4.66: Hysteresis loss ratio in NBR under cyclic compression loading at 0.01 s^{-1} strain rate. Results correspond to 30 days of immersion duration in various biodiesel blends.

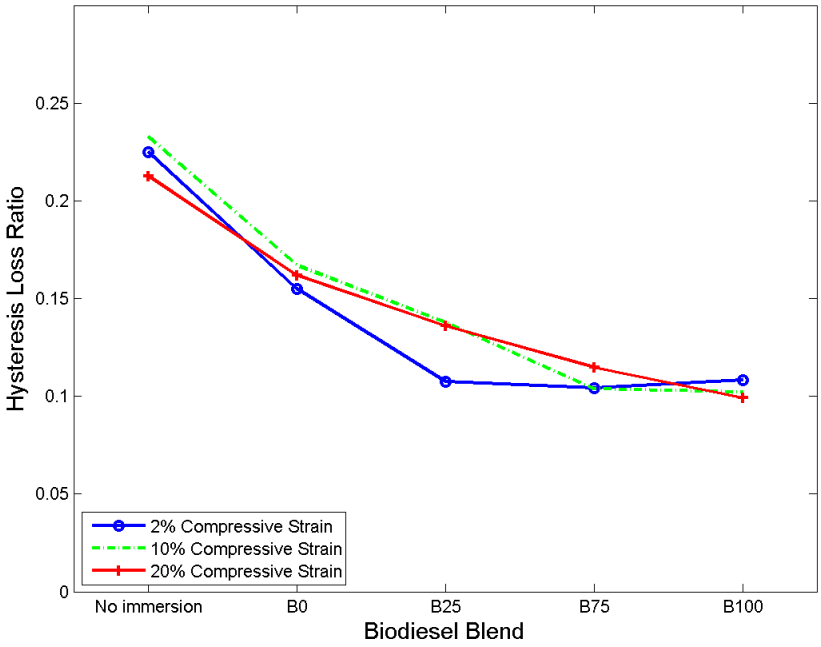

Figure 4.67: Hysteresis loss ratio in NBR under cyclic compression loading at 0.01 s^{-1} strain rate. Results correspond to 90 days of immersion duration in various biodiesel blends.

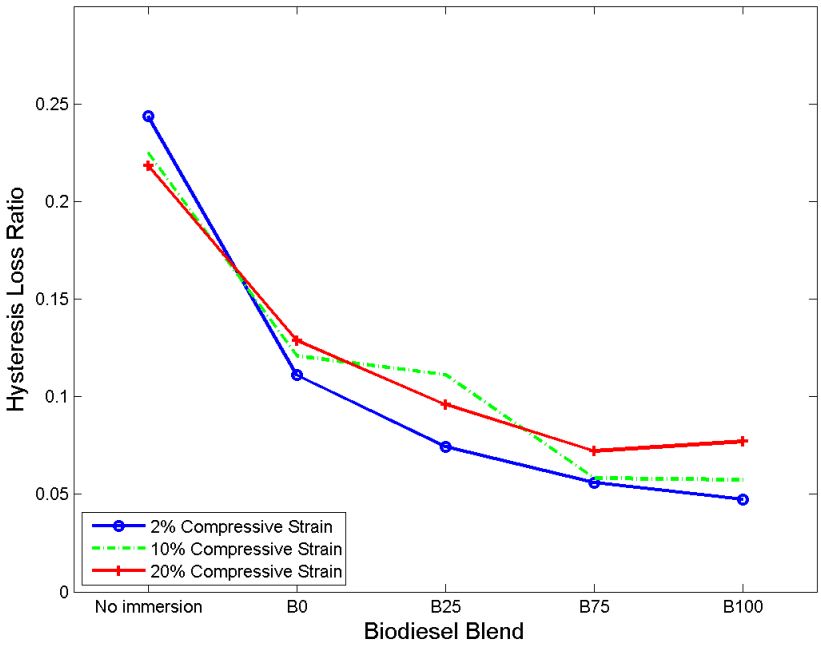

Figure 4.68: Hysteresis loss ratio in CR under cyclic compression loading at 0.01 s^{-1} strain rate. Results correspond to 30 days of immersion duration in various biodiesel blends.

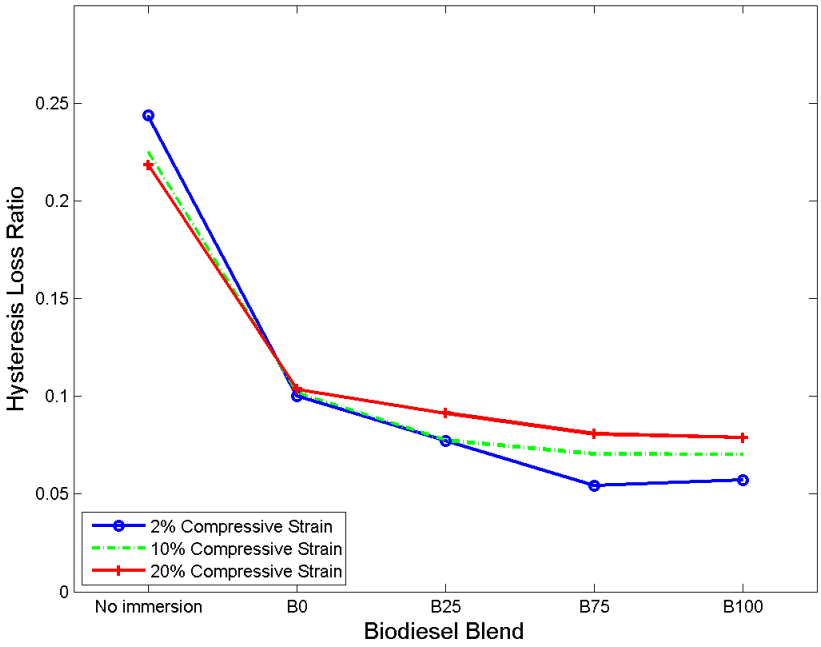

Figure 4.69: Hysteresis loss ratio in CR under cyclic compression loading at 0.01 s^{-1} strain rate. Results correspond to 90 days of immersion duration in various biodiesel blends.

4.2.2 (e) Stress Relaxation

Following the description in Section 4.1.2 (d) in Chapter 4, the stress relaxation for NBR and CR in different biodiesel blends at 30% compressive strain during uploading is reported in Figures 4.70 to 4.73. The curves reveal that the stress relaxation occurs rapidly during the first 200 seconds but subsequently becomes slower as indicated by the near-horizontal curve. Moreover, one can notice that stress relaxation is reducing with the increase of biodiesel content. This suggests that the biodiesel content has a significant influence on the viscoelastic response.

To close the discussion, note that all inelastic phenomena, e.g. stress-softening and mechanical hysteresis, in rubbers resulting from cyclic loading conditions appear to diminish significantly due to the presence of liquids, i.e. the macroscopic mechanical response of swollen rubbers approaches the response of hyperelastic materials. Nevertheless, the physical mechanism by which the presence of liquids modify the mechanical response under the above loading condition remains unknown.

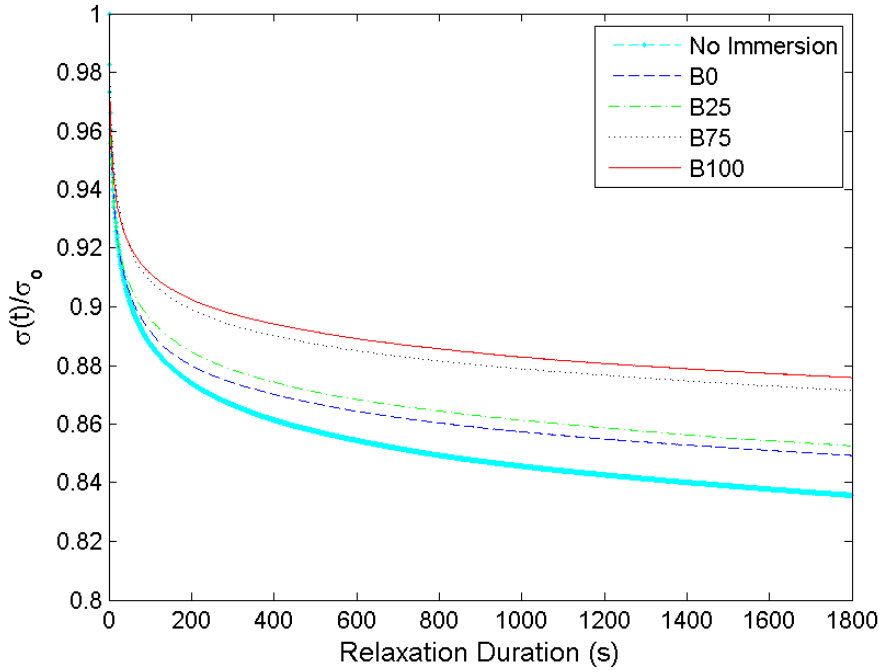

Figure 4.70: Stress relaxation of NBR under compressive strain levels of 30% during 1800 s. Results correspond to 2% pre-compressive strain and 30 days of immersion in various biodiesel blends.

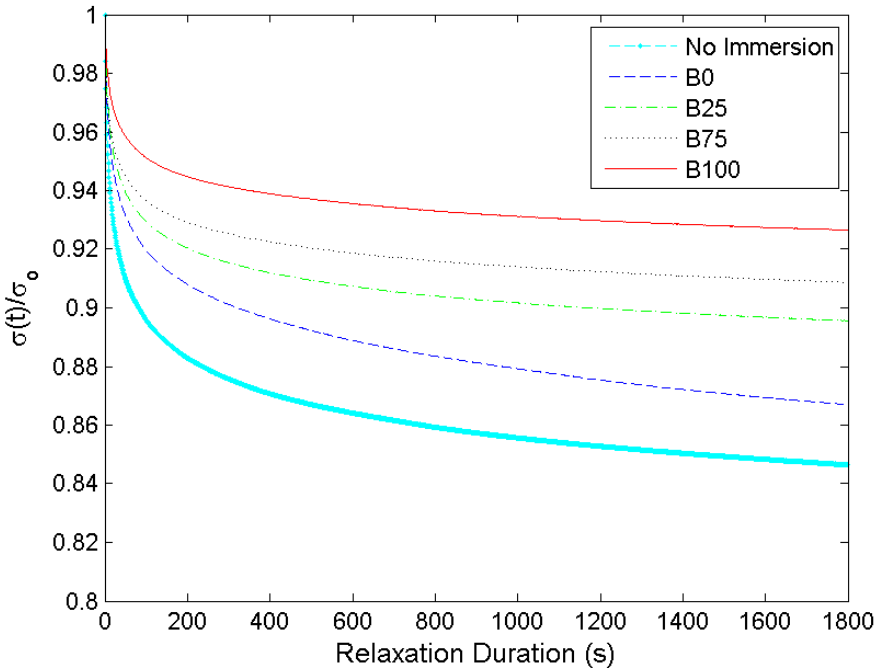

Figure 4.71: Stress relaxation of NBR under compressive strain levels of 30% during 1800 s. Results correspond to 2% pre-compressive strain and 90 days of immersion in various biodiesel blends.

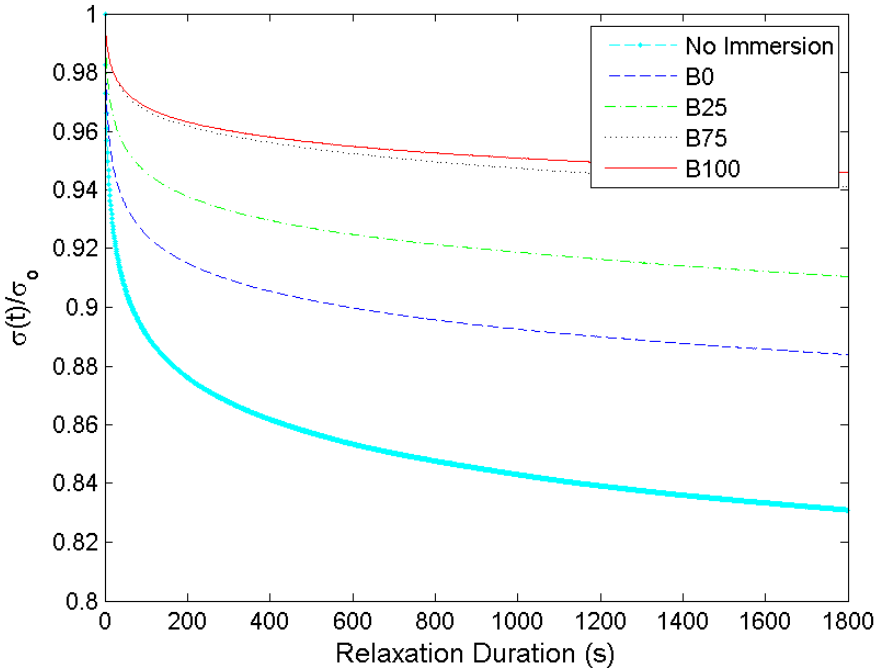

Figure 4.72: Stress relaxation of CR under compressive strain levels of 30% during 1800 s. Results correspond to 2% pre-compressive strain and 30 days of immersion in various biodiesel blends.

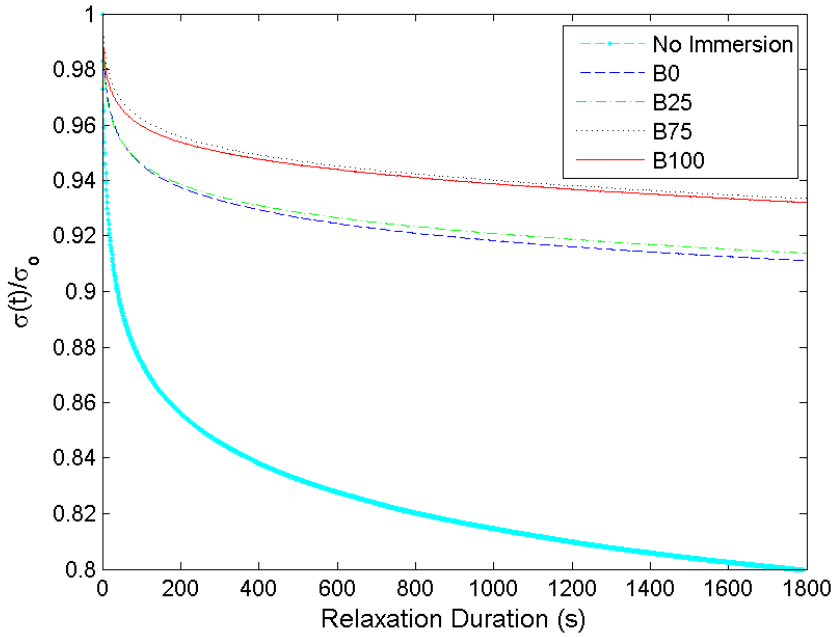

Figure 4.73: Stress relaxation of CR under compressive strain levels of 30% during 1800 s. Results correspond to 2% pre-compressive strain and 90 days of immersion in various biodiesel blends.

4.3 Comparison between experimental results of swelling tests on stress-free and uniaxially-stressed specimens

Comparing the swelling results between the stress-free and uniaxially stressed specimens, it is found that the pre-compressive strains restrict the swelling in the uniaxially-stressed specimens. Although the immersion durations varied between these two tests, the swelling results are qualitatively similar. Concerning the mechanical responses, the effect of pre-compressive strain during immersion on the resulting mechanical responses is not significant. This could be due to the fact that the swelling between the three pre-compressive strains (2%, 10% and 30%) imposed is not significant to cause the degree of swelling to vary significantly. As such, comparing the mechanical responses, i.e. the stress-softening, hysteresis, stress-relaxation between the stress-free swollen rubbers with the highest degree of swelling in the uniaxially stressed swollen rubbers, relatively similar results are obtained. We can conclude here that the higher the degree of swelling, whether it is due to higher biodiesel content, longer immersion duration, or lower level of pre-compressive strain, the more the inelastic responses, i.e. the stress-softening, hysteresis, stress-relaxation are reduced.

CHAPTER 5

MODELING RESULTS AND DISCUSSION

As we have seen in Chapter 4, the mechanical responses of swollen rubber are complex, and include the responses of stress-softening, hysteresis, stress-relaxation, etc. To simulate the real engineering components in the swollen state, an efficient model taking into account all the observed inelastic responses is required. The development of such model is complex. As a first attempt, only the modeling of the Mullins effect is considered. This chapter presents the modeling results and compares them with the experimental results for stress-softening in swollen rubbers. Furthermore, the three-dimensional nature of the model in capturing the effect of swelling on the stress-softening due to Mullins effect is illustrated in simulations of uniaxial tension, pure shear and equibiaxial tension.

5.1 Data treatment

Since the Mullins effect is the only inelastic response addressed in the continuum mechanical modeling, the results in Figures 4.3 and 4.4 have to be treated. More precisely, only the Mullins effect which occurs between the first and second loading cycles is considered. For this purpose, the data treatment proposed by Chagnon et al. (2004) is considered: (i) the reloading path of the second cycle is assumed to coincide with the downloading path of the first cycle, (ii) the unloading data are horizontally shifted such that they start from zero strain and (iii) the unloading data are extended to rejoin the primary loading path. An example of the comparison between original and corrected data in CR is depicted in Figures 5.1 and 5.2.

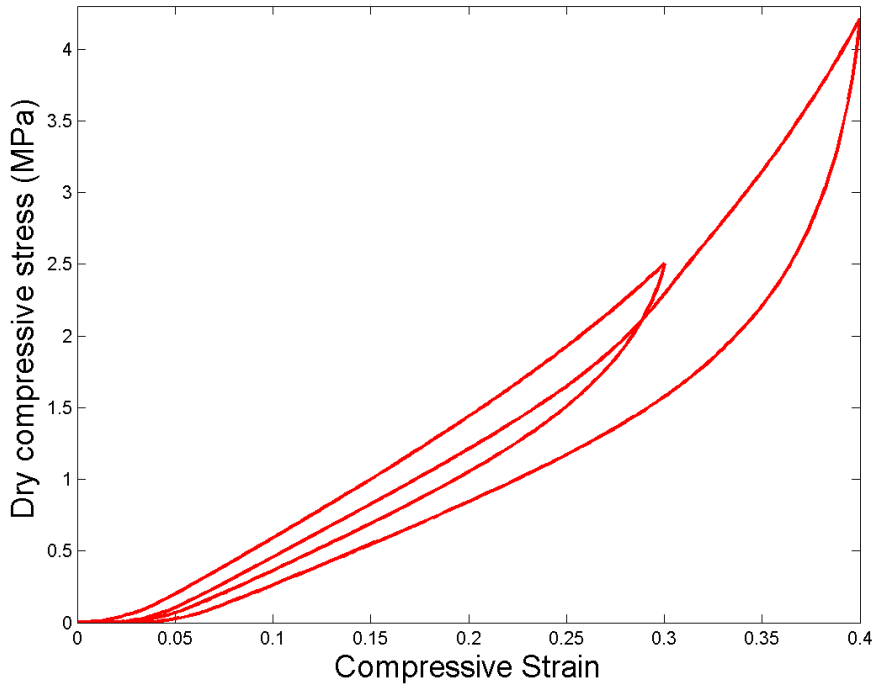

Figure 5.1: Experimental results for dry CR under cyclic compressive test.

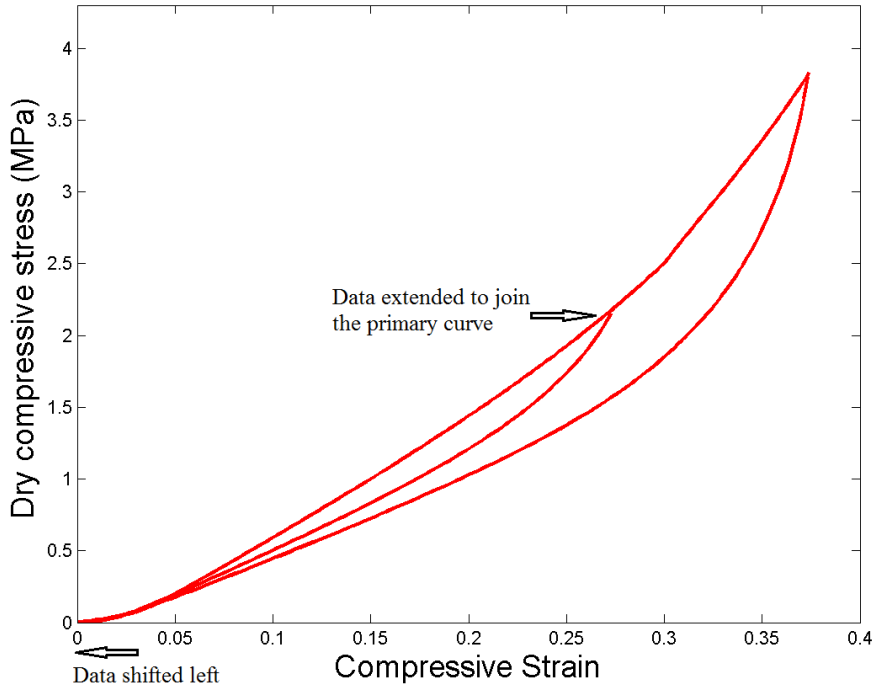

Figure 5.2: Modified data for dry CR under cyclic compressive test.

5.2 Flory-Huggins interaction parameters, χ

To obtain the parameter χ for different rubber-solvent combinations, we first need to determine the volume of the solvent molecules, v.

The volume of the solvent molecules v is given by:

$$v = \frac{M_w}{\rho A_v} \tag{5.1}$$

where,

M_w is the molecular weight of the solvent,

ρ is the density of the solvent,

A_v is the Avogadro number, which is equal to $6.022.10^{23}$ /mol.

The molecular weight of the diesel is obtained from the bibliography. While the molecular weight of the palm biodiesel is approximated from the chemical content of the biodiesel. Detailed calculation is shown in Table 5.1

Table 5.1: Biodiesel molecular weight calculation.

Chemicals	Molecules	C	H	O	Molecular weight	% in biodiesel	
Methyl Laurate	$CH_3(CH_2)_{10}COOCH_3$	12	26	2	214	1.066	2.281
Methyl Myristate	$CH_3(CH_2)_{12}COOCH_3$	15	30	2	242	3.700	8.954
Methyl Palmitate	$CH_3(CH_2)_{14}COOCH_3$	17	34	2	270	44.272	119.534
Methyl Palmitoleate	$CH_3(CH_2)_5CHCH(CH_2)_7COOCH_3$	17	30	2	266	0.497	1.322
Methyl Stearate	$CH_3(CH_2)_{16}COOCH_3$	19	38	2	298	4.128	12.301
Methyl Oleate	$CH_3(CH_2)_7CHCH(CH_2)_7COOCH_3$	19	36	2	296	35.934	106.365
Methyl Arachisate	$CH_3(CH_2)_{18}COOCH_3$	21	42	2	326	0.236	0.769
Total chemical content						89.833 %	251.527
Estimated Molecular weight						100 %	280

The volume of the B0 and B100 molecules is then determined using Equation 5.1. The calculation is shown in Table 5.2

Table 5.2: The volume of the B0 and B100 molecules.

	B0	B100
Molecular weight (g/mol)	280	198.4
Density (g/m^3)	875900	878800
Avogadro number	$6.02x10^{23}$	$6.02x10^{23}$
The volume of the solvent molecules (m^3)	$5.31x10^{-28}$	$3.75x10^{-28}$

Assuming equilibrium swelling occurred after 30 days of immersion for NBR and CR in B0 and B100 and recalling Equation (3.3), the Flory-Huggins Interaction parameter, χ is then calculated using Matlab. The results are shown in Table 5.3.

Table 5.3: Flory-Huggins interaction parameter χ of each rubber-fuel system.

$\chi_{CR-B100}$	0.311
χ_{CR-B0}	1.356
$\chi_{NBR-B100}$	1.285
χ_{NBR-B0}	1.767

5.3 Extended pseudo-elastic model

5.3.1 Form of material functions

In order to describe the general response of swollen rubbers, a simple neo-Hookean hyperelastic strain energy density is retained:

$$\hat{W}_{\mathrm{m}}(J_s, I_{1\mathrm{m}}) = \frac{\mu(J_s)}{2}(I_{1\mathrm{m}} - 3) \tag{5.2}$$

where $\mu(J_s)$ is the shear modulus of swollen rubber. According to Treloar (1975), swelling in rubber is a purely mixing or interdiffusion process with no chemical attraction between rubber and liquid molecules. Furthermore, the only effect of swelling is to reduce the modulus in inverse proportion to the cube root of the degree of swelling without changing the form of the stress-strain curves. Generalizing this idea, the shear modulus of the

swollen rubber $\mu(J_s)$ is assumed to be related to that of dry rubber μ_d through:

$$\mu(J_s) = J_s^{-n}\mu_d \tag{5.3}$$

It follows that the strain energy function of the swollen rubber becomes

$$\hat{W}_{\mathrm{m}}(J_s, I_{1\mathrm{m}}) = J_s^{-n}\frac{\mu_d}{2}(I_{1\mathrm{m}} - 3) \tag{5.4}$$

where n is a parameter to be determined from all sets of experimental data. In this case, the engineering stress in Eq. (3.44) reduces to:

$$\hat{P}_{11} = J_s^{-n}\mu_d(1-d)\left(\lambda_{\mathrm{m}} - \frac{1}{\lambda_{\mathrm{m}}^2}\right) \tag{5.5}$$

where d is given in Eq. (3.39).

In order to determine the explicit forms of $r(J_s, \chi)$ and $m(J_s, \chi)$, the experimental data as shown in Figure 5.2 are considered. More precisely, the experimental values of damage d are plotted as a function of $I_{1\mathrm{m,max}} - I_{1\mathrm{m}}$. The results for CR swollen by B0 and B100 are depicted in Figures 5.3 and 5.4 .

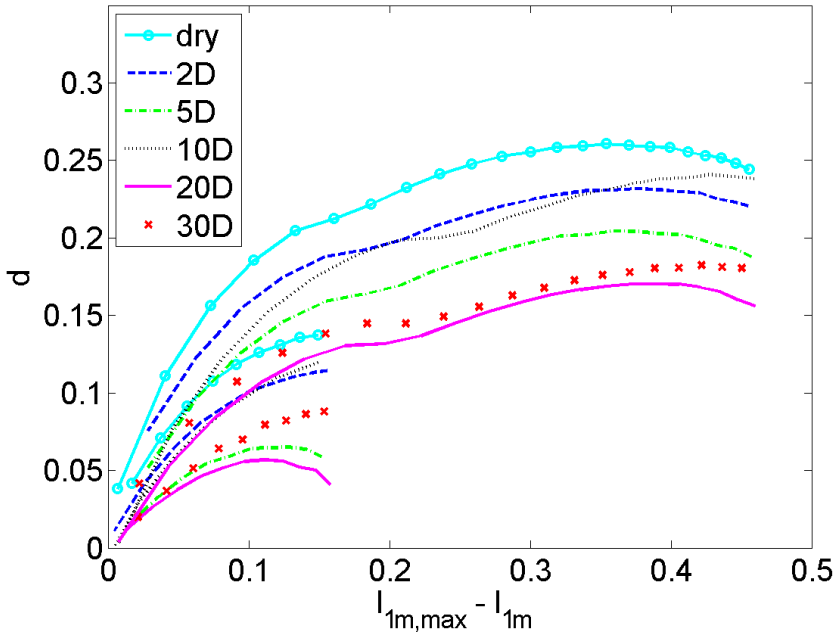

Figure 5.3: Evolution of d in CR swollen by B0. Results correspond to 2, 5, 10, 20 and 30 days of immersion duration. The short and long curves correspond to the maximum compressive strains of 30% ($\lambda = 0.7$) and 40% ($\lambda = 0.6$) respectively.

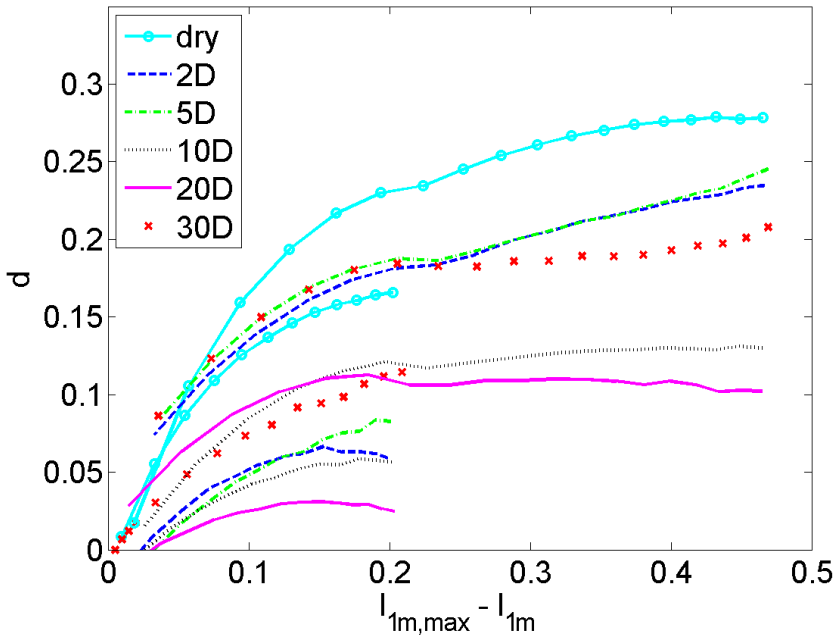

Figure 5.4: Evolution of d in CR swollen by B100. Results correspond to 2, 5, 10, 20 and 30 days of immersion duration. The short and long curves correspond to the maximum compressive strains of 30% ($\lambda = 0.7$) and 40% ($\lambda = 0.6$) respectively.

Note that the corresponding results for NBR swollen by B0 and B100 are not shown since they are qualitatively similar. In the Figures 5.3 and 5.4, d is obtained from the following expressions:

$$d(\text{dry}) = \frac{P_{d1}^{up} - P_{d1}^{un}}{P_{d1}^{up}} \qquad d(\text{swollen}) = \frac{P_{s1}^{up} - P_{s1}^{un}}{P_{s1}^{up}} \tag{5.6}$$

where P_{d1}^{up} is the stress in dry rubber during uploading of the first cycle, P_{d1}^{un} is the stress in dry rubber during unloading of the first cycle, P_{s1}^{up} is the stress in swollen rubber during uploading of the first cycle and P_{s1}^{un} is the stress in swollen rubber during unloading of the first cycle. It is generally observed that the damage is strongly affected by the degree of swelling and the type of rubber-solvent, i.e. interaction between rubber and biodiesel/diesel. More precisely, the Mullins effect appears to decrease with the increase of degree of swelling.

By considering the initial slope and the maximum value of d in Figures 5.3 and 5.4, and recalling the discussion on the last paragraph of Section 3.2.4 (a), it is possible to plot the evolution of both m and r as a function of $\chi\,(J_s - 1)$ as shown in Figures 5.5 and 5.6.

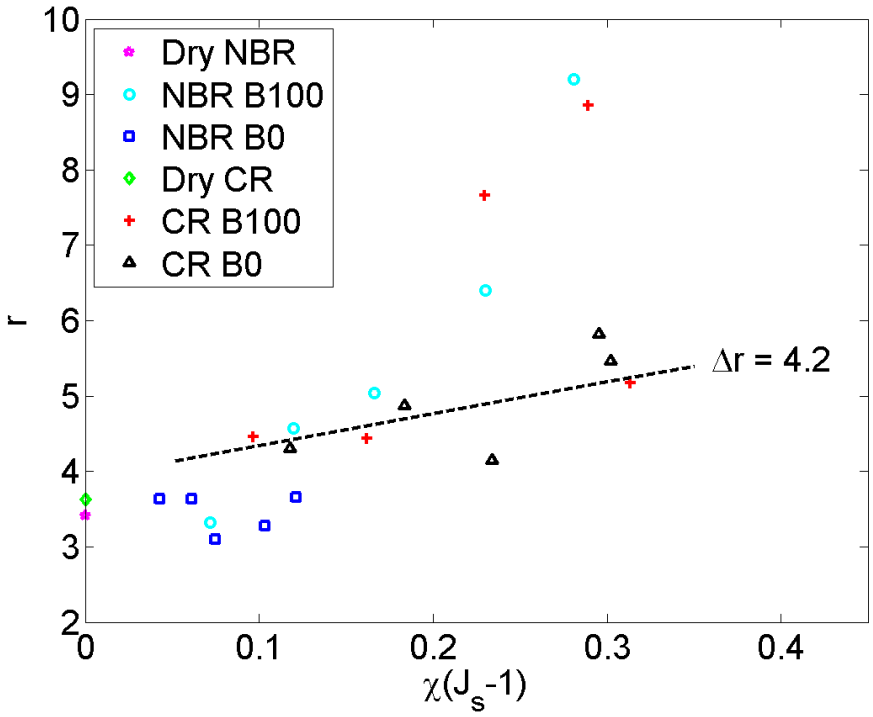

Figure 5.5: Evolution of r as a function of $\chi\,(Js - 1)$. Results correspond to the maximum compressive strain of 40%.

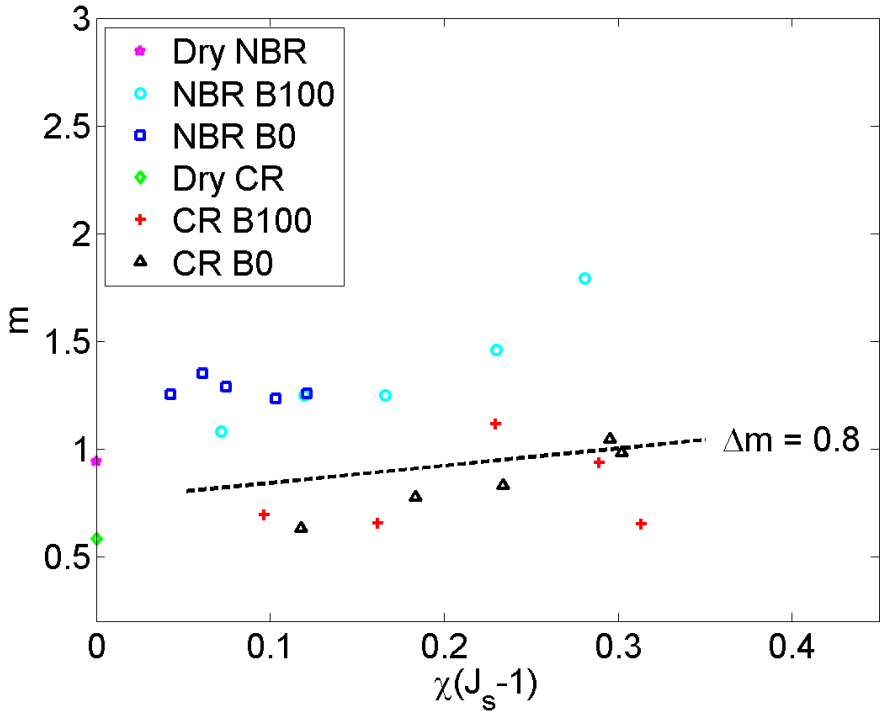

Figure 5.6: Evolution of m as a function of $\chi\,(Js-1)$. Results correspond to the maximum compressive strain of 40%.

In general, it is observed that both r and m are increasing functions of $\chi\,(J_s-1)$. Motivated by this finding, and for the sake of simplicity, the parameters r and m are assumed to evolve in a simple linear way as follow:

$$r = r_d + \Delta r \cdot \chi\,(J_s-1) \qquad\qquad m = m_d + \Delta m \cdot \chi\,(J_s-1)\,. \tag{5.7}$$

where r_d and m_d are the values of r and m for dry rubbers. Δr and Δm are additional material constants. Finally, the damage function d in Eq. (3.39) becomes:

$$d = \frac{1}{r_d + \Delta r \cdot \chi\,(J_s-1)}\,\mathrm{erf}\left[\frac{1}{m_d + \Delta m \cdot \chi\,(J_s-1)}\,(I_{1\mathrm{m,max}} - I_{1\mathrm{m}})\right]. \tag{5.8}$$

To summarize, the following parameters in Table 5.4 have to be identified:

Table 5.4: Summary of material parameters required in the proposed model.

Hyperelasticity (neo-Hookean)	μ_d		
Mullins-effect	r_d	m_d	
Swelling	n	Δr	Δm

5.3.2 Identification of material parameters

In the following, methods to estimate the material parameters of the model are discussed. The parameter μ_d can be obtained by fitting the primary curve of dry rubber using the Neo-Hookean hyperelastic strain energy while r_d and m_d can be identified from the set of secondary curves (downloading) of dry rubber. The power law parameter n, can be estimated by considering the primary curve of dry rubber and primary curves of corresponding swollen rubbers having different degrees of swelling. The parameters Δr and Δm can be estimated by considering the slope of the data in Figures 5.5 and 5.6 respectively. Since the slopes of r and m do not vary significantly for different rubber-solvent combinations, the values of Δr and Δm are assumed to be independent of the types of rubber and solvent and their estimated values are illustrated by dashed lines in Figures 5.5 and 5.6 respectively. Finally, the estimated parameters are summarized in Table 5.5:

Table 5.5: Values of material parameters used in model.

	NBR	CR
μ_d (MPa)	1.7786	1.9102
r_d	4.4340	3.4182
m_d	0.2720	0.1683
n	2.5	
Δr	4.2	
Δm	0.8	

5.3.3 Comparison between model and experiment

The ability of the proposed model to describe Mullins effect in swollen rubbers under cyclic compressive loading conditions is presented in Figures 5.7-5.28. For comparison,

the results related to the dry rubber are also shown in the figure.

In general, it is observed that the proposed model is qualitatively in good agreement with experiments. The primary curves of dry and swollen rubbers are well-described. Moreover, the effects of swelling on the stress-softening due to Mullins effect are well-predicted. Some discrepancies between model and experiments are found for swollen rubbers having relatively high degree of swelling. Indeed, as shown in Figures 5.13 to 5.23, the model appears to slightly underestimate the stress level in highly swollen rubbers. Furthermore, for the case of CR swollen by B100, the stress level and Mullins effect predicted by the model are significantly smaller than the ones obtained from the experiments as presented in Figures 5.24 to 5.28 . The corresponding discrepancies could be attributed to the value of parameters Δr and Δm used in the present model. Indeed, for the sake of simplicity, they are chosen to be independent of the rubber type and rubber-solvent combination. Furthermore, it was also assumed that Treloar's theory holds for all swollen rubbers (Treloar, 1975), i.e. there is no chemical attraction between rubber and solvent molecules in swollen rubbers. While this assumption appears to be acceptable for relatively low degree of swelling, its validity in the case of highly swollen rubber such as CR in B100 becomes questionable. Indeed, as discussed in Haseeb et al. (2011), chemical reaction and interaction occurs between the B100 molecules and CR backbone resulting to the degradation of its mechanical properties.

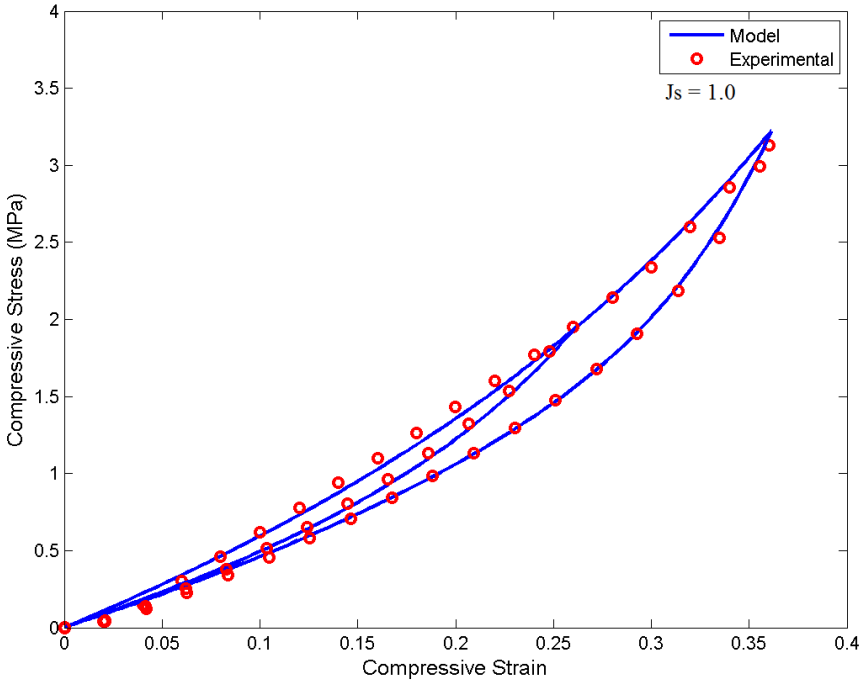

Figure 5.7: Comparison between pseudo-elastic model and experiment for dry NBR.

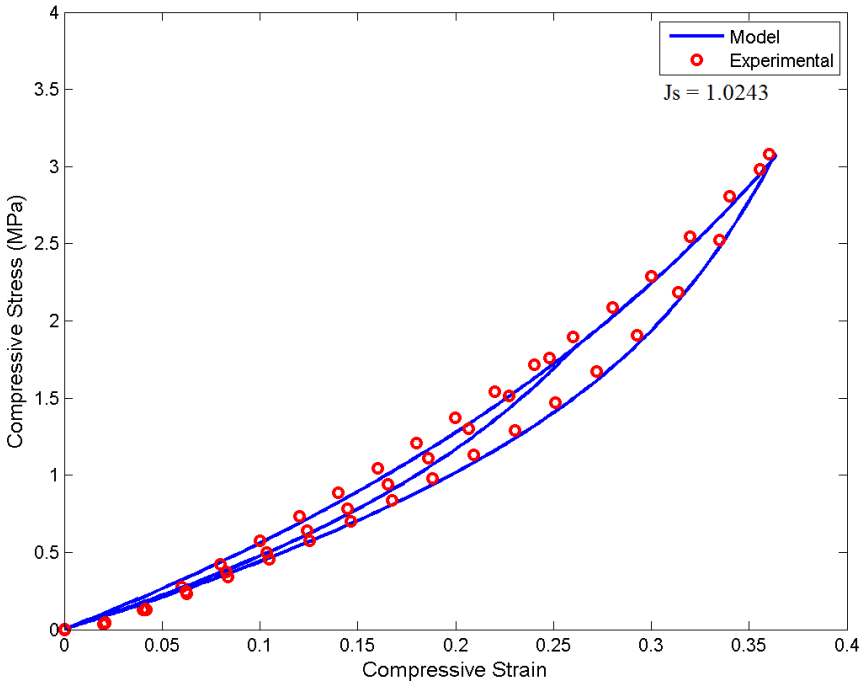

Figure 5.8: Comparison between pseudo-elastic model and experiment for NBR swollen by B0 after 2 days immersion ($\chi = 1.7669$).

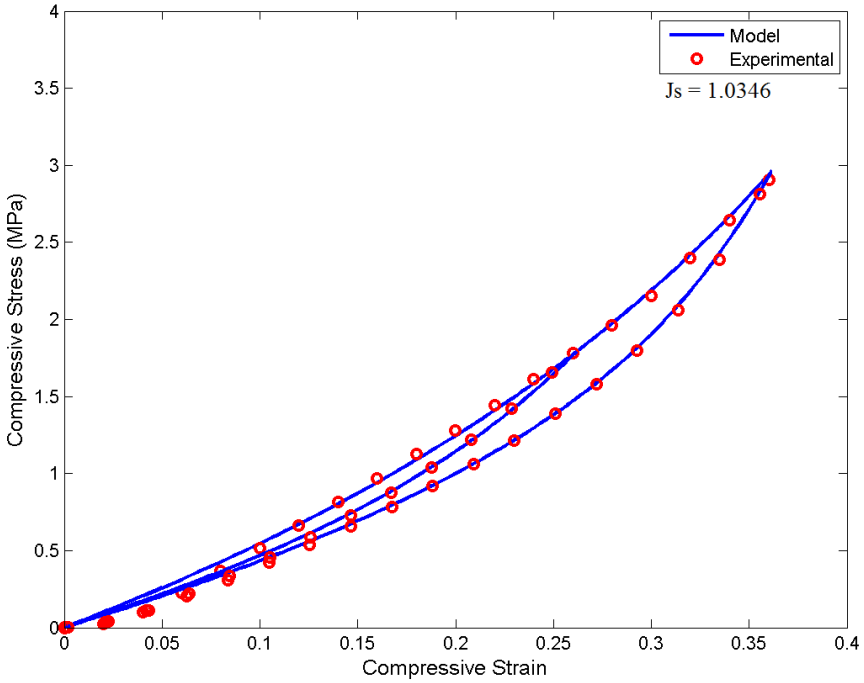

Figure 5.9: Comparison between pseudo-elastic model and experiment for NBR swollen by B0 after 5 days immersion ($\chi = 1.7669$).

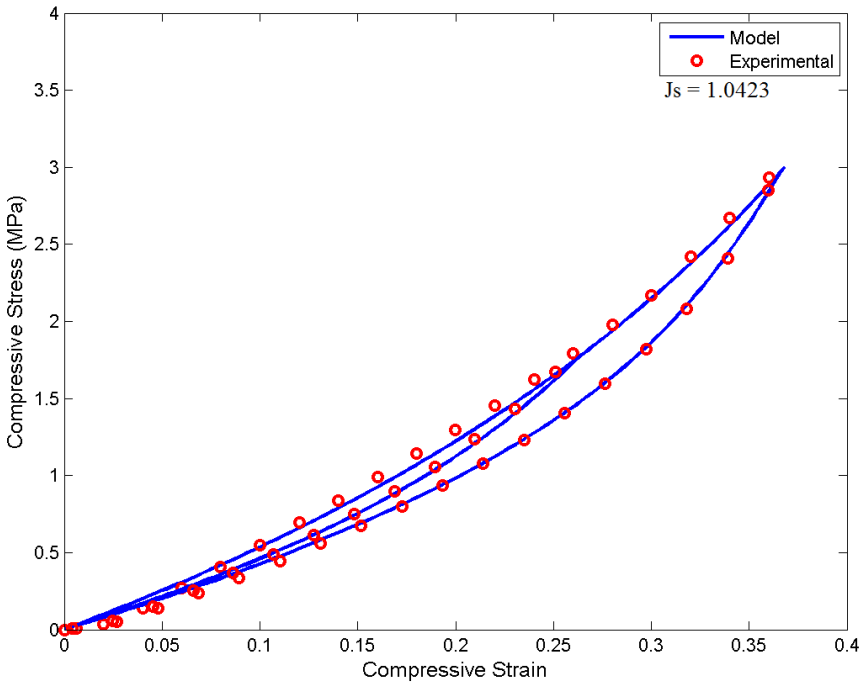

Figure 5.10: Comparison between pseudo-elastic model and experiment for NBR swollen by B0 after 10 days immersion ($\chi = 1.7669$).

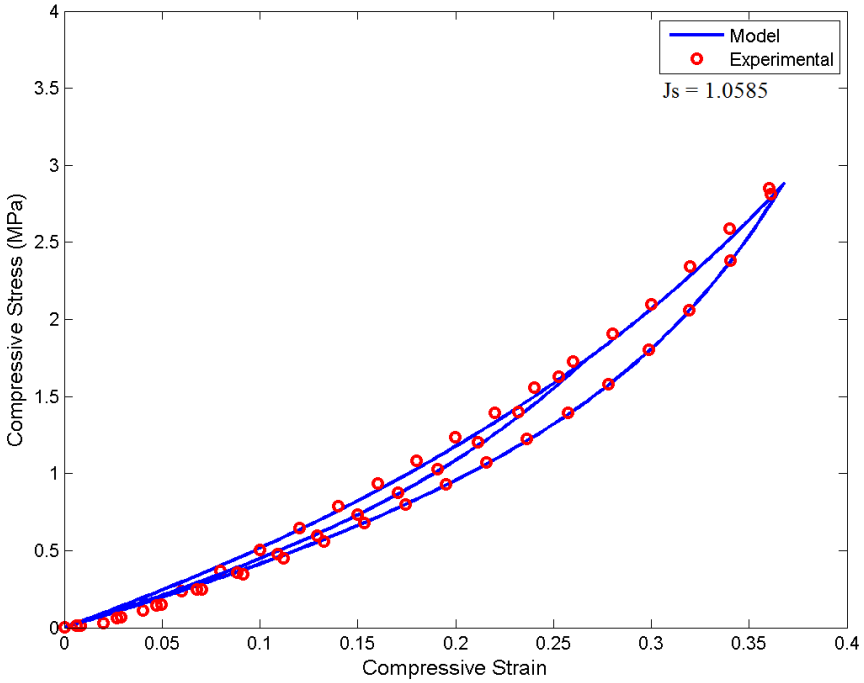

Figure 5.11: Comparison between pseudo-elastic model and experiment for NBR swollen by B0 after 20 days immersion ($\chi = 1.7669$).

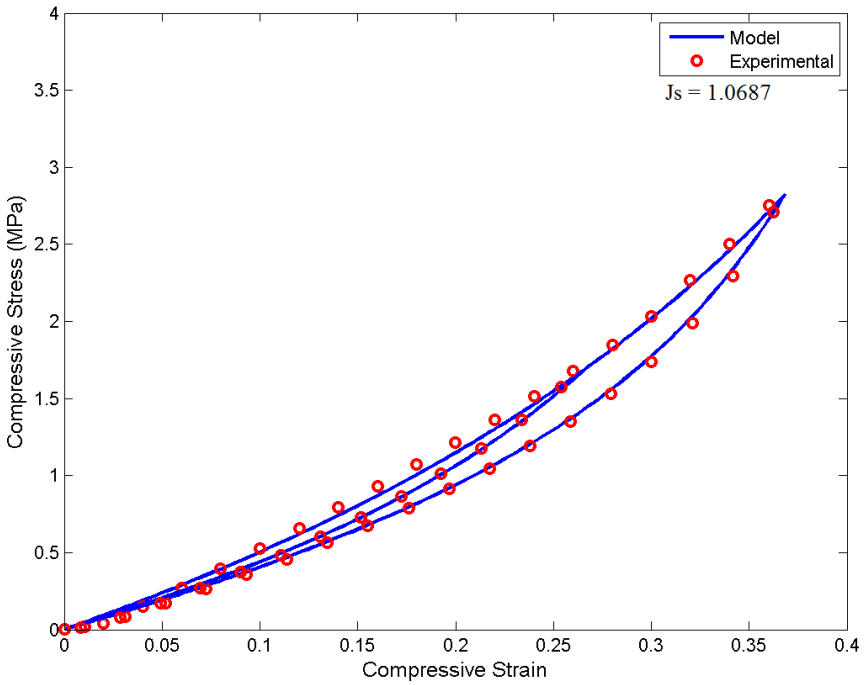

Figure 5.12: Comparison between pseudo-elastic model and experiment for NBR swollen by B0 after 30 days immersion ($\chi = 1.7669$).

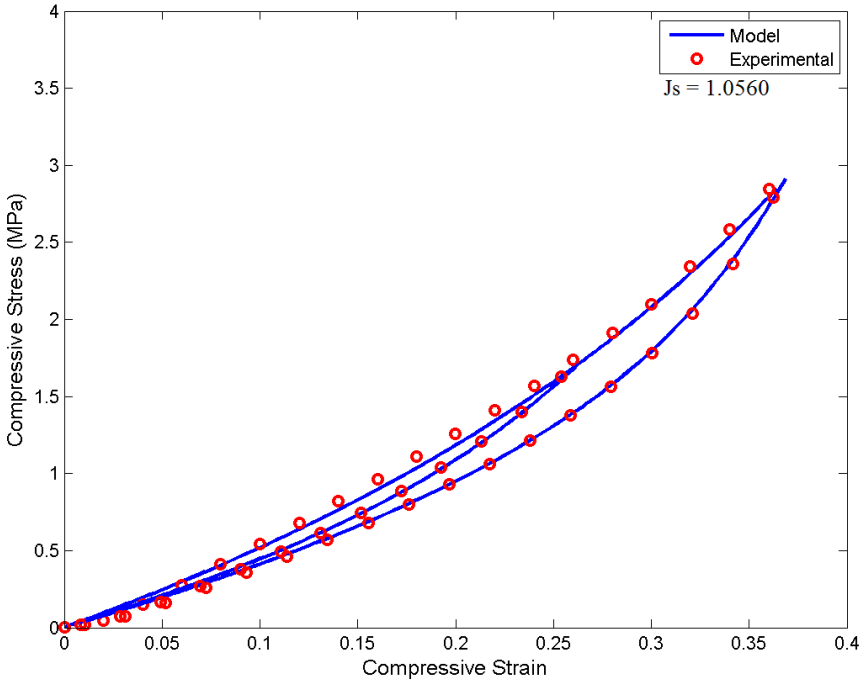

Figure 5.13: Comparison between pseudo-elastic model and experiment for NBR swollen by B100 after 2 days immersion ($\chi = 1.2855$).

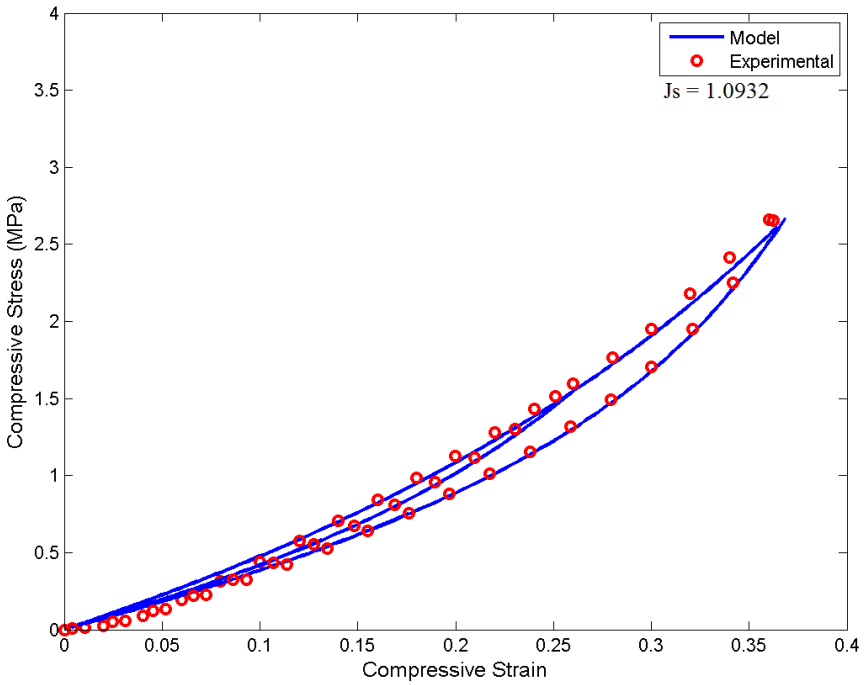

Figure 5.14: Comparison between pseudo-elastic model and experiment for NBR swollen by B100 after 5 days immersion ($\chi = 1.2855$).

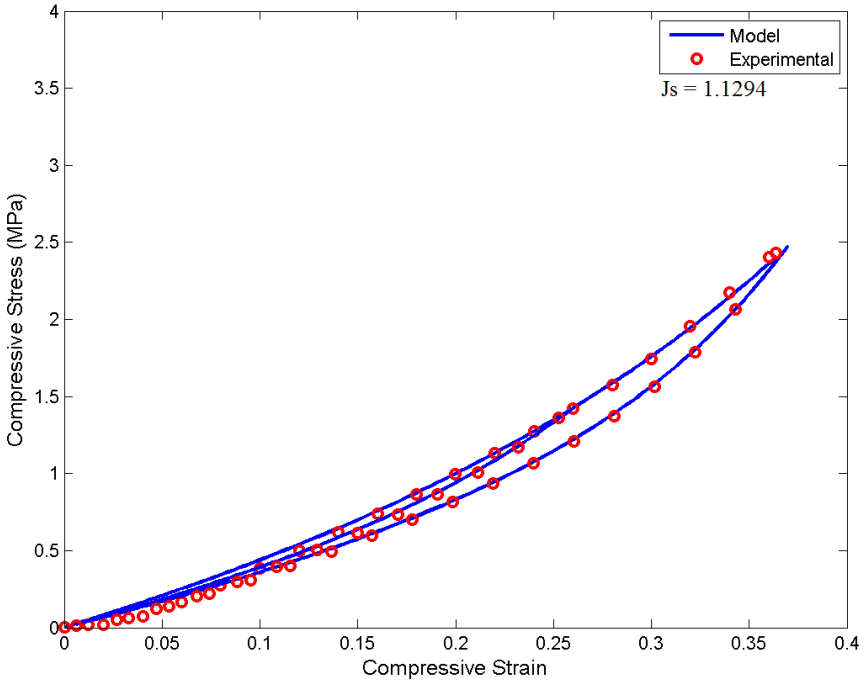

Figure 5.15: Comparison between pseudo-elastic model and experiment for NBR swollen by B100 after 10 days immersion ($\chi = 1.2855$).

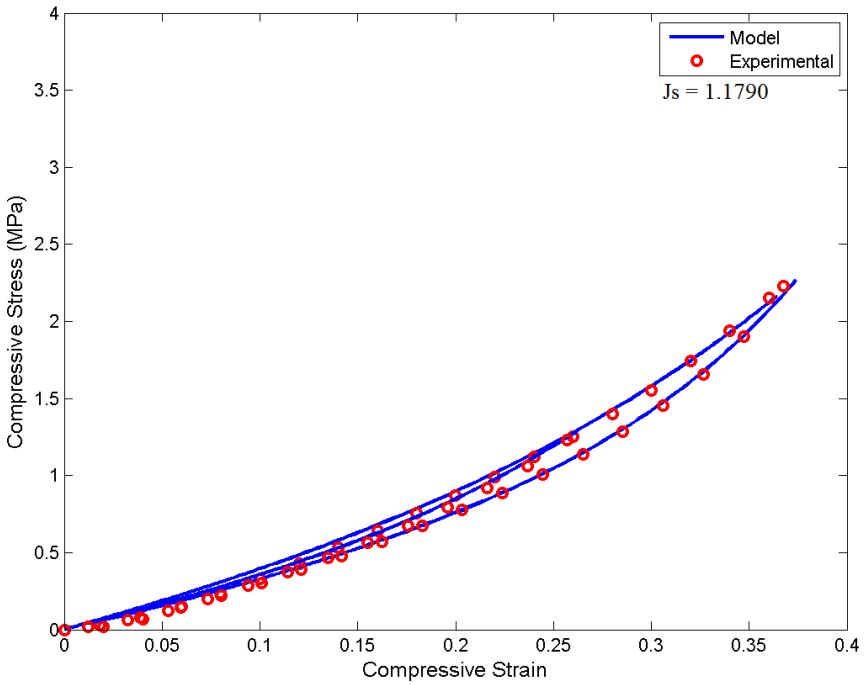

Figure 5.16: Comparison between pseudo-elastic model and experiment for NBR swollen by B100 after 20 days immersion ($\chi = 1.2855$).

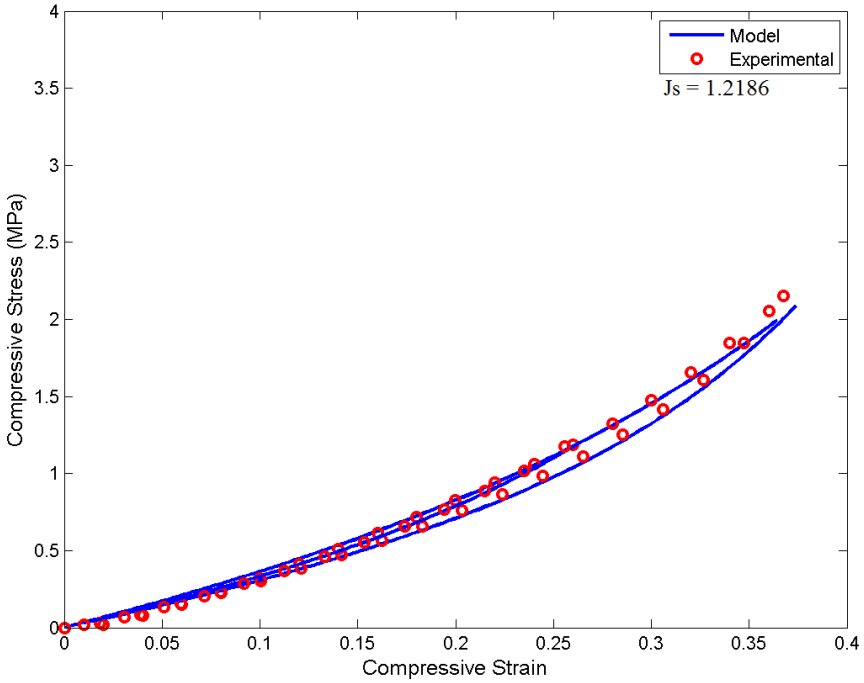

Figure 5.17: Comparison between pseudo-elastic model and experiment for NBR swollen by B100 after 30 days immersion ($\chi = 1.2855$).

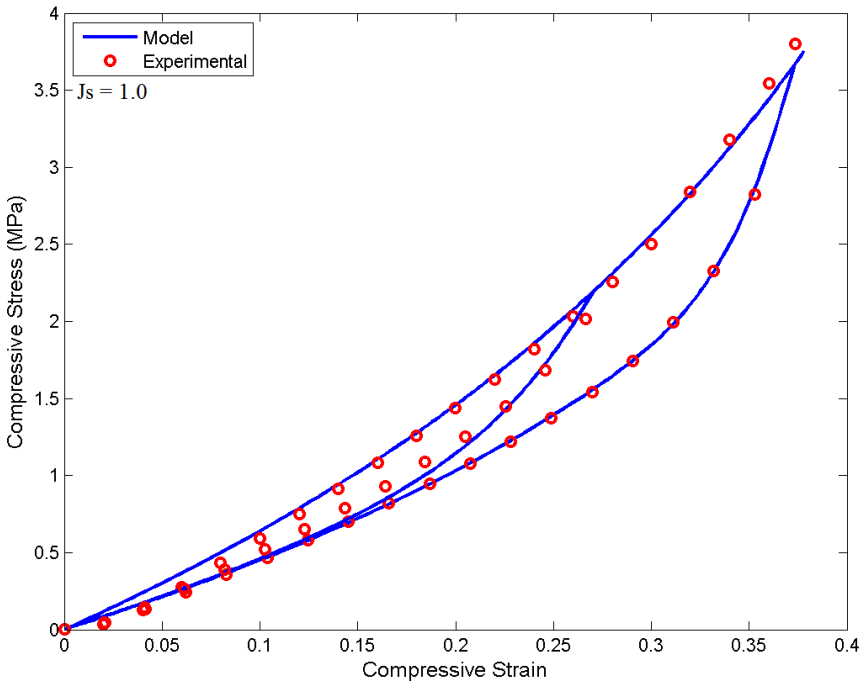

Figure 5.18: Comparison between pseudo-elastic model and experiment for dry CR.

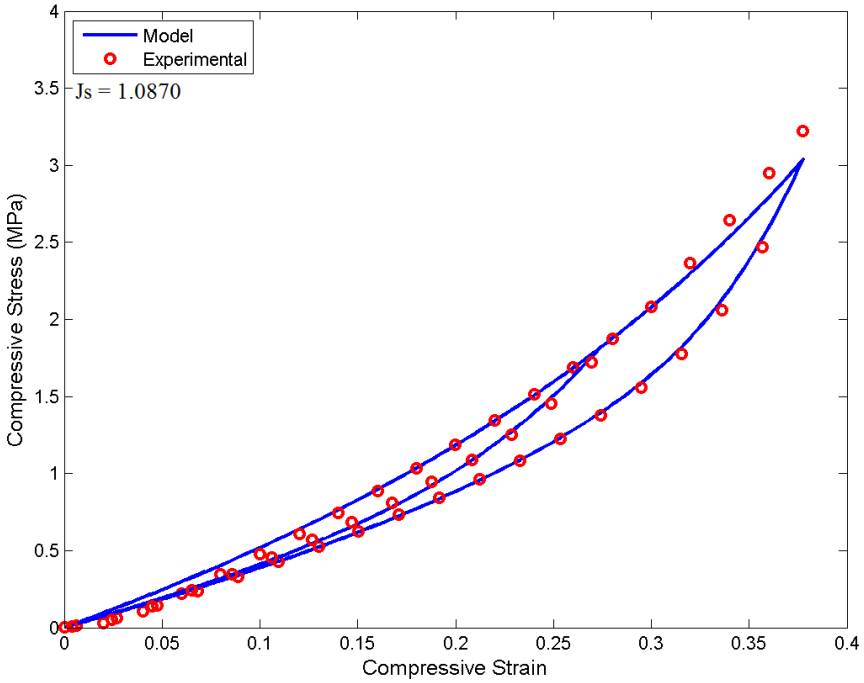

Figure 5.19: Comparison between pseudo-elastic model and experiment for CR swollen by B0 after 2 days immersion ($\chi = 1.3561$).

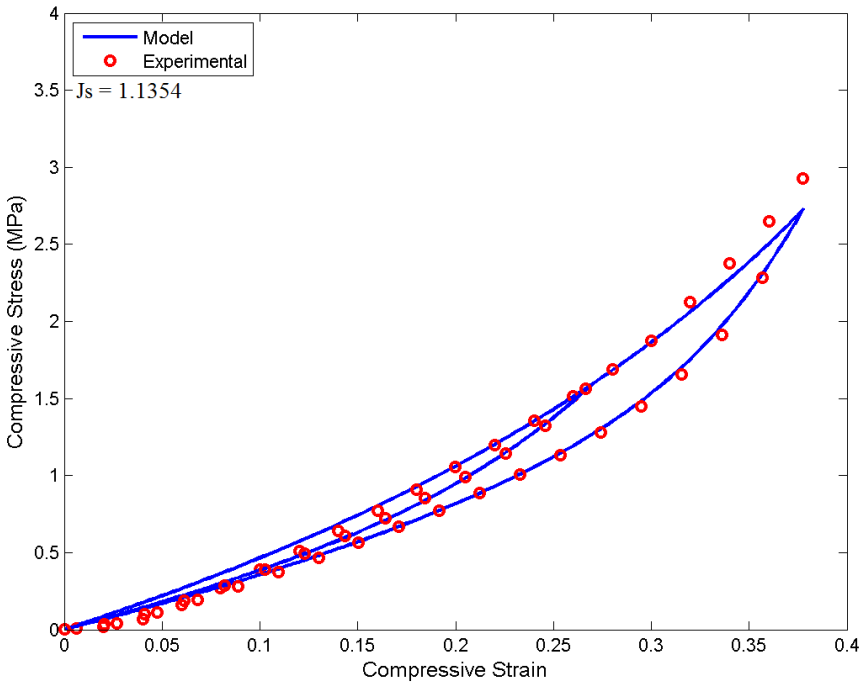

Figure 5.20: Comparison between pseudo-elastic model and experiment for CR swollen by B0 after 5 days immersion ($\chi = 1.3561$).

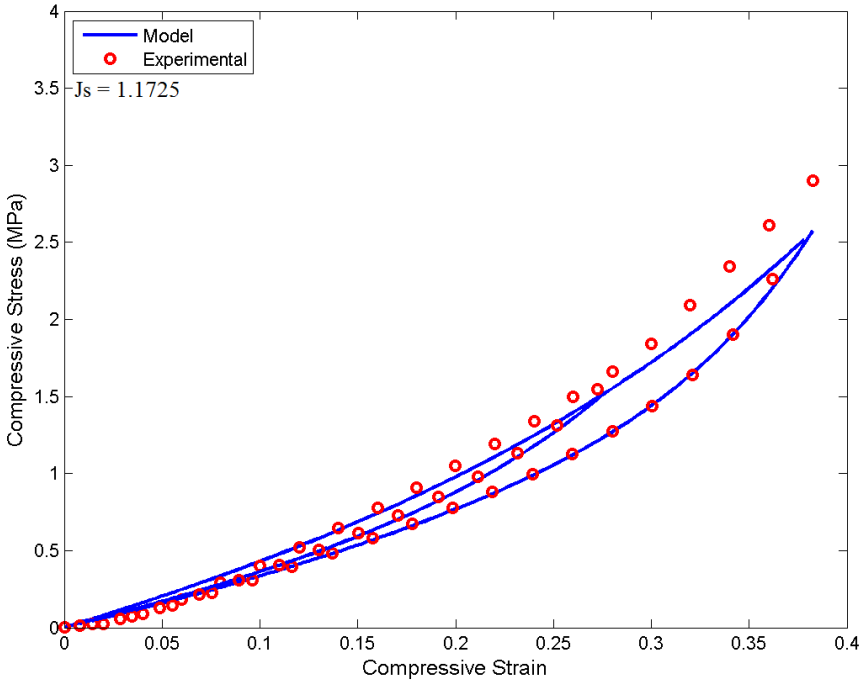

Figure 5.21: Comparison between pseudo-elastic model and experiment for CR swollen by B0 after 10 days immersion ($\chi = 1.3561$).

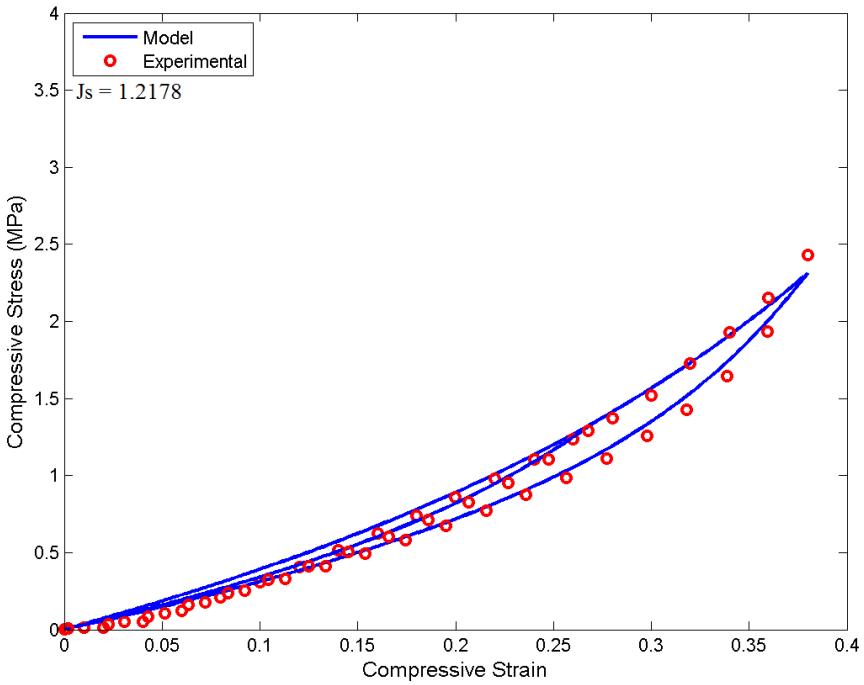

Figure 5.22: Comparison between pseudo-elastic model and experiment for CR swollen by B0 after 20 days immersion ($\chi = 1.3561$).

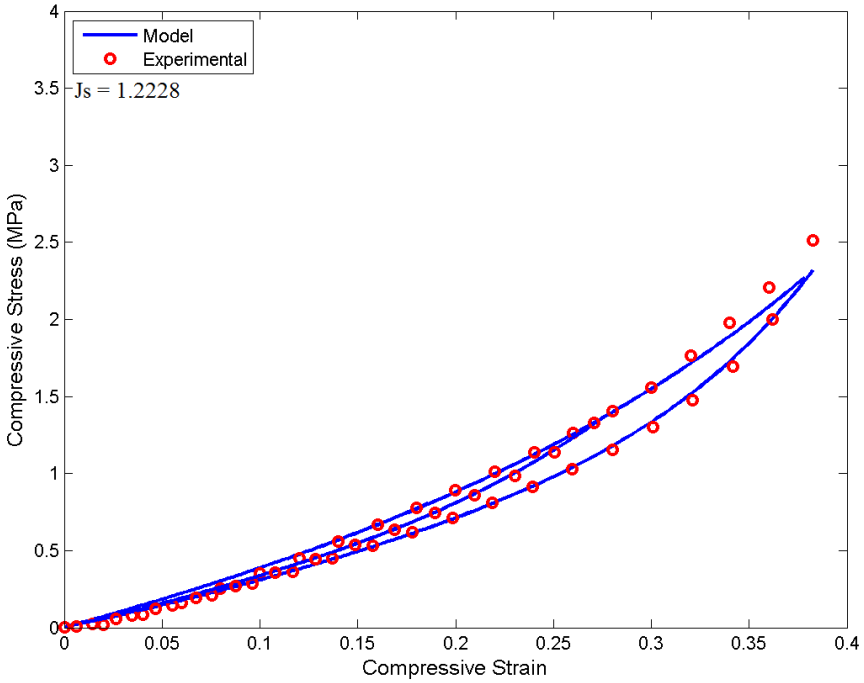

Figure 5.23: Comparison between pseudo-elastic model and experiment for CR swollen by B0 after 30 days immersion ($\chi = 1.3561$).

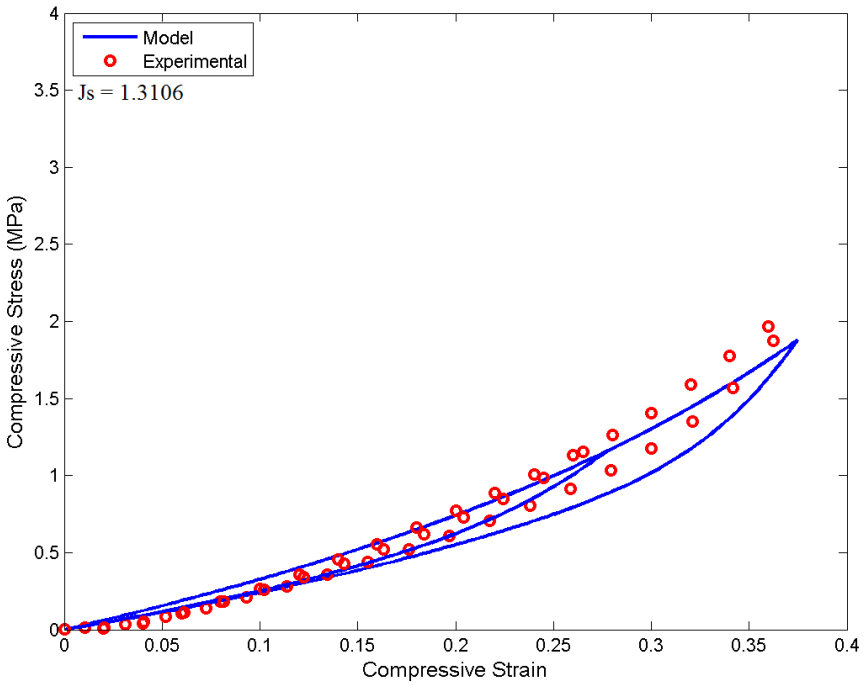

Figure 5.24: Comparison between pseudo-elastic model and experiment for CR swollen by B100 after 2 days immersion ($\chi = 0.3113$).

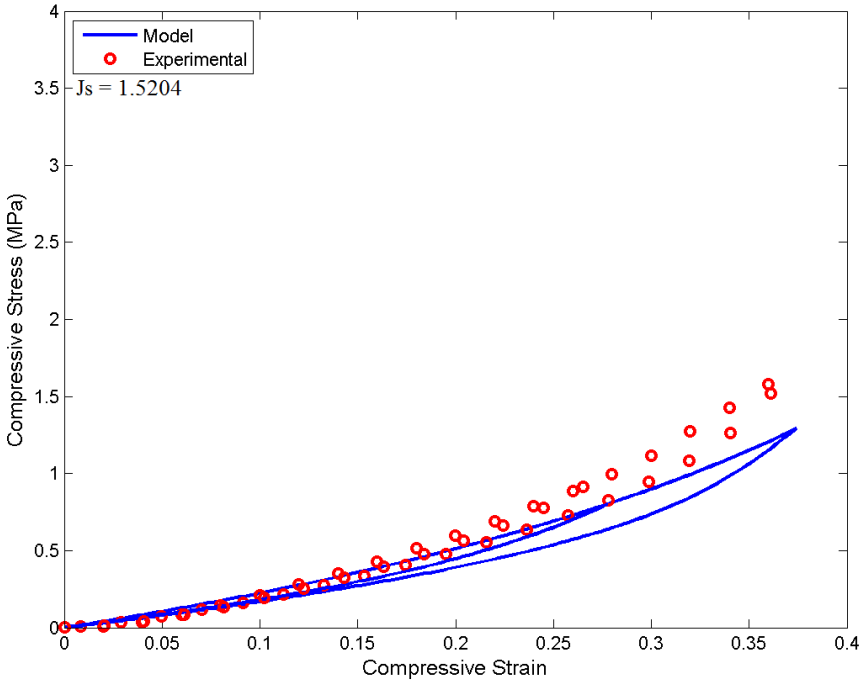

Figure 5.25: Comparison between pseudo-elastic model and experiment for CR swollen by B100 after 5 days immersion ($\chi = 0.3113$).

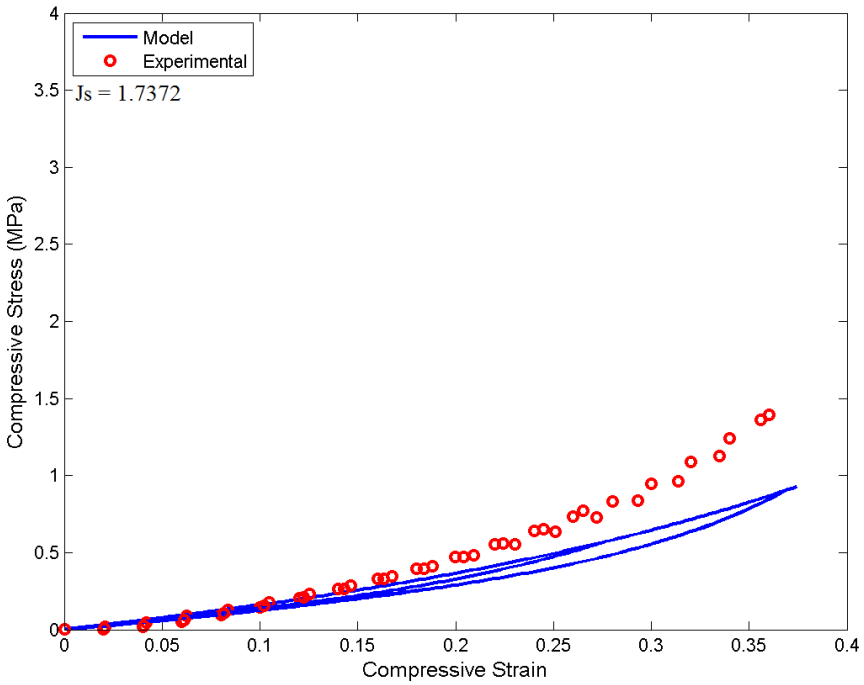

Figure 5.26: Comparison between pseudo-elastic model and experiment for CR swollen by B100 after 10 days immersion ($\chi = 0.3113$).

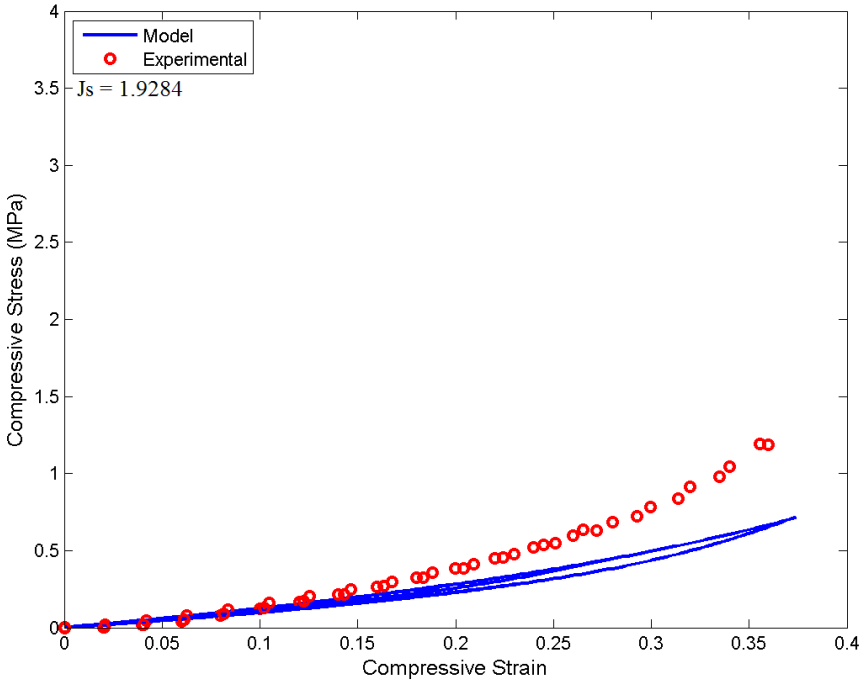

Figure 5.27: Comparison between pseudo-elastic model and experiment for CR swollen by B100 after 20 days immersion ($\chi = 0.3113$).

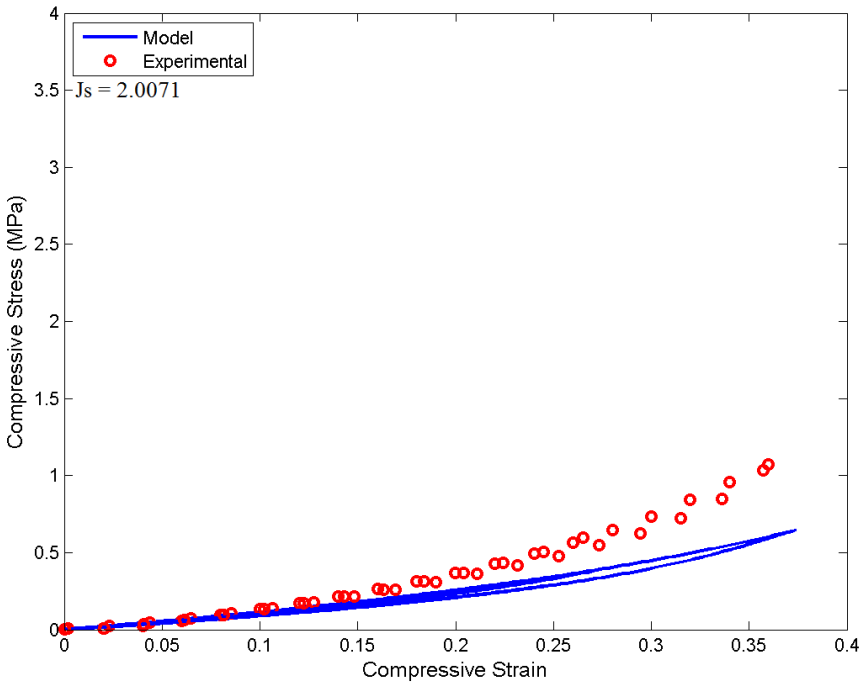

Figure 5.28: Comparison between pseudo-elastic model and experiment for CR swollen by B100 after 30 days immersion ($\chi = 0.3113$).

5.3.4 Simulation for other deformation modes

To simulate the response of the extended pseudo-elastic model under multiaxial loading conditions, deformation modes of uniaxial extension, pure shear and equibiaxial extension are considered in the following. The material is simulated to undergo cyclic loading to two maximum strain levels: ε=0.25 and 0.50. Using the material parameters fitted from the extended pseudo-elastic model under uniaxial compression test results, different degrees of swelling are considered in the simulation. For illustration purpose, only NBR swollen in B0 and B100 for 10 and 20 days and CR swollen in B0 and B100 for 5 and 10 days are simulated.

5.3.4 (a) Uniaxial extension

Simulation of uniaxial extension loading-unloading curves For uniaxial extension, the governing equation needed is given by:

$$\hat{P}_{11} = J_s^{-n} \mu_d \left(1-d\right) \left(\lambda_{\mathrm{m}} - \frac{1}{\lambda_{\mathrm{m}}^2}\right) \tag{5.9}$$

where λ_{m} is the uniaxial extension stretch. The uniaxial extension loading-unloading curves simulated with extended pseudo-elastic model are illustrated in Figures 5.29 to 5.38.

From these figures, it is clearly shown that the proposed extended pseudo-elastic model well predicts that the uniaxial extension loading-unloading curves are affected by the degree of swelling, i.e. lower stress level is produced for rubbers experiencing higher degree of swelling. Furthermore, smaller stress-softening is well predicted when the degree of swelling increases.

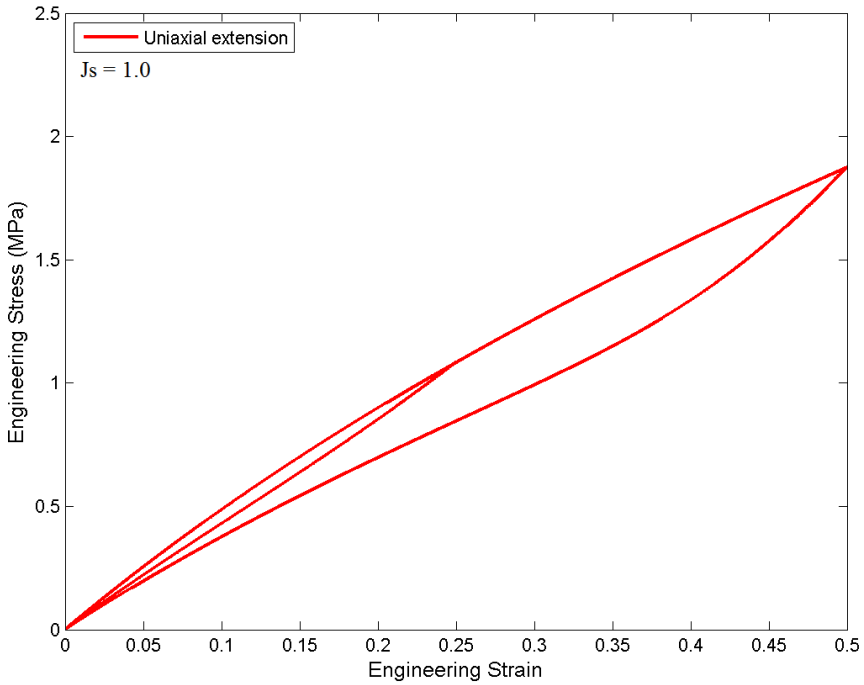

Figure 5.29: Pseudo-elastic model response under uniaxial extension for dry NBR.

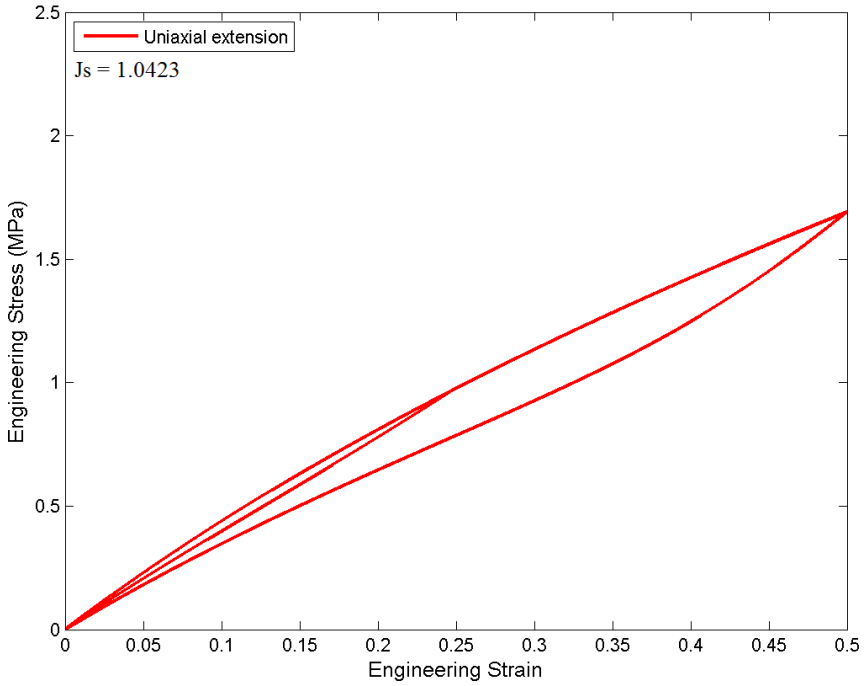

Figure 5.30: Pseudo-elastic model response under uniaxial extension for NBR swollen by B0 after 10 days immersion.

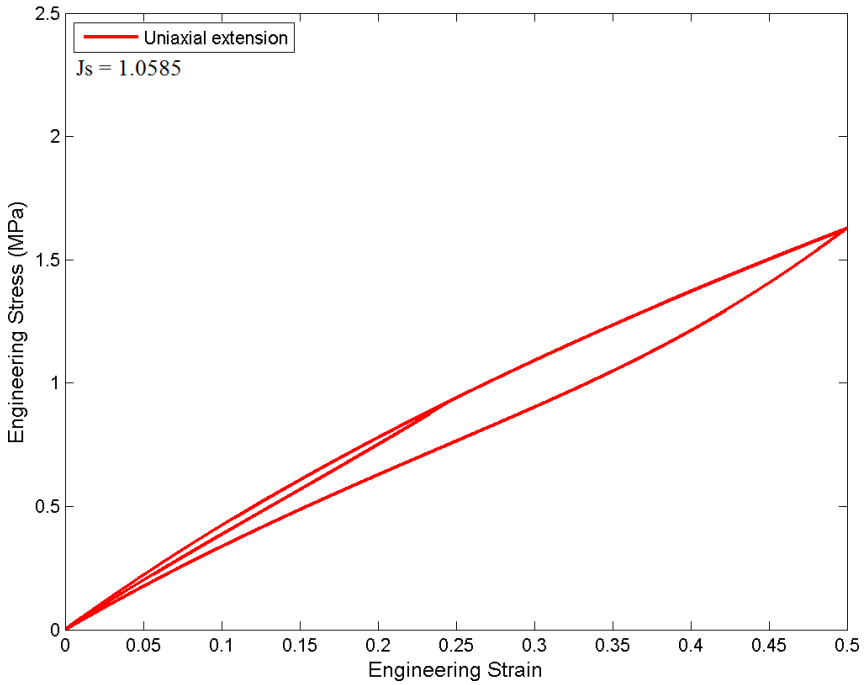

Figure 5.31: Pseudo-elastic model response under uniaxial extension for NBR swollen by B0 after 20 days immersion.

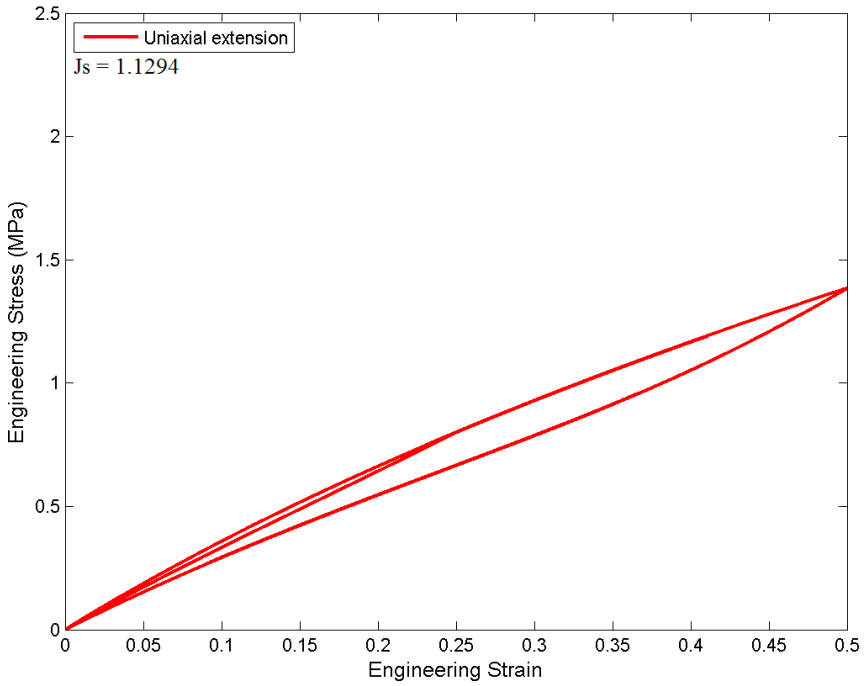

Figure 5.32: Pseudo-elastic model response under uniaxial extension for NBR swollen by B100 after 10 days immersion.

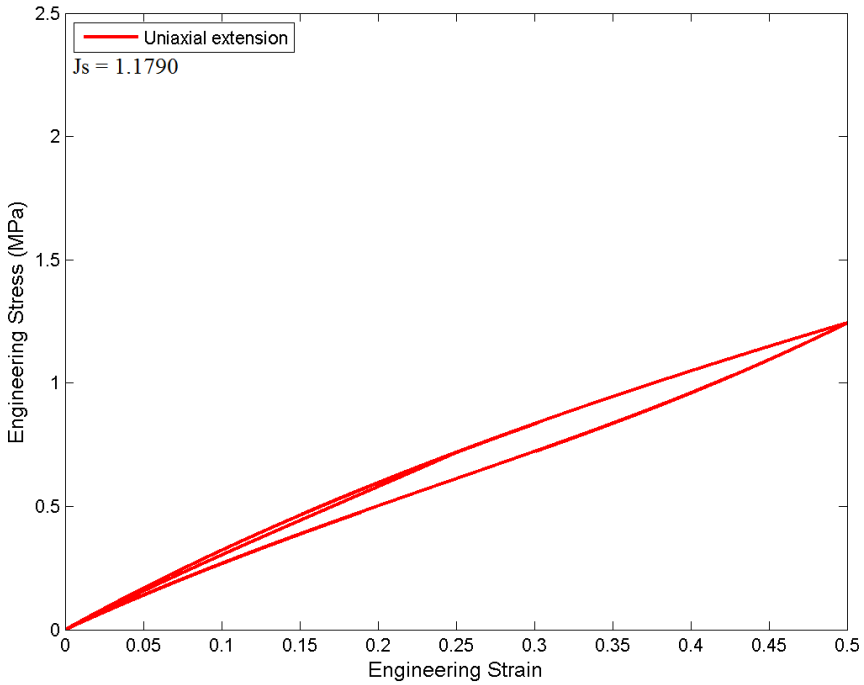

Figure 5.33: Pseudo-elastic model response under uniaxial extension for NBR swollen by B100 after 20 days immersion.

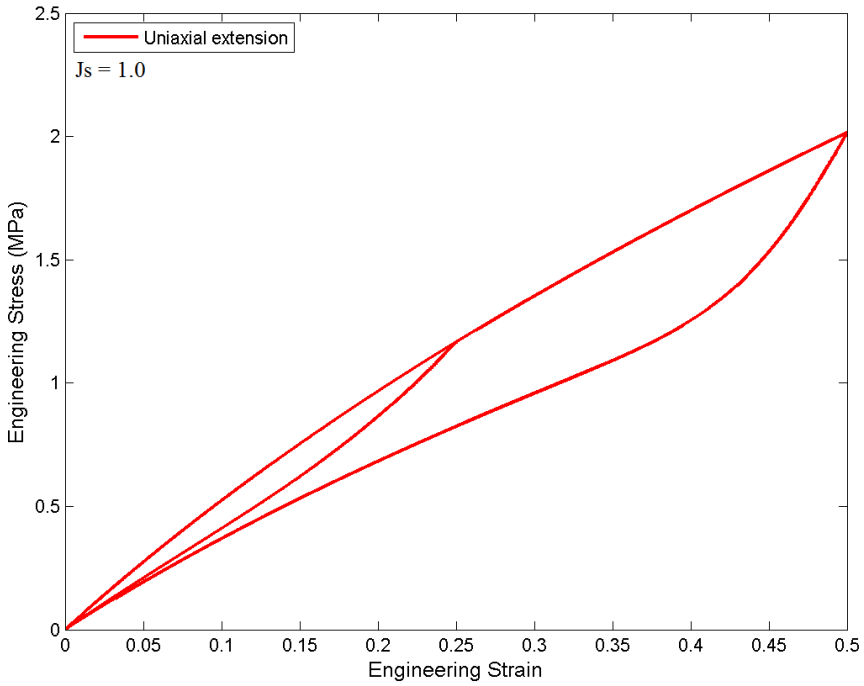

Figure 5.34: Pseudo-elastic model response under uniaxial extension for dry CR.

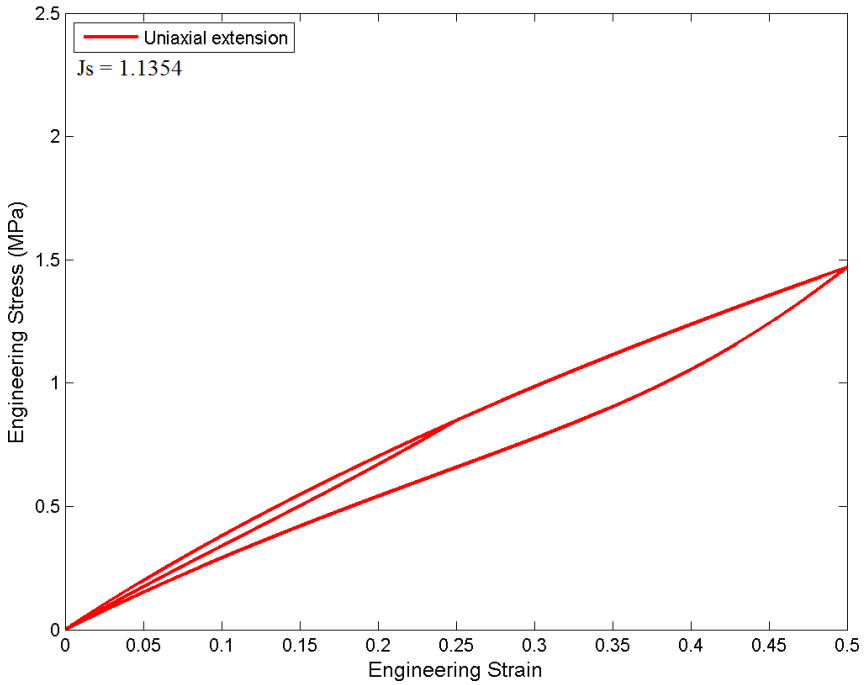

Figure 5.35: Pseudo-elastic model response under uniaxial extension for CR swollen by B0 after 5 days immersion.

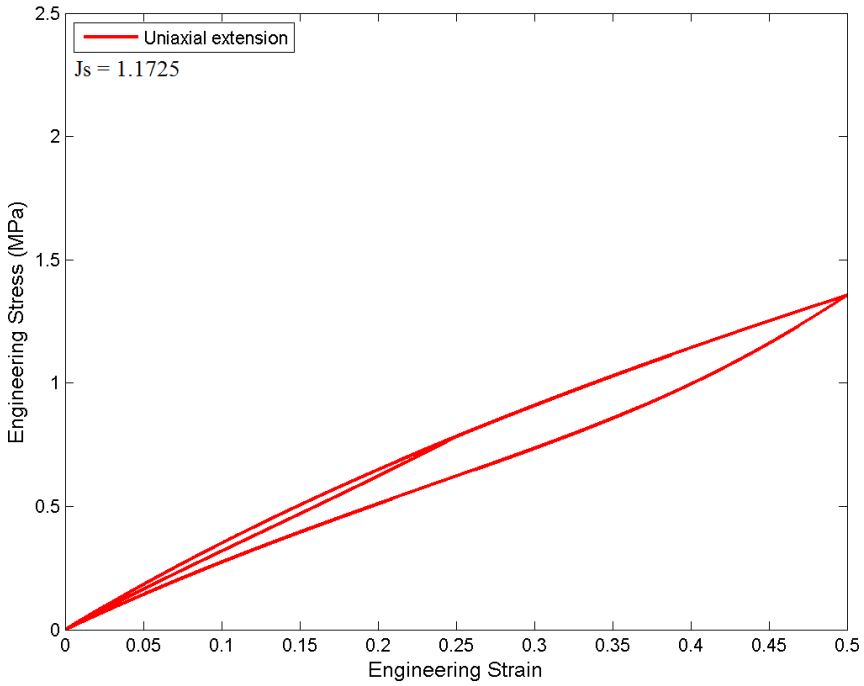

Figure 5.36: Pseudo-elastic model response under uniaxial extension for CR swollen by B0 after 10 days immersion.

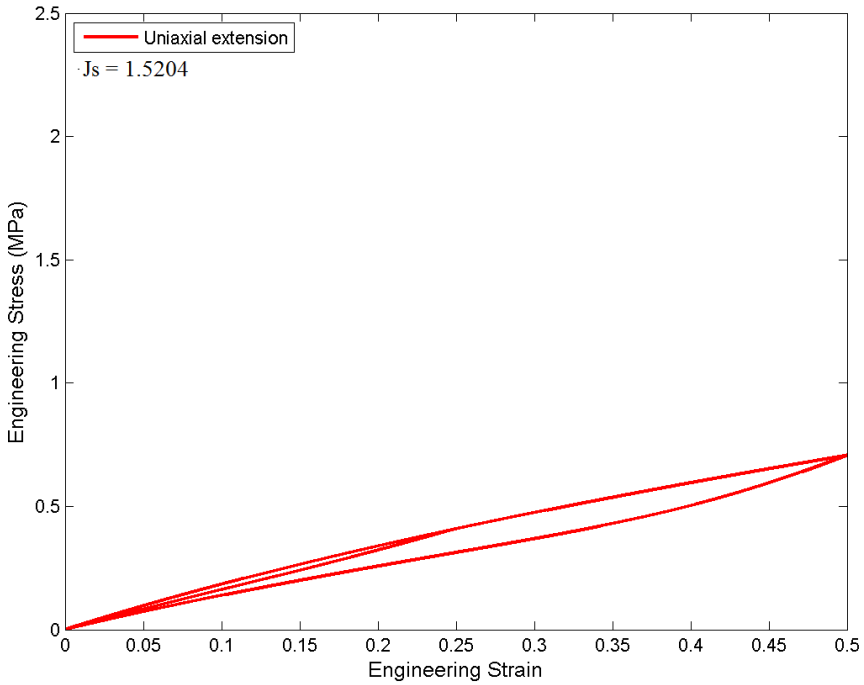

Figure 5.37: Pseudo-elastic model response under uniaxial extension for CR swollen by B100 after 5 days immersion.

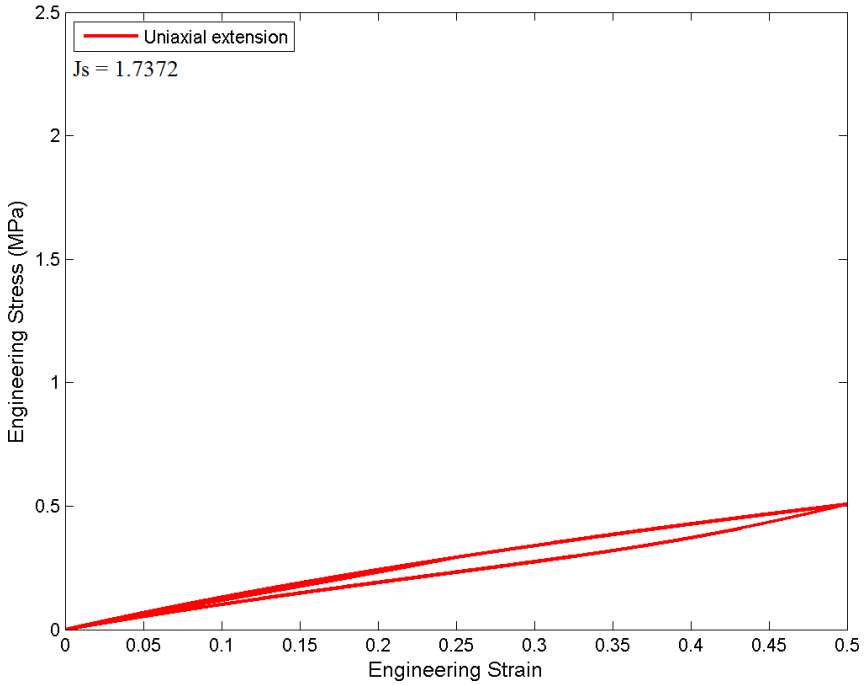

Figure 5.38: Pseudo-elastic model response under uniaxial extension for CR swollen by B100 after 10 days immersion.

Evolution of damage d The evolution of damage d as a function of $I_{1\mathrm{m,max}} - I_{1\mathrm{m}}$ in the uniaxial extension tests during loading to $\varepsilon = 0.5$ for NBR and CR swollen by B100 are depicted in Figures 5.39 and 5.40. It is generally observed that the damage is strongly affected by the degree of swelling and the type of rubber-solvent, i.e. interaction between rubber and biodiesel. More precisely, the Mullins effect appears to decrease with the increase of degree of swelling.

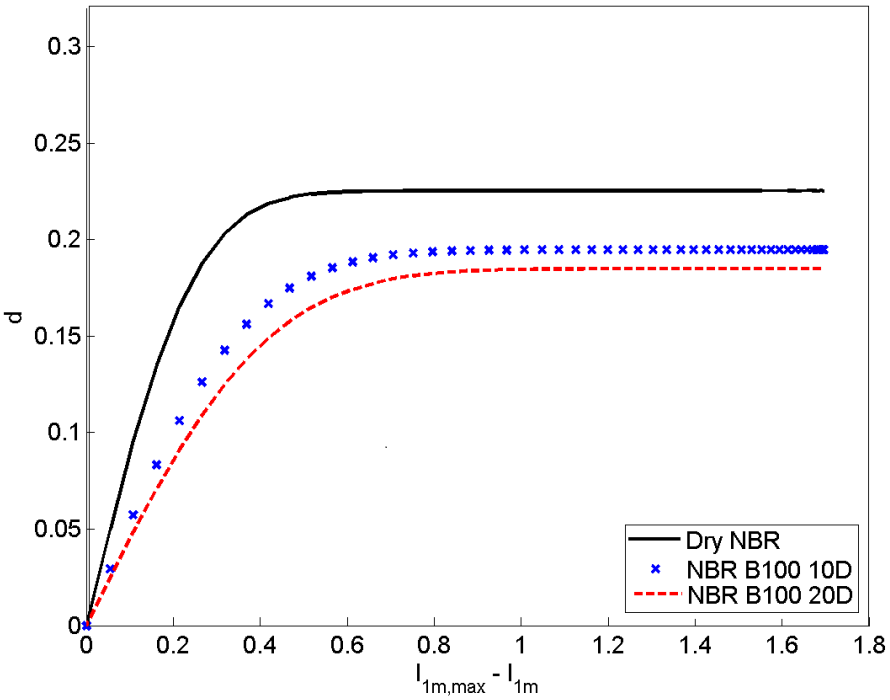

Figure 5.39: Evolution of d under uniaxial extension deformation for NBR swollen by B100. Results correspond to 10 and 20 days of immersion duration.

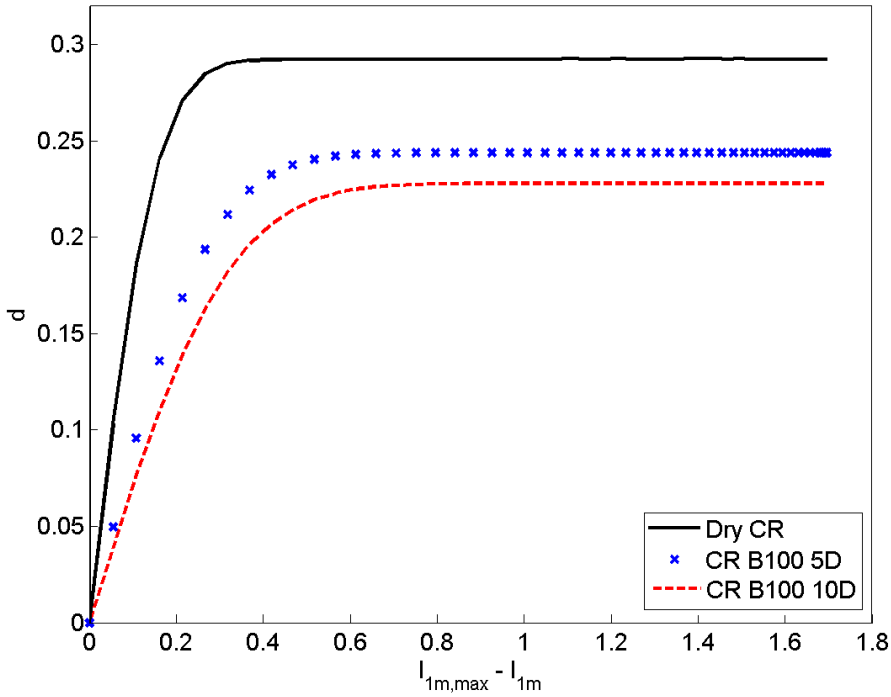

Figure 5.40: Evolution of d under uniaxial extension deformation for CR swollen by B100. Results correspond to 5 and 10 days of immersion duration.

5.3.4 (b) Pure shear

Simulation of pure shear loading-unloading curves For pure shear, the governing equation needed is given by:

$$\hat{P}_{11} = J_s^{-n}\mu_d\,(1-d)\left(\lambda_{\mathrm{m}} - \frac{1}{\lambda_{\mathrm{m}}^3}\right) \tag{5.10}$$

where λ_{m} is the pure shear stretch. The pure shear loading-unloading curves simulated with extended pseudo-elastic model are illustrated in Figures 5.41 to 5.50. From these figures, it is shown that the materials exhibit a slightly more stiff response during unloading/reloading in pure shear than in uniaxial extension. This is because in pure shear the material is subjected to a slightly higher molecular chain stretch than in uniaxial extension at a given strain level. Thus, higher softening is observed in pure shear.

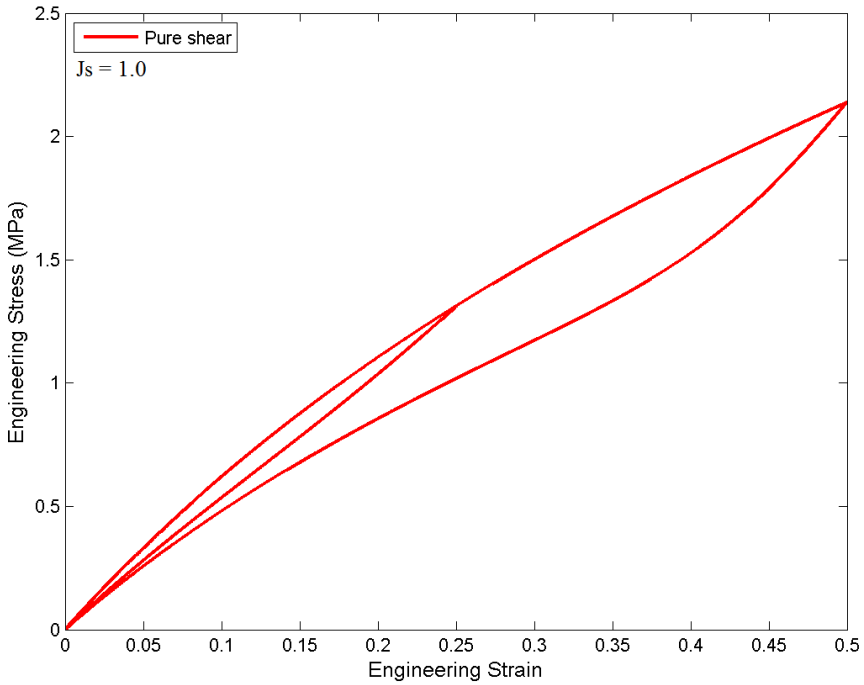

Figure 5.41: Pseudo-elastic model response under pure shear for dry NBR.

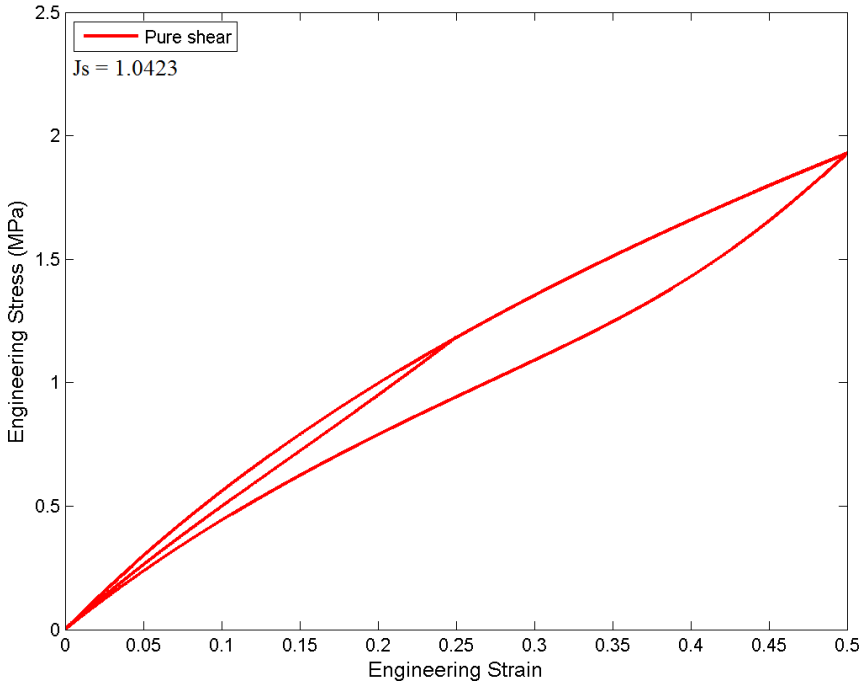

Figure 5.42: Pseudo-elastic model response under pure shear for NBR swollen by B0 after 10 days immersion.

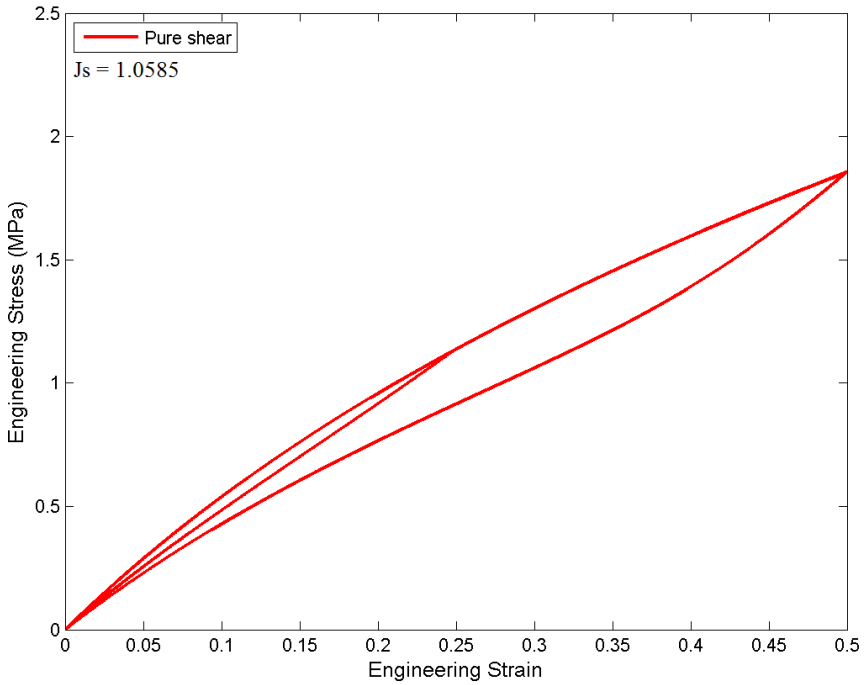

Figure 5.43: Pseudo-elastic model response under pure shear for NBR swollen by B0 after 20 days immersion.

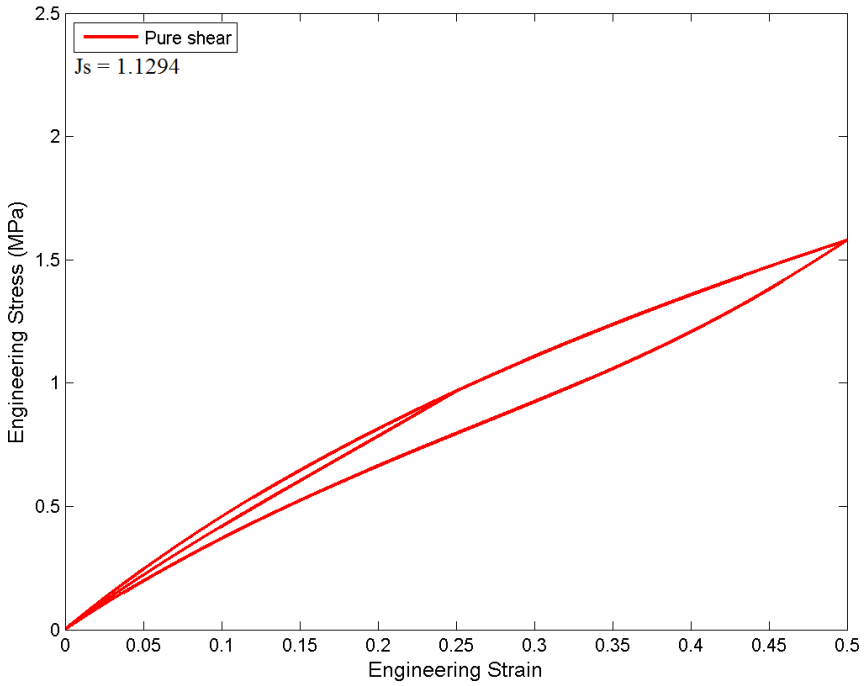

Figure 5.44: Pseudo-elastic model response under pure shear for NBR swollen by B100 after 10 days immersion.

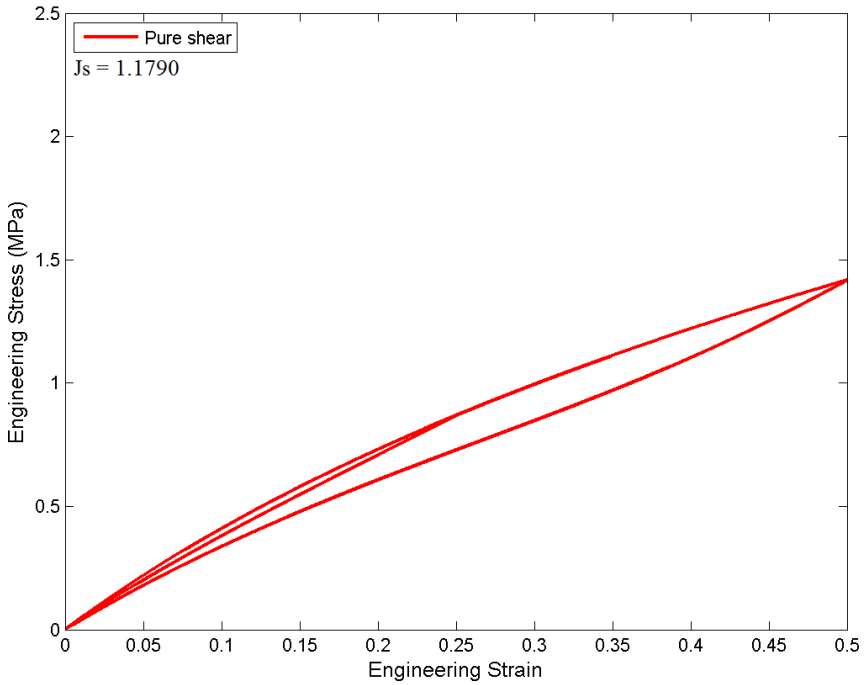

Figure 5.45: Pseudo-elastic model response under pure shear for NBR swollen by B100 after 20 days immersion.

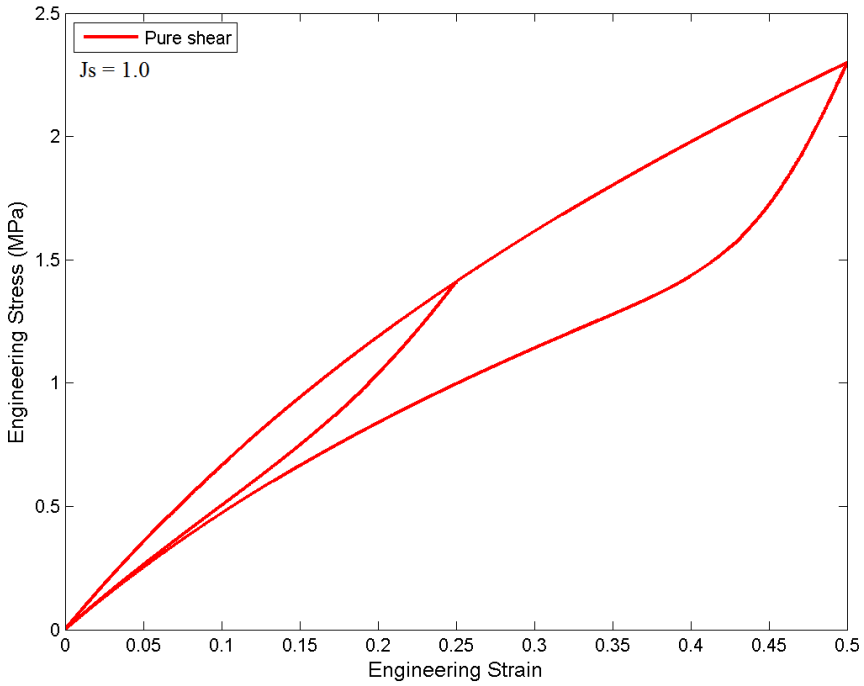

Figure 5.46: Pseudo-elastic model response under pure shear for dry CR.

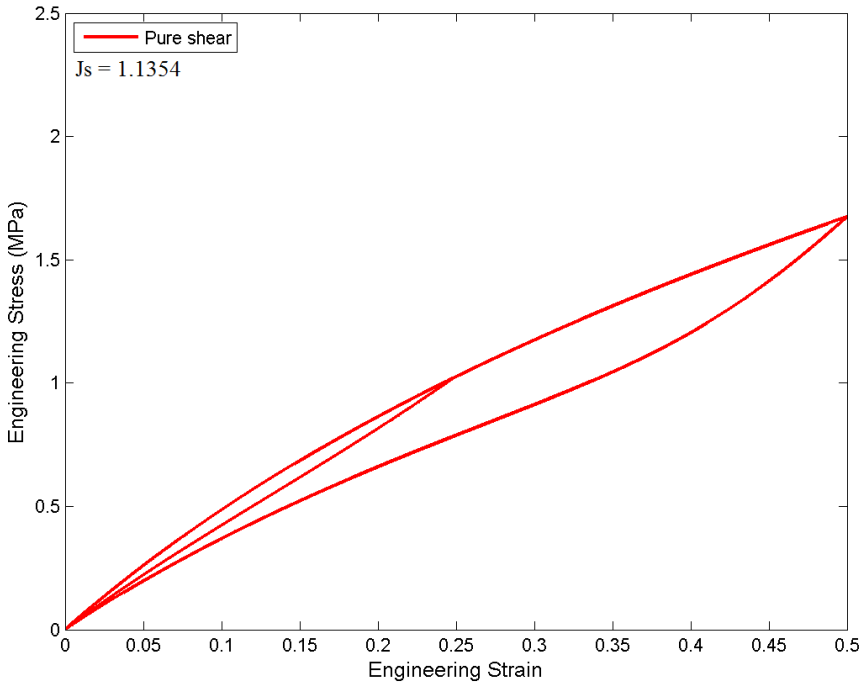

Figure 5.47: Pseudo-elastic model response under pure shear for CR swollen by B0 after 5 days immersion.

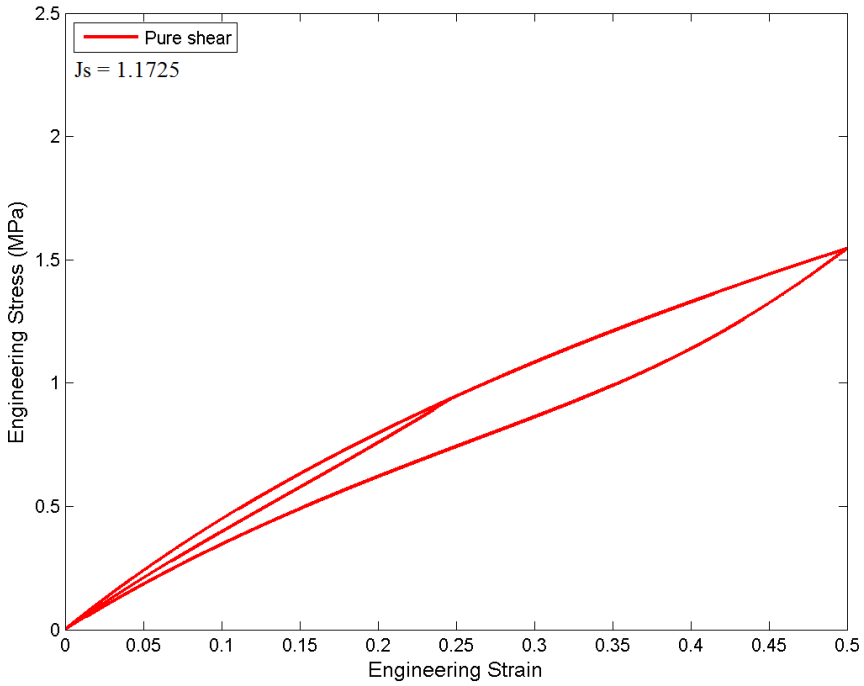

Figure 5.48: Pseudo-elastic model response under pure shear for CR swollen by B0 after 10 days immersion.

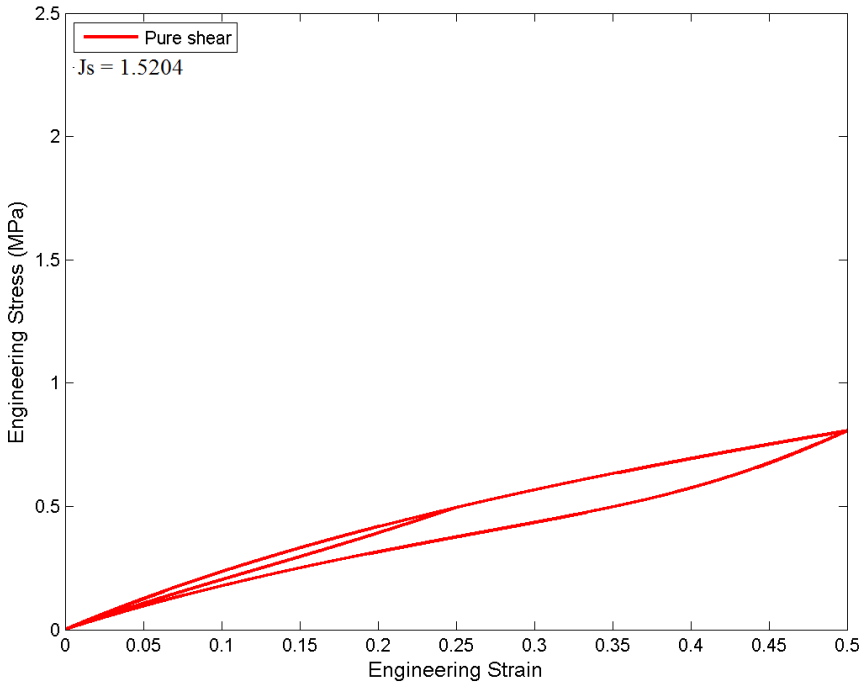

Figure 5.49: Pseudo-elastic model response under pure shear for CR swollen by B100 after 5 days immersion.

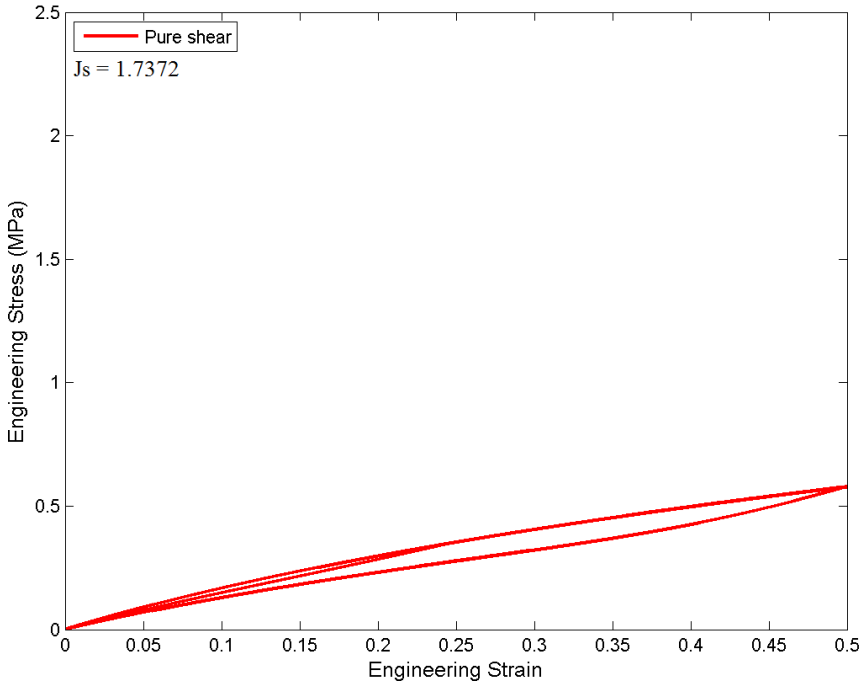

Figure 5.50: Pseudo-elastic model response under pure shear for CR swollen by B100 after 10 days immersion.

Evolution of damage d The evolution of damage d as a function of $I_{1\mathrm{m,max}} - I_{1\mathrm{m}}$ in the pure shear tests during loading to $\varepsilon = 0.5$ for NBR and CR swollen by B100 are depicted in Figures 5.51 and 5.52. The evolution of damage in pure shear is similar to the case of uniaxial extension as shown in Figures 5.39 and 5.40.

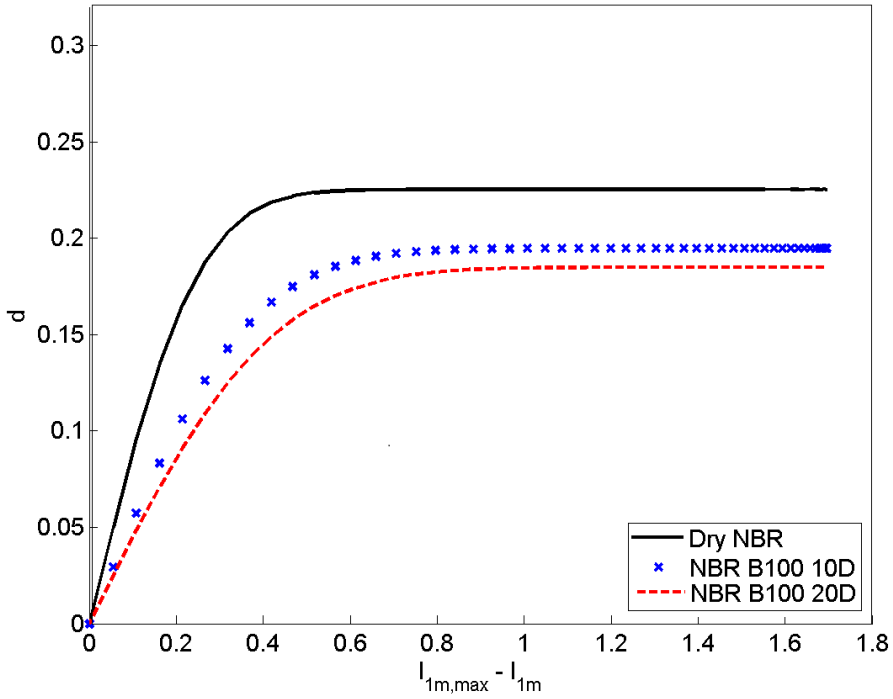

Figure 5.51: Evolution of d under pure shear deformation for NBR swollen by B100. Results correspond to 10 and 20 days of immersion duration.

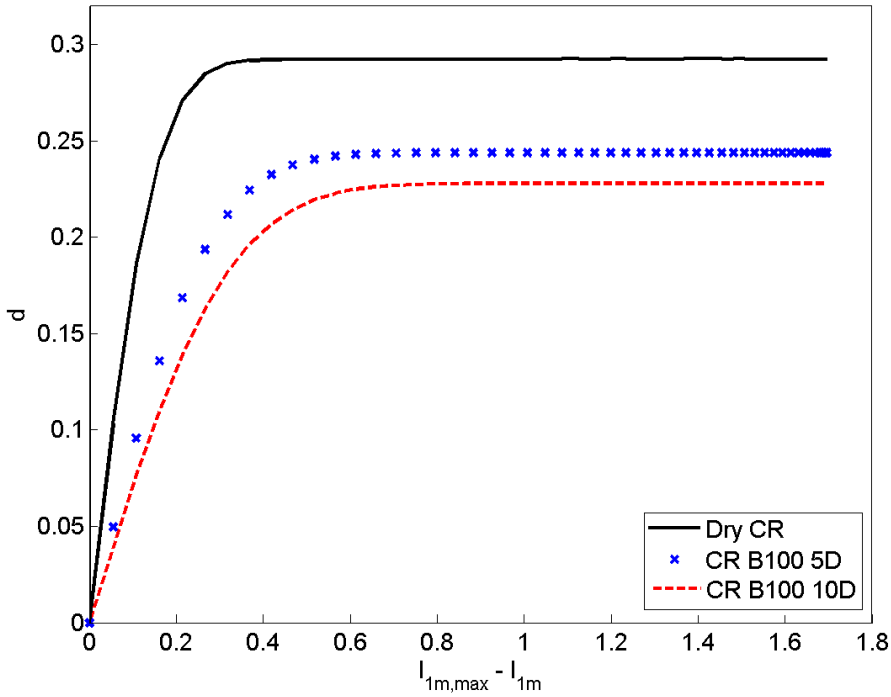

Figure 5.52: Evolution of d under pure shear deformation for CR swollen by B100. Results correspond to 5 and 10 days of immersion duration.

5.3.4 (c) Equibiaxial extension

Simulation of equibiaxial extension loading-unloading curves For equibiaxial extension, the governing equation needed is given by:

$$\hat{P}_{11} = J_s^{-n}\mu_d\,(1-d)\left(\lambda_{\mathrm{m}} - \frac{1}{\lambda_{\mathrm{m}}^5}\right) \tag{5.11}$$

where λ_{m} is the equibiaxial extension stretch. The equibiaxial extension loading-unloading curves simulated with extended pseudo-elastic model are illustrated in Figures 5.53 to 5.62. From these figures, it is demonstrated that the materials show a greater amount of softening (a more compliant response) during reloading in equibiaxial extension than in uniaxial extension. This is because in equibiaxial extension the material is subjected to a higher molecular chain stretch than when in uniaxial extension at a given strain level.

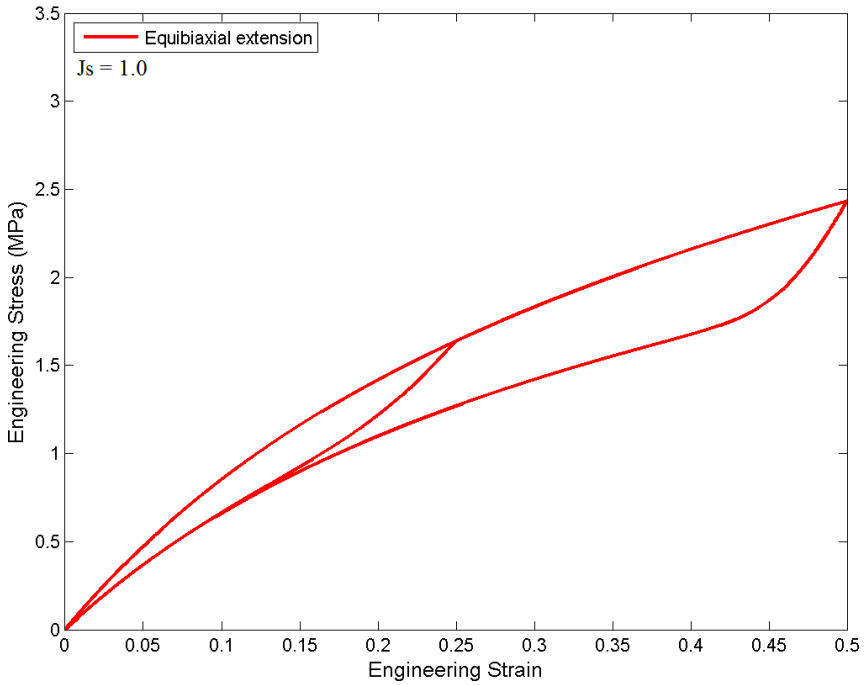

Figure 5.53: Pseudo-elastic model response under equibiaxial extension for dry NBR.

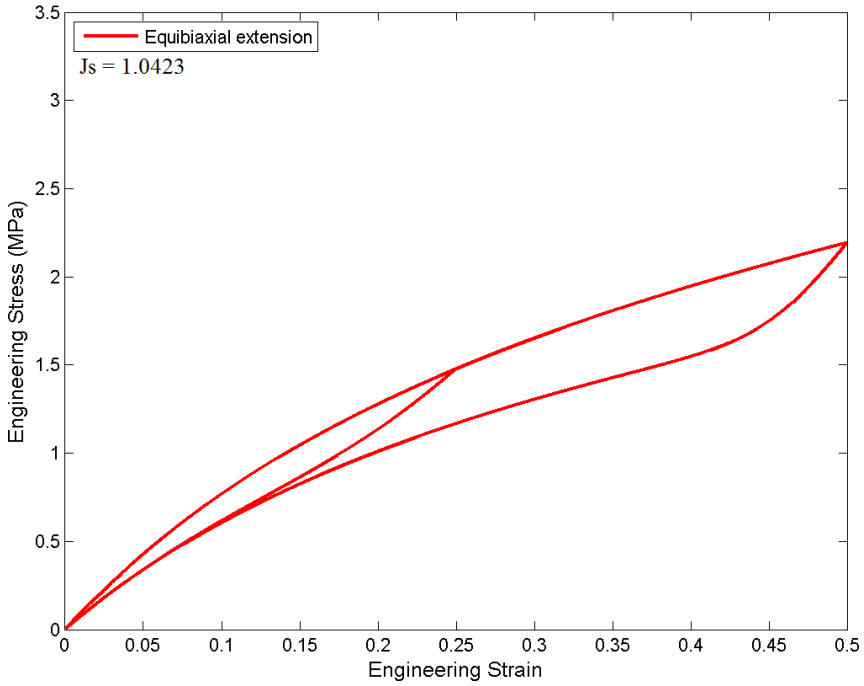

Figure 5.54: Pseudo-elastic model response under equibiaxial extension for NBR swollen by B0 after 10 days immersion.

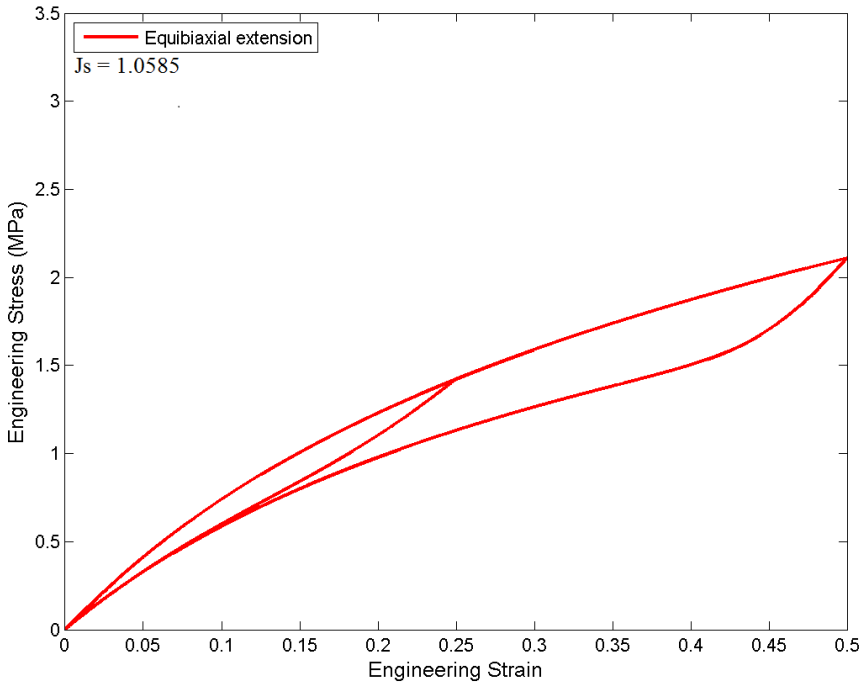

Figure 5.55: Pseudo-elastic model response under equibiaxial extension for NBR swollen by B0 after 20 days immersion.

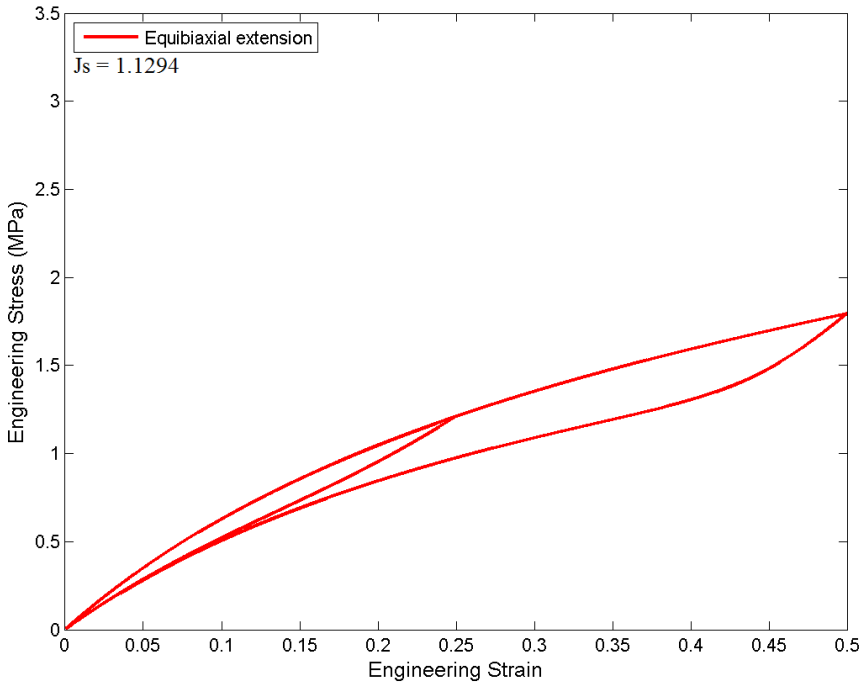

Figure 5.56: Pseudo-elastic model response under equibiaxial extension for NBR swollen by B100 after 10 days immersion.

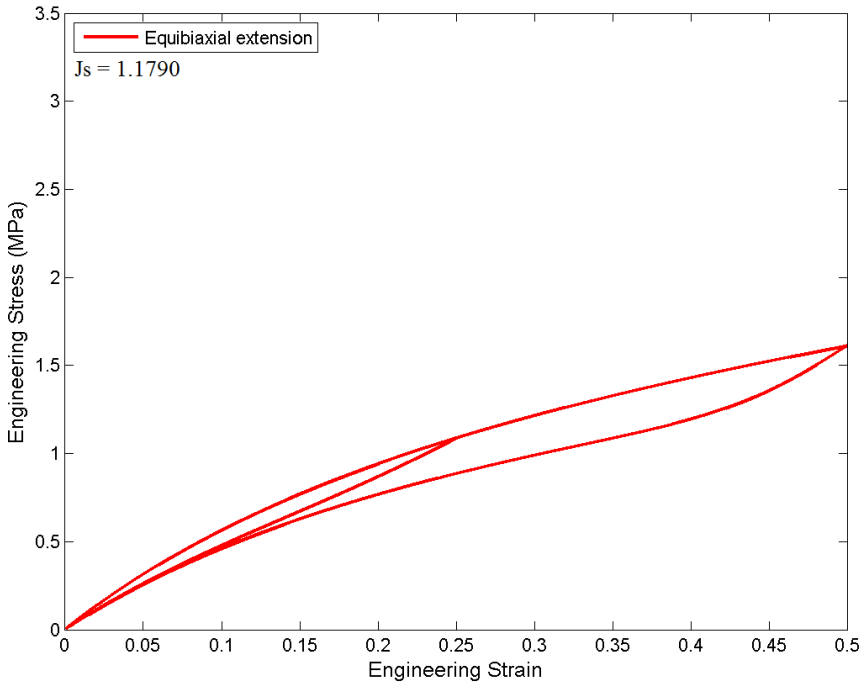

Figure 5.57: Pseudo-elastic model response under equibiaxial extension for NBR swollen by B100 after 20 days immersion.

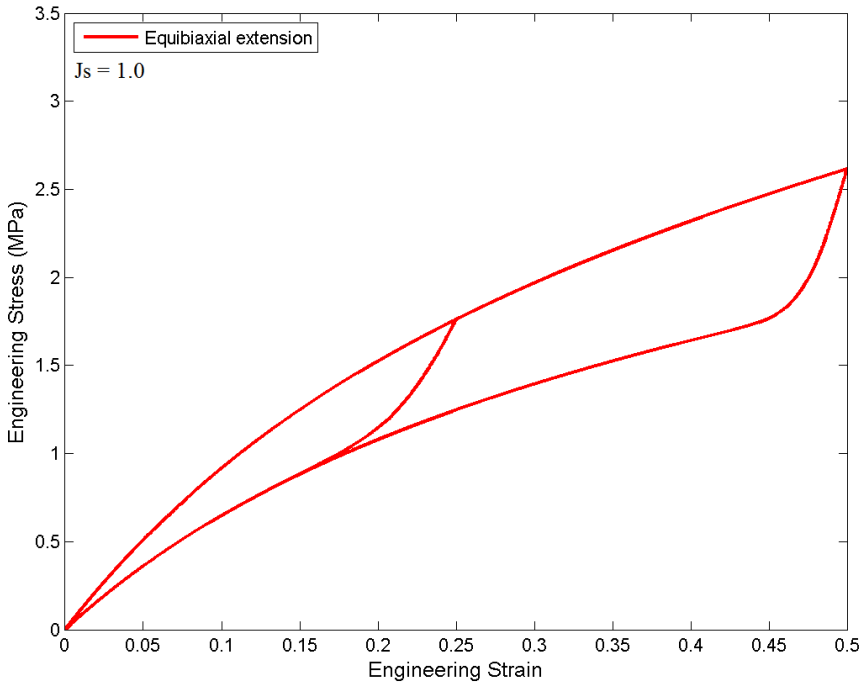

Figure 5.58: Pseudo-elastic model response under equibiaxial extension for dry CR.

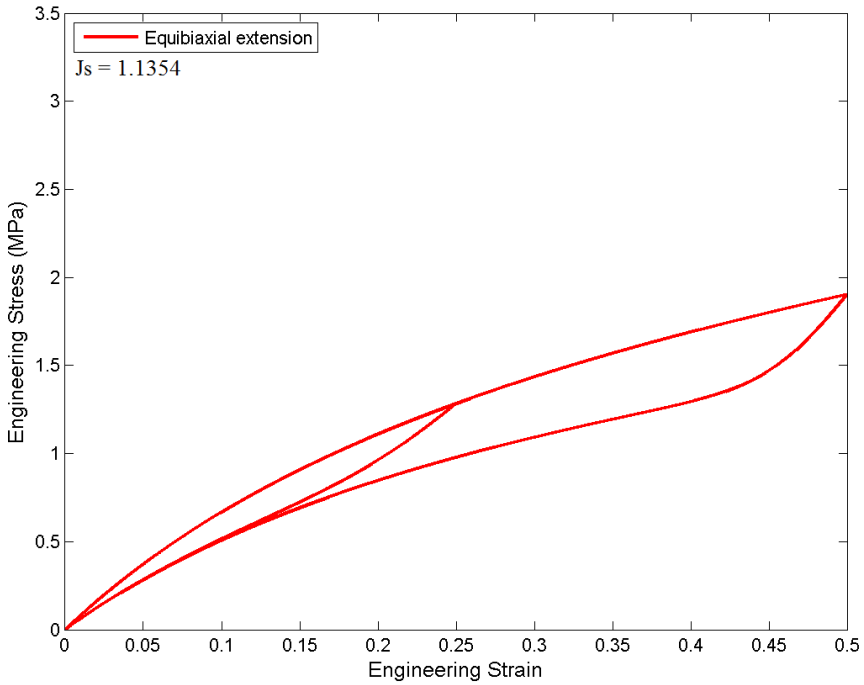

Figure 5.59: Pseudo-elamstic model response under equibiaxial extension for CR swollen by B0 after 5 days immersion.

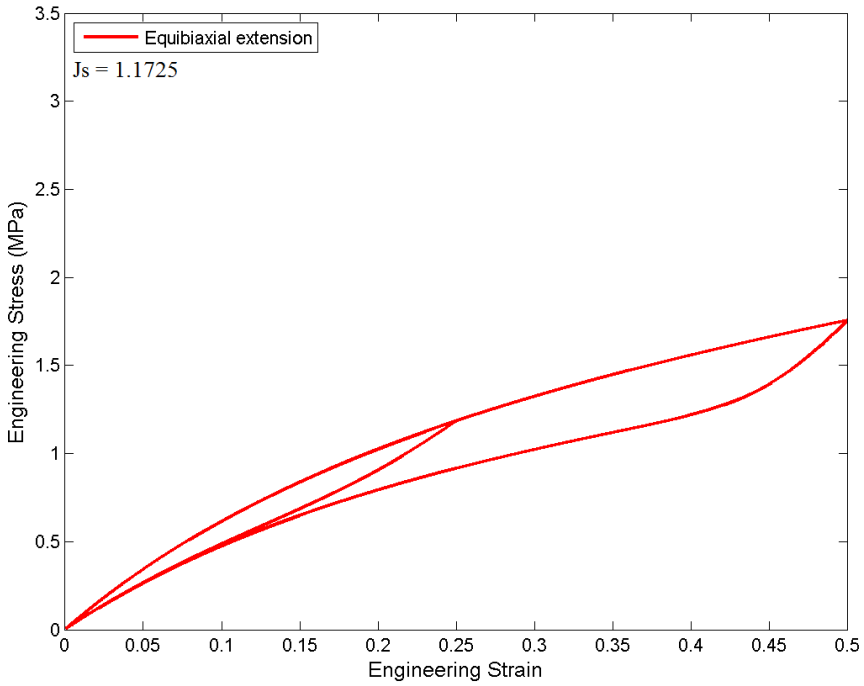

Figure 5.60: Pseudo-elastic model response under equibiaxial extension for CR swollen by B0 after 10 days immersion.

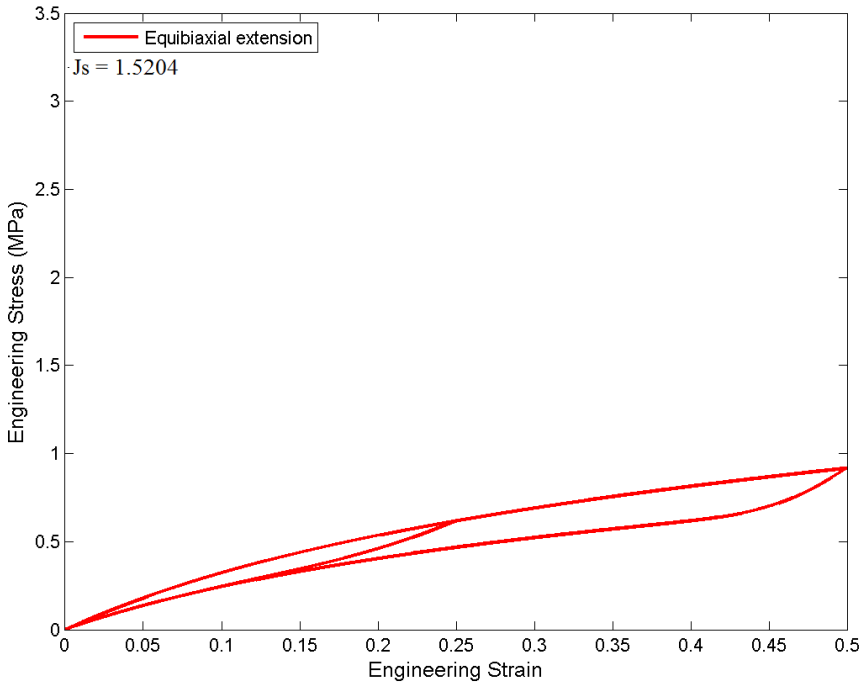

Figure 5.61: Pseudo-elastic model response under equibiaxial extension for CR swollen by B100 after 5 days immersion.

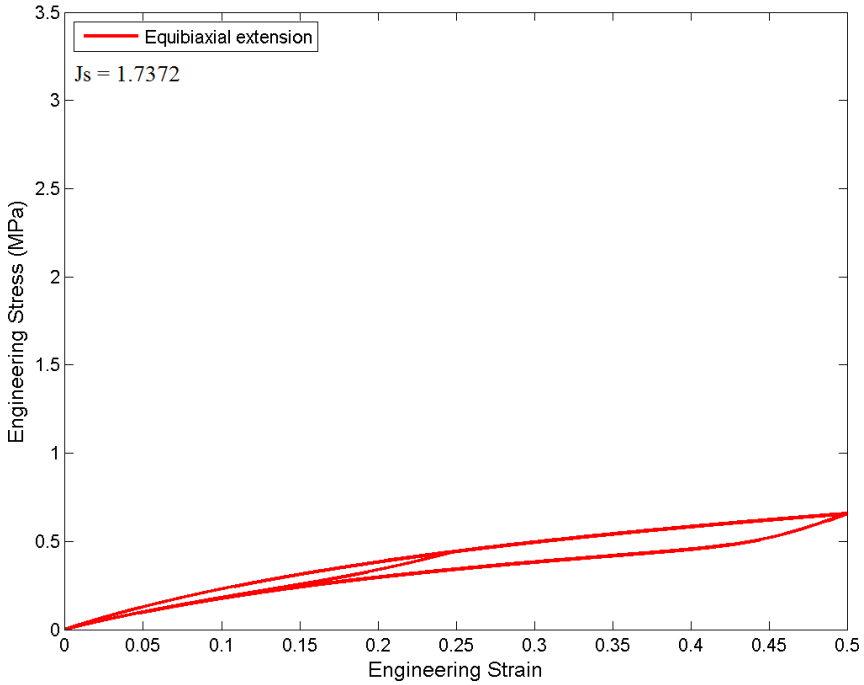

Figure 5.62: Pseudo-elastic model response under equibiaxial extension for CR swollen by B100 after 10 days immersion.

Evolution of damage d The evolution of damage d as a function of $I_{1\mathrm{m,max}} - I_{1\mathrm{m}}$ in the equibiaxial extension tests during loading to $\varepsilon = 0.5$ for NBR and CR swollen by B100 are depicted in Figures 5.63 and 5.64. For a given degree of swelling, it is clearly shown that damage at any given strain is the largest in the case of equibiaxial extension, compared to uniaxial extension and pure shear conditions. Moreover, higher degree of swelling reduces the damage due to Mullins effect

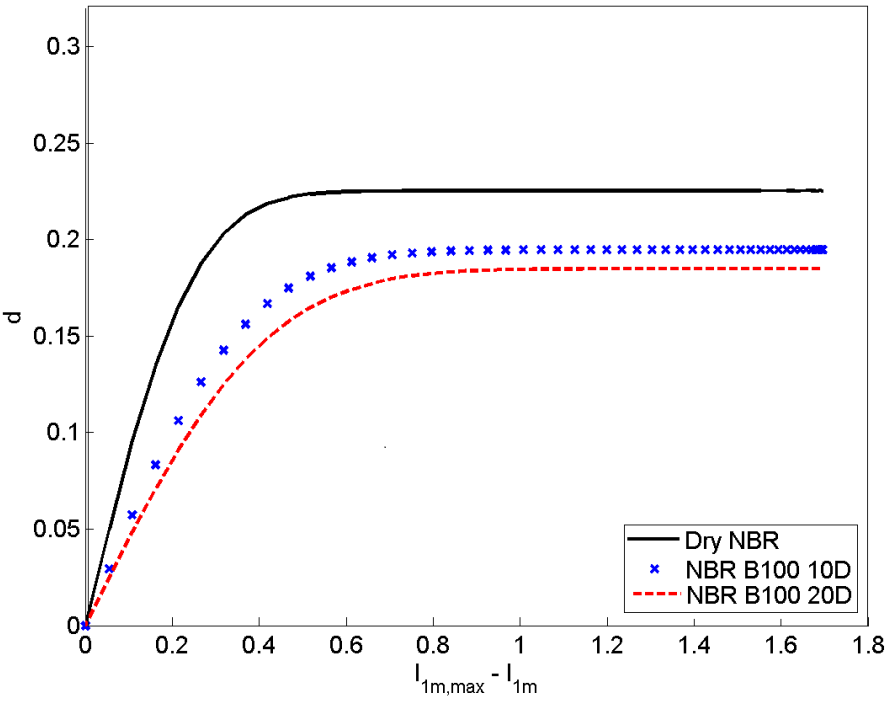

Figure 5.63: Evolution of d under equibiaxial extension deformation for NBR swollen by B100. Results correspond to 10 and 20 days of immersion duration.

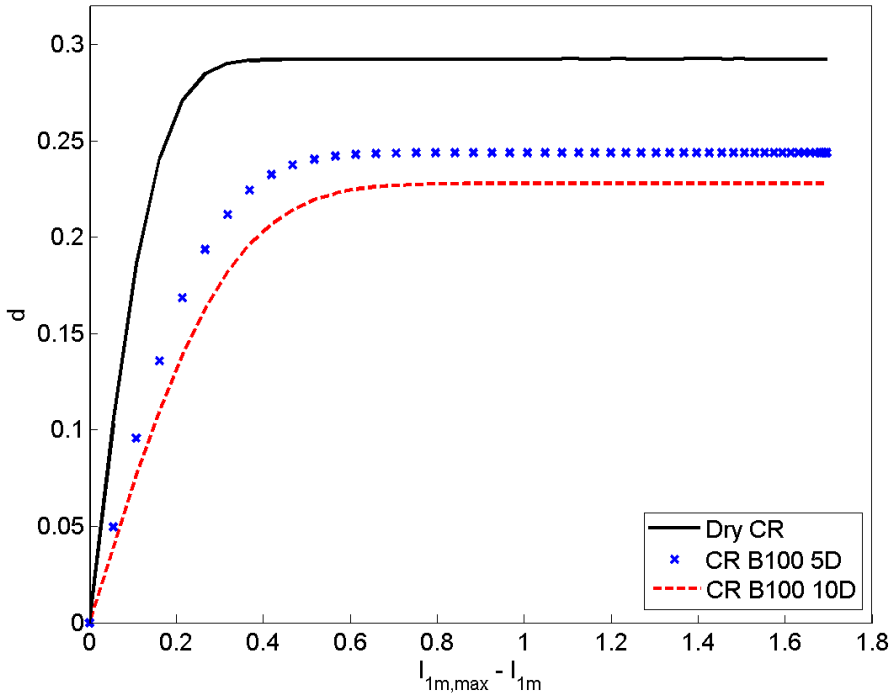

Figure 5.64: Evolution of d under equibiaxial extension deformation for CR swollen by B100. Results correspond to 5 and 10 days of immersion duration.

5.4 Extended two-phase model

5.4.1 Form of material functions

In order to describe the general response of swollen rubbers, Yeoh's hyperelastic strain energy density is specified to describe the mechanical response of dry rubber in the large strain domain:

$$\hat{W} = C_{10}(I_{1\mathrm{m}} - 3) + C_{20}(I_{1\mathrm{m}} - 3)^2 + C_{30}(I_{1\mathrm{m}} - 3)^3. \tag{5.12}$$

where C_{10}, C_{20} and C_{30} are the material constants. Generalizing the idea of Treloar (1975) and following Equation (5.3), it follows that the strain energy function of the soft phase of swollen rubber is given by:

$$\hat{W}_{\text{m-2p}} = \upsilon_s J_s^{-n} \mu_d \tag{5.13}$$

where explicit expression of μ_d from Yeoh's model is given by (Holzapfel, 2000):

$$\mu_d = 2C_{10} + 4C_{20}(I_1 - 3) + 6C_{30}(I_1 - 3)^2. \tag{5.14}$$

In this case, the engineering stress in Eq. (3.59) reduces to:

$$\hat{P}_{11} = J_s^{-n} 2\upsilon_s \left(\lambda_{\mathrm{m}} - \frac{1}{{\lambda_{\mathrm{m}}}^2}\right)(XC_{10} + 2X^2C_{20}(I_{1\mathrm{m}} - 3) + 3X^3C_{30}(I_{1\mathrm{m}} - 3)^2) \tag{5.15}$$

This constitutive equation must be complemented by an evolution equation describing the change in the internal variable υ_s consistent with the second law of thermodynamics. Here, we choose to replace $\dot{\lambda}_{chain}^{max}$ in Equation (3.52) by $\dot{I}_{1\mathrm{m}}^{max}$ for the sake of simplicity. Thus, Equation (3.52) becomes:

$$\dot{\upsilon}_s = A(\upsilon_{ss} - \upsilon_s)\dot{I}_{1\mathrm{m}}^{max}. \tag{5.16}$$

where $\dot{I}_{1\mathrm{m}}^{max}$ is the amplified maximum first invariant of the corresponding stretch.

To summarize, the following parameters in Table 5.6 have to be identified:

Table 5.6: Summary of material parameters required in the proposed model.

Hyperelasticity (Yeoh)	C_{10}	C_{20}	C_{30}
Mullins-effect	υ_s	υ_{ss}	A
Swelling	n		

5.4.2 Identification of material parameters

In the following, the methods to estimate material parameters of the proposed model are discussed. First of all, the material parameters corresponding to dry rubber are determined. The properties of the soft domain in dry rubber can be obtained by considering the last unloading curve (see Figure 5.2 for example). The volume fraction of soft domain at this point ($\varepsilon_{\max} = 0.4$) is first estimated to be $\upsilon_s \approx 0.80$ for both CR and NBR. Using this value, the parameters C_{10}, C_{20} and C_{30} are determined by fitting the same curve using the Yeoh hyperelastic strain energy. Next, the initial soft phase fraction of dry rubber, $\upsilon_{so,d}$, υ_{ss} and A can be identified by fitting simultaneously the primary curve and all the unloading curves of the dry rubber.

For swollen rubbers, the power law parameter n and the initial soft phase fraction of swollen rubber $\upsilon_{so,s}$ are estimated by fitting simultaneously the primary curve and all the unloading curves of the swollen rubbers. To study the effect of swelling on the soften-

ing, the dependence of the initial volume fraction of the soft phase υ_{so} on the degree of swelling J_s need to be examined. For the sake of simplicity, it is assumed that swelling only affects the υ_{so} in the swollen rubber, but not υ_{ss} and A. More precisely, swelling increases υ_{so} available in swollen rubber during deformation. This assumption is motivated by the discussion provided in Section 3.2.3 (a). The estimated parameters are summarized in the Table 5.7 to 5.9.

Table 5.7: Values of material parameters used in model.

	NBR	CR
C_{10}	0.27	0.27
C_{20}	-0.01	-0.01
C_{30}	0.01	0.025
$\upsilon_{so,d}$	0.38	
υ_{ss}	0.9	
A	0.5	0.79
n	2.5	

Table 5.8: $\upsilon_{so,s}$ for swollen NBR.

	B0 2D	B0 5D	B0 10D	B0 20D	B0 30D	B100 2D	B100 5D	B100 10D	B100 20D	B100 30D
$\upsilon_{so,s}$	0.38	0.38	0.38	0.38	0.38	0.38	0.38	0.42	0.42	0.42

Table 5.9: $\upsilon_{so,s}$ for swollen CR.

	B0 2D	B0 5D	B0 10D	B0 20D	B0 30D	B100 2D	B100 5D	B100 10D	B100 20D	B100 30D
$\upsilon_{so,s}$	0.38	0.42	0.42	0.42	0.42	0.48	0.48	0.48	0.48	0.48

Referring to Table 5.8 and 5.9, it is observed that the initial volume fraction of the soft phase in swollen rubber $\upsilon_{so,s}$ increases with degree of swelling J_s. Figure 5.65 depicts the plot of $\upsilon_{so,s}$ as a function of J_s. It appears that the dependence of initial effective volume fraction of soft domain in swollen rubber $\upsilon_{so,s}$ on degree of swelling J_s can be

approximately described by:

$$\upsilon_{so,s} = \upsilon_{so,d} + \left[\frac{\upsilon_{so,m} - \upsilon_{so,d}}{2}\right] + \left[\frac{\upsilon_{so,m} - \upsilon_{so,d}}{2}\right][\tanh(22J_s - 26)] \tag{5.17}$$

where $\upsilon_{so,m}$ = 0.48 is the maximum initial soft phase fraction of the swollen rubber and $\upsilon_{so,d}$ is the initial soft phase fraction of the dry rubber as given in Table 5.7.

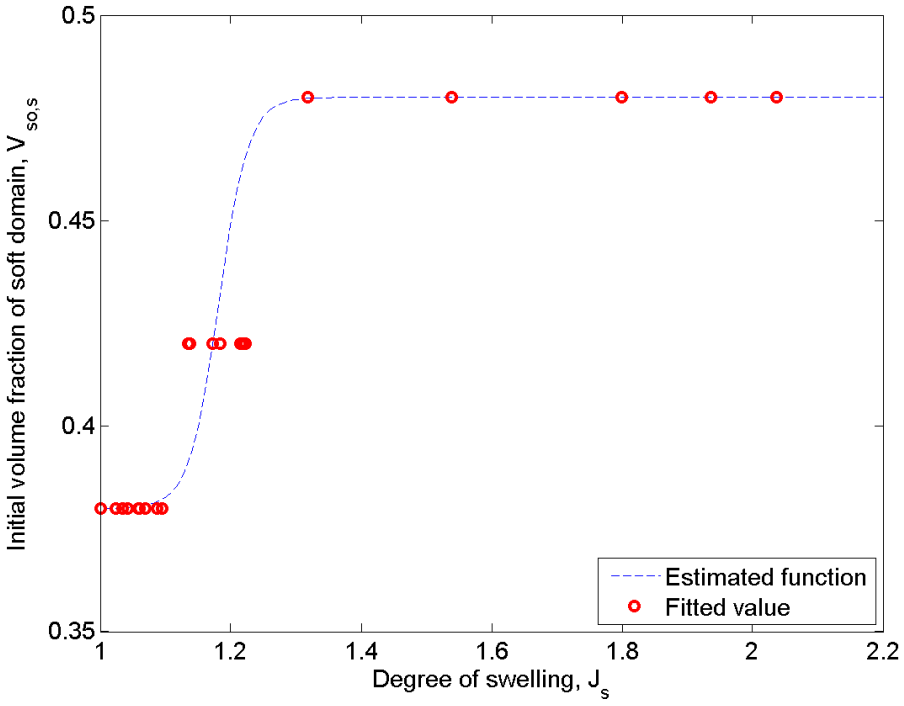

Figure 5.65: Initial effective volume fraction of soft domain as a function of degree of swelling .

5.4.3 Comparison between model and experiment

The ability of the proposed model to describe the Mullins effect in swollen rubbers under cyclic compressive loading conditions is presented in Figures 5.66-5.87. For comparison, results related to the dry rubber are also shown.

In general, it is observed that the proposed model shows good agreement with experimental data. The primary curves of dry and swollen rubbers are well-captured. Moreover, the effects of swelling on the stress-softening due to Mullins effect are well-predicted. However, some discrepancies between model and experiments are found for swollen rubbers having relatively high degree of swelling (i.e. CR swollen in B100). The proposed

model predicted smaller stress-softening, i.e. the simulated unloading curves are closer to the primary curve. This could be attributed to some simplifying assumptions in the model: only n and $\upsilon_{so,s}$ are assumed to be affected by the degree of swelling, the dependence of υ_{ss} and A on the degree of swelling are not considered in the model. Further more, the discrepancies explanation (deviation from Treloar's theory) given in Section 5.3.3 holds true for extended two-phase model.

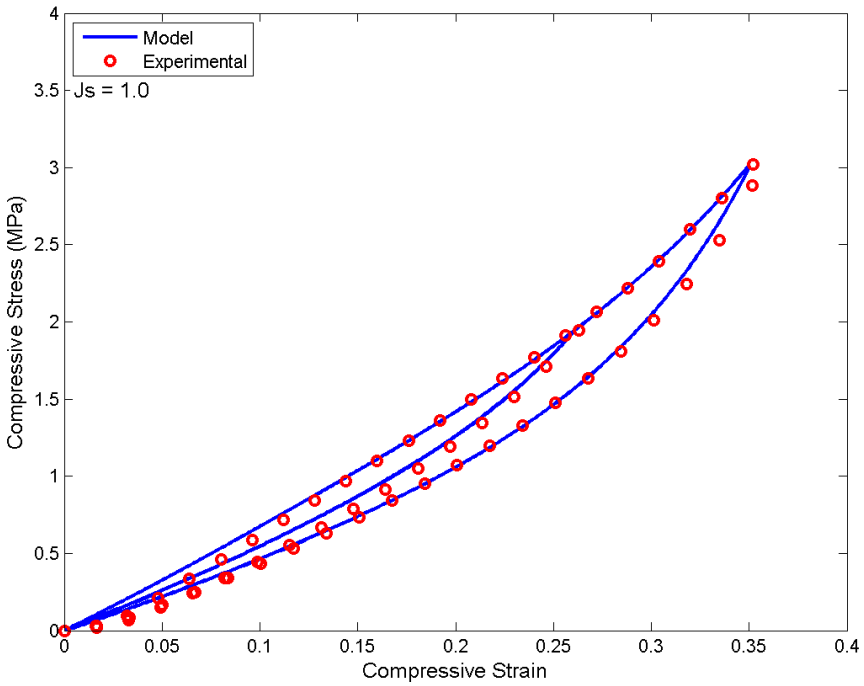

Figure 5.66: Comparison between two-phase model and experiment for dry NBR.

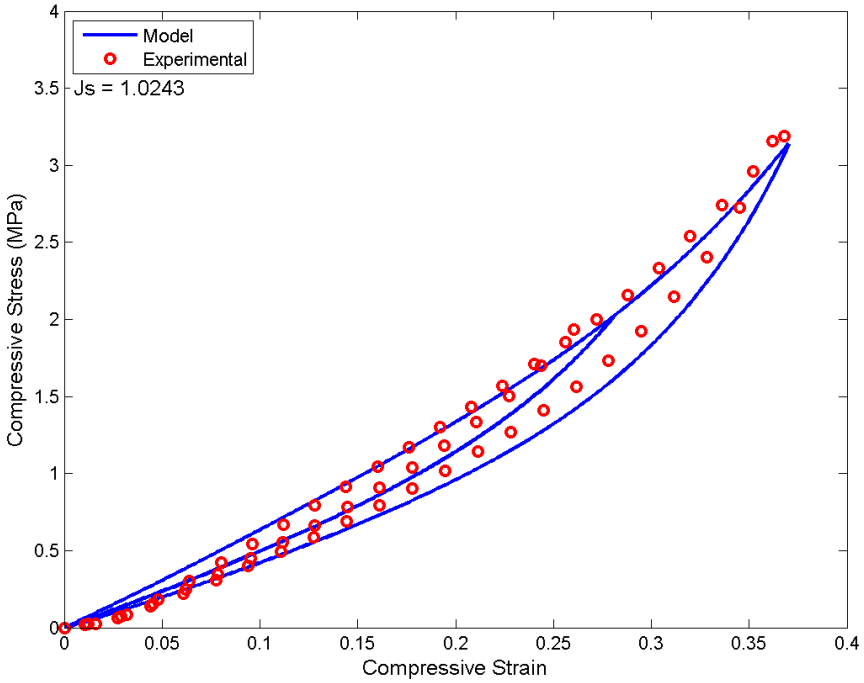

Figure 5.67: Comparison between two-phase model and experiment for NBR swollen by B0 after 2 days immersion.

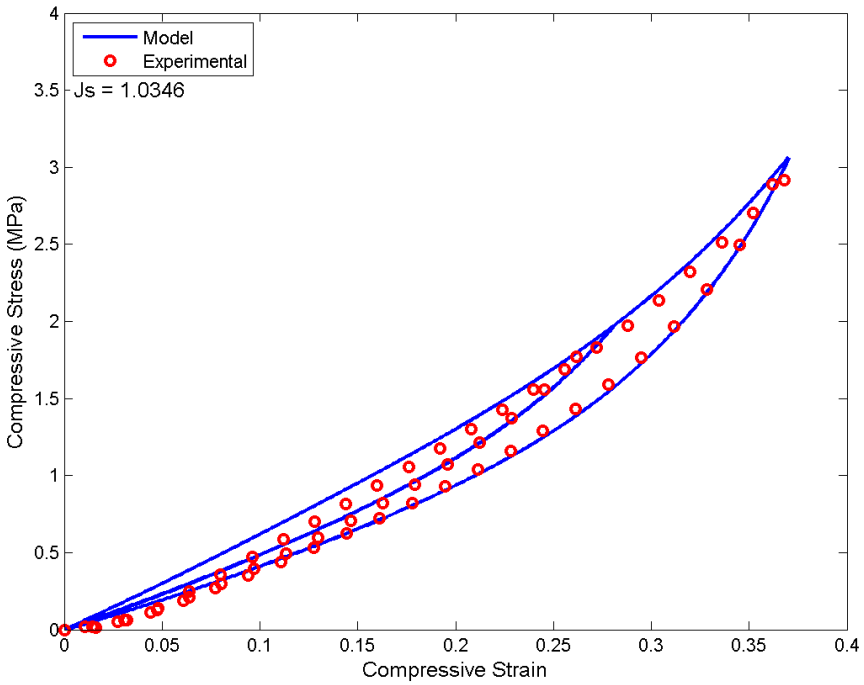

Figure 5.68: Comparison between two-phase model and experiment for NBR swollen by B0 after 5 days immersion.

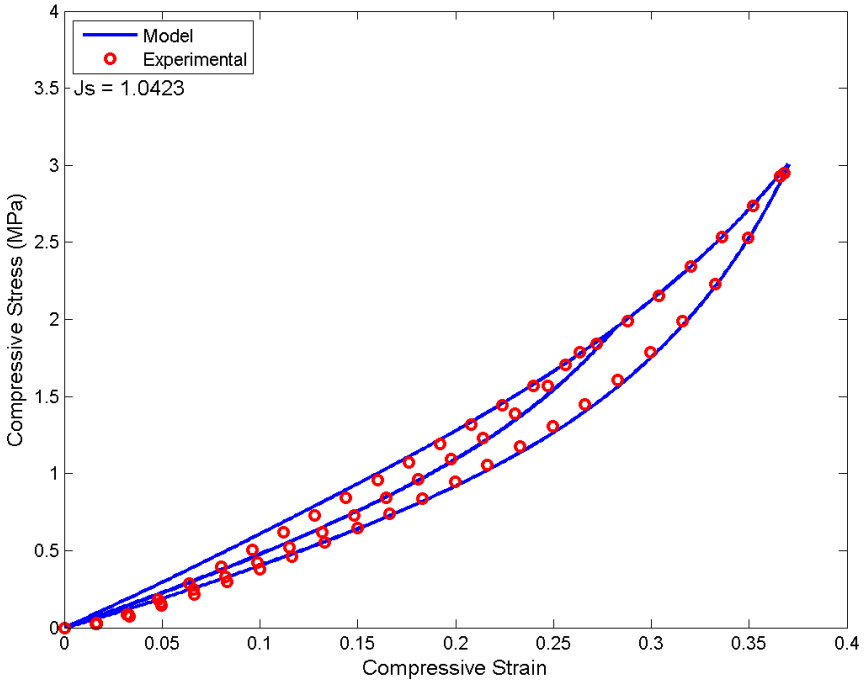

Figure 5.69: Comparison between two-phase model and experiment for NBR swollen by B0 after 10 days immersion.

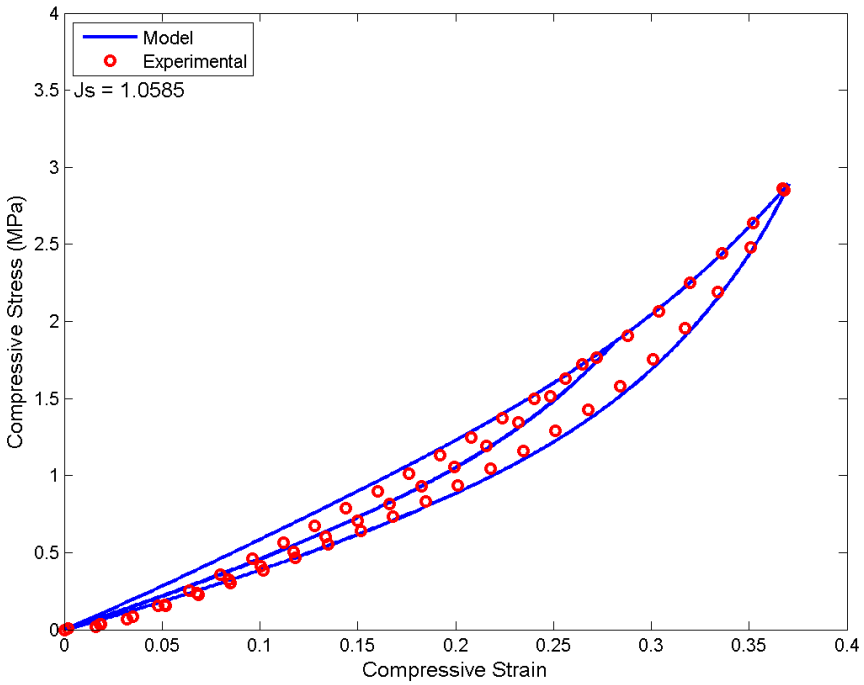

Figure 5.70: Comparison between two-phase model and experiment for NBR swollen by B0 after 20 days immersion.

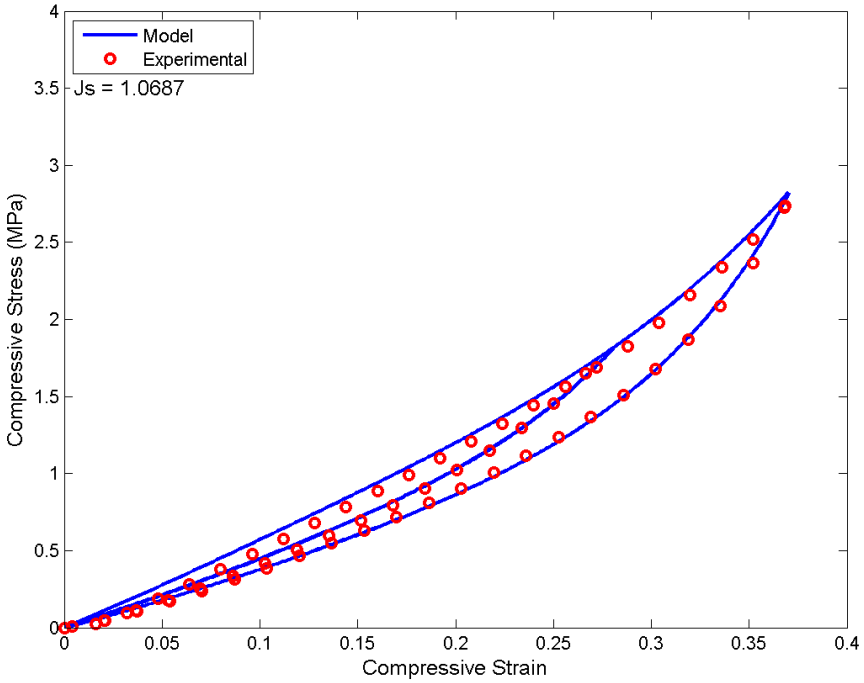

Figure 5.71: Comparison between two-phase model and experiment for NBR swollen by B0 after 30 days immersion.

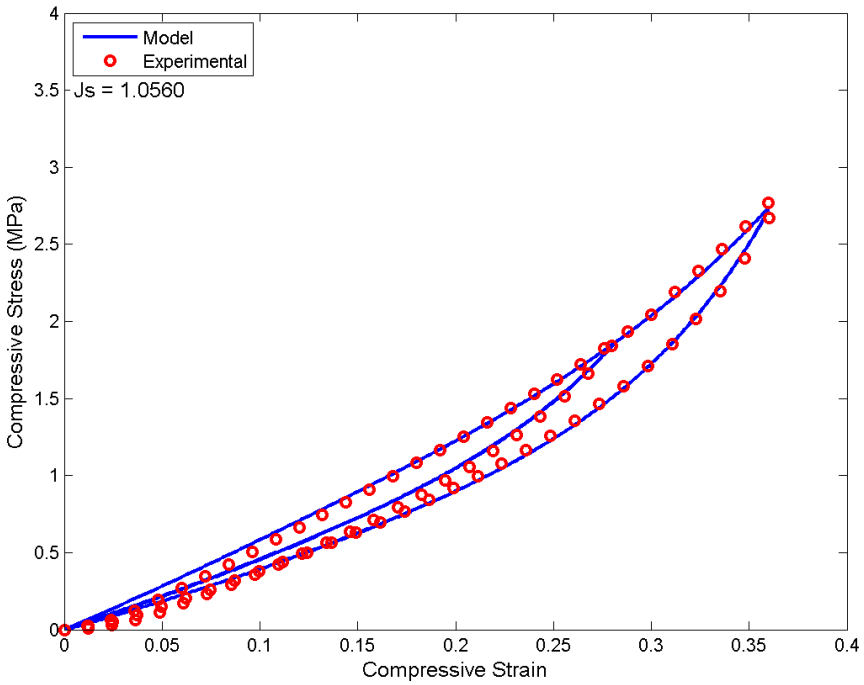

Figure 5.72: Comparison between two-phase model and experiment for NBR swollen by B100 after 2 days immersion.

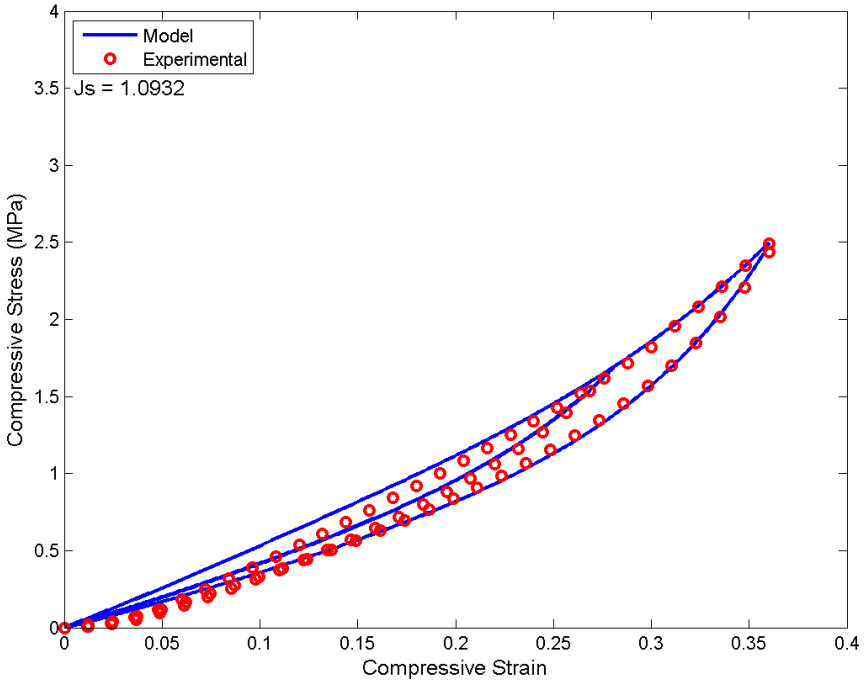

Figure 5.73: Comparison between two-phase model and experiment for NBR swollen by B100 after 5 days immersion.

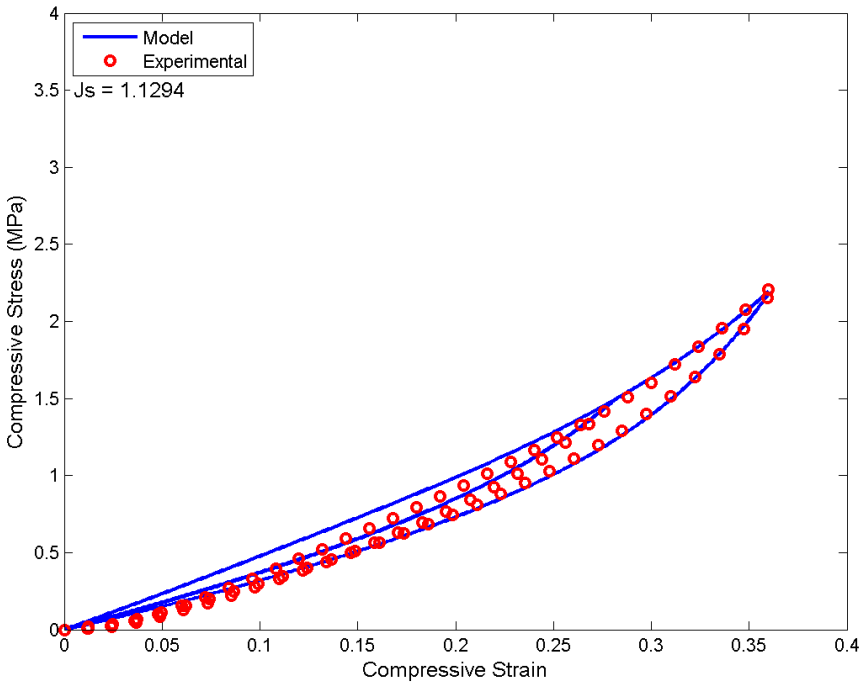

Figure 5.74: Comparison between two-phase model and experiment for NBR swollen by B100 after 10 days immersion.

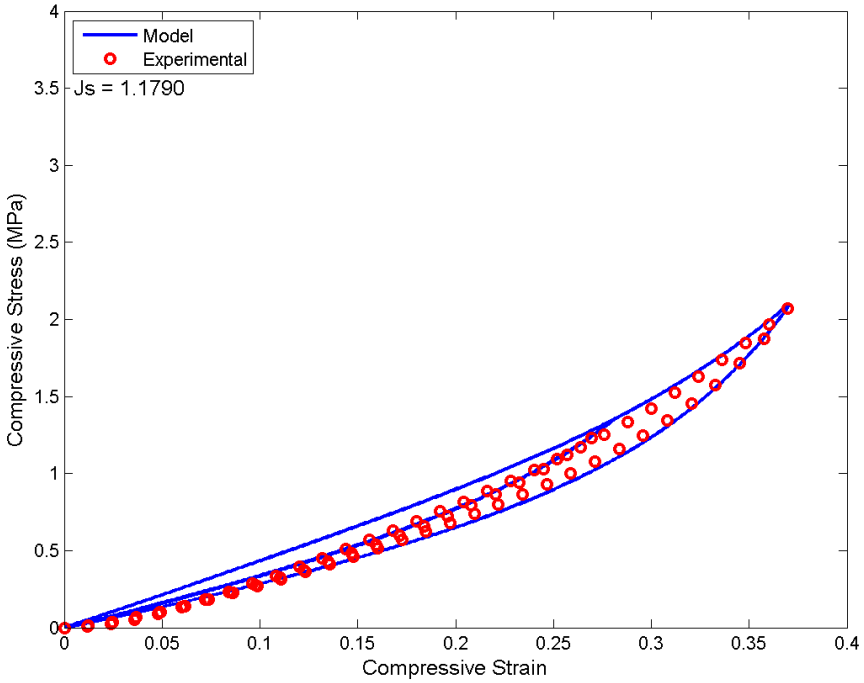

Figure 5.75: Comparison between two-phase model and experiment for NBR swollen by B100 after 20 days immersion.

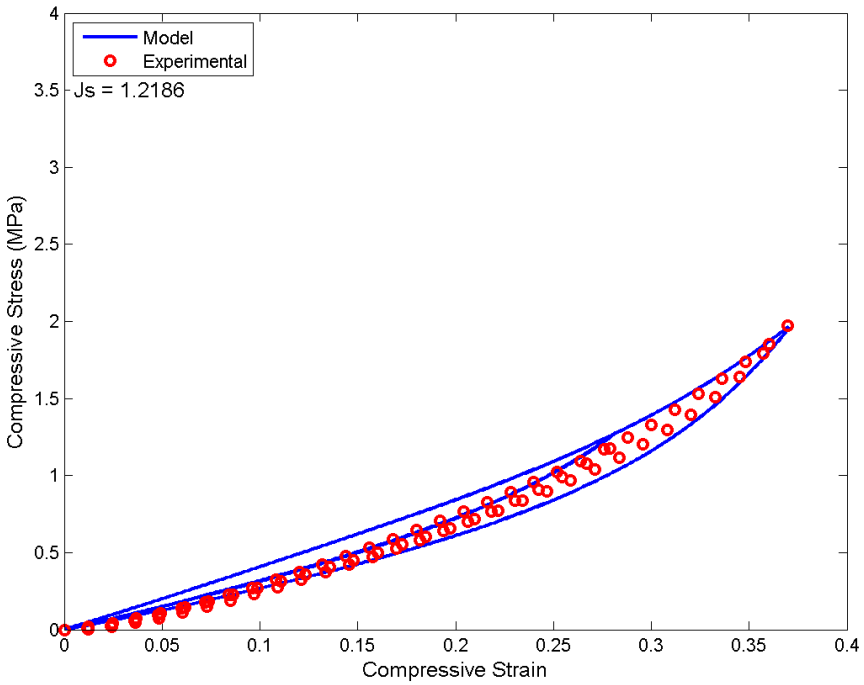

Figure 5.76: Comparison between two-phase model and experiment for NBR swollen by B100 after 30 days immersion.

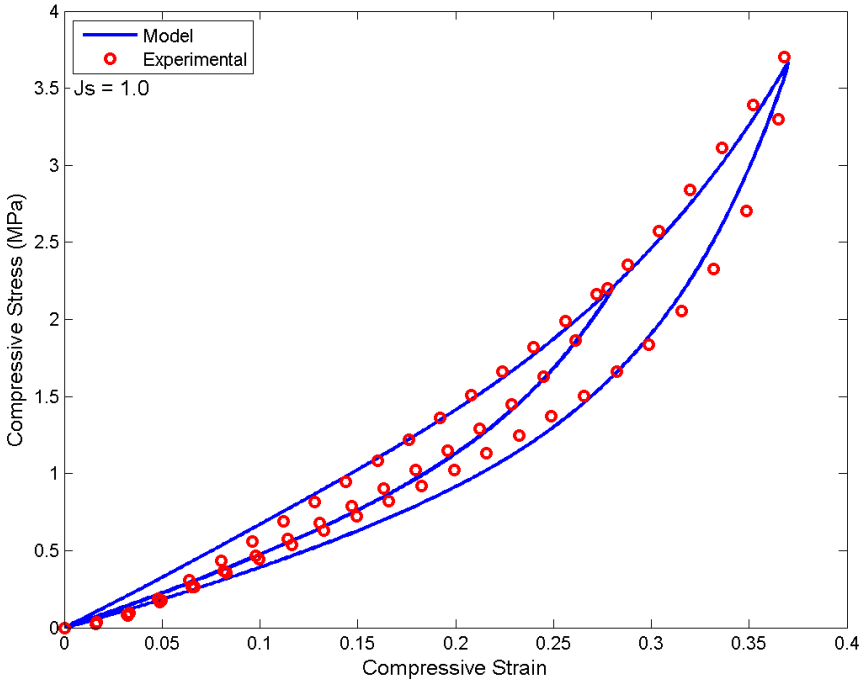

Figure 5.77: Comparison between two-phase model and experiment for dry CR.

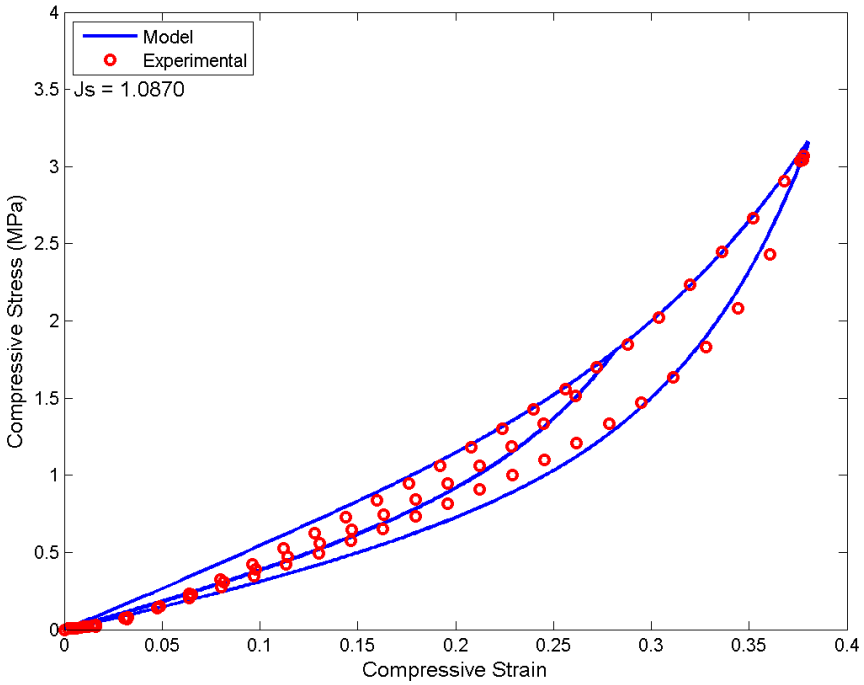

Figure 5.78: Comparison between two-phase model and experiment for CR swollen by B0 after 2 days immersion.

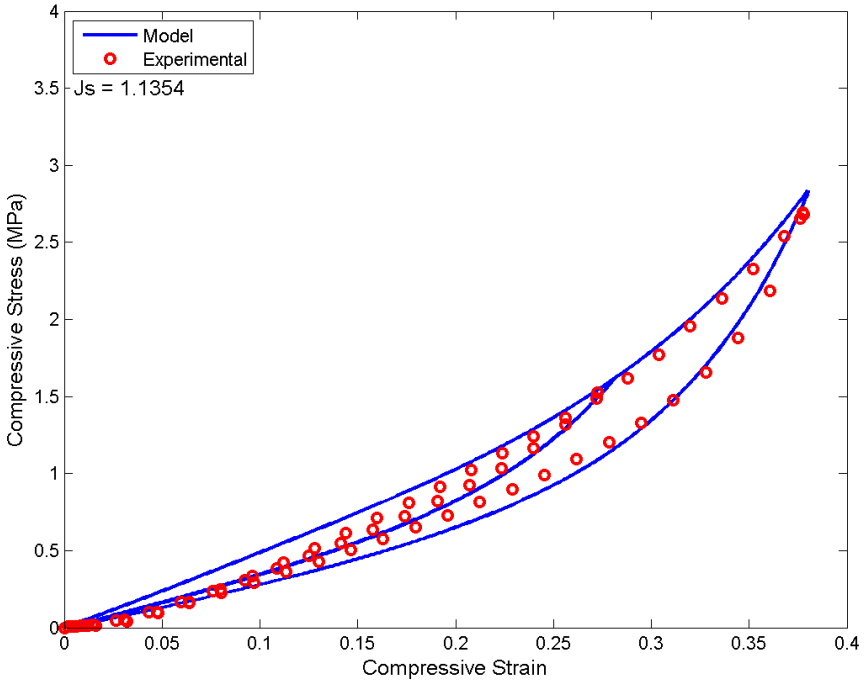

Figure 5.79: Comparison between two-phase model and experiment for CR swollen by B0 after 5 days immersion.

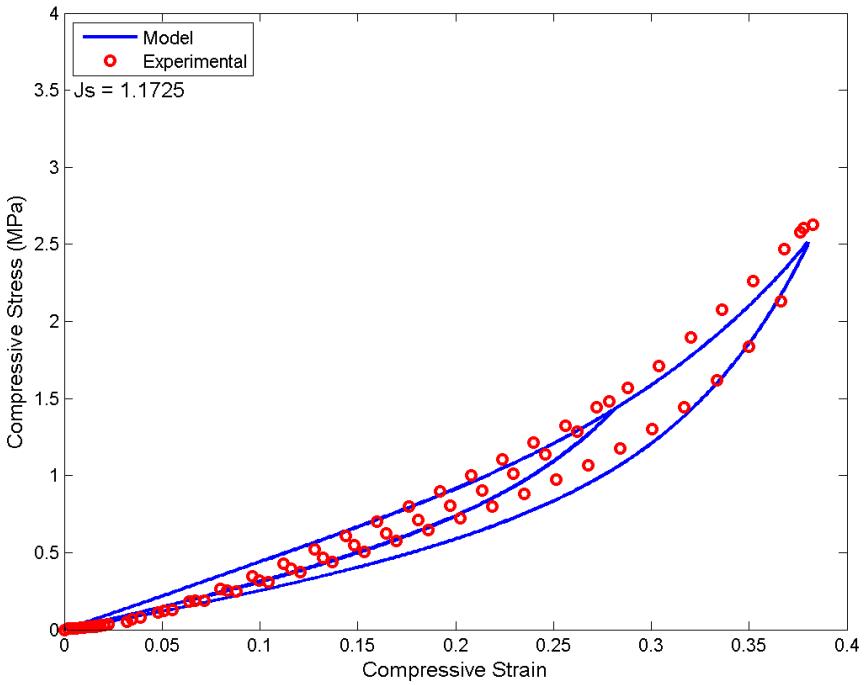

Figure 5.80: Comparison between two-phase model and experiment for CR swollen by B0 after 10 days immersion.

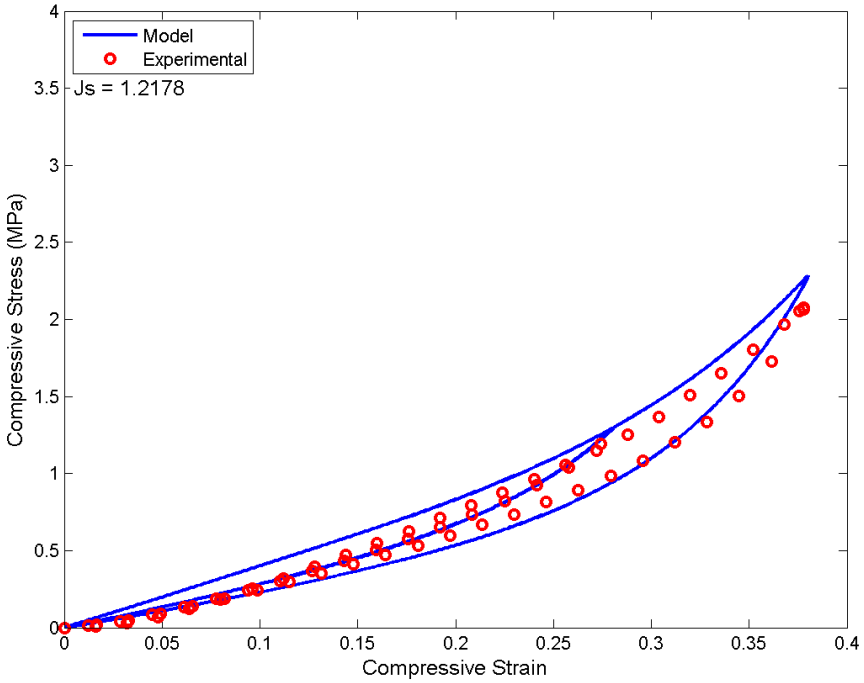

Figure 5.81: Comparison between two-phase model and experiment for CR swollen by B0 after 20 days immersion.

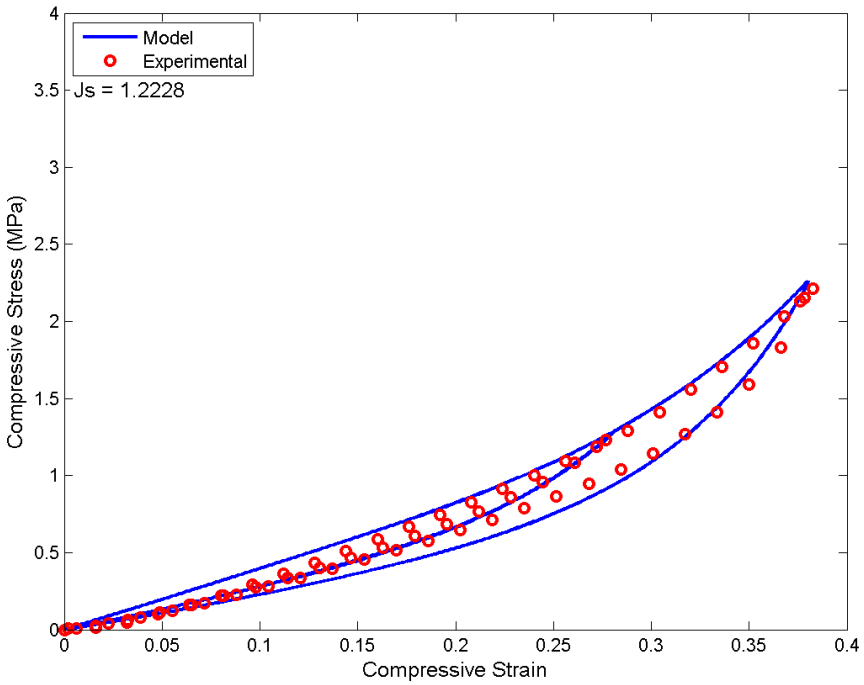

Figure 5.82: Comparison between two-phase model and experiment for CR swollen by B0 after 30 days immersion.

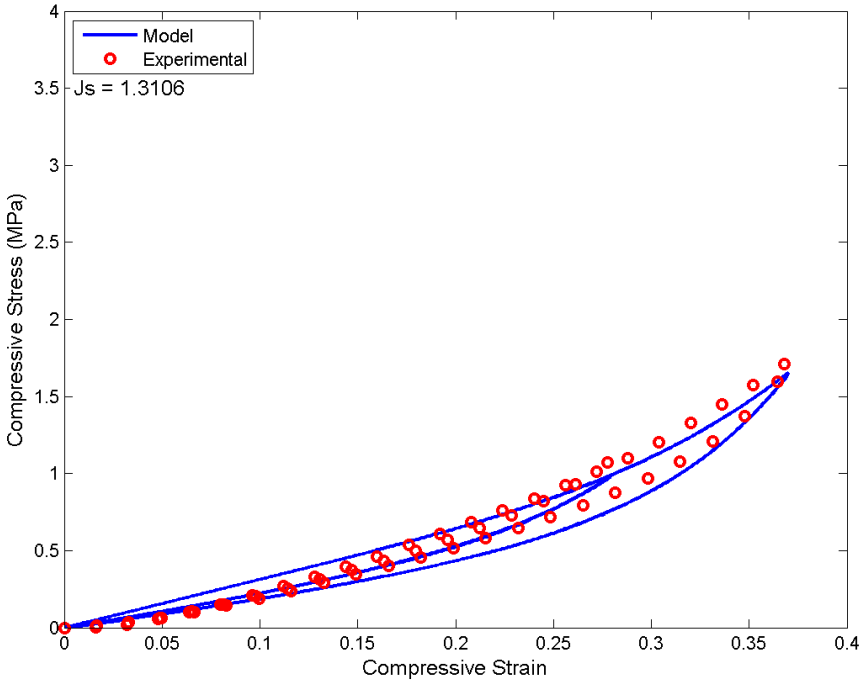

Figure 5.83: Comparison between two-phase model and experiment for CR swollen by B100 after 2 days immersion.

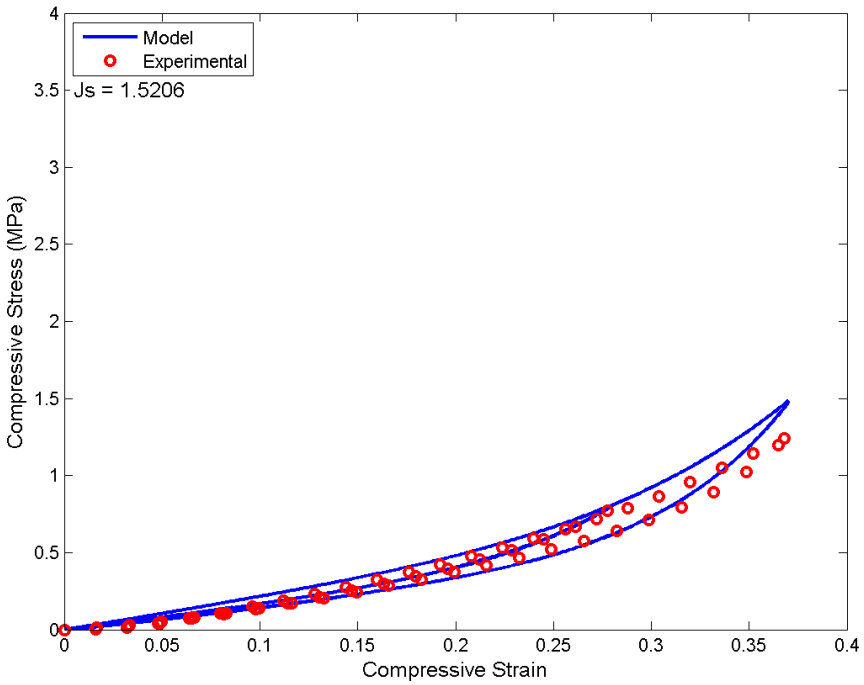

Figure 5.84: Comparison between two-phase model and experiment for CR swollen by B100 after 5 days immersion.

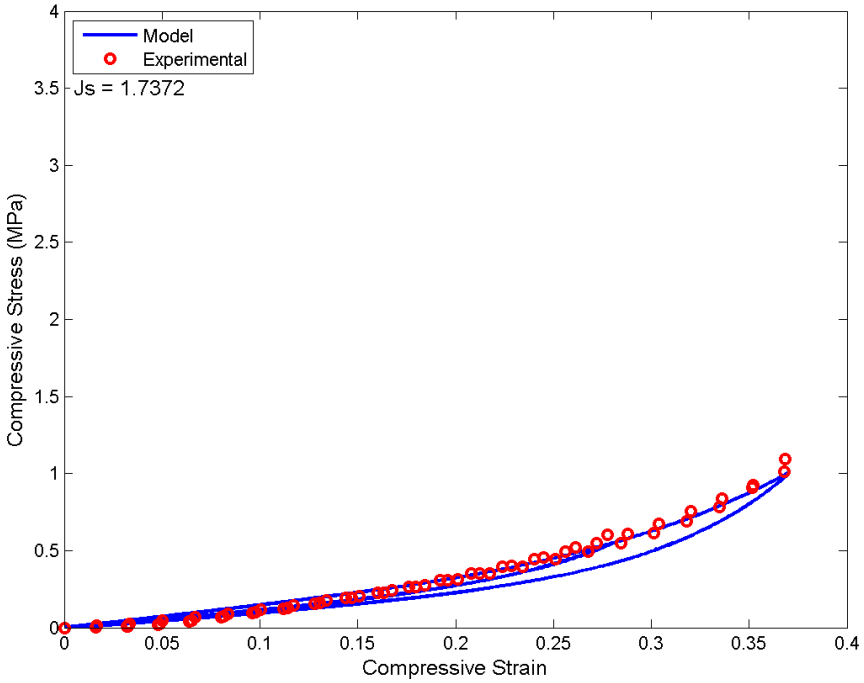

Figure 5.85: Comparison between two-phase model and experiment for CR swollen by B100 after 10 days immersion.

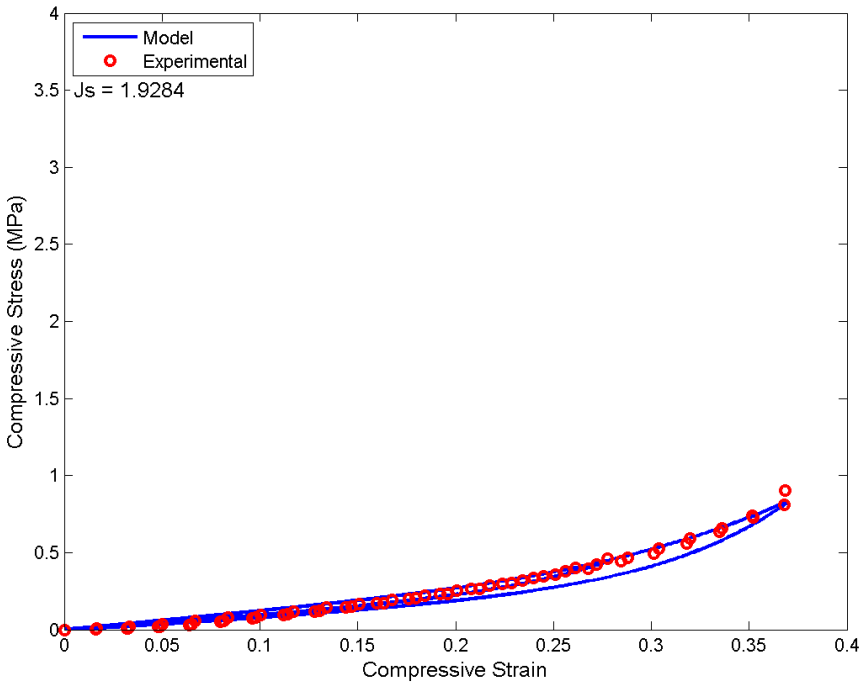

Figure 5.86: Comparison between two-phase model and experiment for CR swollen by B100 after 20 days immersion.

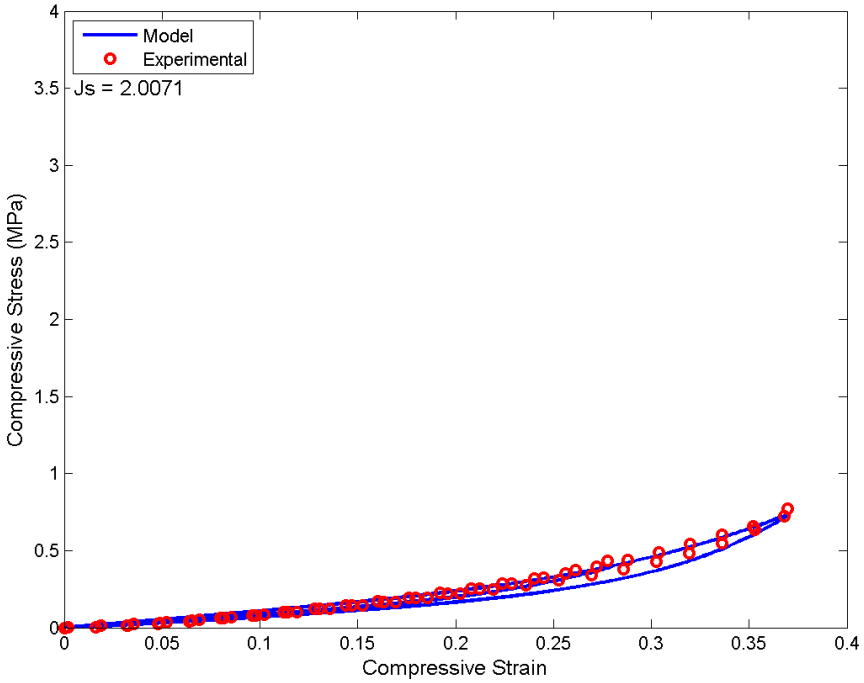

Figure 5.87: Comparison between two-phase model and experiment for CR swollen by B100 after 30 days immersion.

5.4.4 Simulation for other deformation modes

In order to simulate the response of the extended two-phase model under multiaxial loading conditions, deformation modes of uniaxial extension, pure shear and equibiaxial extension are considered in the following. Similar to simulation for other deformation modes using extended pseudo-elastic model, the material is simulated to undergo cyclic loading to two maximum strain levels: ε=0.25 and 0.50. Using the material parameters fitted from the extended two-phase model under uniaxial compression test results, different degrees of swelling are considered in the simulation. Only NBR swollen in B0 and B100 for 10 and 20 days and CR swollen in B0 and B100 for 5 and 10 days are simulated for illustration purpose.

5.4.4 (a) Uniaxial extension

Simulation of uniaxial extension loading-unloading curves For uniaxial extension, the governing equation needed is given by:

$$\hat{P}_{11} = J_s^{-n} 2\upsilon_s \left(\lambda_{\mathrm{m}} - \frac{1}{\lambda_{\mathrm{m}}{}^2}\right)(XC_{10} + 2X^2C_{20}(I_{1\mathrm{m}} - 3) + 3X^3C_{30}(I_{1\mathrm{m}} - 3)^2) \qquad (5.18)$$

where λ_{m} is the uniaxial extension stretch and $I_{1\mathrm{m}} = \lambda_{\mathrm{m}}^2 - \frac{2}{\lambda_{\mathrm{m}}}$. The uniaxial extension loading-unloading curves simulated with the extended two-phase model are illustrated in Figures 5.88 to 5.97.

From these figures, it becomes clearly that the proposed extended two-phase model well predicts that the uniaxial extension loading-unloading curves are affected by the degree of swelling, i.e. a lower stress level is produced for rubbers experiencing higher degree of swelling. Furthermore, smaller stress-softening is well predicted when the degree of swelling increases.

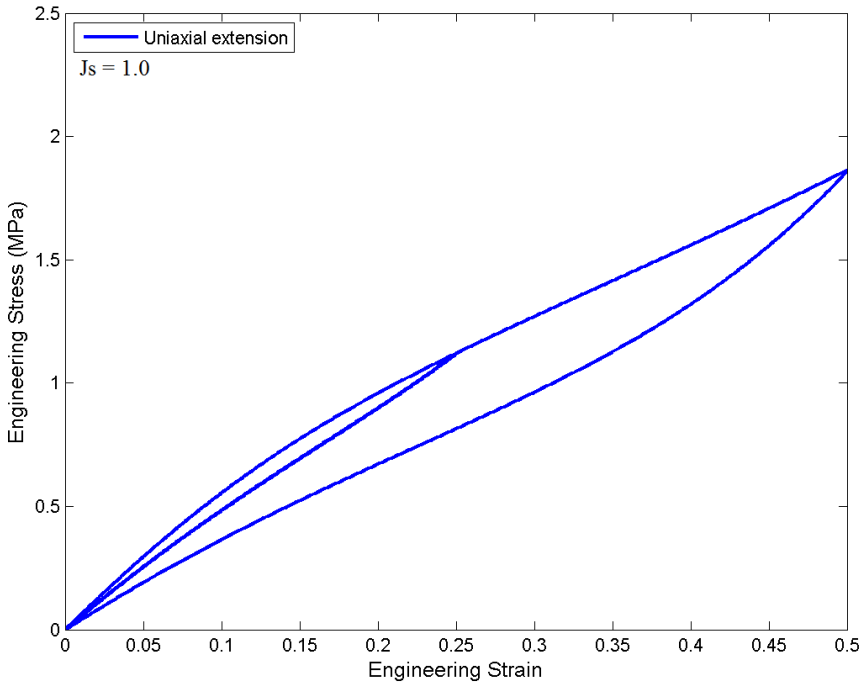

Figure 5.88: Two-phase model response under uniaxial extension for dry NBR.

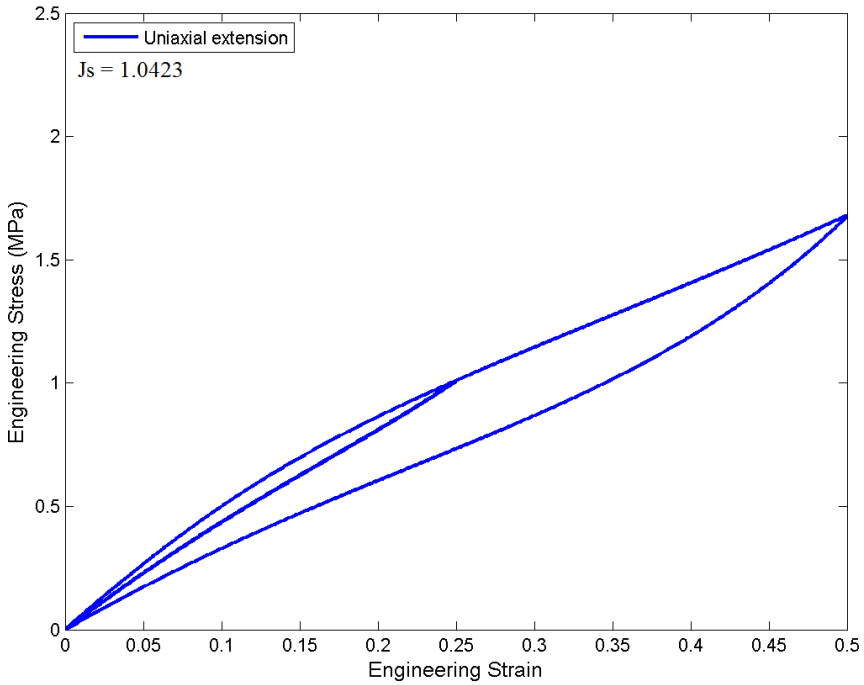

Figure 5.89: Two-phase model response under uniaxial extension for NBR swollen by B0 after 10 days immersion.

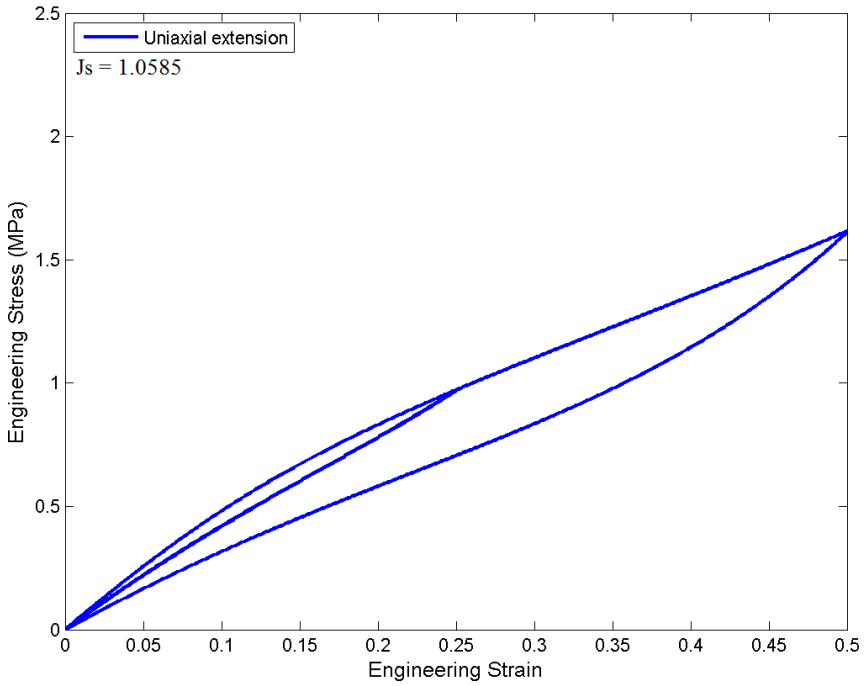

Figure 5.90: Two-phase model response under uniaxial extension for NBR swollen by B0 after 20 days immersion.

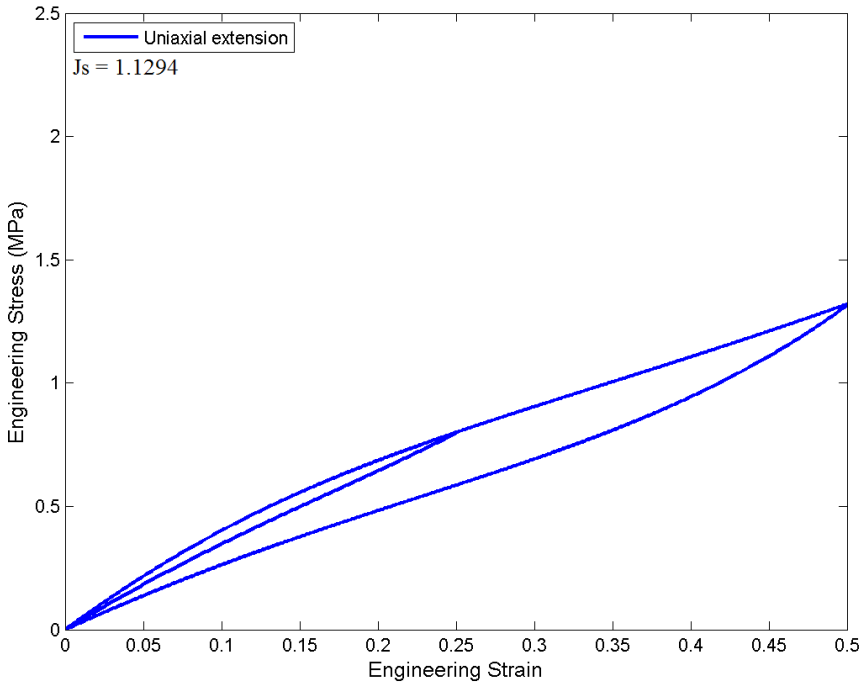

Figure 5.91: Two-phase model response under uniaxial extension for NBR swollen by B100 after 10 days immersion.

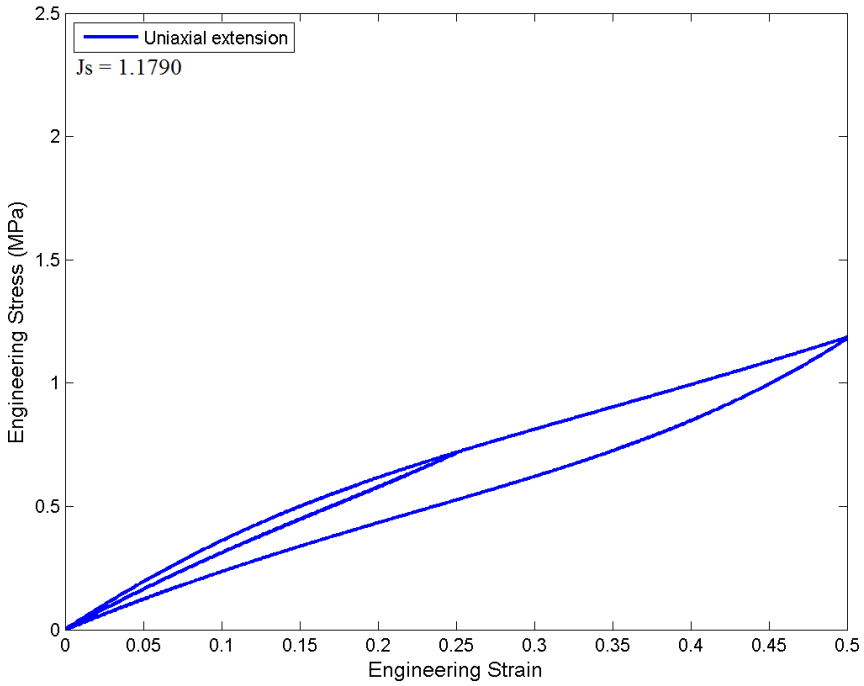

Figure 5.92: Two-phase model response under uniaxial extension for NBR swollen by B100 after 20 days immersion.

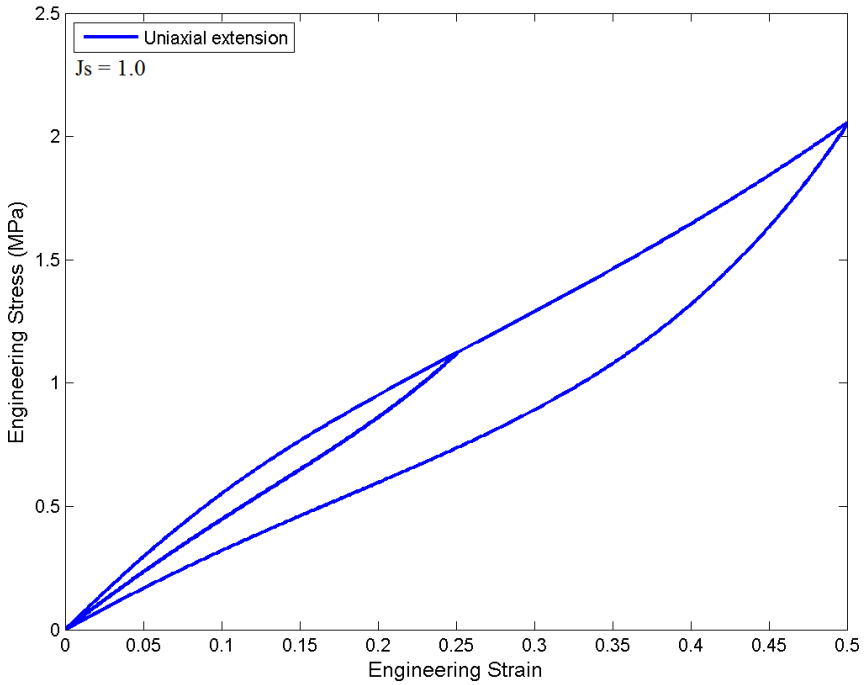

Figure 5.93: Two-phase model response under uniaxial extension for dry CR.

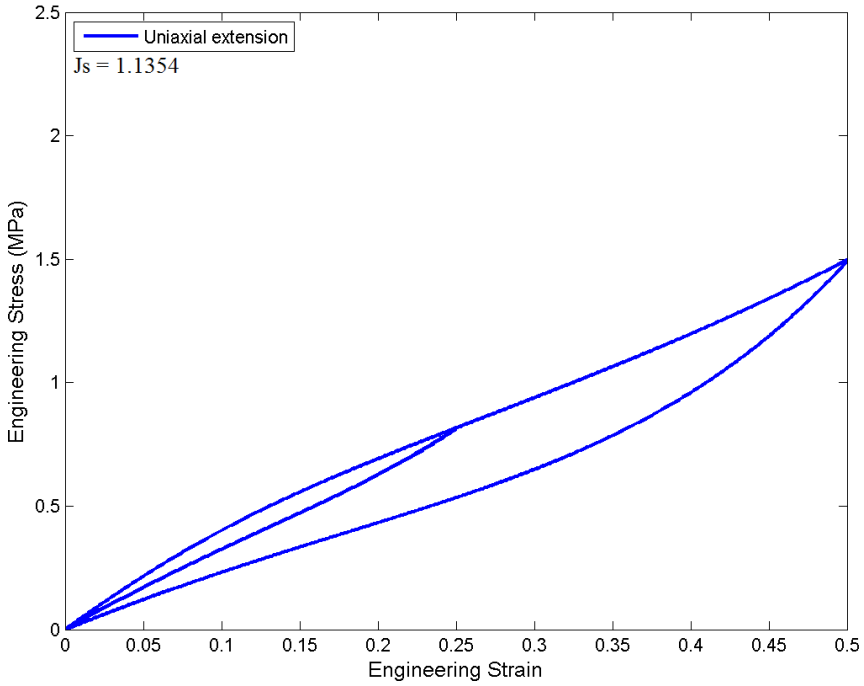

Figure 5.94: Two-phase model response under uniaxial extension for CR swollen by B0 after 5 days immersion.

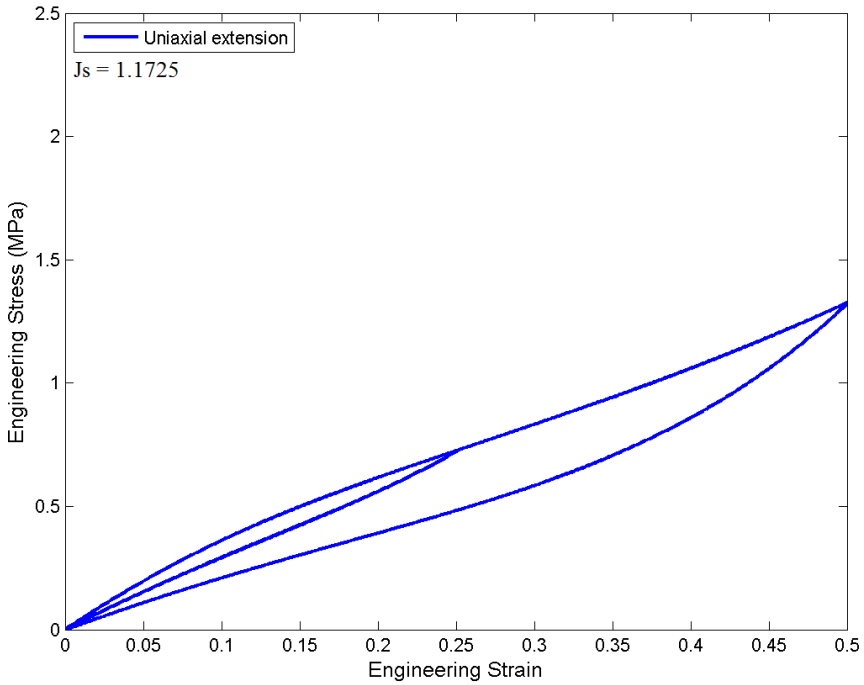

Figure 5.95: Two-phase model response under uniaxial extension for CR swollen by B0 after 10 days immersion.

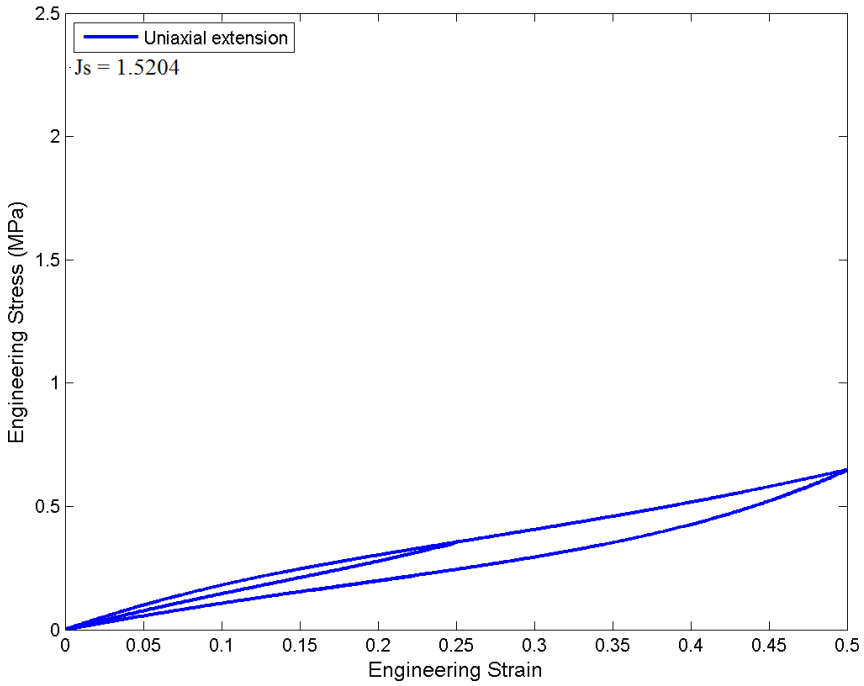

Figure 5.96: Two-phase model response under uniaxial extension for CR swollen by B100 after 5 days immersion.

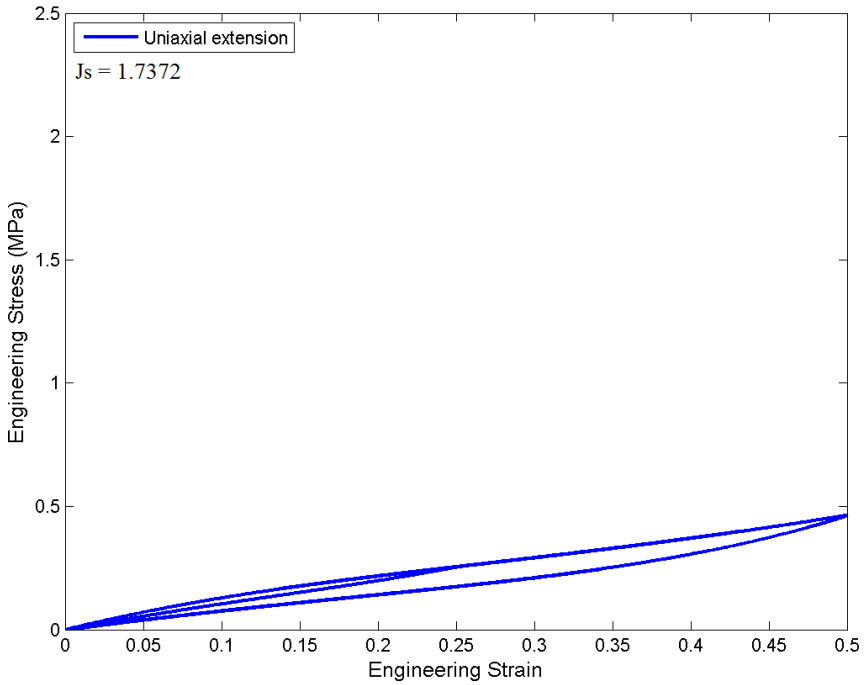

Figure 5.97: Two-phase model response under uniaxial extension for CR swollen by B100 after 10 days immersion.

Evolution of effective volume fraction of soft phase The evolution of the effective volume fraction of the soft phase υ_s for dry and swollen NBR and CR in the uniaxial extension tests during the first virgin material loading to $\varepsilon = 0.5$ are shown in Figures 5.98 and 5.99. It is found that the evolution curve of υ_s for NBR swollen in B100 for 10 days coincides with the one swollen in B100 for 20 days (similar to CR swollen in B100 for 5 days which coincide with the one swollen in B100 for 10 days). This is due to the fact that the values of the parameter $\upsilon_{so,s}$ for these materials are the same in swollen state, independent of the immersion duration as given in Table 5.8 and 5.9. Furthermore, the evolution rule given in Equation (5.16) is not depending on the degree of swelling J_s.

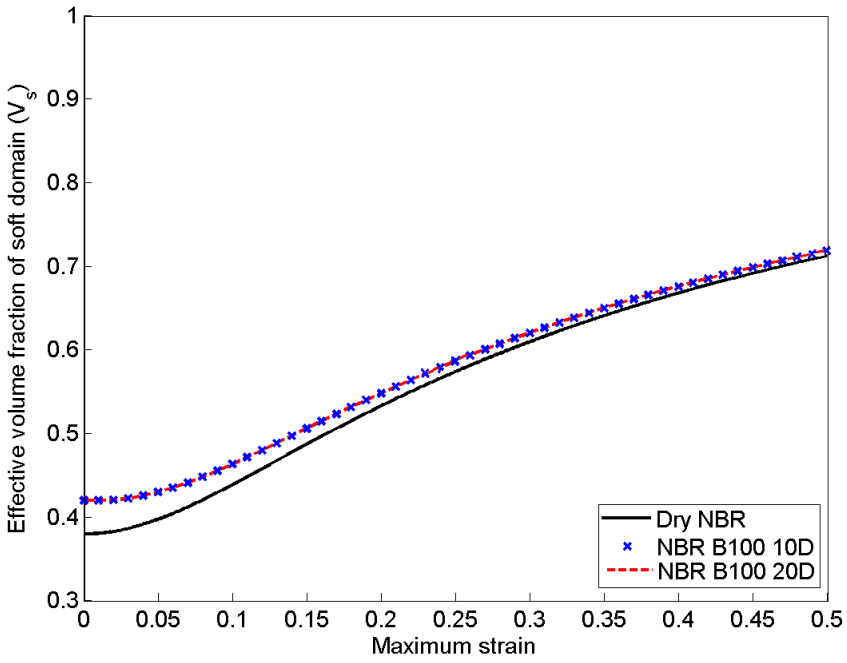

Figure 5.98: Evolution of effective volume fraction of soft phase under uniaxial extension deformation for NBR swollen by B100. Results correspond to 10 and 20 days of immersion duration.

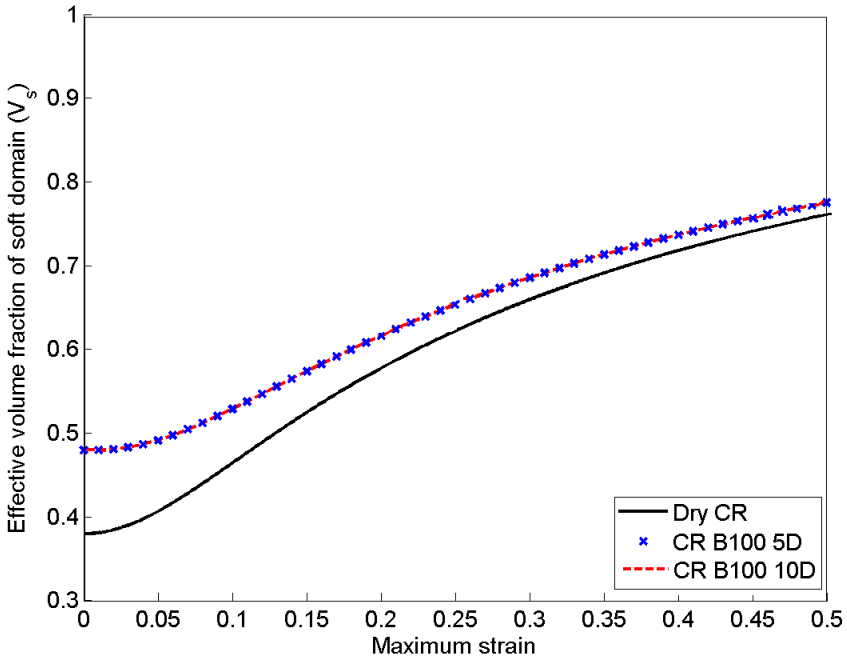

Figure 5.99: Evolution of effective volume fraction of soft phase under uniaxial extension deformation for CR swollen by B100. Results correspond to 5 and 10 days of immersion duration.

5.4.4 (b) Pure shear

Simulation of pure shear loading-unloading curves For pure shear, the governing equation needed is given by:

$$\hat{P}_{11} = J_s^{-n} 2\upsilon_s \left(\lambda_m - \frac{1}{\lambda_m{}^3}\right)(XC_{10} + 2X^2C_{20}(I_{1m} - 3) + 3X^3C_{30}(I_{1m} - 3)^2) \qquad (5.19)$$

where λ_m is the pure shear stretch and $I_{1m} = \lambda_m^2 - \frac{1}{\lambda_m^2} + 1$. The pure shear loading-unloading curves simulated with extended two-phase model are illustrated in Figures 5.100 to 5.109. From these figures, it is shown that the materials exhibit a slightly more stiff response during unloading/reloading in pure shear than in uniaxial extension. This is because in pure shear the material is subjected to a slightly higher molecular chain stretch than in uniaxial extension at a given strain level. Thus, higher softening is predicted in pure shear.

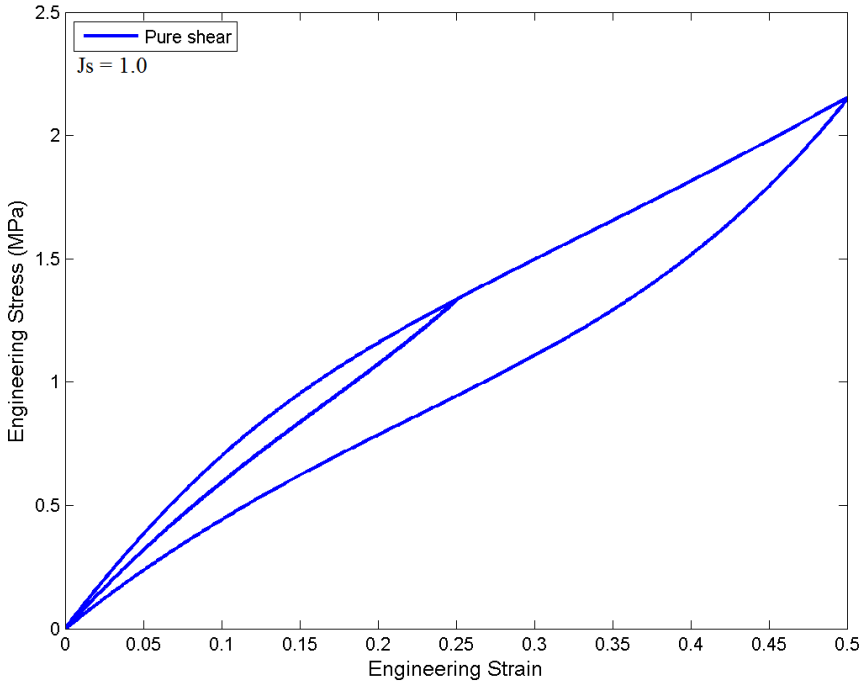

Figure 5.100: Two-phase model response under pure shear for dry NBR.

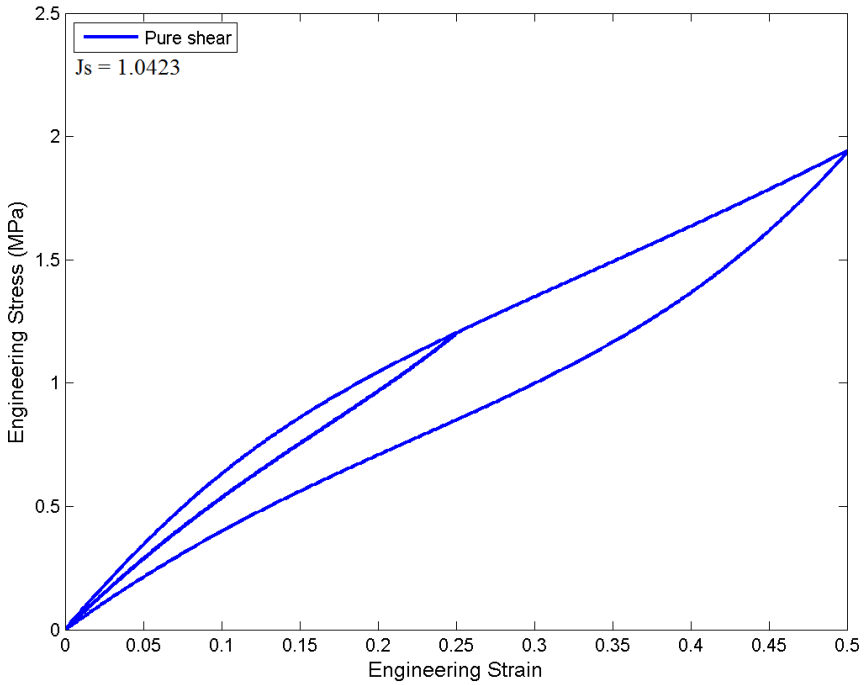

Figure 5.101: Two-phase model response under pure shear for NBR swollen by B0 after 10 days immersion.

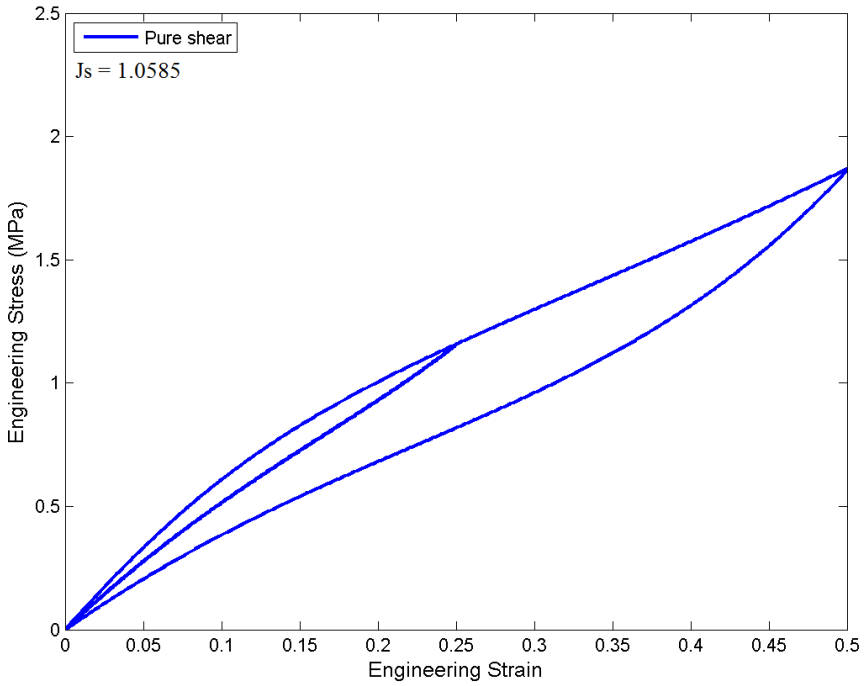

Figure 5.102: Two-phase model response under pure shear for NBR swollen by B0 after 20 days immersion.

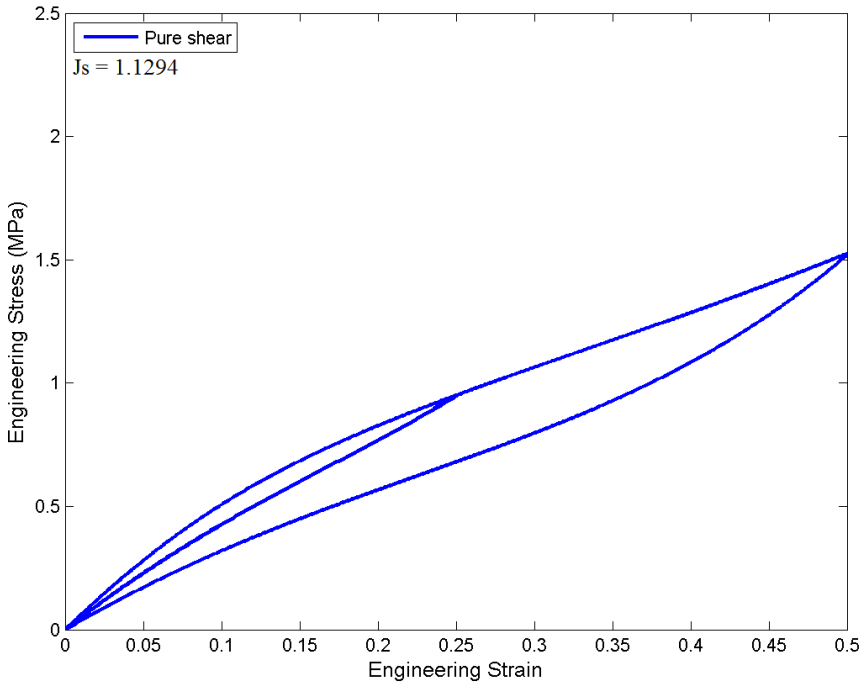

Figure 5.103: Two-phase model response under pure shear for NBR swollen by B100 after 10 days immersion.

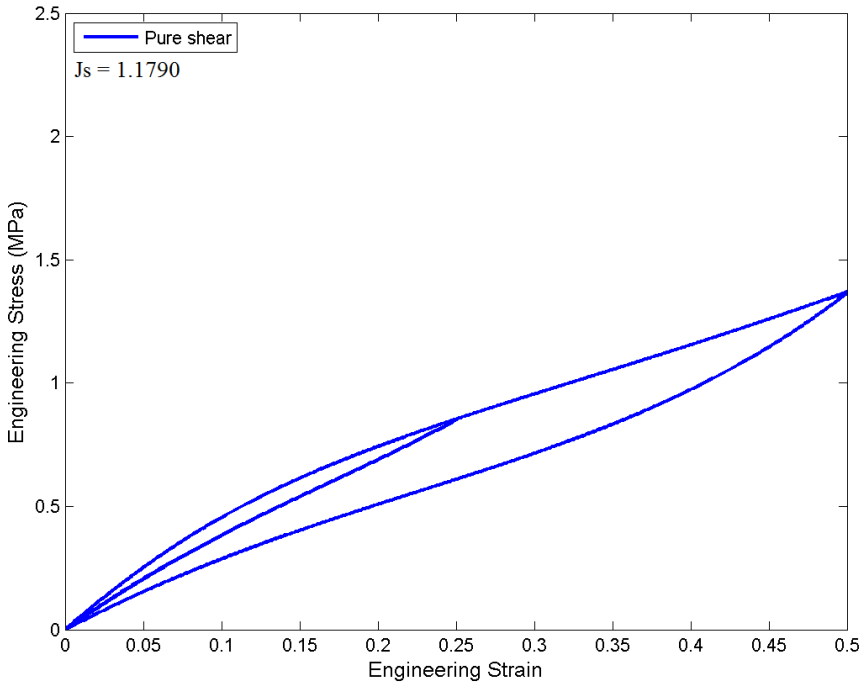

Figure 5.104: Two-phase model response under pure shear for NBR swollen by B100 after 20 days immersion.

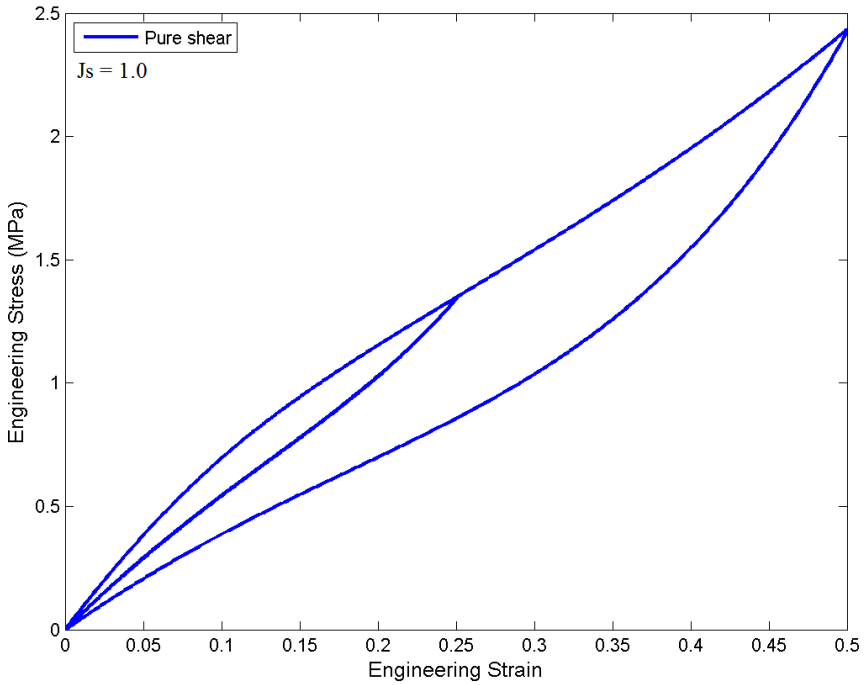

Figure 5.105: Two-phase model response under pure shear for dry CR.

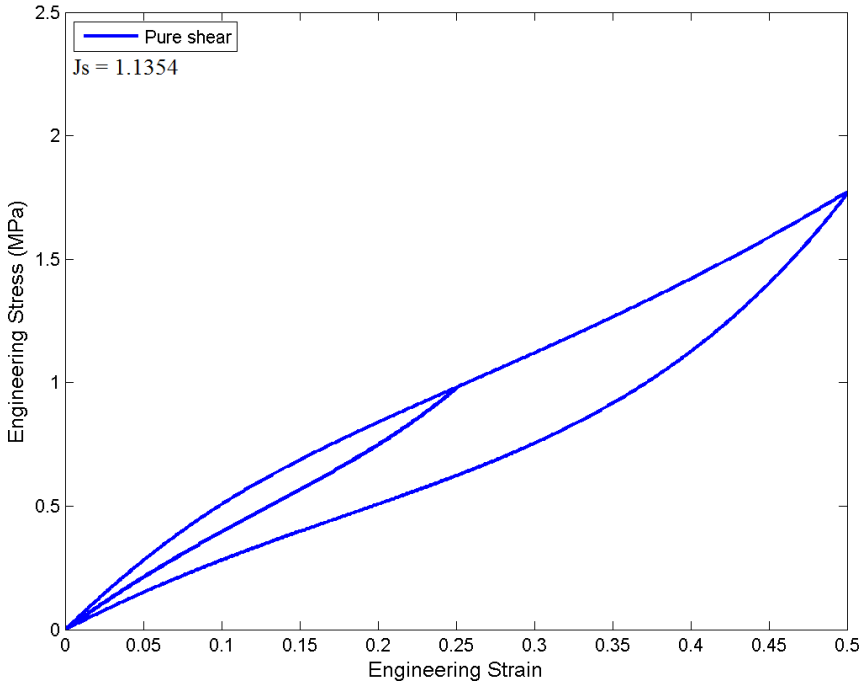

Figure 5.106: Two-phase model response under pure shear for CR swollen by B0 after 5 days immersion.

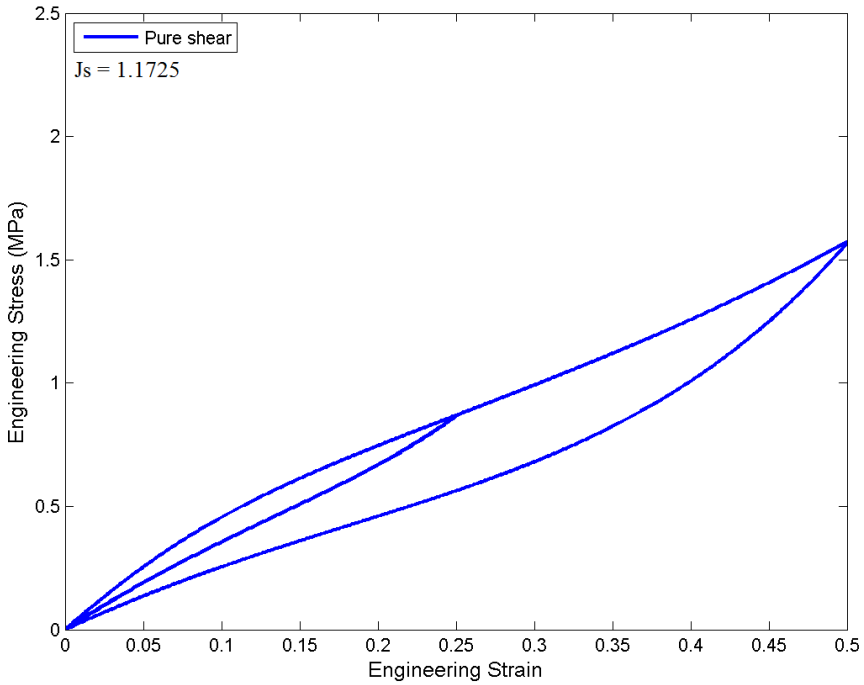

Figure 5.107: Two-phase model response under pure shear for CR swollen by B0 after 10 days immersion.

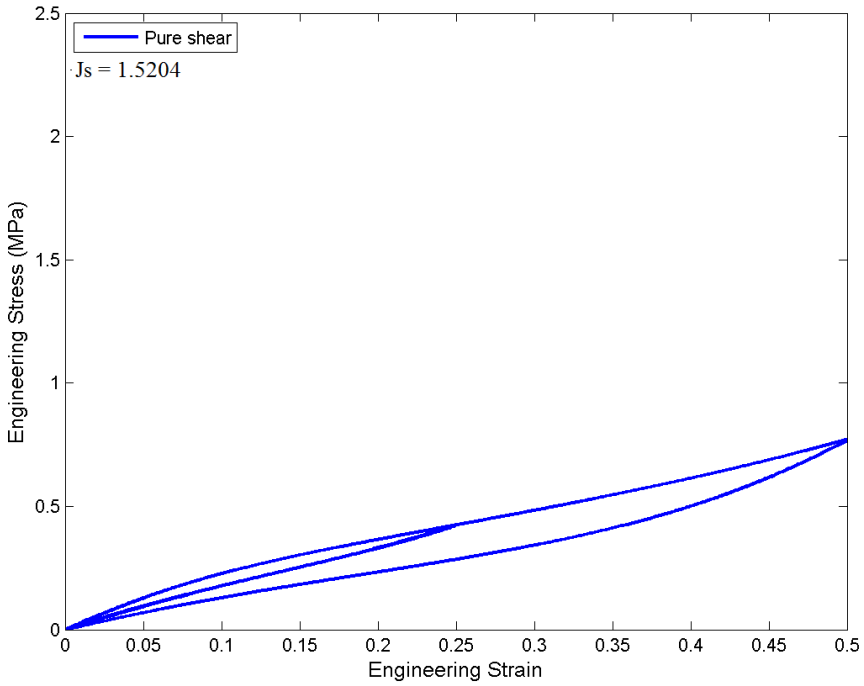

Figure 5.108: Two-phase model response under pure shear for CR swollen by B100 after 5 days immersion.

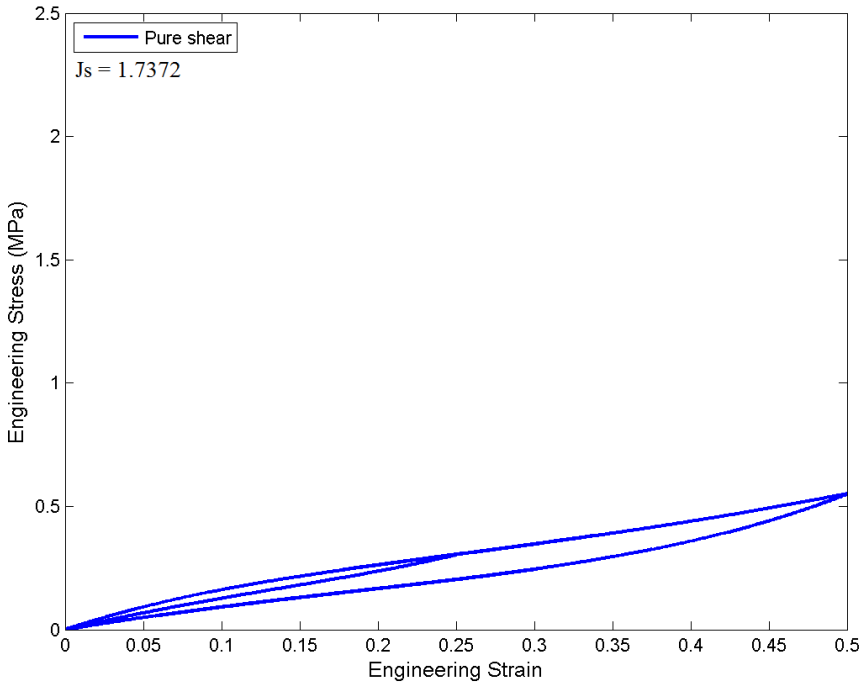

Figure 5.109: Two-phase model response under pure shear for CR swollen by B100 after 10 days immersion.

Evolution of effective volume fraction of soft phase The evolution of the effective volume fraction of the soft phase υ_s for dry and swollen NBR and CR in the pure shear tests during the first loading of the virgin material to $\varepsilon = 0.5$ are shown in Figures 5.110 and 5.111. The dependence of the υ_s on the deformation mode is clearly shown in these two figures when compared to the case of uniaxial extension as shown in Figures 5.98 and 5.99.

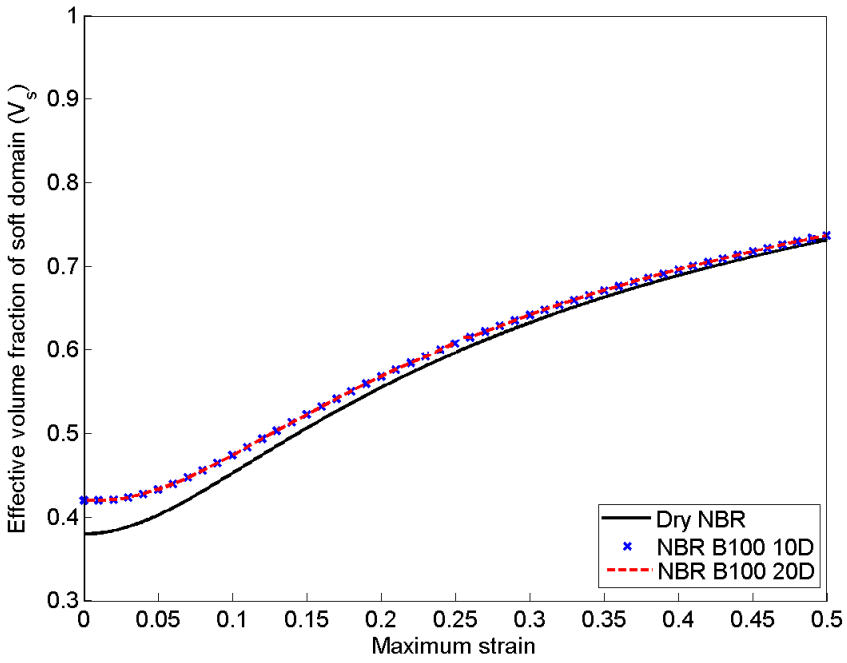

Figure 5.110: Evolution of effective volume fraction of soft phase under pure shear deformation for NBR swollen by B100. Results correspond to 10 and 20 days of immersion duration.

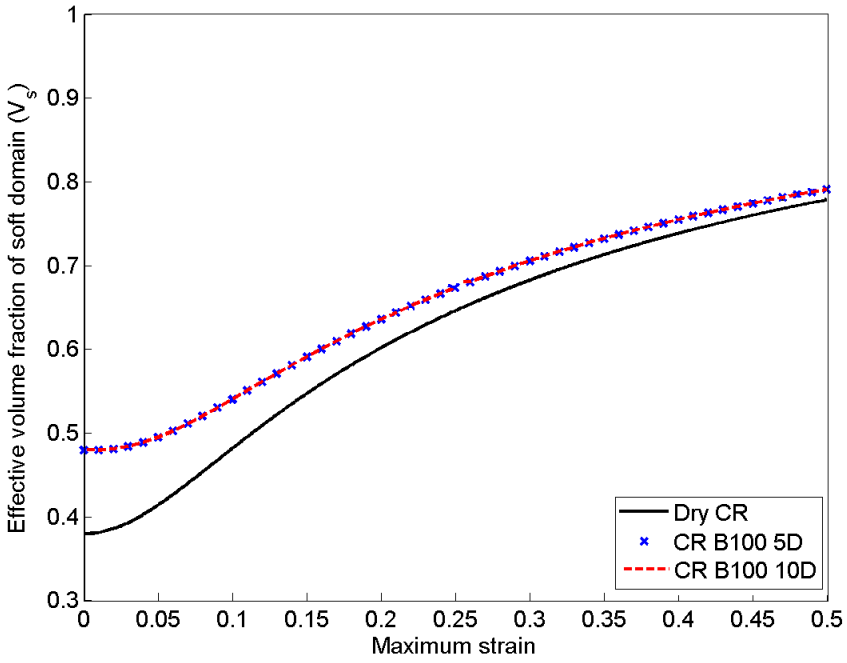

Figure 5.111: Evolution of effective volume fraction of soft phase under pure shear deformation for CR swollen by B100. Results correspond to 5 and 10 days of immersion duration.

5.4.4 (c) Equibiaxial extension

Simulation of equibiaxial extension loading-unloading curves For equibiaxial extension, the governing equation needed is given by:

$$\hat{P}_{11} = J_s^{-n} 2\upsilon_s \left(\lambda_{\mathrm{m}} - \frac{1}{\lambda_{\mathrm{m}}^{5}}\right)\left(XC_{10} + 2X^2C_{20}(I_{1\mathrm{m}} - 3) + 3X^3C_{30}(I_{1\mathrm{m}} - 3)^2\right) \qquad (5.20)$$

where λ_{m} is the equibiaxial extension stretch and $I_{1\mathrm{m}} = 2\lambda_{\mathrm{m}}^2 - \frac{1}{\lambda_{\mathrm{m}}^4}$. The equibiaxial extension loading-unloading curves simulated with extended two-phase model are illustrated in Figures 5.112 to 5.121. These figures demonstrate that the materials show a greater amount of softening (a more compliant response) during reloading in equibiaxial extension than in uniaxial extension. This is because in equibiaxial extension the material is subjected to a higher molecular chain stretch than when in uniaxial extension at a given strain level.

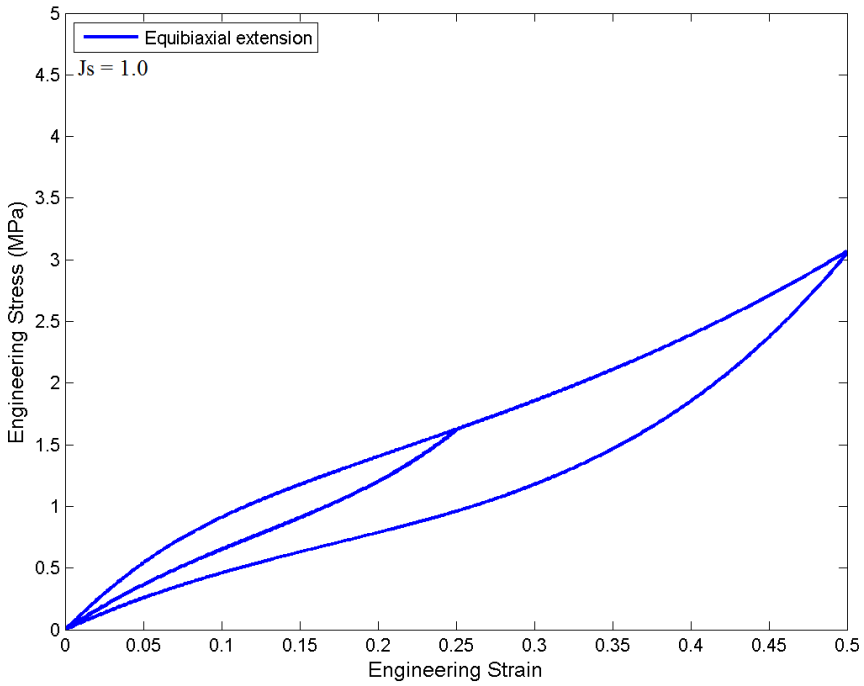

Figure 5.112: Two-phase model response under equibiaxial extension for dry NBR.

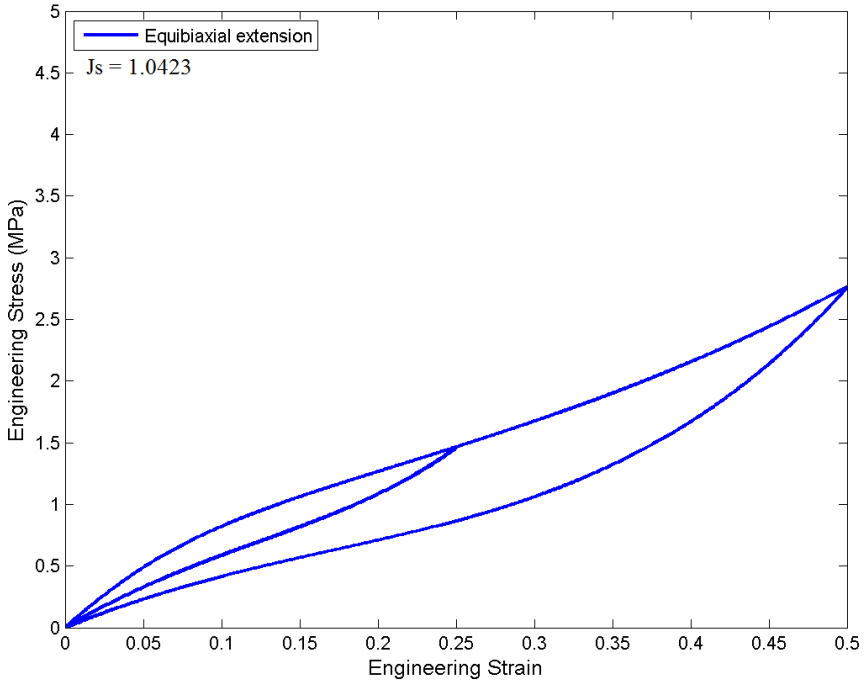

Figure 5.113: Two-phase model response under equibiaxial extension for NBR swollen by B0 after 10 days immersion.

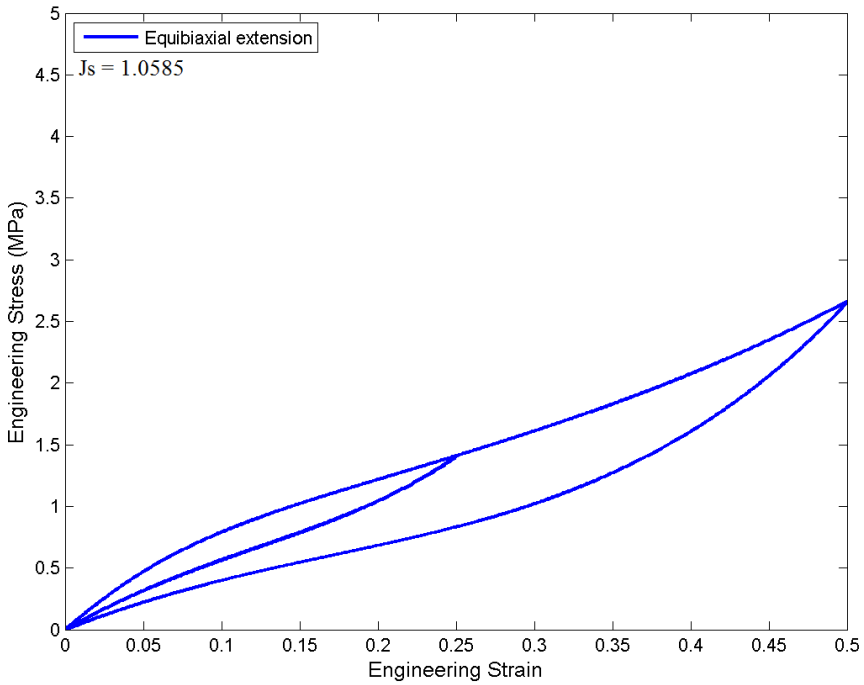

Figure 5.114: Two-phase model response under equibiaxial extension for NBR swollen by B0 after 20 days immersion.

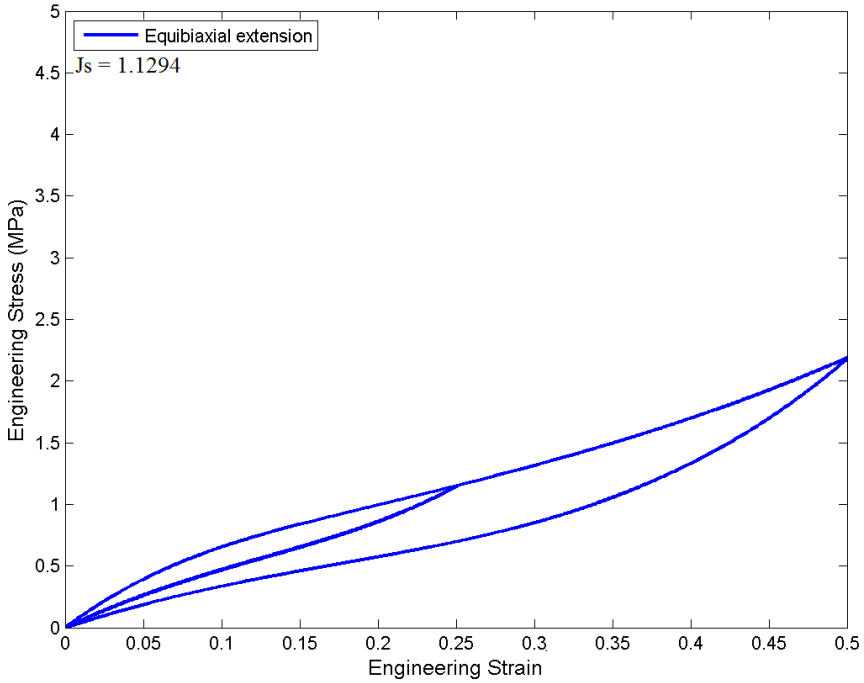

Figure 5.115: Two-phase model response under equibiaxial extension for NBR swollen by B100 after 10 days immersion.

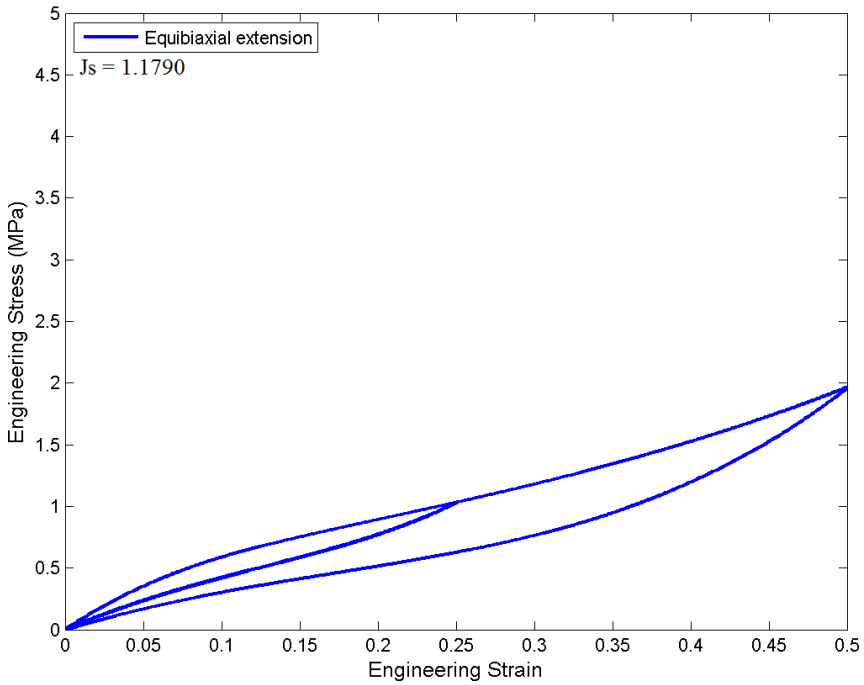

Figure 5.116: Two-phases model response under equibiaxial extension for NBR swollen by B100 after 20 days immersion.

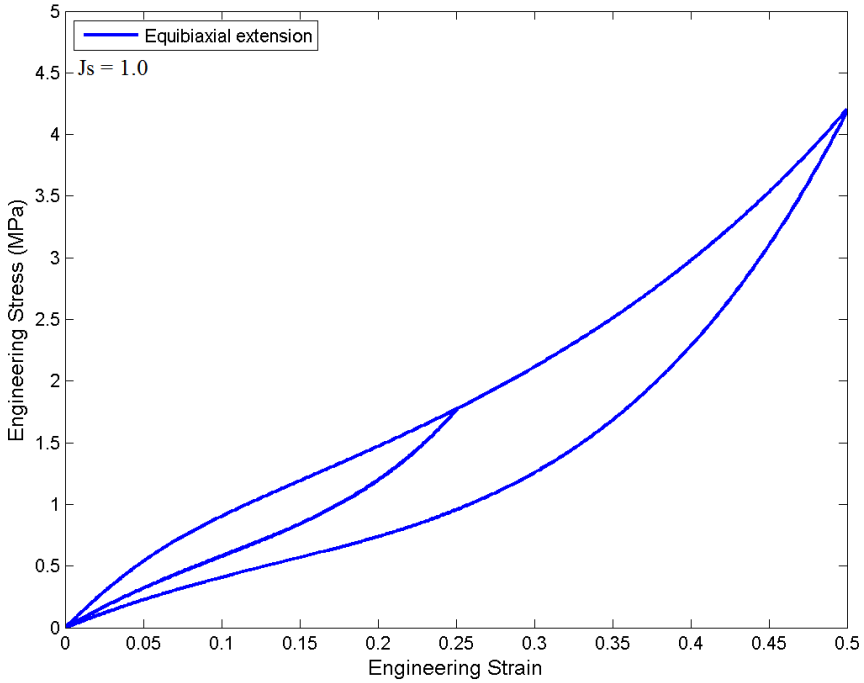

Figure 5.117: Two-phase model response under equibiaxial extension for dry CR.

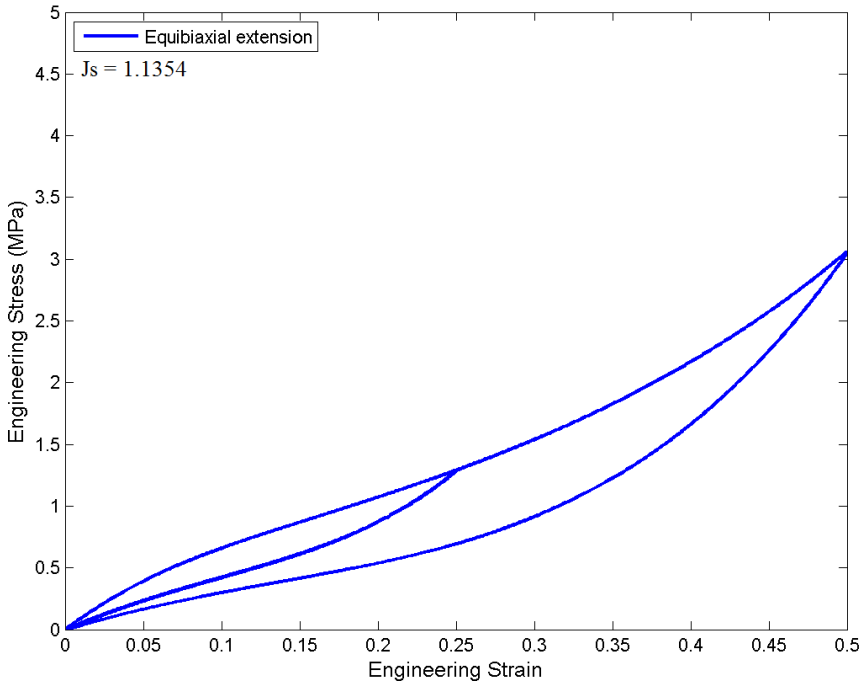

Figure 5.118: Two-phase model response under equibiaxial extension for CR swollen by B0 after 5 days immersion.

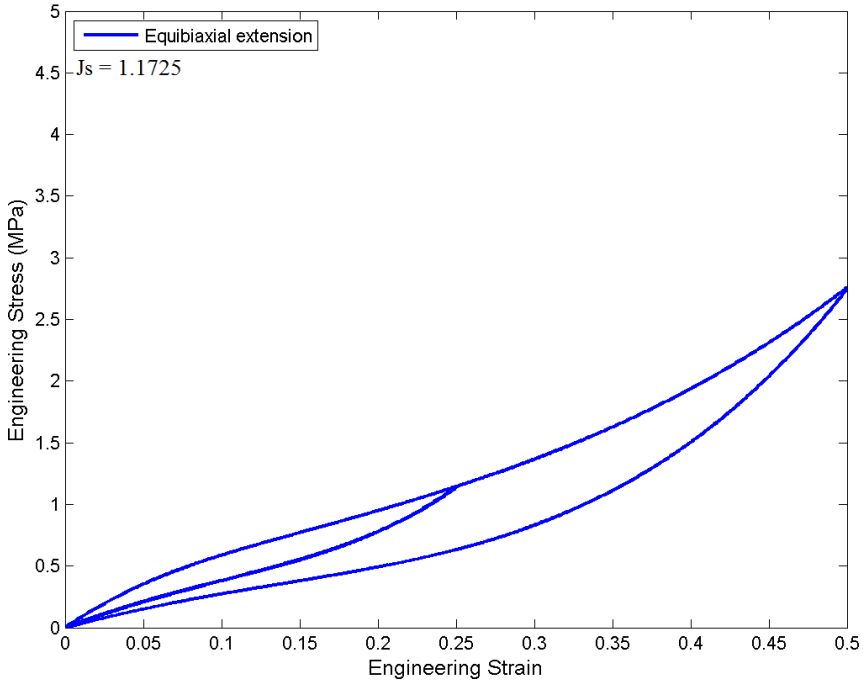

Figure 5.119: Two-phase model response under equibiaxial extension for CR swollen by B0 after 10 days immersion.

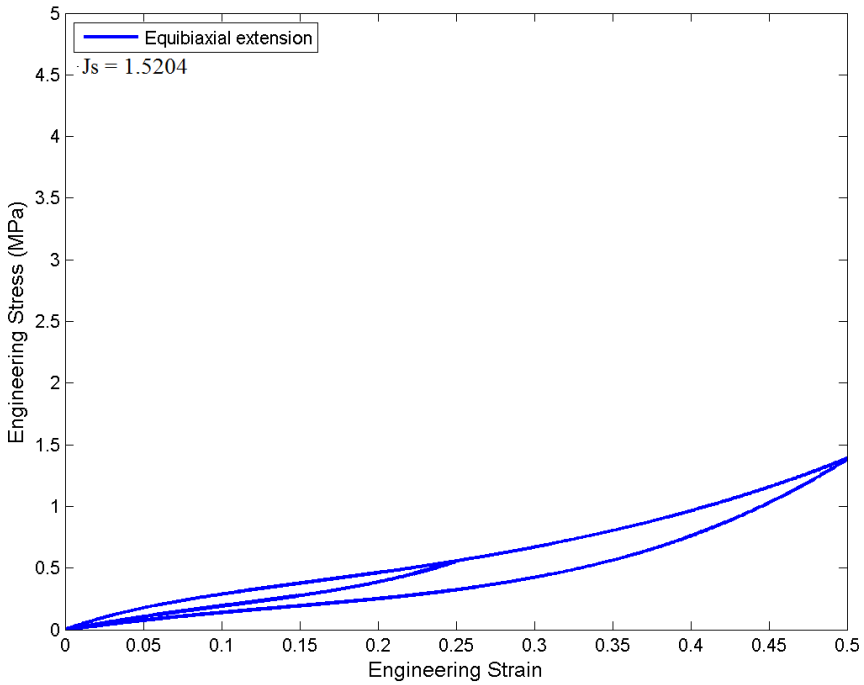

Figure 5.120: Two-phase model response under equibiaxial extension for CR swollen by B100 after 5 days immersion.

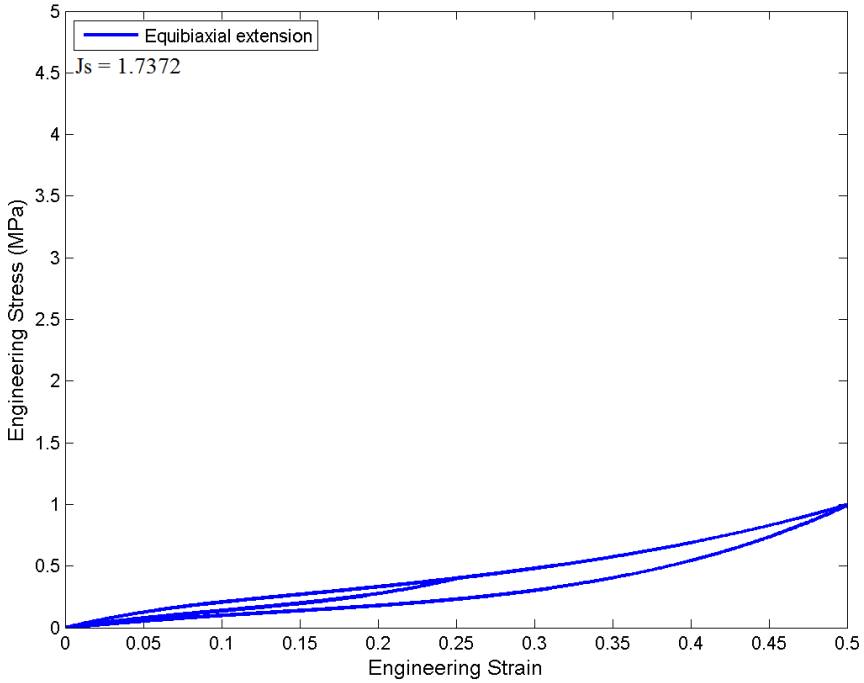

Figure 5.121: Two-phase model response under equibiaxial extension for CR swollen by B100 after 10 days immersion.

Evolution of effective volume fraction of soft phase The evolution of the effective volume fraction of the soft phase for dry and swollen NBR and CR in the equibiaxial extension tests during the first virgin material loading to $\varepsilon = 0.5$ are shown in Figures 5.122 and 5.123. For a given degree of swelling, it is clearly shown that the amount of volume fraction of the soft domain at any given strain is the largest in the case of equibiaxial extension, compared to uniaxial extension and pure shear conditions.

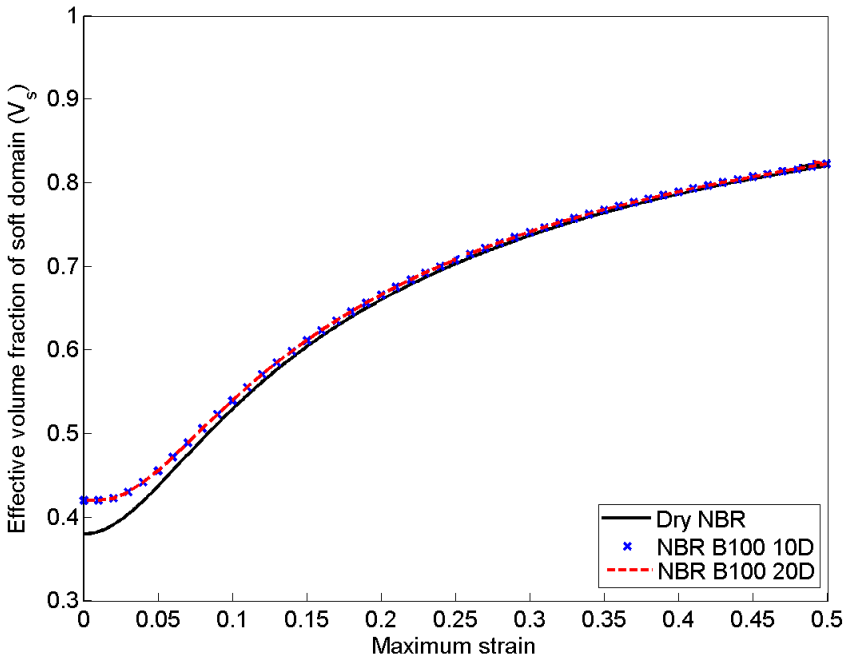

Figure 5.122: Evolution of effective volume fraction of soft phase under equibiaxial extension deformation for NBR swollen by B100. Results correspond to 10 and 20 days of immersion duration.

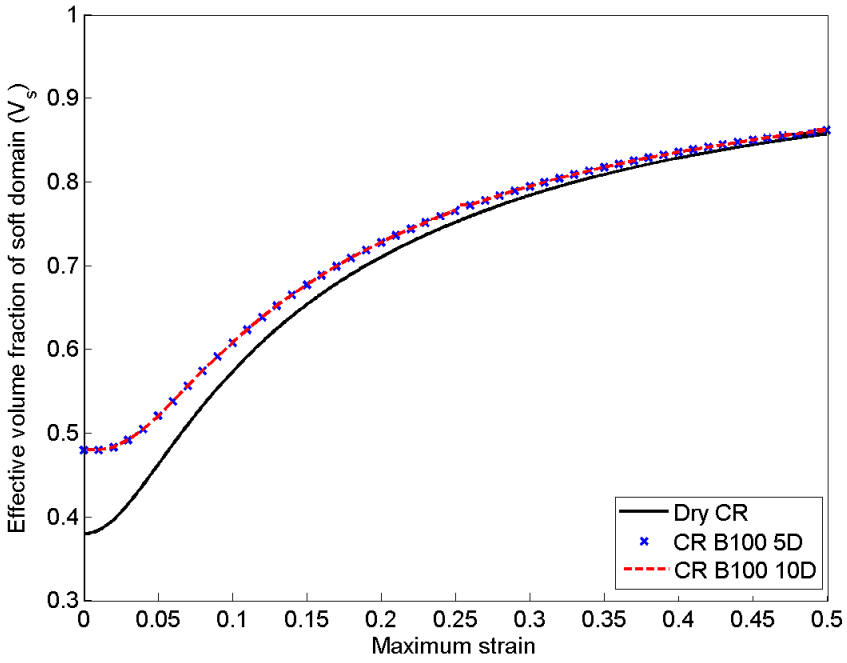

Figure 5.123: Evolution of effective volume fraction of soft phase under equibiaxial extension deformation for CR swollen by B100. Results correspond to 5 and 10 days of immersion duration.

5.5 Comparison between modeling results of extended pseudo-elastic model and two-phase model

Comparing the modeling results of the extended pseudo-elastic model and the extended two-phase model, it is found that the extended pseudo-elastic model is limited to model the stress-softening response of elastomers with low degree of swelling. For high degree of swelling, i.e. CR after immersed in B100 for 30 days, the simulated curve deviates from the experimental curve. The corresponding discrepancies between experiment and model can be attributed to the choice of parameters Δm and Δr which are assumed to be independent of the interaction parameter χ. Obviously, as clearly illustrated in Figures 5.5 and 5.6, better performance of the model can be obtained if we include the dependence on the interaction parameter χ in the expression of Δm and Δr. In spite of these discrepancies, the extended pseudo-elastic model appears to have advantage of being ease to use because of its simplicity. Indeed, it is found that using simple Neo-Hookean strain energy function which required only a single material parameter, the model is capable to capture general feature of Mullins effect in swollen elastomers.

The extended two-phase model appears to capture well the stress-softening response in the swollen elastomers for a wide range of degree of swelling. However, it requires larger number of material parameters than those needed in extended pseudo-elastic model. Moreover, the procedure required for the identification of material parameters is relatively more complex.

CHAPTER 6

CONCLUSIONS AND FUTURE WORKS

6.1 Conclusions

In order to conclude, all research objectives stated in Chapter 1 have been achieved. They are detailed in the following:

1. *Investigation of the swelling of elastomer in solvent:*

   An experimental setup was developed to investigate the swelling of elastomers in biodiesel. Different levels of swelling resulting from different immersion durations of stress-free elastomeric specimens were considered. It was found that the rate of swelling is relatively high at short immersion times and becomes lower at longer immersion duration. For given immersion duration, the swelling in CR was systematically higher than in NBR.

2. *Investigation of the effect of the presence of static mechanical loading on the swelling of elastomer:*

   An original test device for the analysis of the interaction between the diffusion of biodiesel and large deformation in rubber was developed. The test conducted is the first of its kind in investigating the effect of the presence of static mechanical loading on the biodiesel diffusion in rubber. The specially designed compression device consists of four stainless steel plates with spacer bars in between. The presence of spacer bars allows the application of pre-compressive strain while simultaneously exposing the rubber specimens to biodiesel. It was found that the swelling in rubbers increases with the increase of palm biodiesel content and decreases with the increase of pre-compressive strain.

3. *Investigation of the effect of swelling on the mechanical response of elastomers under cyclic loading condition:*

The diffusion of biodiesel into rubber appeared to reduce its strength. Under cyclic loading conditions, both swollen NBR and swollen CR exhibited inelastic responses, i.e. stress-softening, hysteresis and stress relaxation. However, the amount of these inelastic responses in swollen rubbers was significantly lower than that found in dry rubbers. The evolution of shear modulus ratio of swollen and dry rubbers as a function of applied compressive stress was investigated. It was found that this ratio deviates from the one predicted by Treloar.

4. *Development of a continuum mechanical model for the Mullins effect in swollen rubber:*

   An original approach in modeling the Mullins effect taking into account swelling was proposed. Extensions of the pseudo-elastic model of Ogden and Roxburgh (1999) and the two-phases model of Mullins and Tobin (1957) and Qi and Boyce (2004) were developed to describe the Mullins effect in swollen rubber. The models were considered and modified in order to account for the degree of swelling. Results showed that in general the proposed models were qualitatively in good agreement with experimental observations.

6.2 Suggestions for future works

Based on the experimental results, it is suggested that further investigations of the influence of multiaxial stress states on the swelling and the resulting mechanical response are needed. The suggested test will aid in understanding the fatigue failure of elastomers in hostile environment. This can be done by designing special multiaxial test equipment and redesigning the test specimens such that the testing time can be reduced. A further suggestion on the experimental work to conduct swelling tests with a wide range of biodiesel to understand the swelling behavior of elastomers.

On the continuum mechanical modeling, the proposed models for the Mullins effect in swollen rubbers are based on the existing pseudo-elastic model due to Ogden and Roxburgh (1999) and two-phases model due to Mullins and Tobin (1957) and Qi and Boyce (2004). Further development and validation of the proposed model are needed. The models could be improved by considering other material parameters to be dependent on the swelling of elastomers, i.e. υ_{ss} and A in the extended two-phases model. Other

inelastic responses such as permanent set and hysteresis in swollen rubber can also be included in the model. The next step would be implementing the developed models into finite element code to simulate the response of industrial rubber components.

BIBLIOGRAPHY

Abu-Abdeen, M. (2010). Single and double-step stress relaxation and constitutive modeling of viscoelastic behavior of swelled and un-swelled natural rubber loaded with carbon black. *Mater. Design*, *31*(4), 2078–2084.

Amin, A. F. M. S., & Lion, A. (2010). Temperature dependence of mullins softening-healing phenomena: An outline for theoretical description based on experiments. In G. Heinrich, M. Kaliske, A. Lion, & S. Reese (Eds.), *Constitutive models for rubber vi* (pp. 497–503). Taylor & Francis Group.

Andriyana, A., Chai, A. B., Verron, E., & Johan, M. R. (2012). Interaction between diffusion of palm biodiesel and large strain in rubber: Effect on stress-softening during cyclic loading. *Mech. Res. Commun*, *43*, 80–86.

Andriyana, A., Saintier, N., & Verron, E. (2010). Configurational mechanics and critical plane approach: Concept and application to fatigue failure analysis of rubberlike materials. *Int. J. Fatigue*, *32*(10), 1627–1638.

Arruda, E. M., & Boyce, M. C. (1993). A three dimensional constitutive model for the large stretch behavior of rubber elastic materials. *J. Mech. Phys. Solids*, *41*(2), 389–412.

ASTM. (1957). *Standard test method for rubber property-change in properties of elastomeric vulcanizates resulting from immersion in liquids.* (ASTM No. D 471). Philadelphia.

Baek, S., & Srinivasa, A. R. (2004). Diffusion of a fluid through an elastic solid undergoing large deformation. *Int. J. Nonlinear Mech.*, *39*(2), 201–218.

Bauman, J. (2008). *Fatigue, stress, and strain of rubber components: A guide for design engineers*. Hanser.

Beatty, M., & Krishnaswamy, S. (2000). A theory of stress-softening in incompressible isotropic materials. *J. Mech. Phys. Solids.*, *48*, 1931–1965.

Bergström, J. S., & Boyce, M. C. (1998). Constitutive modeling of the large strain time-dependent behavior of elastomers. *J. Mech. Phys. Solids*, *46*(5), 931–954.

Bergström, J. S., & Boyce, M. C. (1999). Mechanical behavior of particle filled elastomers. *Rubber Chem. Tech.*, *72*, 633–656.

Berlanga-Labari, C., Albistur-Goñi, A., Barado-Pardo, I., Gutierrez-Peinado, M., & Fernández-Carrasquilla, J. (2011). Compatibility study of high density polyethylene with bioethano-gasoline blends. *Mater. Design*, *32*(1), 441–446.

Botros, S. H., & Sayed, A. M. E. L. (2001). Swelling Behavior of NR / EPDM Rubber Blends Under. *Polymer*, 3052–3057.

Bouasse, H., & Carrière, Z. (1903). Courbes de traction du caoutchouc vulcanisé. *Ann. Fac. Sci. Toulouse*, *5*, 257–283.

Boyce, M. C., & Arruda, E. M. (2001). Swelling and mechanical stretching of elastomeric materials. *Math. Mech. Solids*(6), 641–659.

Brieu, M., Diani, J., Mignot, C., & Moriceau, C. (2010). Response of a carbon-black filled sbr under large strain cyclic uniaxial tension. *Int. J. Fatigue*, *32*(12), 1921–1927.

Busfield, J. J. C., Deeprasertkul, C., & G, T. A. (2000). The effect of liquids on the dynamic properties of carbon black filled natural rubber as a function of pre-strain. *Polymer*, *41*(26), 9219–9225.

Cai, S., Lou, Y., Ganguly, P., Robisson, A., & Suo, Z. (2010). Force generated by a swelling elastomer subject to constraint. *J. Appl. Phys.*, *107*, 1–7.

Callister, W. D. (2007). *Materials science and engineering: An introduction*. John Wiley & Sons.

Chagnon, G., Verron, E., Gornet, L., Marckmann, G., & Charrier, P. (2004). On the relevance of continuum damage mechanics as applied to the mullins effect in elastomers. *J. Mech. Phys. Solids*, *52*(7), 1627–1650.

Chagnon, G., Verron, E., Marckmann, G., & Gornet, L. (2006, November). Development of new constitutive equations for the Mullins effect in rubber using the network alteration theory. *Int. J. Solids Struct.*, *43*(22-23), 6817–6831.

Chai, A. B., Andriyana, A., Verron, E., & Johan, M. R. (2013). Mechanical characteristics of swollen elastomers under cyclic loading. *Mater. Design*, *44*, 566–572.

Chai, A. B., Andriyana, A., Verron, E., Johan, M. R., & Haseeb, A. S. M. A. (2011). Development of a compression test device for investigating interaction between diffusion of biodiesel and large deformation in rubber. *Polym. Test.*, *30*, 867–875.

Chai, A. B., Verron, E., Andriyana, A., & Johan, M. R. (2013). Mullins effect in swollen rubber: Experimental investigation and constitutive modeling. *Polym. Test.*, *32*, 748–759.

Cho, K., Jang, K. J., Lee, D., Chun, H., & Chang, Y.-W. (2000). Fatigue crack growth of elastomers in the swollen state. *Polym*, *41*, 179–183.

Coleman, B., & Gurtin, M. (1967). Thermodynamics with internal state variables. *J. Chem. Phys.*, *47*, 597–613.

Deng, H., & Pence, T. J. (2009). Equilibrium states of mechanically loaded saturated and unsaturated polymer gels. *J. Elasticity*, *99*(1), 39–73.

Deng, H., & Pence, T. J. (2010). Shear induced loss of saturation in a fluid infused swollen hyperelastic cylinder. *Int. J. Eng. Sci.*, *48*(6), 624–646.

Diani, J., Fayolle, B., & Gilormini, P. (2009). A review on the Mullins effect. *Eur. Polym. J.*, *45*(3), 601–612.

Dick, J. S. (Ed.). (2001). *Rubber technology: Compounding and testing for perfomance*. Hanser.

Dorfmann, A., & Ogden, R. W. (2004). A constitutive model for the mullins effect with permanent set in particle-reinforced rubber. *Macromolecules*, *41*(7), 1855–1878.

Flory, P. J. (1942). Thermodynamics of high polymer solutions. *J. Chem. Phys.*, *10*, 51–61.

Flory, P. J. (1953). *Principles of polymer chemistry*. Cornell University Press.

Flory, P. J. (1961). Thermodynamics relation for high elastic materials. *Trans. Faraday Soc.*, *57*, 829–838.

Flory, P. J., & Rehner, J. (1943a). Statistical mechanics of cross-linked polymer networks ii. swelling. *Rubber Chem. Technol.*, *11*, 521–526.

Flory, P. J., & Rehner, J. (1943b). Statistical mechanics of cross-linked polymer networks i. rubberlike elasticity. *J. Chem. Phys.*, *11*, 512–520.

Fukumori, K., Kurauchi, T., & Kamigaito, O. (1990). Swelling behaviour of rubber vulcanizates: 2. Effects of tensile strain on swelling. *Polymer*, *31*(12), 2361–2367.

Gandhi, M. V. (1989). Combined extension and torsion of a swollen cylinder within the context of mixture theory. *Acta Mech.*, *13*(4), 203–95.

Gent, A. (Ed.). (1992). *Engineering with rubber: How to design rubber components*. Hanser.

George, S. C., Knörgen, M., & Thomas, S. (1999). Effect of nature and extent of crosslinking on swelling

and mechanical behavior of styrene-butadiene rubber membranes. *J. Membrane Sci.*, *163*(1), 1–17.

George, S. C., & Thomas, S. (2001). Transport phenomena through polymeric systems. *Prog. Polym. Sci.*, *26*(6), 985–1017.

Govindjee, S., & Simo, J. C. (1991). A micro-mechanical continuum mechanical model for carbon black filled rubbers incorporating Mullins effect. *J. Mech. Phys. Solids*, *39*, 87–Ű112.

Hanley, J. (2008). *Swelling effects in dynamic equi-biaxial testing of epdm elastomers by the bubble inflation method*. Unpublished doctoral dissertation, Dublin Institute of Technology.

Harwood, J. A. C., Mullins, L., & Payne, A. R. (1966a). Stress softening in natural rubber vulcanizates. Part lll. Carbon black filled vulcanizates. *J. Appl. Polymer Sci.*, *10*, 315–323.

Harwood, J. A. C., Mullins, L., & Payne, A. R. (1966b). Stress softening in natural rubber vulcanizates. Part ll. Stress softening effects in pure gum and filler loaded rubbers. *Rubber Chem. Technol.*, *39*, 814–822.

Harwood, J. A. C., & Payne, A. R. (1966). Stress softening in natural rubber vulcanizates. Part lll. Unfilled vulcanizates. *J. Appl. Polymer Sci.*, *10*, 1203–1211.

Haseeb, A. S. M. A., Jun, T. S., Fazal, M. A., & Masjuki, H. H. (2011). Degradation of physical properties of different elastomers upon exposure to palm biodiesel. *Energy*, *36*(3), 1814–1819.

Haseeb, A. S. M. A., Masjuki, H. H., Siang, C. T., & Fazal, M. A. (2010). Compatibility of elastomers in palm biodiesel. *Renew. Energ.*, *35*(10), 2356–2361.

Hirotsu, S. (2004). Stress relaxation and elastic moduli in the swollen and the shrunken phases of N-Isopropylacrylamide gel. *Macromolecules*, *37*(9), 3415–3424.

Holzapfel, G. A. (2000). *Nonlinear solid mechanics: A continuum approach for engineering*. John Wiley & Sons Ltd.

Hong, W., Liu, Z., & Suo, Z. (2009). Inhomogeneous swelling of a gel in equilibrium with a solvent and mechanical load. *Int. J. Solids Struct.*, *46*(17), 3282–3289.

Hong, W., Zhao, X., Zhou, J., & Suo, Z. (2008). A theory of coupled diffusion and large deformation in polymeric gels. *J. Mech. Phys. Solids*, *56*(5), 1779–1793.

Horkay, F., & Zrinyi, M. (1988). Studies on mechanical and swelling behavior of polymer networks on the basis of the scaling concept. 7. effect of deformation on the swelling equilibrium concentration of gels. *Macromolecules*, *21*(11), 3260–3266.

Huggins, M. L. (1942). Theory of solutions of high polymers . *J. Am. Chem. Soc.*, *64*, 1712–1719.

Huntley, H. E., Wineman, A. S., & Rajagopal, K. R. (1996). Chemorheological relaxation, residual stress and permanent set arising in radial deformation of an elastomeric hollow sphere. *Math. Mech. Solids*, *1*, 267–299.

Huntley, H. E., Wineman, A. S., & Rajagopal, K. R. (1997). Stress softening, strain localization and permanent set in the circumferential shear of an incompressible elastomeric cylinder. *IMA J. Appl. Math*, *59*, 309–338.

Inci, M. N., Erman, B., Okay, O., & Durmaz, S. (2001). Elastic behaviour of solution cross-linked poly(isobutylene) gels under large compression. *Polymer*, *42*(8), 3771–3777.

Ismail, H., Nordin, R., & Noor, A. M. (2002). Cure characteristics, tensile properties and swelling behaviour of recycled rubber powder-filled natural rubber compounds. *Polym. Test.*, *21*(5), 565–569.

Jayed, M. H., Masjuki, H. H., Kalam, M. A., Mahlia, T. M. I., Husnawan, M., & Liaquat, A. M. (2011). Prospects of dedicated biodiesel engine vehicles in Malaysia and Indonesia. *Renew. Sust. Energ. Rev.*,

15, 220–235.

Jayed, M. H., Masjuki, H. H., Saidur, R., Kalam, M. A., & Jahirul, M. I. (2009). Environmental aspects and challenges of oilseed produced biodiesel in Southeast Asia. *Renew. Sust. Energ. Rev.*, *13*, 2452–2462.

Johlitz, M., & Lion, A. (2012). Chemo-thermomechanical ageing of elastomers based on multiphase continuum mechanics. *Continuum Mech. Thermodyn.*, 1–20.

Joshi, N., & Muliana, A. (2010). Deformation in viscoelastic sandwich composites subject to moisture diffusion. *Compos. Struct.*, *92*(2), 254–264.

Kakavas, P. A. (1996). Mechanical properties of bonded elastomer discs subjected to triaxial stress. *J. Appl. Polym. Sci.*, *59*, 251–261.

Kar, K., & Bhowmick, A. (1997). High-strain hysteresis of rubber vulcanizates over a range of compositions, rates, and temperatures. *J. Appl. Polym. Sci.*, *65*, 1429–1439.

Killian, H. G., Strauss, M., & Hamm, W. (1994). Universal properties in filler-loaded rubbers. *Rubber Chem. Technol.*, *67*, 1–16.

Klüppel, M., & Schramm, M. A. (2000). A generalized tube model of rubber elasticity and stress softening of filler reinforced elastomer systems. *Macromol. Theory Simul.*, *9*, 742–7Ű54.

Laboratory, N. R. E. (2009). *Biodiesel handling and use guide: Fourth edition (revised)* (Tech. Rep.). Author.

Laraba-Abbes, F., Ienny, P., & Piques, R. (2003). A new 'Tailor-made' methodology for the mechanical behaviour analysis of rubber-like materials: II. Application to the hyperelastic behaviour characterization of a carbon-black filled natural rubber vulcanizate. *Polymer*, *44*(3), 821–840.

Le Cam, J. B., Huneau, B., & Verron, E. (2008). Description of fatigue damage in carbon black filled natural rubber. *Fatigue Fract. Eng. Mater. Struct*, *31*, 1031–1038.

Le Cam, J. B., Huneau, B., & Verron, E. (2013). Fatigue damage in carbon black filled natural rubber under uni- and multiaxial loading conditions. *Int. J. Fatigue*, *52*, 82–94.

Le Cam, J. B., & Toussaint, E. (2010). The mechanism of fatigue crack growth in tubbers under severe loading: The effect of stress-induced crystallization. *Macromolecules*, *43*, 4708–4714.

Lin, W.-C., Fan, W., Marcellan, A., Hourdet, D., & Creton, C. (2010). Large strain and fracture properties of Poly(dimethylacrylamide)/Silica hybrid hydrogels. *Macromolecules*, *43*(5), 2554–2563.

Lion, A. (1996). A constitutive model for carbon black filled rubber: Experimental investigations and mathematical representation. *Continuum Mech. Thermodyn.*, *8*(3), 153–169.

Lion, A. (1997). On the large deformation behaviour of reinforced rubber at different temperatures. *J. Mech. Phys. Solids*, *45*(11-12), 1805–1834.

Magryta, J., Debek, C., & Debek, D. (2006). Mechanical properties of swelled vulcanizates of polar diene elastomers. *J. Appl. Polym. Sci.*, *99*(5), 2010–2015.

Marckmann, G., & Verron, E. (2006). Comparison of hyperelastic models for rubber-like materials. *Rubber Chem. Technol.*, *79*, 835–858.

Marckmann, G., Verron, E., Gornet, L., Chagnon, G., Charrier, P., & Fort, P. (2002). A theory of network alteration for the mullins effect. *J. Mech. Phys. Solids*, *50*, 2011–2028.

Mark, J. E., Erman, B., & Eirich, F. R. (Eds.). (2005). *Science and technology of rubber*. Elsevier.

Mars, W. V. (2001). *Multiaxial fatigue of rubber*. Unpublished doctoral dissertation, University of Toledo.

Mars, W. V., & Fatemi, A. (2002). A literature survey on fatigue analysis approaches for rubber. *Int. J. Fatigue*, *24*, 949–961.

Maru, M. M., Lucchese, M. M., Legnani, C., Quirino, W. G., Balbo, A., Aranha, I. B., ... Achete, C. A. (2009). Biodiesel compatibility with carbon steel and HDPE parts. *Fuel Process. Techno.*, *90*(9), 1175–1182.

Meyer, K., & Ferri, C. (1935). Sur l'élasticité du caoutchouc. *Helvetica Chimica Acta*, *18*, 570–589.

Miehe, C. (1995). Discontinuous and continuous damage evolution in ogden-type large strain elastic materials. *Eur. J. Mech. A/Solids.*, *14*, 697–720.

Miller-Chou, B. A., & Koenig, J. L. (2003). A review of polymer dissolution. *Prog. Polym. Sci.*, *28*(8), 1223–1270.

Mostafa, A., Abouel-Kasem, A., Bayoumi, M. R., & El-Sebaie, M. G. (2009). Effect of carbon black loading on the swelling and compression set behavior of SBR and NBR rubber compounds. *Mater. Design*, *30*(5), 1561–1568.

Mullins, L. (1948). Effect of stretching on the properties of rubber. *Rubber Chem. Technol.*, *21*, 281–300.

Mullins, L., & Tobin, N. R. (1957). Theoretical model for the elastic behaviour of filler reinforced vulcanized rubbers. *Rubber Chem. Technol.*, *30*, 551–571.

Nah, C., Lee, G., Lim, C. I., Ahn, J., & Gent, A. N. (2011). Swelling of rubber under nonuniform stresses and internal migration of swelling liquid when the stresses are removed. *Macromolecules*, *44*(6), 1610–1614.

Nah, C., Lee, G. B., Lim, J. Y., Kim, Y. H., SenGupta, R., & Gent, A. N. (2010). Problems in determining the elastic strain energy function for rubber. *Int. J. Nonlinear Mech.*, *45*(3), 232–235.

Ogden, R. W., & Roxburgh, D. G. (1999, August). A pseudo-elastic model for the Mullins effect in filled rubber. *P. Roy. Soc. A-Math. Phy.*, *455*(1988), 2861–2877.

Pekcan, Ö., & Uğur, Ş. (2002). Molecular weight effect on polymer dissolution: a steady state fluorescence study. *Polymer*, *43*(6), 1937–1941.

Qi, H. J., & Boyce, M. C. (2004). Constitutive model for stretch-induced softening of the stress-stretch behavior of elastomeric materials. *J. Mech. Phys. Solids.*, *52*, 2187–2205.

Radhakrishnan Nair, N. (1997). *Studies on depolymerized natural rubber*. Unpublished doctoral dissertation, Mahatma Gandhi University.

Ramesan, M. T. (2005). The effects of filler content on cure and mechanical properties of dichlorocarbene modified styrene butadiene rubber/carbon black composites. *J. Polym. Res.*, *11*, 333–340.

Ramtani, S. (2006). Pre-stressed and reinforced hollow cylindrical mixture of non-linearly elastic solid and ideal fluid subjected to combined deformations: A study within the context of the theory of interacting continua. *Int. J. NonLin. Mech.*, *41*(5), 736–750.

Sasaki, S. (2004). Stress relaxation of deformed gel in a good solvent. *The Journal of chemical physics*, *120*(12), 5789–94.

Shackelford, J. F. (2000). *Introduction to materials science for engineers*. Prentice Hall.

Simo, J. C. (1987). On a fully three-dimensional finite-strain viscoelastic damage model: formulation and computational aspects. *Comput. Method Appl. Mech. Eng.*, *60*, 5153–5173.

Soares, J. S. (2009). Diffusion of a fluid through a spherical elastic solid undergoing large deformations. *Int. J. Eng. Sci.*, *47*(1), 50–63.

Trabelsi, A., Albouy, P. A., & Rault, J. (2003). Crystallization and melting processes in vulcanized stretched natural rubber. *Macromolecules*, *36*(20), 7624–7639.

Trakarnpruk, W., & Porntangjitlikit, S. (2008). Palm oil biodiesel synthesized with potassium loaded calcined hydrotalcite and effect of biodiesel blend on elastomer properties. *Renew. Energ.*, *33*(7), 1558–1563.

Treloar, L. R. G. (1950). The swelling of cross-linked amorphous polymers under strain. *T. Faraday Society*, *46*, 783.

Treloar, L. R. G. (1975). *The physics of rubber elasticity*. London: Oxford University Press.

Ueberreiter, K. (1968). The solution process. In J. Crank & G. S. Park (Eds.), *Diffusion in polymers* (pp. 219–257). Academic Press.

Valentín, J. L., Mora-Barrantes, I., Carretero-González, J., López-Manchado, M. A., Sotta, P., Long, D. R., & Saalwächter, K. (2010). Novel experimental approach to evaluate filler-elastomer interactions. *Macromolecules*, *43*, 334–346.

Verron, E., & Andriyana, A. (2008). Definition of a new predictor for multiaxial fatigue crack nucleation in rubber. *J. Mech. Phys. Solids*, *56*, 417–443.

Webber, R., Creton, C., Brown, H., & Gong, J. (2007). Large strain hysteresis and mullins effect of tough double-network hydrogels. *Macromolecules*, *40*, 2919–2927.

Wineman, A. S., & Huntley, H. E. (1994). Numerical simulation of the effect of damaged induced softening on the inflation of a circular rubber membrane. *Int. J. Solids Struct.*, *31*, 3295–Ű3313.

Wypych, G. (Ed.). (2004). *Handbook of plasticizers*. ChemTec Publishing.

Zhang, H., & Cloud, A. (2007). Research progress in calenderable Fluorosilicone with excellent fuel resistance. *SAMPE*.

Zuyev, Y. S., Pravednikova, S. I., Zherebkova, L. S., & Zaitseva, V. D. (1964). The tear-resistance of rubbers in the presence of physically aggressive media. *Polymer Sci. USSR*, *5*, 269–276.

LIST OF PUBLICATIONS

Academic Journals

1. **Chai, A.B.**, Andriyana, A., Ch'ng, S.Y., Verron, E., and Johan, M.R. (2013). Extended two-phase model for mullins effect in swollen rubber. *Mater. Res. Innov.*, Submitted.

2. **Chai, A.B.**, Verron, E., Andriyana, A., and Johan, M.R. (2013). A pseudo-elastic model for the Mullins effect in swollen rubber. *Sains Malays.*, Submitted.

3. **Chai, A.B.**, Verron, E., Andriyana, A., and Johan, M.R. (2013). Mullins effect in swollen rubber: Experimental investigation and constitutive modeling. *Polym. Test.*, 32: 748-759.

4. **Chai, A.B.**, Andriyana, A., Verron, E., and Johan, M.R. (2013). Diffusion of biodiesel in rubber and the resulting mechanical response under cyclic loading. *Defect Diffus. Forum*, 334-335: 111-116.

5. **Chai, A.B.**, Andriyana, A., Verron, E., and Johan, M.R. (2012). Mechanical characteristics of swollen elastomers under cyclic loading. *Mater. Design.*, 44: 566-572.

6. Andriyana, A., **Chai, A.B.**, Verron, E., and Johan, M.R. (2012). Interaction between diffusion of palm biodiesel and large strain in rubber: Effect on stress-softening during cyclic loading. *Mech. Res. Commun.*, 43: 80-86.

7. **Chai, A.B.**, Andriyana, A., Verron, E., Johan, M.R., and Haseeb, A.S.M.A. (2011). Development of a compression test device for investigating interaction between diffusion of biodiesel and large deformation in rubber. *Polym. Test.*,30: 867-875.

Conference Proceedings

1. **Chai, A.B.**, Andriyana, A., Ch'ng, S.Y., Verron, E., Johan, M.R. (2013). Modeling the Mullins effect in swollen rubber. In: *Constitutive Models for Rubber VII*. Gil-Negrete & Alonso (eds). Page 443-448. Taylor & Francis Group Publisher. ISBN 978 1 138 00072 8.

2. Andriyana, A., **Chai, A.B.**, Verron, E., Johan, M.R., and Haseeb, A.S.M.A. (2011). Coupling between diffusion of biodiesel and large deformation in rubber: Effect on the mechanical response under cyclic loading conditions. In: Constitutive Models for Rubber VII. Jerrams and Murphy (eds). Page 283-288. Taylor & Francis Group Publisher. ISBN 978 0 415 68389 0.

3. **Chai, A.B.**, Andriyana, A., Verron, E., Johan, M.R., and Haseeb, A.S.M.A. (2011). Development of an experimental device to investigate mechanical response of rubber under simultaneous diffusion and large strain compression. In: Constitutive Models for Rubber VII. Jerrams and Murphy (eds). Page 391-396. Taylor & Francis Group Publisher. ISBN 978 0 415 68389 0.

Conference Presentations

1. **Chai, A.B.**, Andriyana, A., Ch'ng, S.Y., Verron, E., Johan, M.R. Extended two-phase model for mullins effect in swollen rubber. *International Conference on the Science and Engineering of Materials 2013 (ICoSEM2013)*. Kuala Lumpur, Malaysia. 13-14 November 2013. (Accepted).

2. **Chai, A.B.**, Andriyana, A., Ch'ng, S.Y., Verron, E., Johan, M.R. Modeling the Mullins effect in swollen rubber. *8th European Conference on Constitutive Models for Rubber (ECCMR)*. San Sebastián, Spain. 25-28 June 2013.

3. **Chai, A.B.**, Verron, E., Andriyana, A., Johan, M.R. A pseudo-elastic model for the Mullins effect in swollen rubber. *4th International Conference on Solid State Science and Technology (ICSSST)*. Malacca, Malaysia. 18-20 December 2012.

4. **Chai, A.B.**, Andriyana, A., Verron, E., Johan, M.R. Diffusion of biodiesel in rubber and the resulting mechanical response under cyclic loading. *8th International Conference on Diffusion in Solids and Liquids (DSL)*. Turkey, Istanbul. 25-29 June 2012.

5. Andriyana, A., **Chai, A.B.**, Verron, E., Johan, M.R., and Haseeb, A.S.M.A. (2011). Coupling between diffusion of biodiesel and large deformation in rubber: Effect on the mechanical response under cyclic loading conditions. *8th European Conference on Constitutive Models for Rubber (ECCMR)*. 20-23 September 2011. Dublin, Ireland.

6. **Chai, A.B.**, Andriyana, A., Verron, E., Johan, M.R., and Haseeb, A.S.M.A. (2011). Development of an experimental device to investigate mechanical response of rubber under simultaneous diffusion and large strain compression. *8th European Conference on Constitutive Models for Rubber (ECCMR)*. 20-23 September 2011. Dublin, Ireland.